Self-desiccation and its importance in concrete technology : Proceedings of an International research seminar in Lund, June 10, 1997

Persson, Bertil; Fagerlund, Göran

1997

LUND UNIVERSITY
LUND INSTITUTE OF TECHNOLOGY
Division of Building Materials

Report TVBM-3075

SELF-DESICCATION AND ITS IMPORTANCE IN CONCRETE TECHNOLOGY

B Persson and G Fagerlund, Editors

Proceedings of an International Research Seminar in Lund, June 10, 1997

ISRN LUTVDG/TVBM--97/3075--SE(1-255)
ISSN 0348-7911 TVBM
ISBN 91-630-5528-7

Lund Institute of Technology
Division of Building Materials
Box 118
S-221 00 Lund, Sweden

Telephone: 46-46-2227415
Telefax: 46-46-2224427

PREFACE

Self-desiccation is a well-known phenomenon. It has also been known for a very long time that the magnitude of self-desiccation increases with decreasing waterlcement ratio. Self-desiccation in low-porosity cement paste with a waterlcement ratio as low as 0.17 was described almost 60 years ago in a paper by Gause and Tucker,[1]. The phenomenon was theoretically explained by Powers,[2]. Further experimental and theoretical studies were presented by Copeland and Bragg in 1955,[3]. The mechanical effects of self-desiccation, such as different types of shrinkage and cracking, were described by Wittmann in 1968,[4]. The RH-reducing effect of self-desiccation in concrete with low water/cement ratio, and the importance of this effect for reducing the drying time of concrete, was investigated and marketed quite early in Sweden by Ahlgren in 1973,[5], and later by Nilsson in 1977,[6]. The increased drying rate of high performance concrete has been widely exploited in Sweden during the last 5 years. More than 1 million square meters of concrete slabs have been produced with so-called self-drying, or rapid-drying, concrete.

The effects - positive and negative - of self-desiccation are negligible in traditional concrete because of the small effect of self-desiccation on the internal RH of such concrete. Therefore, self-desiccation is hardly noticed, or considered, in traditional concrete technology. The growing interest in high performance concrete has changed the situation. A reduction in the waterlcement ratio to levels far below 0.40 and use of silica fume cause such big changes in the internal pore structure that self-desiccation becomes important. The RH-level can be very much reduced, causing rapid drying and improved durability. But it also has negative effects such as shrinkage and cracking. Therefore, self-desiccation cannot be neglected in high performance concrete.

It is clear that we need more information and a better understanding of self-desiccation; of the mechanism, and of the effects on the properties of the finished concrete, especially the durablity. It is the purpose of this seminar to collect and discuss information from ongoing research within this important field.

Lund, May 16,1997

Göran Fagerlund

---

[1]) Gause, Tucker (1940) J. of Research, National Bureau of Standards Vol 25, p. 403.

[2]) Powers (1947) A discussion of cement hydration in relation to the curing of concrete, Higway Research Board, Proc. 27.

[3]) Copeland, Bragg (1955) Self desiccation in portland cement pastes, ASTM Bulletin No 204.

[4]) Wittmann (1968) Surface tension, shrinkage and strength of hardened cement paste, Materials and Strucures, No 6.

[5]) Ahlgren (1973) Moisture in concrete floors with impermeable coatings, Byggmastaren, Nr 6.

[6]) Nilsson (1977) Moisture problems at concrete floors, Division of Building Materials, Lund Institute of Technology, Report TVBM-3002

TABLE OF CONTENTS PAGE

HIGH PERFORMANCE CONCRETE (HPC) AT EARLY AGES: SELFGENERATED STRESSES DUE TO AUTOGENOUS SHRINKAGE AND TEMPERATURE

ØYVIND BJØNTEGAARD, ERIK J. SELLEVOLD
The Norwegian University of Science and Technology,
Department of Structural Engineering, Trondheim.

TOR ARNE HAMMER
The research institution SINTEF Civil and Environmental
Engineering, Trondheim.

ABSTRACT

There are two main driving forces to the generation of stresses in concrete during hardening under restraint: Thermal dilation and autogenous shrinkage. The results in the paper demonstrates that the autogenous shrinkage contribution may be substantial. The magnitude of the autogenous shrinkage is very sensitive to the binder phase composition of the concrete, the available water content in the aggregate and to temperature. It is shown that for a given concrete, with a constant initial temperature through setting, the subsequent autogenous shrinkage at different temperature developments may be described using the maturity concept. However, both the rate and magnitude of the shrinkage depends on the initial temperature level. The temperature sensitivity of autogenous shrinkage is presently badly understood and requires more work.

INTRODUCTION AND TEST PROGRAM

Practical use of HPC has shown it to be sensitive to cracking at early ages. Several mechanisms are active: (1) Plastic shrinkage may develop very early due to minimal bleeding, (2) chemical shrinkage due to hydration reactions resulting in autogenous shrinkage, and **(3)** the temperature rise is high due to high cement contents resulting in tensile stress development during subsequent cooling. The control of such cracking is the goal of the Norwegian NOR-IPACS project. The total project involves determination of the required material properties, temperature and stress calculation programs and field testing at construction sites. FIG.-1 shows a principle sketch of the interaction between the different project parts. The "Stress-Rig" (FIG.-2) has a central role. It measures the stress generation under full restraint (via a feedback system) in a concrete from about 6 hours after mixing. **A** "Shrinkage-Rig" is also constructed to measure the unrestrained (free) movement caused by temperature change (thermal dilation) and autogenous shrinkage. The Shrinkage-Rig may be operated so that the 2 contributions to movement can be separated. The temperature of the concrete is controlled in both rigs, to produce either isothermal conditions (to measure the contribution of autogenous shrinkage alone) or a realistic temperature history to simulate practical conditions. Thus, the Stress-Rig may be used directly to characterize the stress generation in a given concrete composition, or as a "facit" to check the

accuracy of calculations of stress development based on the materials properties: heat development, autogenous shrinkage, thermal dilation, E-modulus and creep/relaxation.

A comprehensive test program is underway to determine these properties, and, in particular, to determine the minimum number of tests that are required in order to determine the properties with sufficient accuracy for practical applications. Drying shrinkage is not included in the program so far, hence, the concrete is sealed from moisture exchange in the experiments.

The whole field of stress predictions and crack limitation is quite active presently, particularly in Europe and Japan. A comprehensive view of the field is given in the RILEM symposium proceedings[1)].

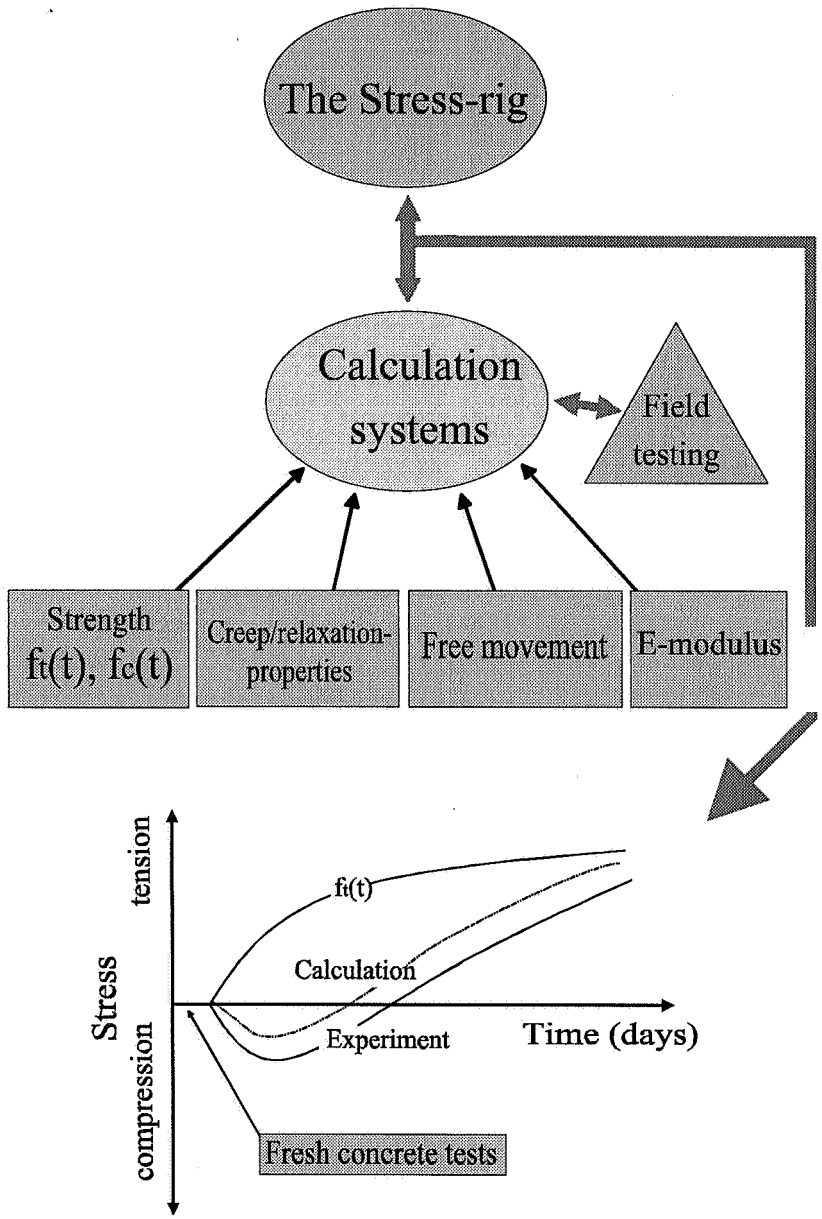

FIG.-1 NOR-IPACS, principle sketch

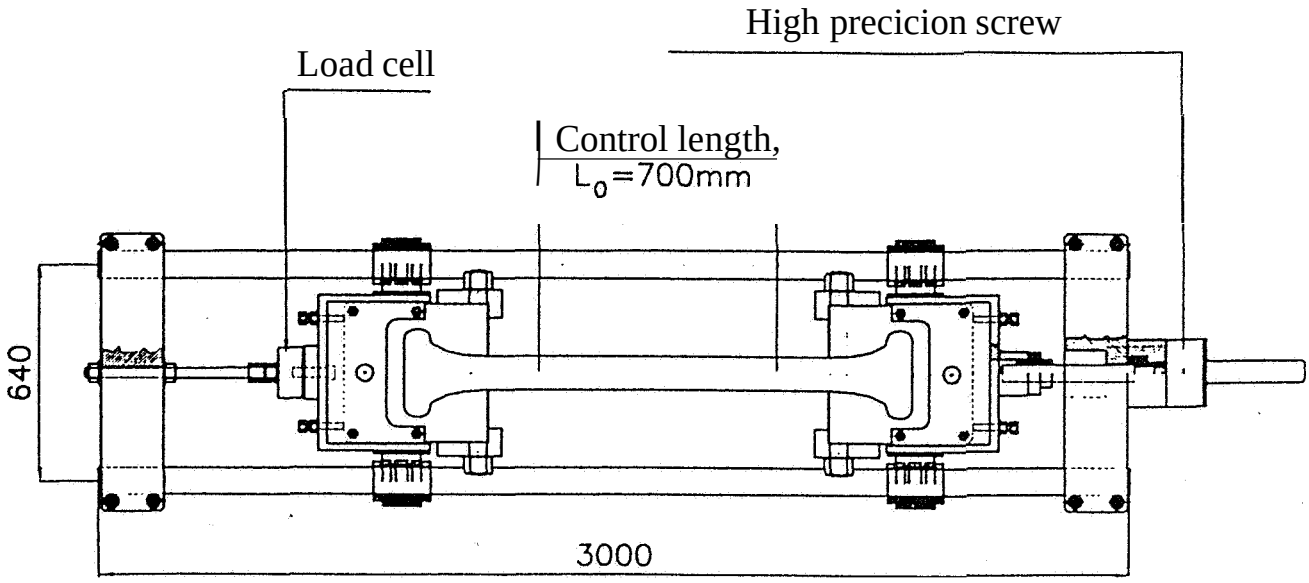

FIG.-2 The Stress-rig

PRELIMINARY RESULTS

Stress development

The fact that autogenous shrinkage may contribute substantially to stress generation in HPC is illustrated in FIGs. 3 and 4. FIG.-3 shows autogenous shrinkage and stress development during a 20°C isothermal test. Stress developes from about 6 hrs. Autogenous shrinkage starts earlier, but is zeroed at the time stress is generated since before this time the E-modulus is too low to produce stresses. Note that the stress increases during the test period (14 days), i.e. the relaxation effect is not sufficient to counteract the autogenous shrinkage contribution during this whole period. FIG.-4 shows restraint stresses at isothermal and two more realistic temperature histories, plotted against maturity (equivalent time at 20°C). The two specimens with realistic temperature histories (maximum temperatures of 42°C and 54°C) failed in tension after 27 and 33 maturity hours, respectively (15 and 13 hrs. real time). Considering the stress values in FIG.-4, it can be seen that the autogenous shrinkage contributes substantially to the stress development, and cannot be ignored in stress calculations. The magnitude of the effect, however, varies greatly as discussed in the following.

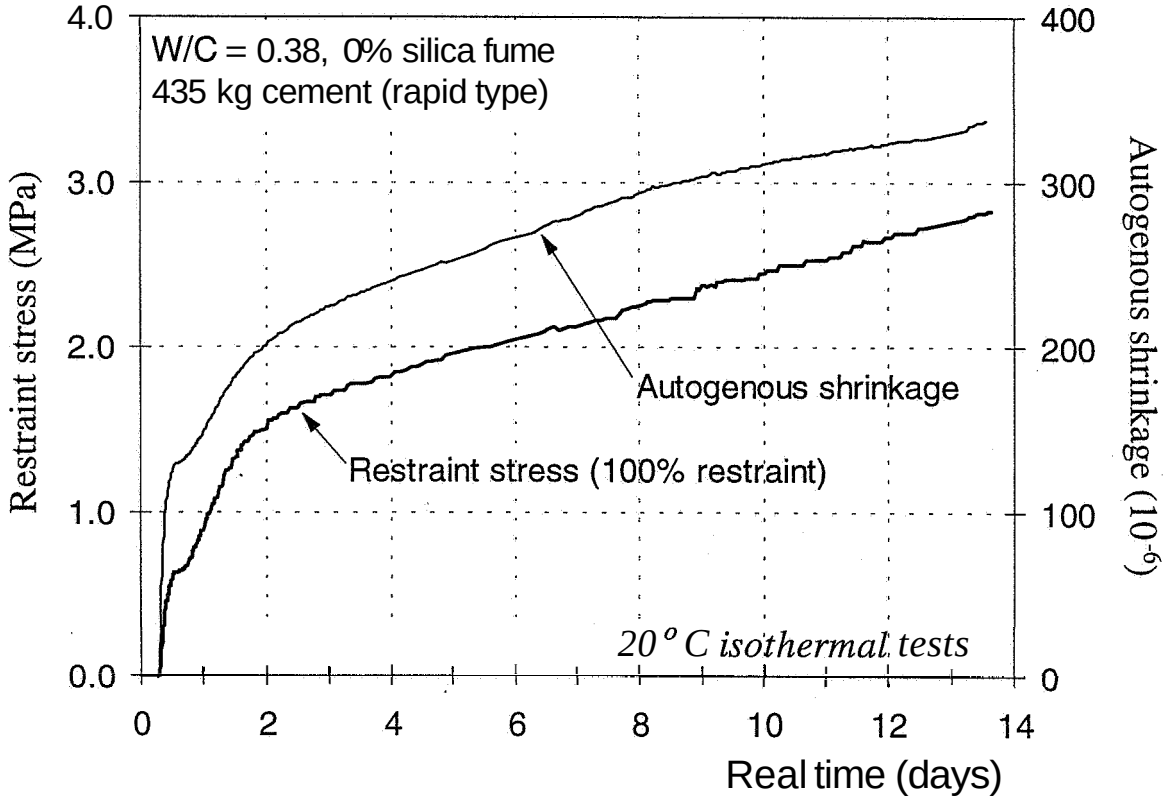

FIG.-3 Autogenous shrinkage and restraint stress in parallell isothermal tests at 20°C

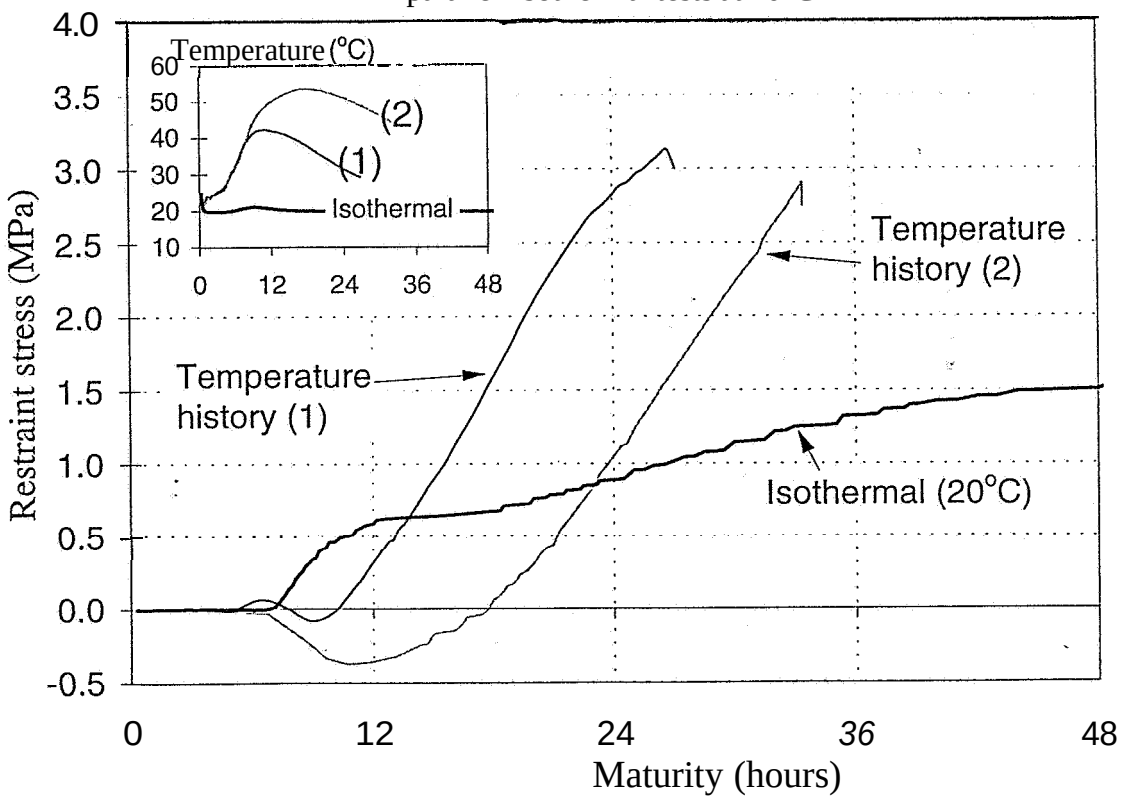

FIG.-4 Effect of temperature history on restraint stress. Same concrete as in FIG.-3

Autogenous shrinkage - water supply

Little systematic data on autogenous shrinkage of concrete is available. Comparison between unpublished results from our and other Scandinavian laboratories indicate large differences and strong dependence on the concrete binder composition. One, possibly very important, factor should be noted: Autogenous shrinkage is a result of the internal chemical shrinkage associated with cement hydration. After a sufficiently rigid skeleton is formed in the binder, this chemical shrinkage results in empty pore space and the development of capillary forces in the pore water, which again produces external volume contraction, i.e. autogenous shrinkage. However, the amount of empty pore space is very small. F.inst. a concrete with 400 kg cement/m^3 will only form 0.012 m^3/m^3 empty pore space at about 50 % degree of hydration. If this amount of water is available in the aggregate, the autogenous shrinkage may be eliminated. Tests at our laboratory have shown that for light weight aggregate HPC there is no autogenous shrinkage, demonstrating that 'the water in the aggregate is available to compensate for the chemical shrinkage. Even normal aggregate contains some water, thus, the variations in autogenous shrinkage are possibly caused by differences in available water in the aggregates as well as differences in binder composition.

Autogenous shrinkage - temperature

The effects of different isothermal temperatures on autogenous shrinkage is an obvious starting point in the task to separate the two effects of thermal dilation and autogenous shrinkage on the total movement. Such experiments were carried out for the "Basic" HPC, i.e. a concrete with water to binder ratio of 0.38 containing 5 % silica fume (a typical Norwegian concrete for bridges). The concretes were mixed as near the intended temperatures as possible using water + cem + aggregate at different temperatures. After placing the concretes in the Shrinkage-Rig, they reached the intended isothermal temperatures within one hour. The results are shown in FIG.-5. The curves are zeroed at the time when stress developed in the parallel Stress-Rig, thus only the "stressgenerating" part of the autogenous shrinkage is plotted for clarity. The results are rather unsystematic, however, duplicate runs were made at 5°C and 20°C demonstrated good reproducibility. Clearly, the temperature variation of the autogenous shrinkage of this Basic concrete cannot be described using the maturity concept. In order to obtain data under more realistic conditions two series of new tests were made with the same concrete: The initial temperature was kept constant at 13°C and 20°C until after setting (about 15 and 8 hours), and then increased in steps during short periods (less than 1 hrs) to reach a new isothermal level. The two series were as follows: 13°C, 13-20°C and 13-20-27-35°C, and 20°C, 20-27°C, 20-27-35°C and 20-27-35-45"C. The latter temperature for each test denotes the final isothermal temperature which was maintained for one week. The results for the two series are shown in FIG.-6. The thermal dilations caused by the temperature steps are eliminated in the curves. The maturity hours are calculated using an activation energy of 91500 J/mole in the Arrhenius equation, in contrast to the "normal" value of 31500 J/mole used to describe heat - and strength development in concrete. This high value means a much greater temperature sensitivity for autogenous shrinkage than for heat and strength. FIG.-6 shows that for a given initial temperature the subsequent autogenous shrinkage development at different temperatures may be described using the maturity concept. However, with different initial temperature levels both the rate and magnitude of the autogenous shrinkage differ. From a practical application point of

view the results in FIG.-6 are useful, but clearly much more work is needed before a more general characterization of the autogenous shrinkage can be formulated.

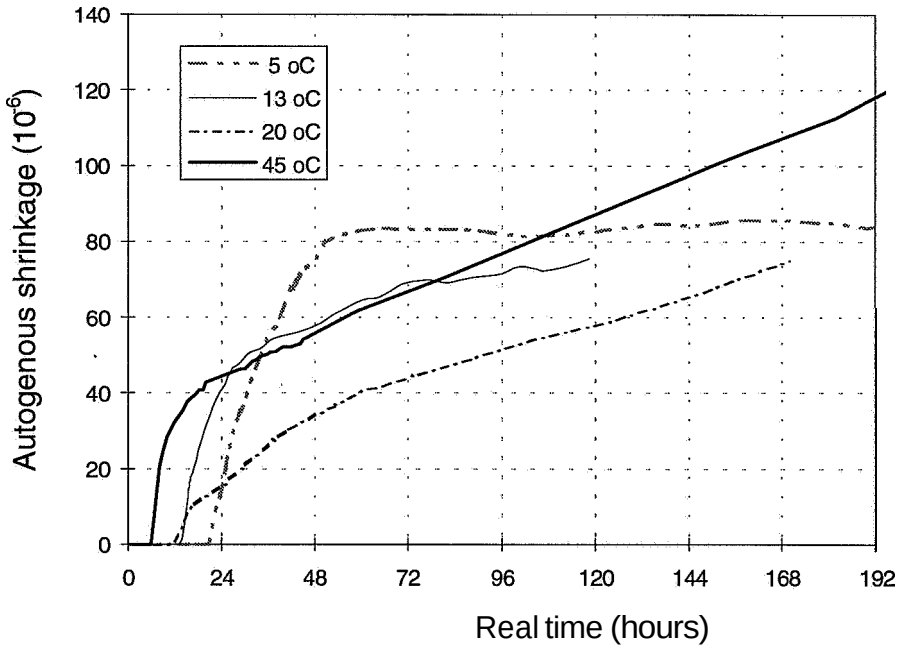

FIG.-5 Autogenous shrinkage at different isothermal temperatures from mixing for the "basic" concrete

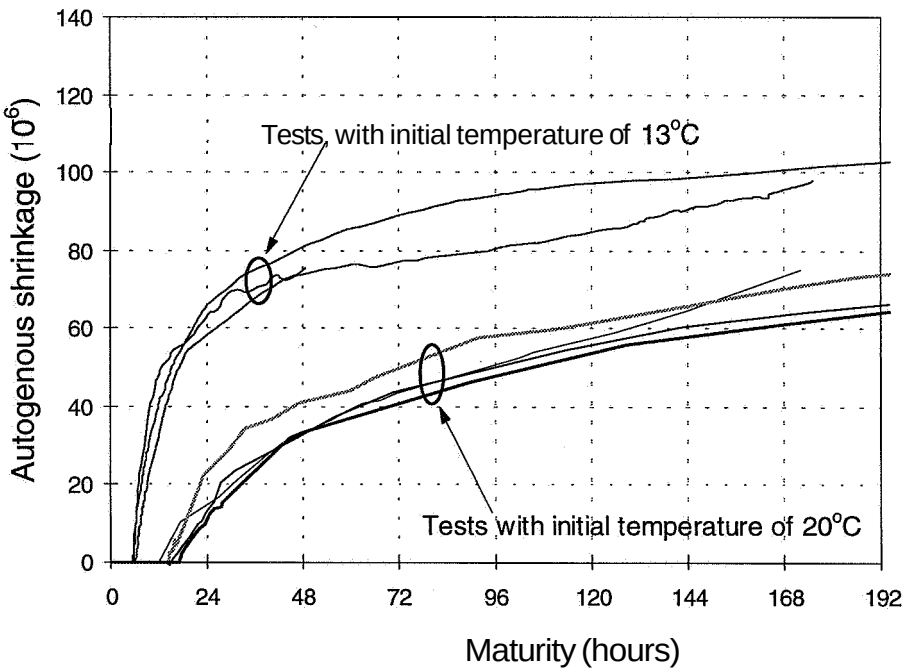

FIG.-6 Autogenous shrinkage for the "basic" concrete with two different initial temperatures until after setting, when the temperature was increased in steps to reach different isothermal levels

CONCLUSIONS

The autogenous shrinkage starts immediately upon mixing of the concrete. In the present paper autogenous shrinkage is defined as "stressgenerating" shrinkage, i.e. only what occurs after stress development is recorded in the Stress-Rig is considered.

Autogenous shrinkage may be a major contributor to stress generation in concrete hardening under full restraint.

The magnitude and rate of development of autogenous shrinkage depend strongly on the concrete binder composition, the entire temperature history of the concrete since mixing and the amount of water available in the aggregates.

For a given initial temperature in the concrete through the setting, the subsequent development of the autogenous shrinkage may be described by the maturity concept, but the activation energy is higher (greater temperature sensitivity) than for compressive strength development.

More research is needed on autogenous shrinkage to increase our understanding of the mechanisms, and in order to develop a model to describe the property in a generalised way.

ACKNOWLEDGEMENT

The present work is part of the Norwegian project NOR-IPACS supported by NFR (Norwegian Research Council) with the following partners: Selmer ASA (project leader), Elkem ASA Materials, Norcem A/S, Fesil ASA, The Directorate of Roads (The Road Laboratory) and NTNU (Norwegian University of Science and Technology). The national project will from mid 1997 be integrated with a new European Brite-Euram project (IPACS) with Sweden (Scancem) as project leader and partners from Norway, Germany, Italy and The Netherlands.

REFERENCES

1) Springenschmied, B. ed. "Thermal Cracking in Concrete at Early Ages", Proceedings of the International RILEM Symposium, Miinchen, oct. 1994. Rilem Proceedings 25, 1995.

This paper will also be presented as a supplementary paper at the "Third CANMET/ACI International Symposium on Advances in Concrete Technology", Auckland, New Zeeland, August 25-27, 1997

EFFECT OF SELF-DESICCATION ON VOLUME CHANGE AND FLEXURAL STRENGTH OF CEMENT PASTE AND MORTAR

EI-ICHI TAZAWA[*1] and SHINGO MIYAZAWA[*2]

*1 Hiroshima University, Department of Civil Engineering
1-4-1, Kagamiyama, Higashi I-Iiroshima, 739 JAPAN

*2 Ashikaga Institute of Technology, Department of Civil Engineering
268-1 Ohmae, Ashikaga, 326 JAPAN

ABSTRACT

Moisture movement due to self-desiccation in cement paste and mortar specimens with low water to cement ratio was experimentally investigated. Volume change and flexural strength of specimens under moist and sealed conditions were also observed, and relationship between self-desiccation and these properties was studied. It is proved that self-desiccation can be observed in the central core of a specimen during water curing and that the moisture distribution has an considerable effect on length change and flexural strength.

INTRODUCTION

Absolute volume of cement plus water decreases as hydration proceeds. This phenomenon has been called as chemical shrinkage. When excessive water is not applied to cement paste, intrinsic voids should be generated by chemical shrinkage after the framework of hydrate is formed by setting. This phenomenon is called self-desiccation[1]). The experiments done by Copeland[2)] shows that the relative humidity in a container holding some pieces of young cement paste decreases with time. Whether self-desiccation occurs uniformly in a cross section of a specimen has not been understood. In this study, moisture distribution in a cross section of sealed cement paste and mortar specimens was measured by oven drying. Volume change and flexural strength of specimens with different water to cement ratio, which had been cured under moist and sealed conditions, were also observed, and influence of self-desiccation on these properties was also discussed.

MOISTURE MOVEMENT DUE TO HYDRATION

In order to study moisture movement in a sealed cement paste specimen, 220×220×30mm specimens were used for measuring distribution of moisture content. Cement paste was placed between two 220×220×10mm polyethylene plates spaced out 30mm apart. Two sides, the

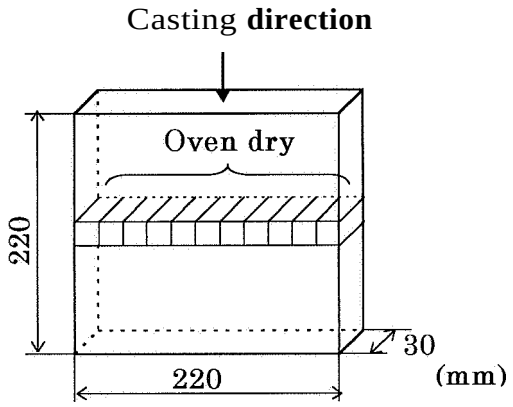

Fig.1 Measrument of moisture content

bottom and the top surface were sealed to prevent evaporation. Samples of 20×20×30mm pieces from different portions of a specimen were used for the measurement of moisture content, as shown in Fig.1. Moisture content was measured from the weight reduction of the samples when they were oven dried (105℃), after specified period of sealed curing, 1, 4, and 7 days. The test results are shown in Fig. 2. For 0.45 w/c cement paste, the moisture content near the surface of a specimen is less than that near the center at the age of 7 days. For 0.30 w/c specimen, the moisture reduction near the surface has already been observed at the age of 1 day.

Fig.3 shows the weight loss of 0.3 w/c cement paste after oven drying during. The test was done at the ages of 0, 4, 10, 24 hours and 2 and **3** days after casting. Cement paste was cast in a ϕ 65×110mm plastic mold and sealed on the top surface. Samples were taken from the portion within 10 mm from the side and the portion of the central 20×20mm section. The data shows that moisture movement inward a specimen begins to occur at about 10 hours after casting.

For cement paste with 0.2 wlc, moister distribution is not be clearly observed, as show in Fig.2. This may be because the cement paste has very little amount of free water in the mixture and because the cement hydrate is so dense that free water can not move inward.

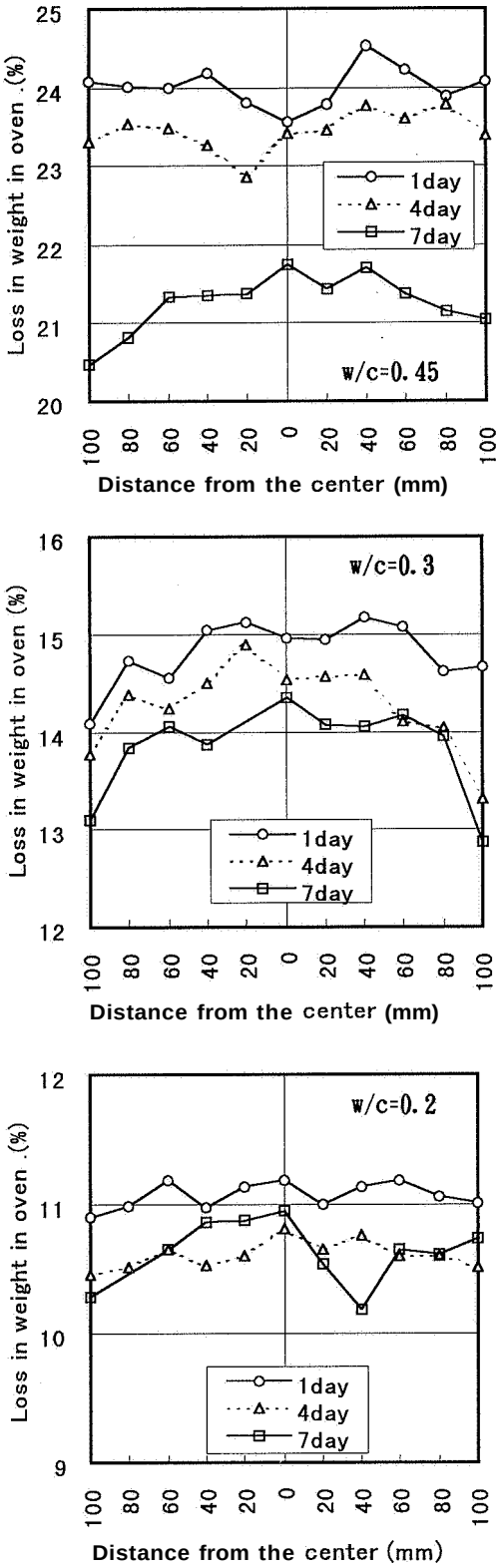

Fig.2 Distribution of moisture content in cement paste

It can be considered, from these experimental results, that degree of self-desiccation should not be uniformly observed in cross section of a cement paste specimen with 0.3 and 0.45 of water to cement ratio. Because the absolute volume of cement plus water decreases with progressive hydration, voids will be formed in the space which has been occupied by cement and water before hydration. Since free water will keep continuity by attracting force between the molecules, water will move into the inner part of the specimen, compensating the absolute volume reduction. ` Driving for of the water movement may be capillary tension and atmospheric pressure[3].

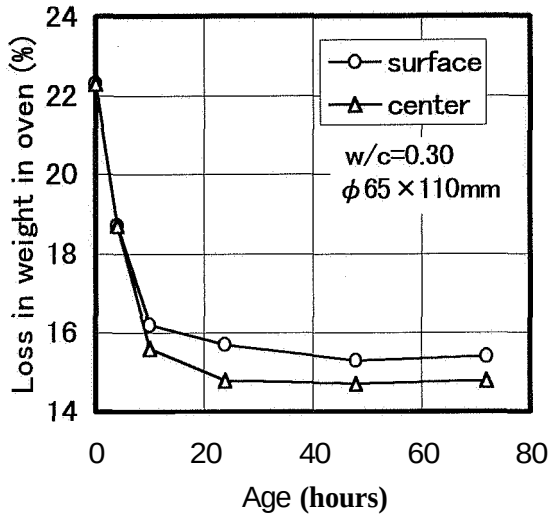

Fig.3 Moisture content of cement paste versus time

VOLUME CHANGE IN MOIST CONDITIONS

In order to study the influence of specimen size on self-desiccation and length change of a moist cured specimen, different sized cement paste specimens, 13x25x279 mm, 25x25x279 mm, 38x38x279 mm, 76x76x279 mm and 102x102x279 mm, were prepared. ASTM type I cement was used and water to cement ratio was 0.3. After demolding at the age of 1 day, the specimens were stored in moist conditions at 20℃(in a fog room) and length and weight changes over time were measured. Details of the experiments are presented in a published paper[4].

The specimens which were smaller than 38x38x279 mm increased in length continuously in moist conditions, while the larger specimens decreased in length during the first two weeks, as shown in Fig. 4. Length of the larger specimens decreased down to 140×10^{-6} as linear strain and thereafter it gradually increased. It was observed that the weight of the specimens continuously increased, as shown in Fig. 4, which shows the gain in mass by the cement paste specimens as a percentage of the original weight. It can be said that the volume of capillary void due to chemical shrinkage was increasing and that physical absorption of water into the capillary void occurred in hydrating cement paste. As expected, the gain decreased with increasing specimen size. The maximum gain in mass curve as a function of time can be theoretically estimated from the chemical equations of cement hydration described in the following equations(eq. 1 ～ eq. 8). The rate of hydration of each mineral compound, which was given by Copeland[5] was used in the calculations.

$$2C_3S+6H_2O \rightarrow C_3S_2H_3+3Ca(OH)_2 \quad \cdots\cdots (1)$$

$$2C_2S+4H_2O \rightarrow C_3S_2H_3+Ca(OH)_2 \quad \cdots\cdots (2)$$

$$C_3A+3(CaSO_42H_2O)+26H_2O \rightarrow C_3A3CaSO_432H_2O \quad \cdots\cdots (3)$$

$$2C_3A+C_3A3CaSO_432H_2O+4H_2O \rightarrow 3[C_3ACaSO_412H_2O] \quad \cdots\cdots (4)$$

$$C_3A+Ca(OH)_2+12H_2O \rightarrow C_3ACa(OH)_212H_2O \quad \cdots\cdots (5)$$

$$C_4AF+3(CaSO_4 2H_2O)+27H_2O \rightarrow C_3(A\cdot F)3CaSO_4 32H_2O+Ca(OH)_2 \quad (6)$$

$$2C_4AF+C_3(A\cdot F)3CaSO_4 32H_2O+6H_2O \rightarrow 3[C_3(A\cdot F)CaSO_4 12H_2O]+2Ca(OH)_2 \quad (7)$$

$$C_4AF+10H_2O+2Ca(OH)_2 \rightarrow C_3AH_6\text{-}C_3FH_6(\text{solid solution}) \quad (8)$$

where, C=CaO, S=SiO_2, A=Al_2O_3, F=Fe_2O_3, H=H_2O.

Observed gain in mass is less than the theoretical values which is presented as a dotted line in Fig.4. Assuming that curing water permeates into a specimen uniformly from the surfaces, the average thickness of saturated portion can be calculated from both observed and theoretical gain in mass. The calculated thickness of saturated portion is shown in Fig.5. The thickness increases with specimen size for the smaller specimens, but it does not increase significantly for the larger specimens. It can be seen that the curing water only permeates the surface layer of the specimens due to the low permeability of the specimen(w/c=0.3), while the inside of the specimen may be subjected to self-desiccation. The ratio of observed gain in mass to the theoretical one, which is also shown in Fig.5, decreases with the specimen size. This suggests that degree of self-desiccation increases with increase in specimen size. It can be seen that length change in moist conditions is influenced by autogenous shrinkage of the inner portion and swelling of the portion

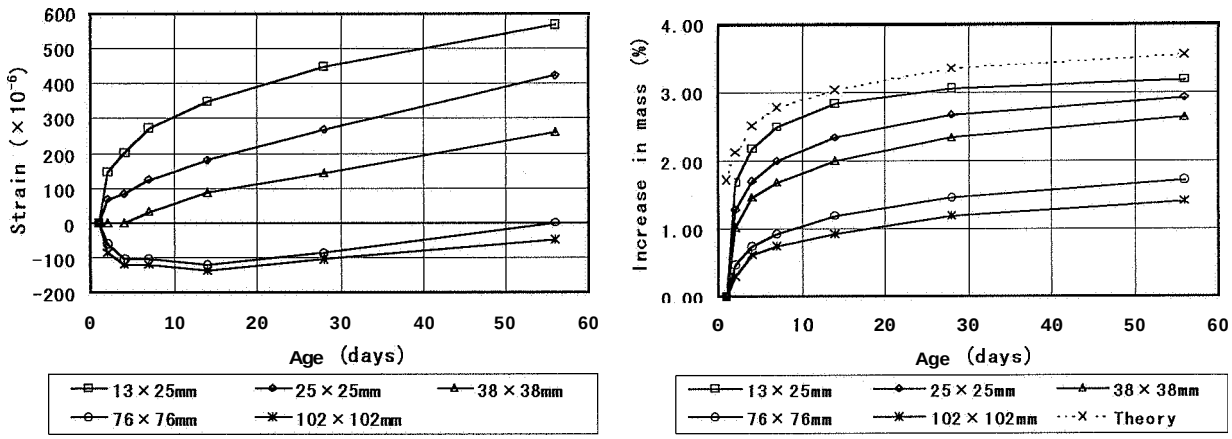

Fig.4 Length change and gain in mass of cement paste specimens (w/c=0.30)

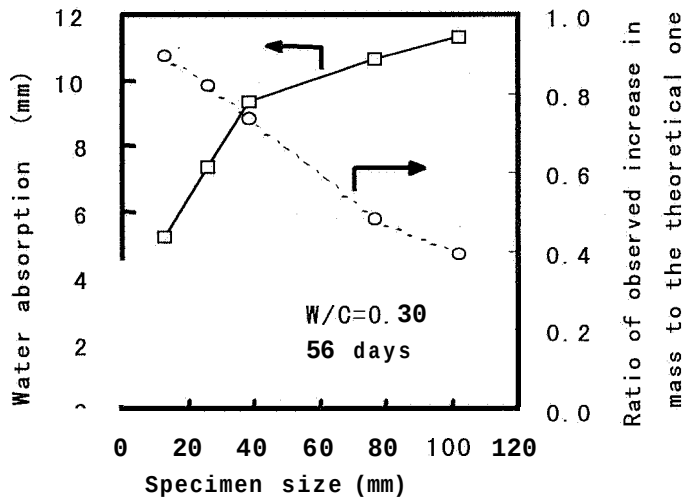

Fig.5 Water absorption in cement paste(w/c=0.30)

near the surface. The moisture distribution may also cause internal stress, which is described in the next chapter.

EFFECT OF SELF-DESICCATION ON FLEXURAL STRENGTH

It has been said self-desiccation has an influence of compressive strength of concrete. In order to study the effect of self-desiccation on compressive and flexural strength, two kind of cement paste specimens (40×40×160mm), one had been cured under water and the other had been sealed before the tests[3]. After the specified period of curing, flexural strength was tested and compressive strength was tested with pieces of the specimens which had been used for flexural strength tests. Compressive strength observed is almost the same for the both type of the specimens, as shown in Fig.6. Flexural strength of the sealed specimens, however, is much lower than that of those cured under water, when water to binder ratio is less than 0.40, as shown in

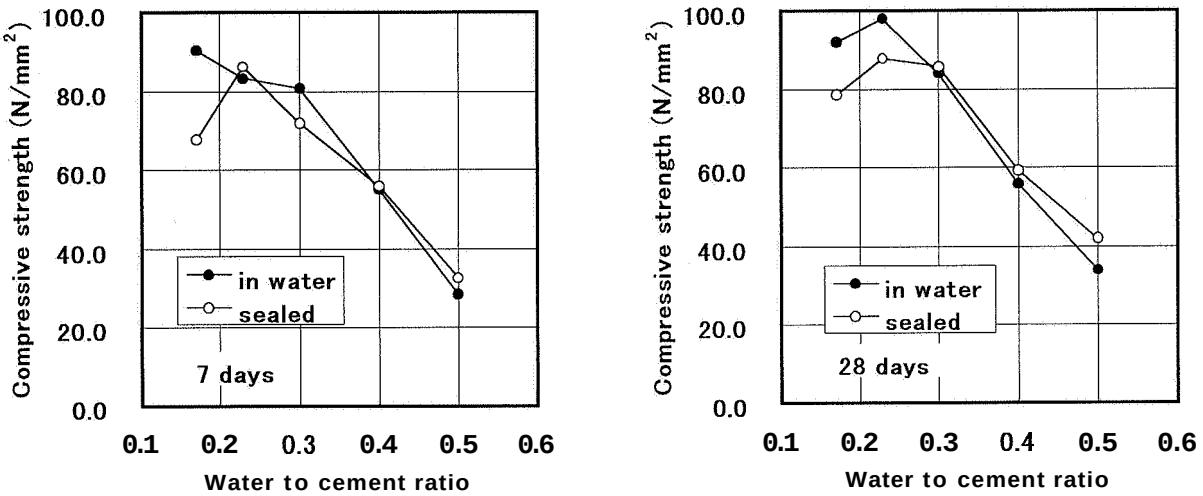

Fig.6 Compressive strength of cement paste specimen (For specimens with 0.17 and 0.23 w/c, ten percent of cement was replaced by silica fume)

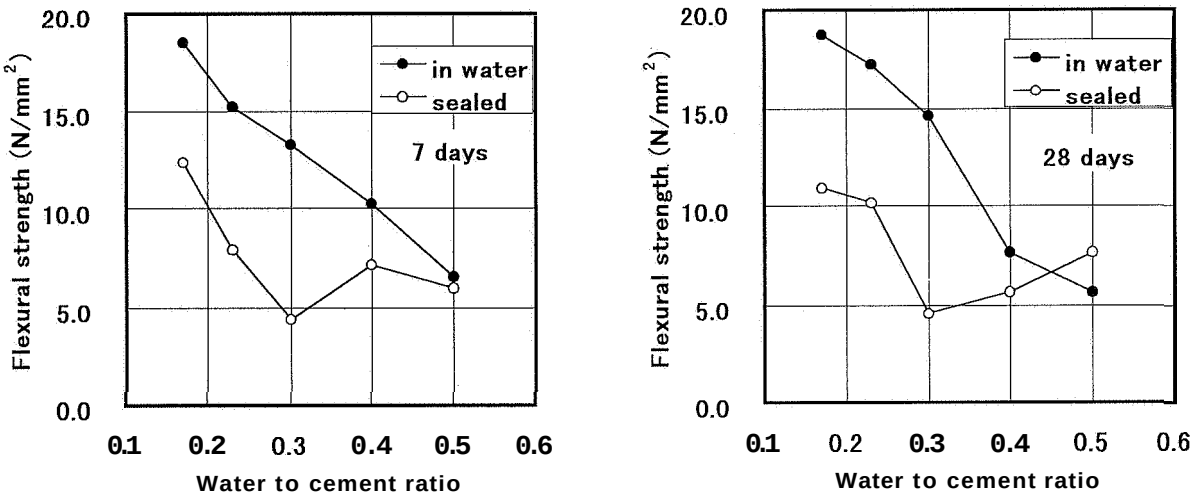

Fig.7 Flexural strength of cement paste specimen (For specimens with 0.17 and 0.23 w/c, ten percent of cement was replaced by silica fume)

Fig.7. This phenomenon may be explained by moisture distribution in a cross section of the specimens. Self-desiccation in periphery portion of the sealed specimens, which has been previously mentioned, may be generated tensile self stress near the surface. On the other hand, compressive self stress may be generated due to swelling near the surface of the water cured specimens.

Another experiments were conducted in order to study the influence of moisture movement in a specimen after water curing. High-early strength Portland cement was used and 100 × 100 × 400 mm mortar specimens with different water to cement ratio were prepared. The specimens were cured under water for the first 7 days, and then they were sealed to prevent evaporation. Flexural strength was measured after specified period of sealed curing, 0, 3, 7, 14, 28 and 84 days. Details of the experiments are presented in a published paper[6]. As shown in Fig.8, flexural strength of 0.5 w/c and 0.7 w/c mortars did not change or slightly increased with time elapsed, while flexural strength of 0.30 w/c mortar decreased without evaporation approximately by 40% and then gradually increased. This phenomenon for high-strength mortar may be explained as follows. During the period of water curing, free swelling near the surface may have been internally restrained due to the moisture difference in a cross section and compressive self stress generated near the surface. Therefore, the apparently higher flexural strength was recorded at the end of the water curing. After the specimen was sealed, compressive self stress decreased as moisture moved into the inner part of the specimen. It may also have been relaxed by creep of mortar. Furthermore, tensile self stress may have been generated when flexural strength of 0.3 w/c specimen decreased to the level of 0.50 w/c specimen. Recovery of flexural strength at later ages can be explained by decreasing tensile self stress caused by moisture movement and creep. It has been reported that tensile strength of mortar decreased with increasing moisture content under equilibrium conditions[7]), but the experimental results previously mentioned suggests that the effect of self stress has the greater influence on flexural strength of mortar under moisture gradient.

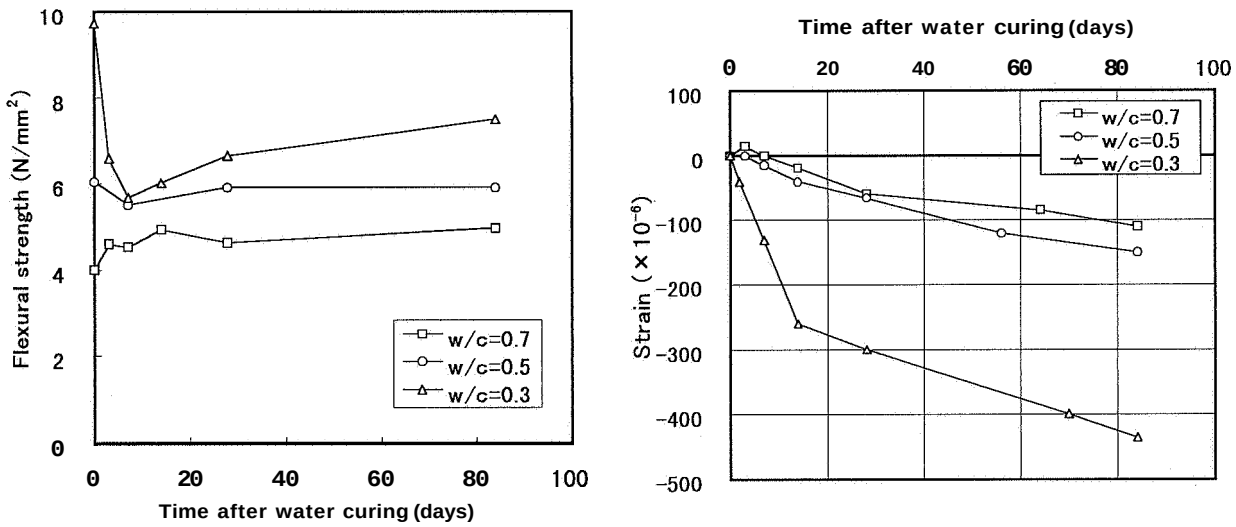

Fig.8 Flexural strength and length change of mortar specimens
(water curing for 7 days thereafter sealed curing, high-early strength Portland cement, 100 × 100 × 400mm mortar specimens)

Length change of the sealed specimens after water curing is also shown in Fig.8. Large shrinkage was observed for 0.3 w/c specimen. This suggests that self-desiccation of the inner part of a specimen has great influence on volume change.

CONCLUSIONS

In this study, moisture distribution in a cross section of a specimen and flexural strength were measured with cement paste and mortar with different water to cement ratio. Weight and length change of different sized cement paste specimens under water were also observed. It is proved that differential moisture content is generated in a cross section of a specimen under water curing and sealed condition. The moisture distribution has an considerable effect on length change and flexural strength of mortar with low water to cement ratio.

REFERENCES

1) Powers T.C. and Brownyard T.L., Study of the physical properties of hardened portland cement paste, Part 9, Bulletin No.22, PCA, 1948
2) Copeland L.E. and Bragg R.H., Self-desiccation in Portland-cement paste, Bulletin of PCA, No.52, 1955, pp.1-11
3) Tazawa E. and Miyazawa S., Autogenous shrinkage of cement paste with condensed silica fume, Proceedings of the 4th CANMET/ACI International Conference on Fly Ash, Silica Fume, Slag and Natural Pozzolans in Concrete, ACI, 1992, pp.875-894
4) Miyazawa S. and Monteiro P.J.M., Volume change of high-strength concrete in moist conditions, Cement and Concrete Research, Vol.26, No.4, 1996, pp.567-572
5) Copeland L. E. and Kantro D. L., Kinetics of the Hydration of Portland Cement, Proceedings of the 4th International Symposium on the Chemistry of Cement, 1960, pp.443-453
6) Tazawa E. and Miyazawa S., Tensile and flexural strength of cement mortar subjected to non-uniform self stress, Magazine of Concrete Research, Vol.44, No.161, 1992, pp.241-248
7) Pihlajavaara S.E., A review of some of the main results of a research on the ageing phenomena of concrete: Effect of moisture conditions on strength, shrinkage and creep of mature concrete, Cement and Concrete Research, Vol.4, No.5, 1974, pp.761-771

EFFECT OF SELF STRESS ON FLEXURAL STRENGTH OF GYPSUM POLYMER COMPOSITE

EI-ICHI TAZAWA
Hiroshima University, Department of Civil Engineering
4-1, kagamiyama 1 chome, Higashi Hiroshima,
739 Japan

ABSTRACT

Self stress generated in polymer impregnated gypsum (referred as GPC) when it is composed, is estimated and its influence cn flexural strength is discussed. The estimation of the self stress is based on measured values of shrinkage caused by polymerization of impregnated monomer and elastic moduli of dried gypsum base just before impregnation. Effect of this self stress on flexural strength of GPC is investigated. It was found that the equation - (1) is valid to predict flexural strength of polymer impregnated gypsum (6b) in terms of the self stress as a variable.

$$\sigma_b = \sigma_{gb} + V_p \ (\sigma_p - \sigma_{sp}) \quad \text{.....} \quad (1)$$

where σ_{gb} : flexural strength of gypsum base
V_p : specific volume of polymer
σ_p : tensile strength of polymer
σ_{sp} : self stress generated in polymer phase

If extremely low water gypsum ratio is adopted to prepare gypsum base, cracking is observed just after polymerization preceding any flexural loading. For somewhat higher water gypsum ratio, specimens are not cracked, but their flexural strength is decreased after polymer impregnation. The self stress corresponding to this case turns out to be higher than the tensile strength of polymethyl methacryrate (PMMA) used for the impregnation. Since prediction of σ_{sp} in the equation (1) is based on tri-axial compressive strain of gypsum base that is within its elastic region, σ_{sp} in polymer phase should positively exist. Even for this condition the validity of the equation (1) seems to be maintained although the value in the parenthesis of the equation (1) becomes minus. Based on this fact an unstable physical state where one phase of a composite material is stressed beyond its macroscopic strength as an individual material owing to the crack arresting effect of the other phase (gypsum in this case) has been postulated. This state is designated as "superstressed" state taking its resemblance with supercooling or supersaturation into consideration.

INTRODUCTION

Polymer impregnated gypsum (GPC) is manufactured by impregnating gypsum base with monomer and polymerizing it in situ by thermal-catalytic reaction, where drying of base material, evacuation of impregnation vessel and impregnation of monomer, are required prior to polymerization. A new type of material that exhibits high strength and high impermeability can be produced.

In order to reduce the total cost of the product, optimization of base material with reference to facility of processing, polymer content and performance of the product is required.

For these purposes, optimization of porosity of gypsum base is experimentally conducted. Through this investigation, a seemingly contradicting fact that flexural strength is decreased after impregnation of polymer for positive polymer loading, is found.

An analysis of this phenomenon is presented in this paper together with a proposal of a crack propagation model and a composite law based on this model.

PREPARATION OF SAMPLE

Four gypsum bases having different porosity are prepared using three types of gypsum α and β as shown in TABLE-1. These bases are dried in a draft type of oven at 48℃ for 5 days for gypsum A, B and D, and for 3 days for gypsum C. These bases are placed in a container evacuated down to 6~7mmHg for *30* min. Then, methyl methacrylate (MMA) monomer mixed with *0.5%* of azobisisobutyronitrile is introduced to the container for impregnation. After 1 hour of impregnation, impregnated polymer is polymerized for 20 hours at 60℃ in a heat medium that could minimize monomer loss from the bases.

TABLE-1
Properties of Gypsum

Name	A	B	C	D
Type of Gypsum	α	α	β	α
Row Material	Synthesized	Natural	Natural	Synthesized
Mixed Water (%)	30	39	60	20
Specific Gravity at demolding	1.95	1.86	1.64	mixed with hot water 70℃
Specific Gravity after drying	1.769	1.583	1.207	
Initial Set (min)	6	30	15	
Final Set (min)	35	39	43	
Expansion (after 1 hr.) (%)	0.236	0.016	0.126	
Final Expansion (%)	0.328	0.016	0.126	
PH of Gypsum Paste	7–8	11–11.5	5–6	
V_a	0.246	0.319	0.478	0.174
V_g	0.754	0.681	0.522	0.826
V_p	0.180	0.242	0.363	0.123

V : Specific Volume of Void V_g : Specific Volume of Gypsum

MEASUREMENT METHODS

Flexural strength and compressive strength are measured by a method prescribed as JIS R5201 for beam specimen having dimension 4×4×16cm. Modulus of elasticity and Poisson's ratio are measured by a method prescribed in ASTM C469 for 5 Φ×10cm cylindrical specimen attached with electric strain gauge 20mm in length. These tests are performed after three days after polymerization.

Shrinkage due to polymerization, is measured by a method prescribed as ASTM C490-65 T for beam specimen having dimension 2.5×2.5×28cm. In this test measurement of the original length is taken just before impregnation and the shrinkage is determined for the length just after impregnation when the specimen is cooled down to 20°C.

RESULTS OF MEASUREMENTS

In TABLE-2, the theoretical monomer loading is compared to the observed monomer loading. Theoretical porosity in this Table is calculated from specific gravity of dried gypsum (apparent) and that of dehydrate (assumed as 2.32). In order to get the theoretical polymer loading, all voids are assumed to be filled with monomer of specific gravity 0.959. It is understood that the measured polymer loading is very close to the theoretical one.

TABLE-2
Comparison of Polymer Loading

Type of Gypsum Base	Specify Gravity of Gypsum (dry)	Theoretical Porosity	Theoretical Monomer Loading	Measured Monomer Loading
		(%)	(%)	(%)
A	1.750	24.57	13.46	13.57
B	1.582	31.81	19.28	19.50
C	1.202	48.19	38.44	38.87

TABLE-3
Strength of Dried Gypsum

Type of Gypsum Base	σgb (Mpa) Flexural Strength	σgc (Mpa) Compressive Strength	
A	15.9	43.4	52.3
	16.9	53.9	44.0
	13.6	47.6	49.9
	14.7	63.8	62.1
average	15.8	52.3	
B	8.57	18.7	28.5
	9.08	28.0	24.0
	7.65	26.2	28.2
	8.16	24.4	35.1
average	8.37	26.6	
C	5.31	17.2	16.6
	5.00	20.5	16.1
	5.00	19.4	18.7
	7.04	17.2	19.2
average	5.59	18.2	

TABLE-4
Elastic Moduli of Dried Gypsum

Type of Gypsum Base	$E \times 10^4$ Modulus of Elasticity (Mpa)	μ Poisson's Ratio
A	2.09	0.256
	1.97	0.250
	1.89	0.215
average	1.98	0.240
B	1.31	0.238
	1.36	0.228
	1.10	0.244
average	1.26	0.237
C	0.82	0.222
	0.87	0.228
	0.77	0.215
average	0.82	0.222

Strength and elastic moduli of dried gypsum are shown in TABLE-3 and 4.

Strength of GPC is shown in TABLE-5 and shrinkage of gypsum base due to polymerization of impregnated monomer in TABLE-6.

TABLE-5
Strength of GPC

Type of Gypsum Base	σ_{gb} (Mpa) Flexural Strength	σ_{gc} (Mpa) Compressive Strength	
A	10.6	126.3	-
	10.4	123.1	116.1
	13.1	118.0	120.5
	10.9	111.6	107.8
average	11.3	117.7	
B	13.9	119.0	112.6
	14.7	114.8	96.0
	12.3	116.1	105.2
	14.1	116.1	116.4
average	13.8	111.9	
C	15.4	81.0	86.1
	11.7	91.0	91.6
	14.7	87.0	80.7
	15.4	81.0	84.2
average	14.3	84.7	

From these figures it can be pointed out that flexural strength of gypsum A is decreased after impregnation, although compressive strength is significantly increased for every types of gypsum base after impregnation.

In order to seek for a composite low existing in between these measurements, estimation of self stress is attempted.

TABLE-6
Shrinkage due to Polymerization

Type of Gypsum Base	Sp Shrinkage due to Polymerization (%)		
A	0.092 0.091 0.096	0.095 0.089 0.088	0.091 0.088
average	0.0912		
B	0.083 0.086 0.090	0.088 0.082 0.087	0.090 0.088 0.093
average	0.0874		
C	0.180 0.195 0.187	0.197 0.164 0.204	0.179 0.199 -
average	0.188		

ESTIMATION OF SELF STRESS

Shrinkage due to polymerization (Sp) is considered to be tri-axial in nature, and gypsum base is presumed to be compressed tri-axially up to this strain. So, self stress working in gypsum phase can be calculated from this strain and moduli of elasticity of gypsum base.

Using bulk modulus of elasticity (K) and volumetric strain (ε_v), the macroscopic self stress ($б_{sg}$) is written as,

$$б_{sg} = K\,\varepsilon_v \quad \cdots\cdots (1)$$

while, let modulus of elasticity and Poisson's ratio of gypsum base E and p respectively,

$$K = \frac{E}{3(1-2\mu)}, \quad \varepsilon_v = 3Sp \quad \cdots\cdots (2)$$

Substituting (2) to (1),

$$б_{sg} = E \cdot Sp / (1-2\mu) \quad \cdots\cdots (3)$$

This compressive self stress should be balanced with tensile self stress ($б_{sp}$) working in polymer phase that has cross section Vp in a unit area of gypsum base. Then,

$$б_{sg} + Vp\ б_{sp} = 0 \quad \cdots\cdots (4)$$

Since the strength measurement is performed about three days after the time of shrinkage measurement, effect of relaxation corresponding to this time difference should be taken into account.

Let η the relaxation coefficient, η should be multiplied by the self stress to get true self

stress working at the time of testing. Relaxation ratio for gypsum base for 0.8 of stress ratio is found to be 8% and relaxation ratio of polymer phase is assumed to be 40% from literature. Then the total effect can be estimated as 0.92×0.60, that is, 0.55. While, $(1 - 2p)$ calculated from TABLE-3 is 0.53 in average for three types of gypsum base. Then $\eta/(1 - 2\mu)$ is assumed to be unity in the following analysis for all cases. Spring back due to this relaxation might probably explain negative creep of PIC, a strange phenomenon that has been reported by Steinberg et al. [4),5)]

Therefore,

$$\sigma_{sg} = E \cdot Sp \quad \cdots\cdots (5)$$

$$\sigma_{sp} = -E \cdot Sp / Vp \quad \cdots\cdots (6)$$

Using these equations, self stresses are estimated as in TABLE-7. Tensile self stress working in polymer phase of GPC for A type of gypsum base, is calculated as higher than the tensile strength of PMMA (68.4 Mpa). In this case compressive strain of gypsum A 912×10^{-6} is far below its uni-axial elastic limit $2{,}500 \times 10^{-6}$. So, the tensile stress should exist, if equation (4) do hold.

TABLE-7
Self Stress in Gypsum (σ_{sg}) and polymer phase (σ_{sp})

Type of Gypsum Base	A	B	C
Sp	−0.000912	−0.000874	−0.001880
E(Mpa) $\times 10^4$	1.98	1.26	0.82
Vp	0.180	0.242	0.363
σ_{sg}	−18.05	−10.97	−15.35
σ_{sp} (Mpa)	100.3	45.33	42.28

ESTIMATION OF FLEXURAL STRENGTH OF GPC AS A FUNCTION OF SELF STRESS

Since polymer is formed as continuous phase in a part of void that is originally created in gypsum base and microscopically incorporated with gypsum, series model shown in FIG.-1 could be applied for flexural strength where failure is initiated locally at the outmost skin of specimen.

FIG.-1
Series Model

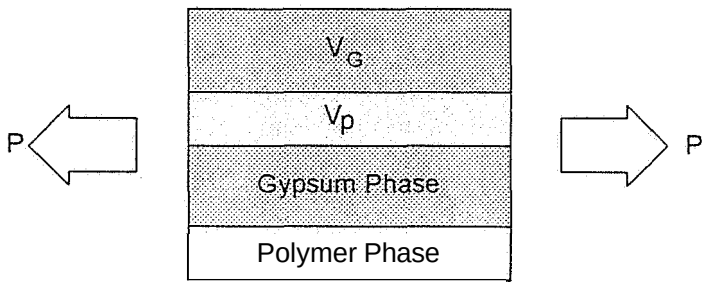

As the first approximation, flexural strength of polymer impregnated gypsum is obtained by

adding the contribution of polymer strength to the flexural strength of gypsum base.

$$\sigma_b = \sigma_{gb} + Vp\ \sigma_p \quad \cdots\cdots (7)$$

An equation as this, however, could not be applied for a two phase composite material where rupture in either phase leads to failure of the total system. (c.f. Tensile strain capacity of polymer is, 10 times or more, greater than that of gypsum.)

But in general, force is transmitted from one phase to another due to bond, friction or mechanical intertwining etc. On this behalf, local rupture of one phase dose not necessarily lead to final failure of a composite material. In case that propagation path of catastrophic crack rarely coincides with cracks pre-existing in one phase, the equation (7) might hold in Griffith's sense of theory even if strain capacity of two phases differs greatly each other, and the difference is compensated with microcracks which should be developed locally before final rupture.

Since experimental data have not proved the equation (7), effect of self stress is introduced as,

$$\sigma_b = \sigma_{gb} - \sigma_{sg} + Vp\,(\sigma_p - \sigma_{sp}) \quad \cdots\cdots (8)$$

But self stresses in this equation cancel each other and the equation (S) reduces to the equation (7). Then, a new model for crack propagation is conceived as shown in FIG.-2, where influence of microcracks that should develop in gypsum phase before rupture of polymer phase is taken into account. Accordingly, the self stress should be locally released on initial microcracking at the cracked ends of gypsum phase and the stress variation due to the subsequent elastic spring back is gradually restrained by bond or friction acting between two phases to give a stress distribution shown in FIG.-2, and self stress in polymer phase is also changed corresponding to this situation.

FIG.-2
Transition of Self Stress and
Propagation Path of Catastrophic Crack

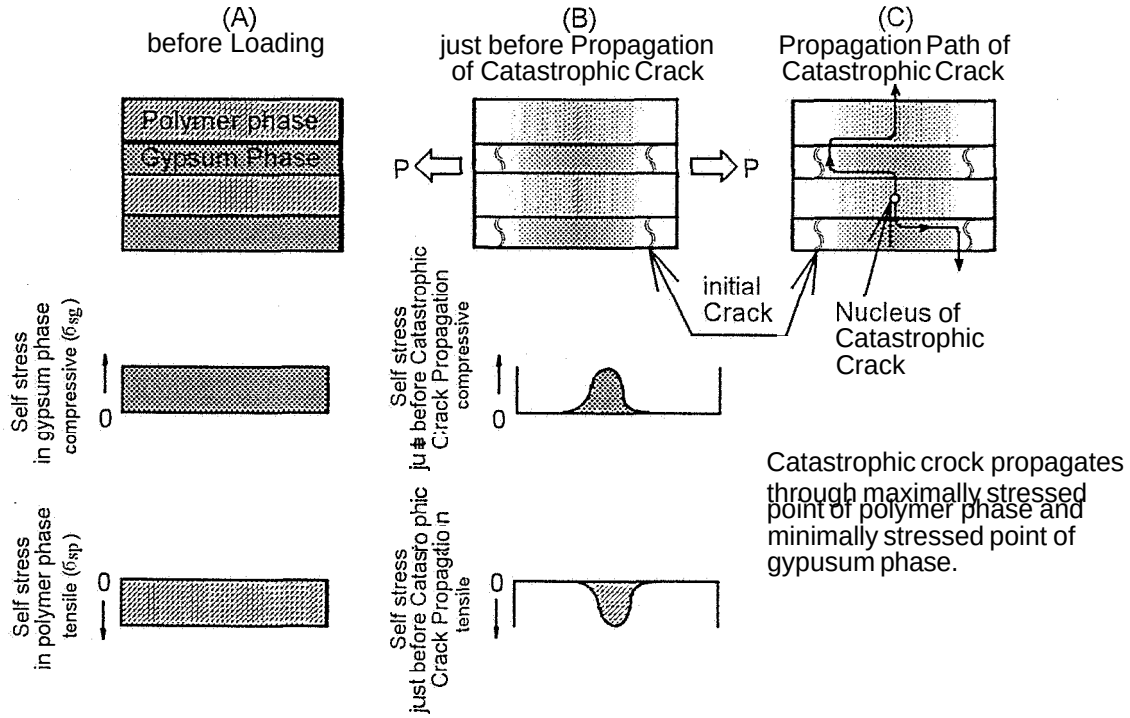

Needless to refer to the principle that the catastrophic crack should propagate through a path so that the minimum energy barrier is required, the catastrophic crack should be initiated in the maximum self stress region of polymer phase and should propagate through the minimum self stress region of the gypsum phase. In an extreme case, the catastrophic crack might selectively propagate along pre-cracked points of gypsum phase. Distribution of the initial microcracks in gypsum phase and their relative size and location in comparison with the nucleus of the catastrophic crack might probably determine which is really the case. Here, it should be kept in mind that location of the maximum self stress region of polymer phase is furthest from location of initial microcracks.

If the former is the case,

$$\sigma_b = \sigma_{gb} + Vp\,(\sigma_p - \sigma_{sp}) \quad \cdots\cdots (9)$$

or substituting equation (6) to (9)

$$\sigma_b = \sigma_{gb} + Vp\,\sigma_p - ES_p \quad \cdots\cdots (10)$$

could be applied.

For an extreme case such as the latter one,

$$\sigma_b = Vp\,(\sigma_p - \sigma_{sp}) \quad \cdots\cdots (11)$$

might be supported.

Using these equations, estimation of flexural strength of GPC is performed as in TABLE-8.

TABLE-8
Theoretical Prediction of Flexural Strength of GPC

Items	Type of Gypsum Base			Unit	Remarks
	A	B	C		
σ_{gb}	15.8	8.37	5.59	Mpa	
Vp	0.180	0.242	0.363	–	
$\sigma_p - \sigma_{sp}$	–31.9	23.0	26.1	Mpa	
$Vp\,(\sigma_p - \sigma_{sp})$	–5.74	5.57	9.47	Mpa	eq.(11)
$\sigma_{gb} + Vp(\sigma_p - \sigma_{sp})$	10.06	13.94	14.97	Mpa	eq.(9)
Observed σ_b	11.3	13.8	14.3	Mpa	

INVESTIGATION INTO FLEXURAL STRENGTH

Observed values of flexural strength of polymer impregnated gypsum are compared to the values estimated by equation (9) and (11) in FIG.-3. It is clearly seen that the equation (9) provides pretty good prediction.

Experimental data are explained by the equation (9) rather than the equation (11). This fact strongly suggests that the initial microcracks that should be developed in gypsum phase are three dimensionally distributed in a quite discontinuous manner and are rarely hit upon with the

catastrophic crack.

FIG.-3
Flexural Strength and Specific Volume of Polymer

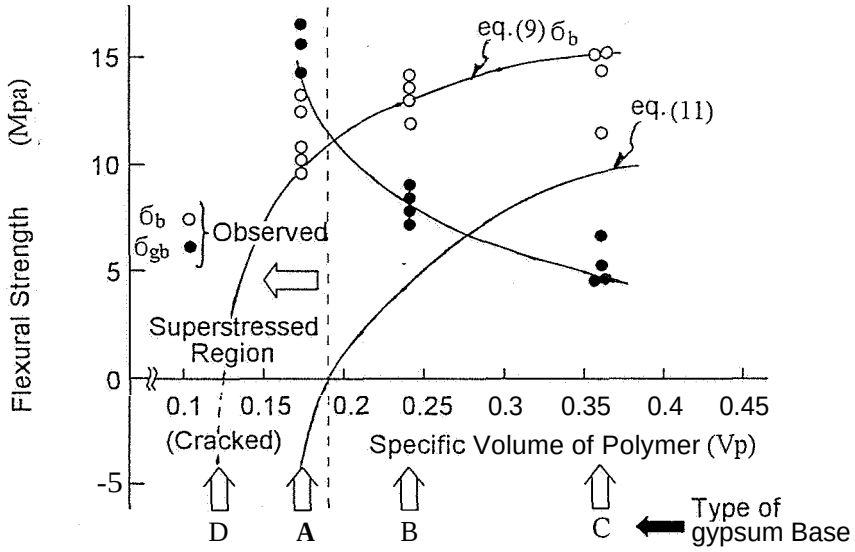

On the basis of the model shown in FIG.-2 and Griffith's theory, it is natural that gypsum phase which is fragmentarily sustained in continuous polymer phase is as resistant as the original gypsum base against propagation of the catastrophic crack, if pre-described situation is really the case.

The term $\sigma_{gb} - \sigma_{sg}$ in the equation (8) could be regarded as flexural strength of gypsum that is prestressed by the shrinkage of polymer. The observed flexural strength of polymer impregnated gypsum is much smaller than this value. The main reason could be understood by the fracture model shown in FIG.-2. It should be noted that self stress that is generated microscopically in a composite material is fundamentally different from prestress that is macroscopically introduced in a material.

SUPERSTRESSED STATE

Flexural strength of polymer impregnated gypsum is decreased after impregnation for type A gypsum. This is quite strange, because original void space that has no contribution to strength is filled with polymer that has tensile strength much higher than that of gypsum.

As shown in TABLE-3, self stress in polymer phase is higher than the tensile strength of polymer for this gypsum, and the term ($\sigma_p - \sigma_{sp}$) in the equation (9) is calculated as minus. By assuming apparent contribution of polymer strength to be minus, the amount of strength decrease is also predicted for this case by the equation (9) as shown in TABLE-8 and FIG.3. Self stress in gypsum phase σ_{sg} corresponding to this σ_{sp} is within elastic limit and is positively working. Therefore, this self stress in polymer phase should also exist. Thus, an unstable physical state where one phase of a composite material is stressed beyond its macroscopic strength owing to the crack arresting effect of the other phase is postulated. This state is termed as superstressed state.

EFFECT OF SELF STRESS ON COMPRESSIVE STRENGTH OF GPC

As described before, dried gypsum base is tri-axially compressed by the shrinkage of the impregnated polymer. Generally it is well known that uni-axial compressive strength (6_1) of a material is increased by lateral pressure ($б_2 = б_3$). In the uni-axial compression loading of GPC, self stress generated in gypsum phase $б_{sg}$ must exhibit the same function as lateral pressure in tri-axial compression test. So, apparent compressive strength of GPC is increased by the self stress regardless of any contribution of polymer phase.

Therefore, compressive strength of polymer impregnated gypsum (6_c) that is strikingly improved by impregnation can be expressed as

$$б_c = б_{gc} + C_{sg} + C_{pl} \quad \cdots\cdots (12)$$

where, $б_{gc}$: compressive strength of gypsum base
C_{sg} : strength increment derived from tri-axial compression effect due to self stress
C_{pl} : strength increment derived from existence of polymer phase

If we know tri-axial compressive strength of gypsum base measured at a lateral pressure equivalent to the self stress in gypsum base ($б_{tc}$), the minimum amount of C_{sg} ($б_{gc}$ is neglected from contribution) is calculated as

$$C_{sg} = б_{tc} - б_{sg} \quad \cdots\cdots (13)$$

Because the tri-axial test is performed for gypsum base without any self stress and in GPC self stress $б_{sg}$ is initially generated in gypsum phase before uni-axial loading.

While, the term C_{pl} could be devided into two contributions independent each other. One is strength increment derived from crack arresting toughness of polymer ($б_{pl}$) and the other is that derived from microscopic change in transmitting path of force caused by the existence of polymer phase ($б_{ex}$). Referring to Griffith's theory, the former can be evaluated as the contribution of surface energy γ of polymer phase and the latter as the contribution of change in crack length c and modulus of elasticity E caused by impregnation. [1)]

Thus, the maximum amount of C_{pl} (If the minimum possible value of C_{sg} is used in eq.(12), the value of C_{pl} is possible maximum.) is expressed as

$$C_{pl} = б_{pl} + б_{ex} \quad \cdots\cdots (14)$$

Substituting (13) and (14) to equation (12)

$$\sigma_c = \sigma_{gc} + \sigma_{tc} - \sigma_{sg} + \sigma_{pl} + \sigma_{ex} \quad \cdots\cdots\cdots\cdots (15)$$

is obtained.

INVESTIGATION INTO COMPRESSIVE STRENGTH

Results of tri-axial compression test of gypsum base, where dried gypsum base wrapped in a rubber membrane is pressurized laterally and loaded, are shown in FIG.-4. Strength of gypsum bases under lateral stress equivalent to self stress σ_{sg} are obtained as shown in this Figure.

FIG.-4
Result of Tri-axial
Test of Dried Gypsum

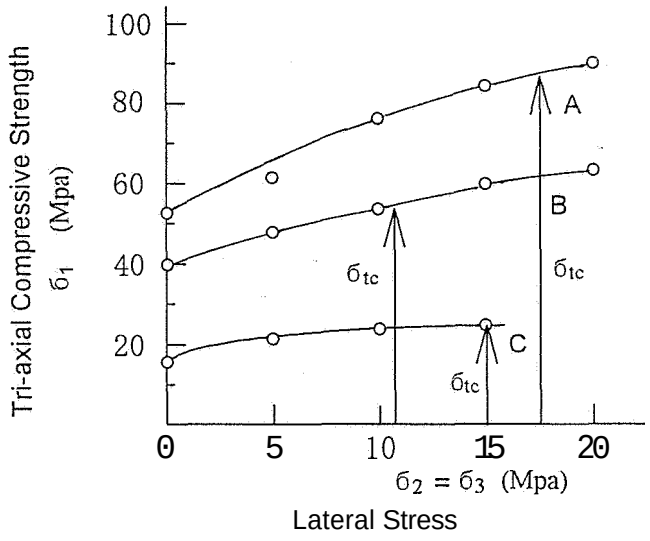

Using these values, the maximum contribution of polymer phase $\sigma_{pl} + \sigma_{ex}$ can be calculated from equation (15) as shown in TABLE-9. (From equation (12) the maximum value of Cpl is obtained if minimum amount of Csg is assumed.)

TABLE-9

Type of Gypsum	(Mpa)				
	σ_c	σ_{gc}	σ_{tc}	σ_{sg}	$\sigma_{pl} + \sigma_{ex}$
A	117.7	52.3	88.5	18.1	-5
B	111.9	26.6	55.1	11.0	41.2
C	84.7	18.2	25.0	15.3	56.8

For gypsum base A, the maximum contribution of polymer phase $\sigma_{pl} + \sigma_{ex}$ is found to be minus. Since $\sigma_{ex} > 0$ for positive polymer loading, σ_{pl} should be mimus for gypsum base A. This means contribution of crack arresting toughness of polymer to the compressive strength of GPC is also minus for superstressed polymer phase existing in GPC manufactured from gypsum base A.

CONCLUSION

(1) Self stress of polymer impregnated material can be obtained from shrinkage due to polymerization and moduli of elasticity of base material before impregnation.

(2) The self stress generated is balanced in two phases of GPC working as compressive in gypsum phase and as tensile in polymer phase.

(3) Strength of GPC is affected by the self stress, and the equation (9) can be applied to predict flexural strength of polymer impregnated gypsum.

(4) The phenomenon that the flexural strength of polymer impregnated gypsum is decreased after impregnation for gypsum mixed with small amount of water is interpreted by an unstable physical state where one phase of a composite material is stressed beyond its macroscopic strength due to crack arresting effect of the other phase. This state is designated as superstressed state.

(5) Tensile superstress existing in polymer phase exibits such an effect that decreases apparent compressive strength of composite material. This is consistent with its effect on flexural strength.

REFERENCES

1) E. Tazawa, S. Kobayashi, Properties and Applications of Polymer Impregnated Cementitious Materials , SP-40, ACI, 1973

2) E. Tazawa, S. Matsuhashi, Self Stress and its Effect on Flexural Strength of Polymer Impregnated Gypsum (in Japanese), Reports of the Technical Research Institute of Taisei Corporation, Nov., 1975.

3) E. Tazawa, Strength of Material Affected by Composite Stress , Transaction of the JCI, 71–79, 1979

4) Steinberg, M., Dikeou, J. T., et al, "Concrete Polymer Material, Second Topical Report", USBR REC-OCE-70-1 and BNL 50275 (T-602), December 1969

5) Dikeou, J. T., Steinberg, M., et al, "Concrete Polymer Material, Third Topical Report", USBR REC-ERC-71-6 and BNL 50275 (T-602), January 1971

EQUIPMENT FOR MEASURING AUTOGENOUS RH-CHANGE AND AUTOGENOUS DEFORMATION IN CEMENT PASTE AND CONCRETE

KURT KIELSGAARD HANSEN and OLE MEJLHEDE JENSEN
Department of Structural Engineering and Materials
Technical University of Denmark
Building 118, 2800 Lyngby
Denmark

ABSTRACT

Equipment for measuring autogenous RH-change and autogenous deformation in cement paste and concrete are presented. The equipment consists of a Rotronic Hygroskop DT including a measuring chamber for measuring autogenous RH-change in cement paste and concrete, a paste dilatometer for measuring autogenous deformation of cement paste and a concrete dilatometer for measuring autogenous deformation of concrete.

ROTRONIC HYGROSKOP DT

The measuring chamber Rotronic WA-14 TH is shown in FIG.-1. Crushed cement paste or concrete is placed in a small enclosed volume with a moisture sensor and a temperature sensor. The measuring range is 0 - 100 %RH. The Rotronic Hygroskop DT is the instrument, which controls and displays measuring signals from the measuring chamber. Before and after every experiment the RH equipment is calibrated with four saturated salt solutions in the range 75 - 100 %RH. This reduces the maximum measurement error to ± 1 %RH when the measuring chamber is placed in a climatic box controlled to ± 0.1 °C.

PASTE DILATOMETER

The paste dilatometer is shown in FIG.-2. The equipment measures the linear deformation of the specimen. **A** special feature of the equipment is that measurements can begin before setting. A special form system of corrugated tubes enables this to be done. The corrugation permits the tubes to deform easily in the longitudinal direction, and the geometry of the cross-section is well-

defined. The sealing prevents exchange of material with the surroundings (CO, and H_2O). During measurements the dilatometer is immersed in a thermostatic bath, controlled to ± 0.1 "C.

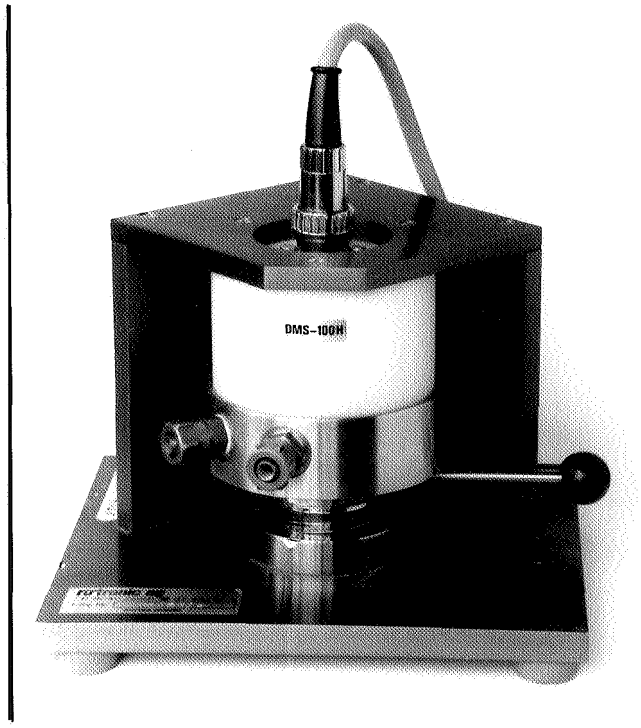

FIG.-1. Rotronic WA-14 TH measuring chamber. Inside the chamber is a Pt-100 temperature sensor and a DMS-100H RH sensor.

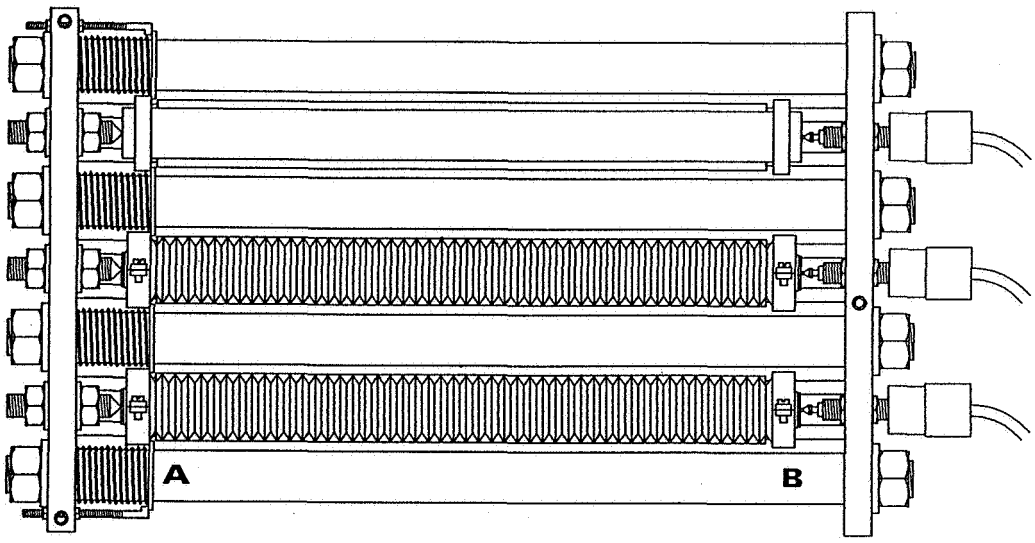

FIG.-2. Sketch of paste dilatometer. Two test specimens and an invar reference rod (uppermost). The specimens are horizontal and are fixed in one end at A. The changes in length are registered by displacement transducers at B. The length of the samples is app. 280 mm.

CONCRETE DILATOMETER

Autogenous deformation of concrete is measured with a concrete dilatometer, see FIG.-3. The concrete dilatometer including the form system functions in principle in the same way as the paste dilatometer described in the previous section. During measurement the equipment is also immersed in a thermostatic bath.

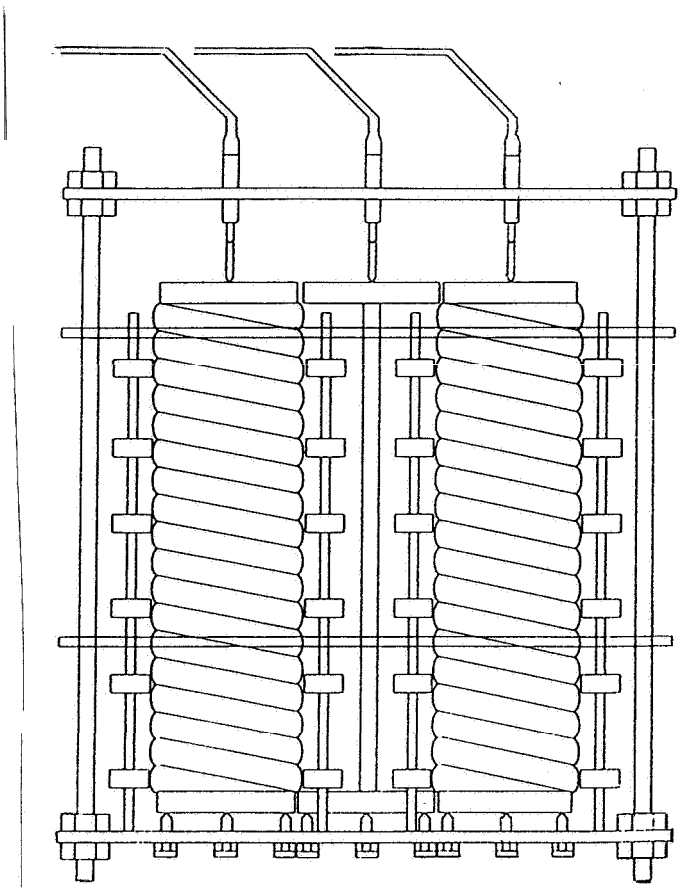

FIG.-3. Sketch of dilatometer for the measurement of autogenous deformation of concrete. Two tests specimens and an invar reference rod are measured simultaneously. The specimens are vertical and are supported by sliding plates of teflon. Changes in length are measured by displacement transducers placed above. The forms are Ø100 · 375 mm long flexible tubes.

REFERENCES

Jensen, O. Mejlhede: Autogenous deformation and change of the relative humidity - self-desiccation and self-desiccation shrinkage (in Danish), Ph.D. thesis, Technical Report 284193, Building Mat. Lab., Techn. Univ. Denmark, 1993.

Jensen, O. M.; Christensen, S. L.; Dela, B.F.; Hansen, J.H.; Hansen, P.F.; Nielsen, A.: Control of early age cracking in concrete. Phase 2: Shrinkage of mortar and concrete. Series I, No 12. Dep. of Struct. Eng. and Mat., Tech. Univ. Denmark, 1997.

Jensen, O. Mejlhede; Hansen, P. Freiesleben: A dilatometer for measuring autogenous deformation in hardening Portland cement paste. Materials and Structures, 27, 1995.

Jensen, O. Mejlhede; Hansen, P. Freiesleben: Autogenous deformation and change of the relative humidity in silica fume modified cement paste. ACI Materials Journal, Nov-Dec issue, 1996.

MEASUREMENT OF MOISTURE IN HIGH PERFORMANCE CONCRETE

GÖRAN HEDENBLAD
Lund Institute of Technology, Division of Building Materials
Box 118, S-221 00 Lund, Sweden

ABSTRACT

Some results from RH-measurements, as presented in newer Swedish literature, are summarised. Results from the author's own measurements in high performance concrete (HPC) are also presented. Two different types of RH-meters and two different HPCs have been used. The overall conclusion is that RH-measurements in HPC are much more difficult to do than in ordinary concrete.

INTRODUCTION

It is difficult to measure the relative humidity (RH) in high performance concrete (HPC). The reason is that the sorption curve is flatter and also that the moisture transport capacity is lower than for ordinary concrete. This means that less moisture can evaporate from or be taken up by the concrete, near an RH-sensor, than for ordinary concrete, i.e. the moisture capacity of the RH-sensor and its filter has a much greater effect on an RH-measurement in high performance concrete than in conventional concrete. When an RH-measurement was done in a measurement hole in high performance concrete, the measurement hole become consumed for a while. This means that if the RH-measurements are made with a relatively short time between the measurements, then lower and lower RH is received.

The above indicates that older RH-measurements in HPC, which are made with a measuring practice developed for conventional concrete, can be marred by errors which are bigger than for conventional concrete.

A SUMMARY OF THE REPORT "MEASURING RELATIVE HUMIDITY IN CONCRETE"

C. Gårlin and M. Hjort have shown in their master's thesis /1/ some different experiments concerning RH-measurements in concrete. The different tests are:

Test 1: The effect of the time of the measurement and the sealing of the measurement hole
Test 2: The effect of the measuring hole's geometry
Test 3: The effect of preparation with salt and evercreate
Test 4: The effect of screeds
Test 5: How the drilling influences RH
Test 6: Measuring RH at a specific depth
Test 7: Measurement with different types of RH-sensors

Not all the tests are described here, but the interested reader is referred to /1/ (in Swedish).

Test 1 (The time of the measurement and the sealing; of the measurement hole)

This test shows how important it is that the tightening of the drilled hole is done correctly. Four different types of sealing have been examined, namely:

I) No sealing
II) Sealing on the concrete surface
III) Sealing at the RH-sensor
IV) Sealing with a PVC-tube

The measurements were made in a concrete of strength class K25 and with Vaisala's HMP 35 RH meter. The arrangement of the test is, in principle, shown in FIG. 1. It is important to notice that the holes were drilled one month before RH-meters were placed in the test hole. The concrete was about 4 months old when the measurements started, and the drying was from one side only (in principle). The standardised measurement depth (40% of the construction thickness 150 mm) for this type of drying is 60 mm. The depth of the measurement holes was 50 mm. This means that the measurements have been made at a depth where the RH-profile changes very strongly. RH is low at the surface and much higher further inside the concrete. The results of the measurements are shown in FIG. 2.

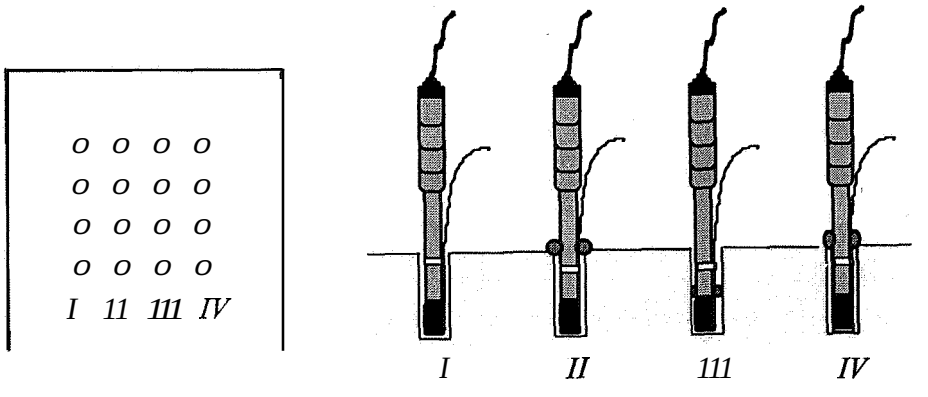

FIG. 1. The experimental arrangement of test 1, in principle. Gårling and Hjort /1/.

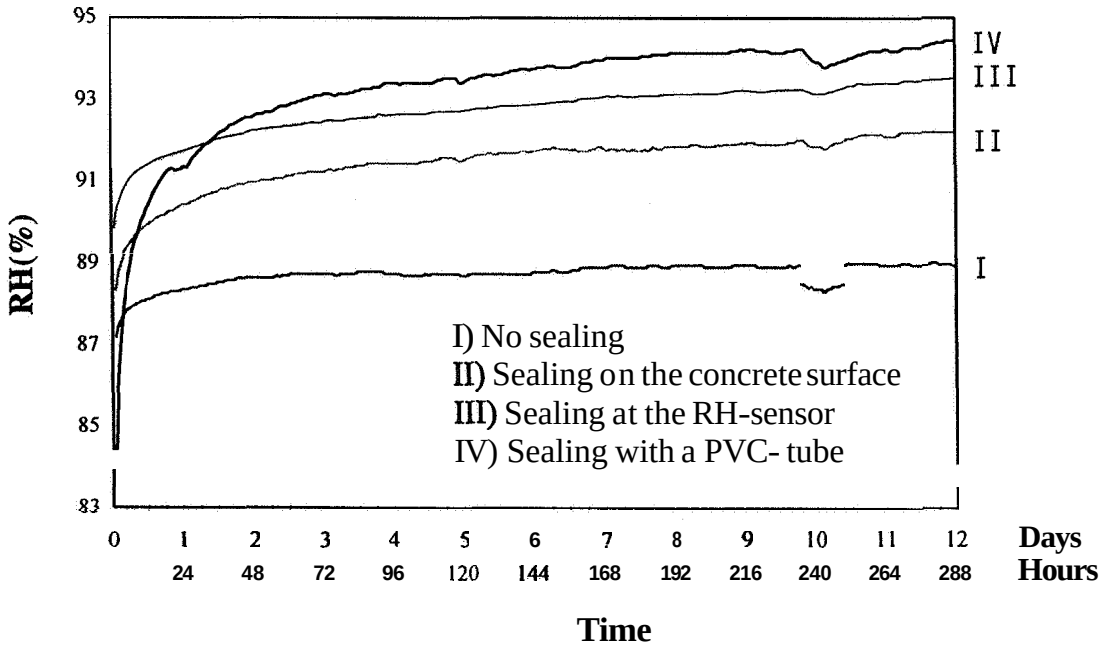

FIG. 2. Measured RH as a function of time and of different sealing of measurement hole. Gårlin and Hjort /1/.

FIG. 2 shows that the type of sealing of the measurement hole has a great influence on the measured result. It is probably only "tube-sealing" that comes close to the truth. The PVC-tube was probably placed immediately after the drilling of the measurement hole. With the other types of sealings, it is not only the type of sealing which is studied but also the redistribution of moisture in the measurement hole. The reason for this is that the hole stood empty for one month before the measurements were made. The most general conclusion is: when you let the drilled hole remain empty and moisture redistribution can occur in the drilled hole, then you can measure any one relative humidity. The result in FIG. 2 would possibly have been more pronounced if the measurements had been made in a concrete with low w/c.

Conclusions: Prevent moisture redistribution from happening in a drilled hole and also check that the measurement depth is well defined.

Test 5 (how the drilling influences RH)

This test has been performed on a concrete of strength class K25 and on a concrete of strength class K40. The later concrete was cast in 1986 and after that it was placed in a normal indoor climate until the measurements in 1993. The experimental arrangement in principle is shown in FIG. 3, where one can see that the drilled holes are only sealed at the concrete surface. In FIG. 4 the measured RH is shown as a function of time after the drilling.

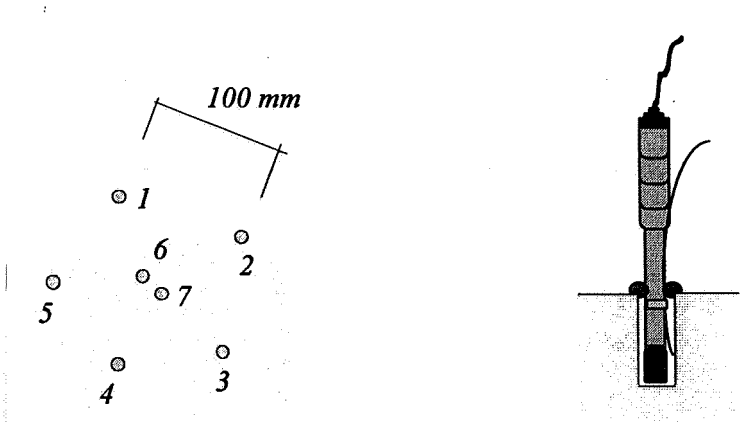

FIG. 3. The experimental arrangement, in principle, of test 5. Gårlin and Hjort /1/.

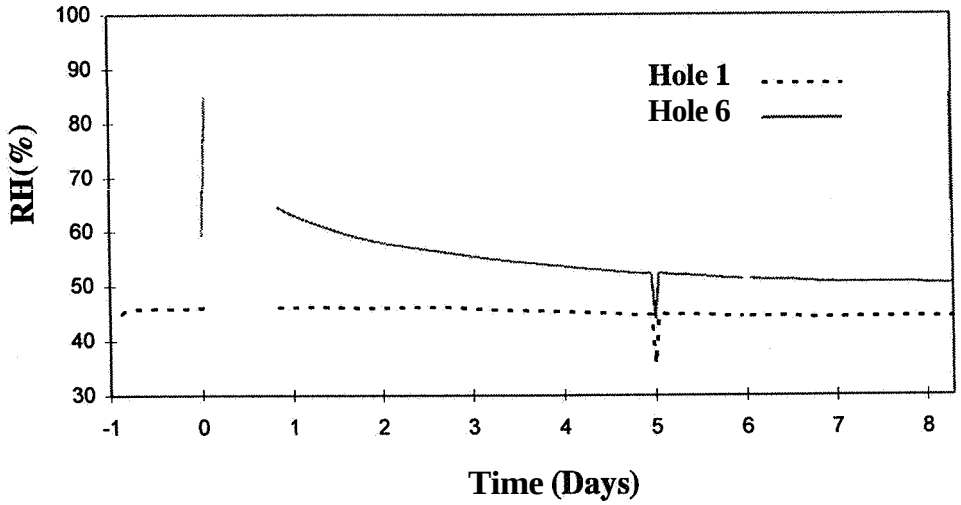

FIG. 4. Change of RH in newly drilled hole (hole 6), and also in an existing hole /1/, at a distance of 100 mm from the middle hole. Concrete K40. RH of the slab is approx. 50%. Gårlin and Hjort /1/.

It is not clearly shown in the report what relative humidity the slab in FIG. 4 had. But one can notice that it took almost one week before the RH sensor in the drilled hole (hole 6) reached equilibrium. With high RH (with concrete K25T) the duration of the transient time is not so long. A similar result has previously been reported by Monica Pastrav /2,3/.

With regard to the lower moisture capacity in the concrete with low w/c compared with ordinary concrete, it is probable that the transient time for HPC concrete is similar to the time in FIG. 4, even with higher RH.

A SUMMARY OF THE PRELIMINARY REPORT "MOISTURE DESIGN OF A CONCRETE FRAME OF A BULDING AND THE FOLLOW-UP OF THE DRYING PROCESS, KV. GÄRDSRÅET UMEÅ"

This report is undergoing the final revision by M. Wappling /4/. The measurements have been performed by Mr. A. Nordström, who has endeavoured to make very careful measurements. Both concrete of strength class K30 and HPC with w/c 0.38 have been studied. Here only RH-measurements for one case are shown. In connection with the RH-measurements, the temperature in surrounding air, in the RH sensor and also in the concrete has been measured.

The outdoor climate is shown in FIG. 5. The measured temperatures are shown in FIG. *6* and the measured and calculated RH-values are shown in FIG. 7. The concrete quality is K30.

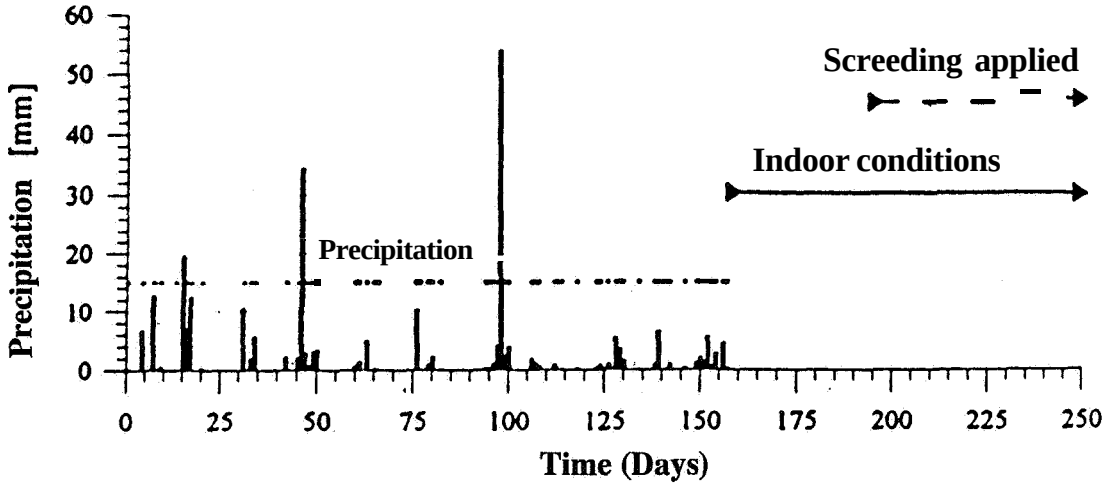

FIG. 5. The outdoor climate of a concrete floor located in Umeå, Sweden. /4/.

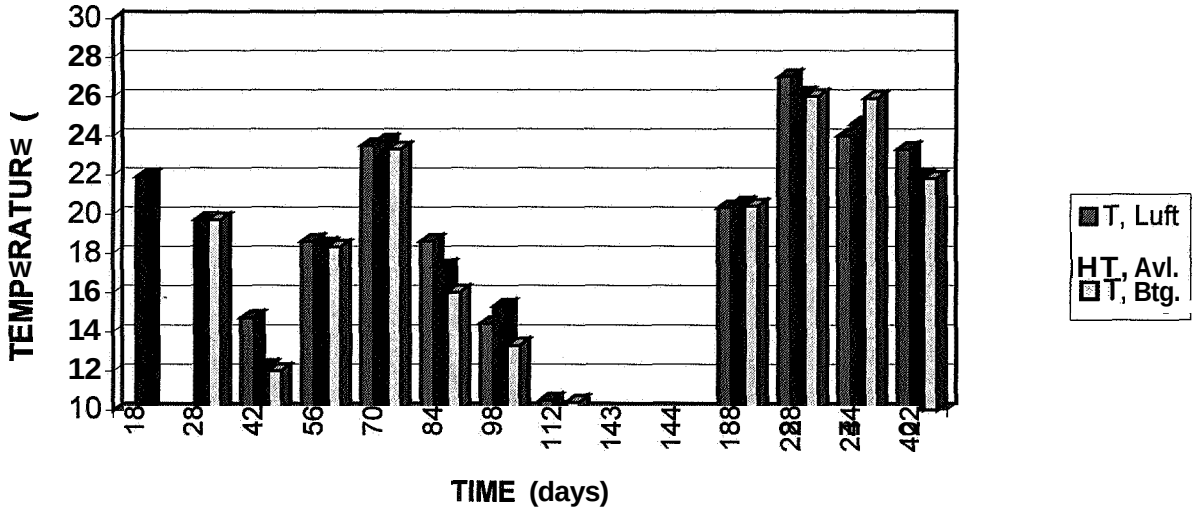

FIG. 6. Measured temperatures of the air (T, Luft), the RH-sensor (T, Avl) and the concrete (T, Btg). From Kv. Gärdsrået, Umeå.

FIG. 6 shows that, above all, at 70, 84, 98 and 234 days, the temperature measured by the RH-sensor differs from the temperature measured at the bottom of the drilled hole (the temperature of the concrete). The latter temperature was measured with a separate thermometer, with a ceramic top. At the RH-measurements a dew point meter was used (Maker Protimeter). With the Protimeter sensor, both the temperature and the dew point temperature were registered. Control has been made afterwards, showing that there was no systematic difference between the temperature measured with the dew point meter and with the separate thermometer (at approx. +20 "C).

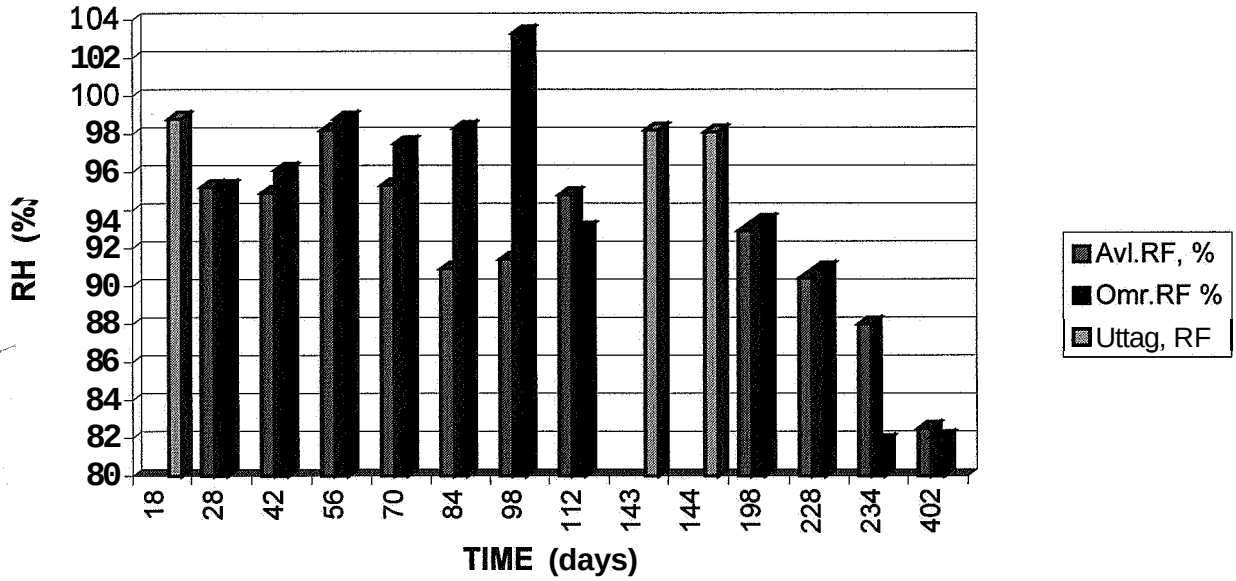

FIG. 7. Measured RH (Avl.RF, %), calculated RH (Omr.RF, %) and RH measured on samples taken out of the concrete (Uttag, RF). From Kv. Gärdsrået, Umeå.

FIG. 5 shows that the building was sealed after about 160 days, i.e. during the five first months the concrete structure was exposed to repeated precipitation. The outdoor temperature appears partially in FIG. 6. From FIG. 5 and FIG. 6 it may be concluded that when the building was sealed the hydration of the concrete had proceeded for a long time that the concrete was almost capillary saturated with water.

FIG. 7 also shows the measured RH of samples taken out of the construction after 18,143 and 144 days. These RH-values are approx. 98%. When the temperature between the RH-sensor and the concrete differs, a recalculation has been made from the RH registered by the RH-sensor to a calculated value in the concrete. These calculations have been made with the formula:

$$\phi_{concrete} = \phi_{read} * \frac{v_s (T_{read})}{v_s (T_{concrete})}$$

where ϕ is the relative humidity (RH) and v, is the vapour concentration at saturation. This formula is theoretically correct, but it is unsuitable in this case because the recalculated RH-values become unreasonable, in one case 103%. When comparing FIG. 6 and FIG. 7 it appears that at 70, 84, 98 and 234 days, when the concrete temperature differs by a few degrees from the

RH-sensor, this gives remarkable RH-values. This is valid for dewpoint meters. We do not know how the results would have been with other types of RH-sensors. Until we arrive at better knowledge the following conclusions can be drawn.

Conclusion: Measure RH when the house is built in and has relatively constant temperature.

STUDIES AT BUILDING MATERIALS, LUND INSTITUTE OF TECHNOLOGY

Suspicions started when RH-measurements were repeated in the same drilled hole (or on samples taken out of the concrete), and we did not got the same measured RH-value on the different occasions. This was valid for concrete with low w/c. A probable reason for the variations in measured RH is that these types of concrete have a flatter equilibrium moisture curve than conventional concrete and at the same time a concrete with low w/c is much tighter than conventional concrete. In other words, there is not so much moisture available on the concrete surface to moisten the RH-sensor and partly it takes time to replace the moisture which is removed by the sensor and by the air on every measurement occasion. To examine whether the suspicions were right, it was decided to perform measurements, both in measurement holes and on samples taken out of the concrete.

The concrete specimens which were used in this study were a few years old, i.e. they had dried to approx. 70% RH. As the equilibrium moisture curve is relatively linear for concrete with low w/c in the range fiom about 30% to 100% RH, it was supposed that if the RH-sensor was dried in 33% RH, about the same amount of water should be removed from the surface of the concrete by the measurement as with a common measurement of moisture.

Repeated RH-measurements in the same measurement hole

The measurements were performed on specimens which had been used earlier. Two different types of concrete were examined, one with w/c 0.32 (sulphate resisting low alkali cement) with 4.8% silica fume, specimen 9-15-3, and one with w/c 0.41 (OPC) with 5.1 % silica fume, specimen 9-6-2. For specimen 9-15-3 RH-measurements were performed both with a dew point meter (Protimeter) and with a capacitive moisture meter (Vaisala).

Specimen 9-15-3 (w/c 0.32 with 4.8% silica fume), measurements with dew point meters

Before the first measurement, the RH-sensors had been conditioned in the climate room where the specimen was stored. This climate room had approx. 60% RH and a temperature of about +20 "C. At the first measurement in the specimen, the RH-sensors were placed in the measurement holes for 27 hours. When the RH-sensors were inserted in the specimen, they had almost the same RH which later was measured. Because of this the moisture loss from the concrete to the meters was small. In other words, it is probable that the measured RH-values are almost the same as the RH of the concrete (except for normal spread in the measured result).

After that the RH-sensors were dried at 33% RH (in calibration vessels with $MgCl_2$) for a few hours. The sensors were then once again placed in the specimen for one day. This was repeated a couple of times, see FIG. 8.

Between 170 and 288 h the meters were placed in the calibration vessels, i.e. during this time the measurement holes were allowed to regain their moisture equilibrium. At 288 h the dew point meters were placed once again in the measurement hole and they stayed there until 434 h.

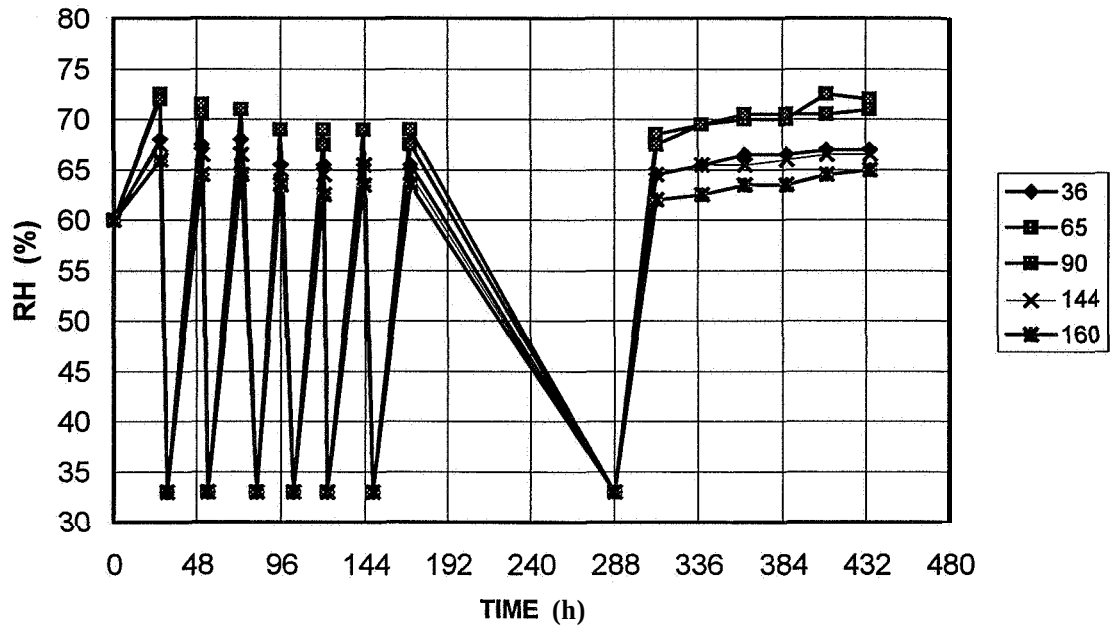

FIG. 8. Measured RH in specimen 9-15-3, with repeated measurements. Dew point meters..

It is obvious from FIG. 8 that the measured relative humidity decreases for every new measurement. No measurements were done between 170 and 288 h and the measurement holes were sealed. During this time (118 h, about 5 days), RH in the measurement holes should have risen to the original values. This probably happened, but when RH rose in the concrete, close to the measurement hole, the moisture content probably did not rise to the same extent. This part of the concrete should have been on an almost entirely horizontal transition curve from the desorption isotherm to the absorption isotherm. That is, RH may change without any remarkable change of the moisture content in the concrete happening.

When the dry RH-sensors are once again placed in the measurement hole and readings are done after about 1 day (312h in FIG. 10) some lower RH-values are read than before. This is quite natural, according to the discussion above, because when the concrete loses moisture to the RH sensors, the outermost part of the concrete in the measurement hole follows the same transition curve but in the other direction until it returns to the desorption curve. The latter has a much greater moisture capacity (inclination) than the transition curve and provides the RH-sensor more easily with moisture than the transition curve.

Between 288 and 434 h the RH sensors are placed all the time in their respective measurement holes. FIG. 8 shows that during this time the measured RH increases almost the whole time. This is distinctly seen in FIG. 9, in which the mean values of all the RH changes are shown. In FIG. 9 the measured RH-values at 27 hours have been set as reference level (the value 0). From that the differences between measured RH-value and the RH-value at 27 h have been calculated. The mean values (for five measurement holes) for the differences have then been calculated and are shown in FIG. 9.

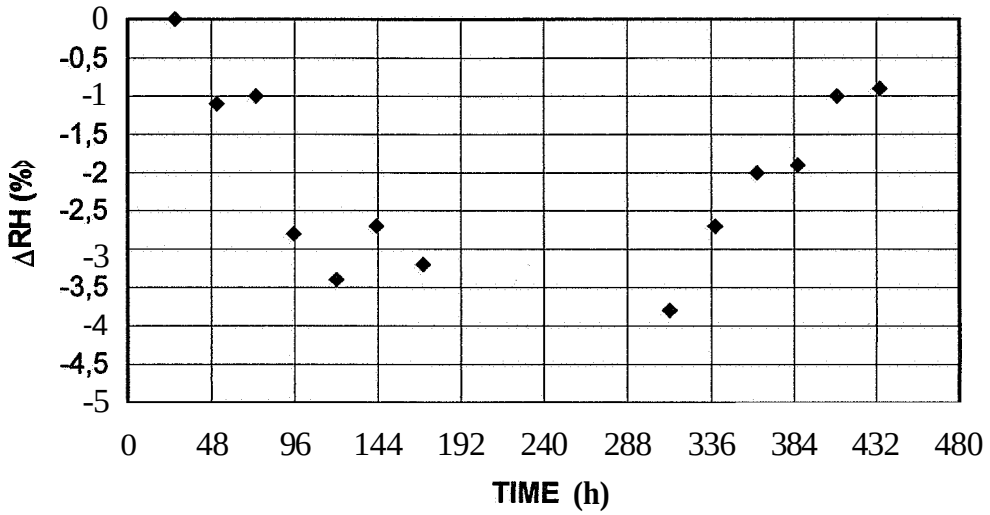

FIG. 9. Mean values of the measured RH-changes in specimen 9-15-3, when the measurements are repeated. Measurements with dew point meters.

It is clearly shown in FIG. 9 that, with repeated measurements in same measurement hole, the measured RH decreases with the number of measurements. It can also be concluded that in the case when the RH-sensors have been in the measurement hole for a longer time (about 6-7 days), from 288 days onwards, RH rose to almost the same level as on the first measuring occasion.

Measurements with capacitive moisture meters in Specimen 9-15-3

Specimen 9-15-3 was allowed to rest for 8 days between the measurements with the dew point meters and the measurements with the capacitive moisture meter. Three meters were used and they were calibrated just before the measurements with different saturated salt solutions, at 33.1, 75.5 and 85.3% RH. The measured RH-changes are shown in FIG. 10, when the measurements are repeated. Repeated measurements were made, with drying of the RH-sensors in 33% RH between every measurements, until the 150 h time. The meters were then continuously placed in the measurement holes from 150 h to about 310 h.

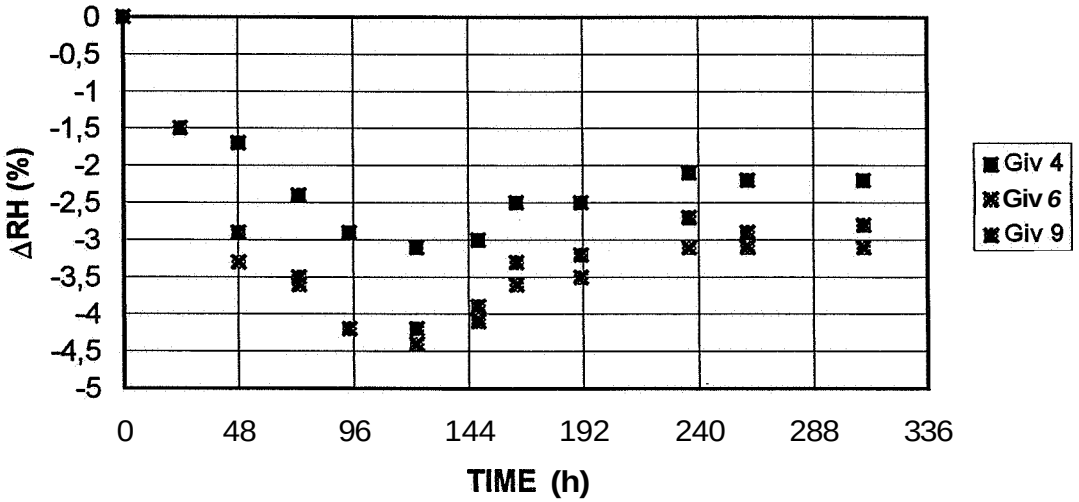

FIG. 10. Measured RH-changes in specimen 9-15-3 when the measurements are repeated. Capacitive moisture meters. At the first reading the time is set to 0 (zero).

From FIG. 10 it is clear that even with this type of RH-meter, lower and lower RH is measured as the measurements are repeated. Besides it is shown that even if the sensors are placed in the measurement hole for one week, the measured RH values will not return to their original value, they are approx. 2.5-3% RH below this value. **A** possible explanation for this may be that capacitive moisture meters have hysteresis in their characteristic curve, i.e. one does not get the same value when the sensor is under desorption as when the sensor is under absorption.

The last calibration point before the measurements started was 85% RH. It can not be excluded that the time of condition, in 33% RH, was too short for the RH-sensors to really reach equilibrium. This could explain some part of the 2.5-3% RH above.

The first measured RH-results with both Protimeter and Vaisala meters are shown in FIG. 11. This RH was measured in the same measurement hole in the test body 9-15-3. The X-axis has the results obtained with Protimeter sensors and the Y-axis has the results measured with Vaisala meters.

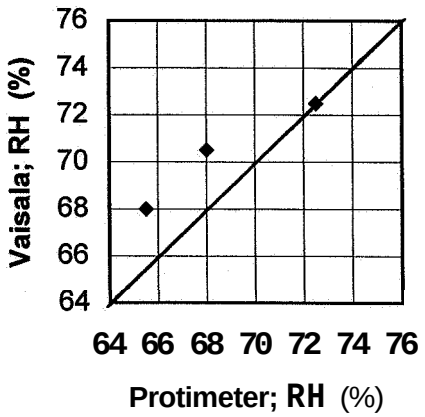

FIG. 11. Comparison of the RH-values measured with dew point meters and with capacitance meters. The first measurements of specimen 9-15-3 with each meter.

The compared results are measured in measurement holes 1, 2 and 3. These have the following distance from their centre lines to the concrete surface: 20, 36 and 65 mm. This means that the measured RH is different in the different measurement holes; the farther into the concrete the higher the RH. If the measured results for the same measurement hole, with the two different types of RH-meters, are similar the result should be the right line in the diagram. This is true of one point, while the other two points are about 2% RH from the line. In view of the fact that there are two measurements for each point and also that every measuring result contains an element of uncertainty (probably of the order of 1-2% RH), the results in FIG. 11 can be regarded as acceptable.

Specimen 9-6-2 (w/c 0.41 with 5.1% silica fume), measurements with dew point meters

To imitate what can happen in a real measuring situation, for example when the RH-meters have been stored in a cold and moist car for a long time and then have been conditioned in the building (in which the measurements are to be made) during a shorter time, the RH-meters were conditioned in 95% RH followed by ½ hour in 60% RH before they were placed in the measurement holes. The measurement holes in the concrete had a diameter of 8-9 mm and a length of approx. 25 mm. These measurement holes in the concrete were smaller than the holes in specimen 9-15-3, where they were about 15 mm in diameter and some 30 mm in length.

During the first five days the sensors were placed all the time in their respective measurement holes followed by drying for 3.5 h in 33% RH. Then they were once again placed in the measurement holes. After this initial period the RH-sensors were alternated between the measurement holes and 33% RH, for about 7 days. The results of the measurements are shown in FIG. 12.

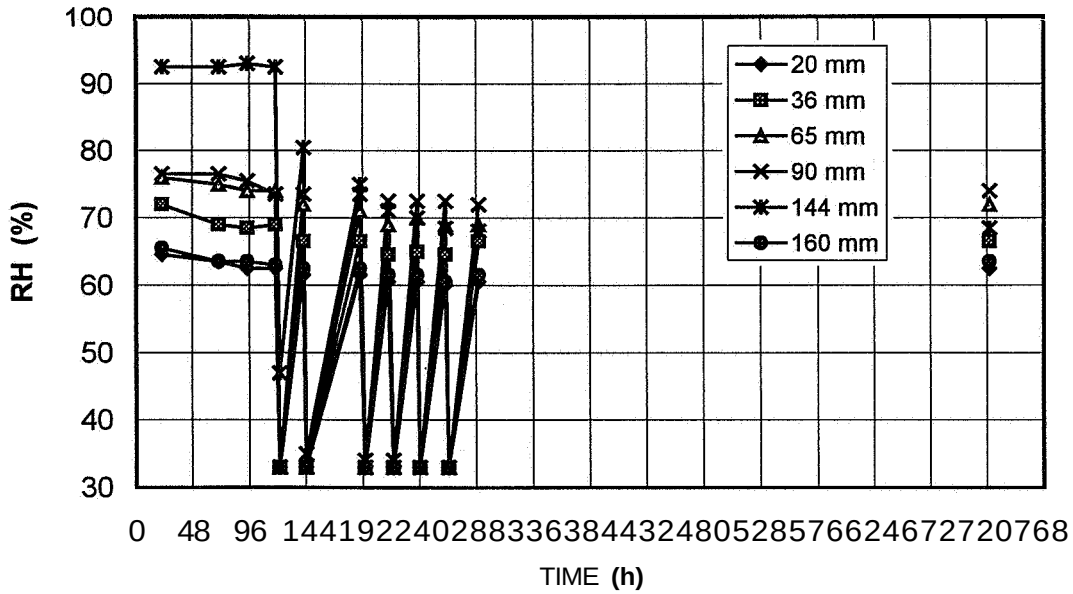

FIG. 12. Measured RH in specimen 9-6-2 at repeated measurements. Measured with dew point meters. The depth of measurement is indicated.

FIG. 12 shows that the introductory conditioning for about ½ hour in the climate room was not enough to dry the RH-meters. One meter shows approx. 93% RH during the first five days. The other five meters show that RH decreases during the first five days, although the sensors were placed in the measurement holes all the time. Possible explanations may be that moisture is emitted fiom the RH-sensors to the surrounding concrete or that there is leakage somewhere. At the first drying at the alternating of RH-sensors, in 33% RH for about 3.5 h, 5 of the sensors dried to 33% RH but the 6th dried to only 48% RH. In other words, in the latter case the drying time, 3.5 h, was not enough. **A** reflection of this is that the next measuring value in the specimen for this sensor (depth 144 mm in FIG. 12) is approx. 80% RH. During the period with "cyclic loads" the measured RH for all sensors decreases for almost every new cycle. This is for a concrete with w/c 0.41.

Conclusions: Let enough time elapse between measurements in the same measurement hole (at least one week) and let the measurement continue long enough. Let the RH-meters including the filters dry to a lower RH than is later measured It is probably easier for the concrete to emit moisture than to take up moisture (in vapour phase), see FIG. 12.

Repeated RH-measurements in test tubes

Specimen 9-15-3 was broken into pieces with the help of a pressure press. The broken specimen was put in plastic bags, where it was kept for 10 days. Pieces of approx. 5-10 mm in diameter were taken out later and immediately put in test tubes. The tubes were sealed with rubber plugs. Mr B. Johansson, who did this work, tried to put samples fiom the same "depth" in the specimen into the same test tube. A total of 8 tests were taken, i.e. 8 test tubes. All the test tubes were first filled entirely and RH-measurements were made twice. Afterwards material was taken fiom 4 of the test tubes, so that different amounts of material were obtained in the test tubes. Counted fiom the bottom of the test tube it was about 2, 4, 6 and 8 cm. Before the measurements of the 4 test tubes were started, the dew point meters were conditioned in 33% RH for about ½ hour. After that, measurements followed for 10-15 hours broken off by conditioning in 33% RH for about ½ h. The results are shown in FIG. 13.

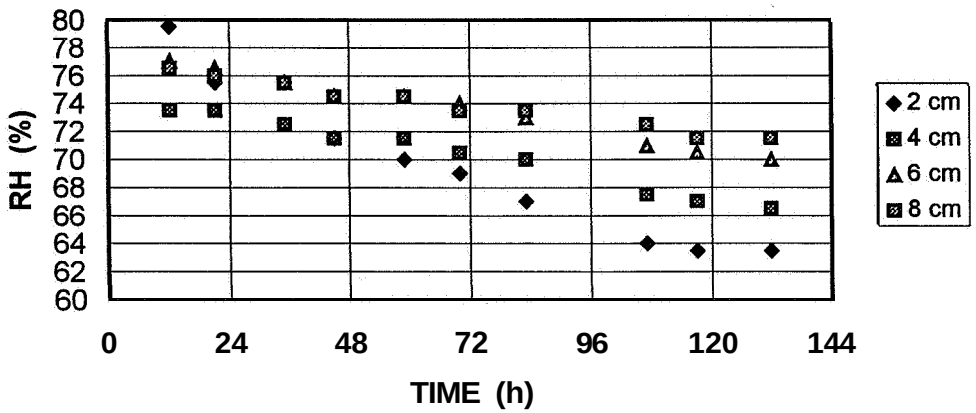

FIG. 13. Repeated RH-measurements in test tubes filled to different depths (2, 4, 6 and 8 cm). Material from specimen 9-15-3, i.e. w/c 0.316 with 4.8% silica fume. Measured with dew point meters.

It is obvious from FIG. 13 that for every new drying period, the measured RH in every test tube decreases. The decrease is faster in the test tube which is only filled to 2 cm. This is clearly shown in FIG. 14, in which the changes of the measured relative hurnidities are shown.

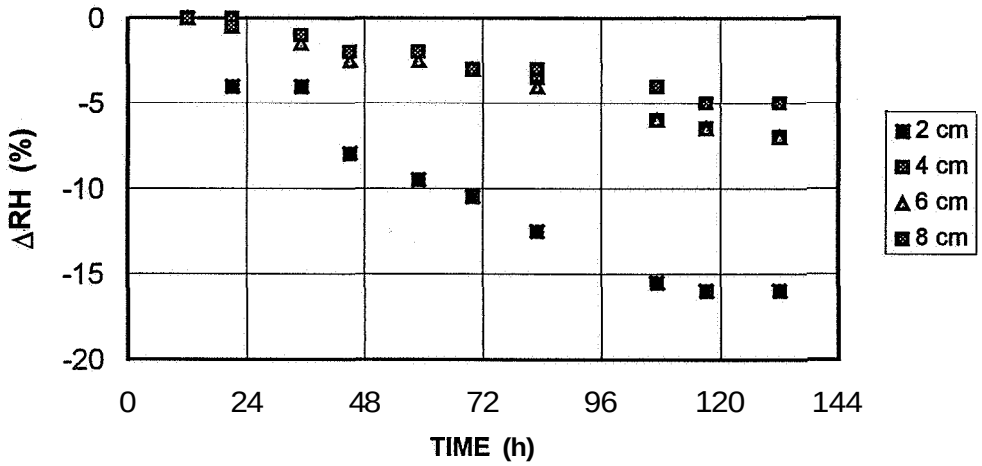

FIG. 14. Measured RH-changes, at repeated measurements, in the test tubes filled with different amounts of concrete material. Measured with dew point meter.

FIG. 14 shows that with only 2 cm filling height in the test tube, the measuring faults can be huge with repeated measurements. On the other hand, it seems that the influence of the filling height is not greater when the height is 4 cm or more. The reduction in RH for these filling heights is pretty much the same in every new round up to about 80 h. After this time the sensors were conditioned for 10.5 h in 33% RH versus roughly ½ hour at the earlier times. This longer conditioning in 33% RH seems to have influenced the tests with 4 and 6 cm filling height more than the test with the height 8 cm. An explanation can be that during this longer time in 33% RH the sensors and especially their filters have time to dry out entirely. As a result the sensors will take up more moisture from the test material the next time they are in the test tubes. This leads to lower measured RH.

The mean values of the RH-changes, measured in test tubes with 4, 6 and 8 cm, are shown in FIG. 15.

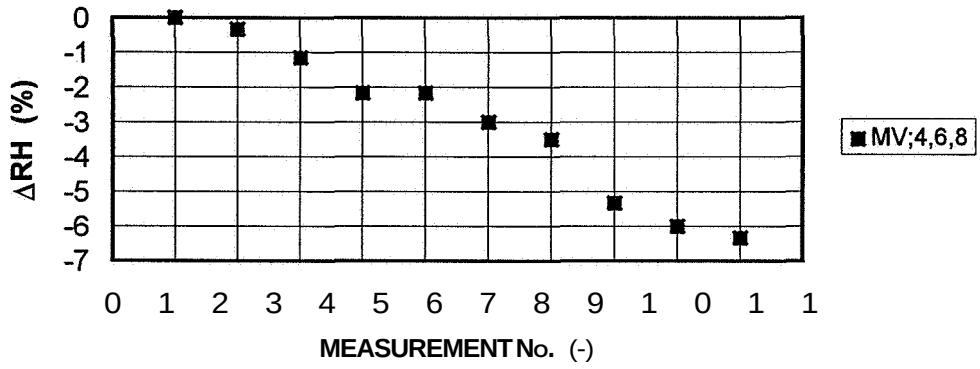

FIG. 15. The mean values of measured RH-changes for test tubes with filling height 4, 6 and 8 cm.

In FIG. 15. it is clear that for every new measurement the RH-change becomes bigger. In other words, even with almost filled test tubes one cannot make repeated measurements in rapid succession. It can not be excluded that a certain moisture redistribution happens in the test tubes from one piece of concrete to the other, which can influence the measured RH values.

Conclusions: Measure only in test tubes which contain a relatively large amount of material and measure only one or two times in same test tube within a brief period. After the sample is taken out from the concrete, let it be conditioned for some days in the test tube before the RH-measurement is done.

RECOMMENDATIONS

This paper shows that it is possible, but requires knowledge, to measure the relative humidity in HPC. The following recommendations can serve as a first base of knowledge.

a)

When measuring RH in drilled holes, check that redistribution of moisture cannot occur in the measurement hole and also check that the measured depth is well defined, that is, that the distance between RH-sensor and the concrete is minimised. Further, the evaporating surface of the concrete against the RH-sensor should be big.

b)

Measure RH only when the house is built in and has a constant temperature.

c)

Let enough time elapse between measurements in the same measurement hole (at least one week). Also let the measurement continue long enough (at least two days). Check that the RH-sensor including its filter has dried to a lower RH than that measured afterwards. It is probably easier for concrete to emit moisture than to take up moisture (in the vapour phase).

d)

When measuring RH in a test tube, do so only with test tubes which contain a relatively large amount of material. Measure only one or two times within a short period. After the sample is taken out of the construction, let it be conditioned for a few days in the test tube before the RH-measurement is made.

ACKNOWLEDGMENTS

This research was supported by the Swedish National Consortium of High Performance Concrete.

REFERENCES

1) Gårlin, C. and Hjort, M., "Measuring Relative Humidity in Concrete", Report SP-AR 1995:62, Building Physics, Swedish National Testing and Research Institute, Borås, Sweden, 1995 (in Swedish).

2) Pastrav, M., "Moisture and Temperature Measurement in Concrete - the Risk of Error in the Measurement in Drilled Holes", Report SP-AR 1989:05, Building Physics, Swedish National Testing and Research Institute, Borås, Sweden, 1989 (in Swedish).

3) Pastrav, M., "Moisture and Temperature Measurements in concrete. Risk for Misleading results when measuring in drilled holes", Proceeding of the 2nd Symposium; BUILDING PHYSICS IN THE NORDIC COUNTRIES, Trondheim, Norway 20 -22 August 1990.

4) Wappling, M., "Moisture Design of a Concrete Frame of a Building and the Follow-up of the Drying Process, Kv. Gärdsrået, Umeå." Report from the company Siab, dated 1996-05-02, Sweden.

INTERNAL EIGENSTRESSES IN CONCRETE DUE TO AUTOGENOUS SHRINKAGE

BIRGITTE FRIIS DELA and HENRIK STANG
Department of Structural Engineering and Materials
Building 118, Technical University of Denmark
2800 Lyngby, Denmark

ABSTRACT

The stress development inside a spherical aggregate embedded in cement paste that undergoes shrinkage is investigated. The shrinkage considered is the autogenous shrinkage of cement paste. Three types of cement paste with different extends of autogenous shrinkage are used in the tests presented in this paper. The development in autogenous shrinkage and modulus of elasticity has been determined. The stresses are measured with the use of a special sensor, currently under development. Experimental results from experiments carried out with two different prototype sensors will be presented.

INTRODUCTION

Autogenous shrinkage of cement paste in ordinary concrete will normally not cause problems regarding cracking in concrete structures to an extend where durability problems can be expected. However, in the presence of large amounts of microsilica, used in concrete where high strength or low porosity is needed, the development of autogenous shrinkage is different. The main difference is that the autogenous shrinkage of cement paste containing micro silica continues over several days and weeks, whereas the autogenous shrinkage of ordinary concrete only takes place within the first couple of days. As the rate of creep and relaxation in very young concrete is high, the stresses that occur at early ages will very rapidly disappear. If, on the other hand, the shrinkage continues to develop increasing eigenstresses will be introduced.

The eigenstresses that develop in concrete as a result of autogenous shrinkage can be divided into 2 categories: Eigenstresses on the macro level resulting from structural restraints and eigenstresses on the meso level resulting from the restraining effect caused by the aggregates in the concrete. The eigenstresses on the macro level can lead to cracking of the concrete structure. These cracks are occasionally visible on the surface of the structure. The stresses that develop on the meso level can lead to micro cracking of the material. These micro cracks will usually form an internal crack pattern oriented perpendicular to the surface

of the larger aggregates and reaching from one aggregate to the other

In order to be able to measure the eigenstresses that develop in and around an aggregate a sensor has to be developed. The sensor serve as an artificial aggregate measuring changes in strains or stresses of the aggregate. Two prototype sensors have been developed. The first sensor was based on strain measurements using a thermometer as "aggregate". This sensor is further developed into a sensor based on stress measurements using electrical resistance. The latter sensor is still under development as part of a Ph.D. project on eigenstresses in hardening concrete. Pilot tests will describe the stress development in one single aggregate embedded in cement paste.

MIXING PROCEDURE FOR CEMENT PASTE

The cement pastes used in the tests has a water-cement ratio of 0,30. The type of cement is a White Portland Cement. The cement pastes contains 0%, 10%, and 20% microsilica (on weight of cement content). In table 1 the mix compositions are listed.

TABLE - 1 Mix composition of the cement pastes

	P00	P10	P20
Water/Cement	0,30	0,30	0,30
Microsilica/Cement	0%	10%	20%
Superplast/Binder	1,05%	1,05%	1,0%
Microsilica	Slurry	Slurry	Powder
Superplast	Melamine	Melamine	Naphthalene

The cement pastes are all mixed in a 5 litre Hobart mixer in the following way: Cement, microsilica and superplasticizer is homogenised by dry mixing for 1 minute. Then 2/3 of the water is added (w/c=0,20). After 3 minutes mixing and 2 minutes break, the remaining part of the water is added and the mixing is continued for another 3 minutes. The mixing procedure at very low water-cement ratio is used to ensure proper dispersion of the microsilica. During mixing evaporation of water is reduced by a metal cover fixed on the mixer.

FACTORS INFLUENCING THE EIGENTSTRESS DEVELOPMENT

The factors influencing the development of eigenstresses around aggregates are numerous. Only those considered most important will be presented here. First of all the autogenous shrinkage and the stiffnesses of cement paste as well as that of the aggregate or sensor are of major influence. If just one of these parameters is negligible no stresses will be initiated. Thus the very early shrinkage of the cement paste will have no influence on the eigenstresses around an aggregate as the stiffness of the cement paste is not developed at this time.

The autogenous shrinkage of the cement pastes used in the tests was measured with the use of a dilatometer developed by [1].The results shown here are carried out at 30°C. The

results of the tests are shown as a function of time in FIG. - 1. The autogenous shrinkage measured 1 hour after start of mixing is used as point of zero shrinkage.

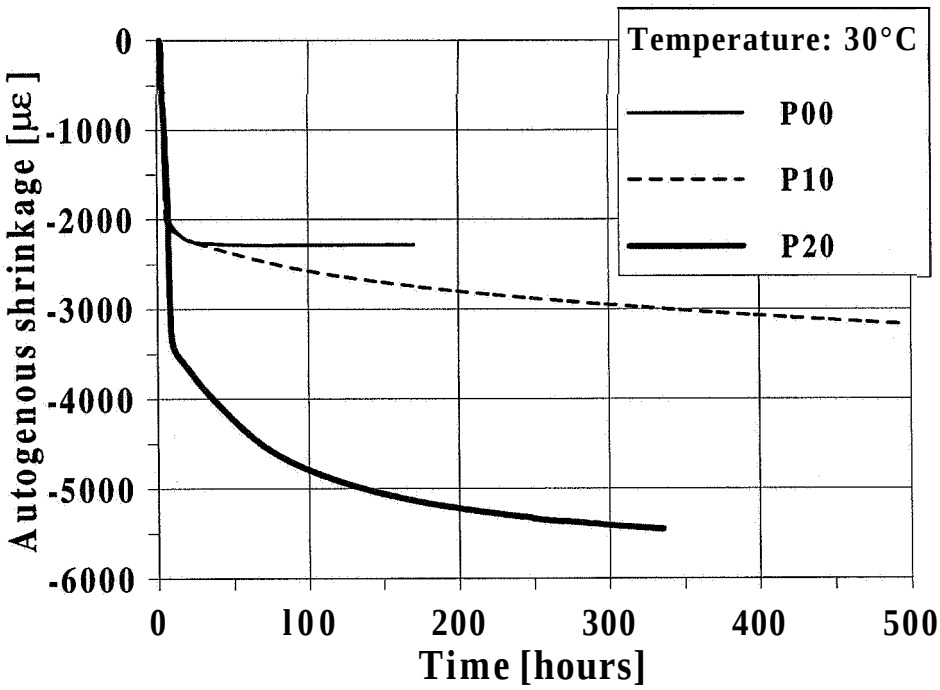

FIG. - 1 Autogenous shrinkage of cement paste containing 0%, 10%, and 20% microsilica, averages of two simultaneous measurements

As mentioned, development of eigenstresses due to shrinkage of cement paste is strongly linked to the stiffness of the cement paste. The stiffness of the cement paste containing 20% microsilica (P20), represented by the modulus of elasticity has been measured as a function of time. Experiments have been carried out in compression as well as in tension. The main part of the tests have been carried out in traditional compression tests on small cylinders (diameter: 25 mm, length: 50 mm (extensometer measuring range: 25 mm)). The specimen for these tests have been stored under sealed conditions at a temperature of approximately $25°C$. A smaller part of the tests have been determined in tension as a part of the loading procedure in relaxation tests. These tests have been carried out in a rebuild set-up in the TSTM (thermal stress testing machine) at TUDelft in the Netherlands. The specimen in this case has a diameter of 30 mm and a measuring range of 130 mm. The hardening temperature in the relaxation tests are $20°C$. The results from both kinds of tests as a function of time are shown in FIG. - 2. The difference in hardening temperature in the two kinds of tests have not been taken into account.

Results from tests similar to the compression tests mentioned above are presented in [2] for paste P00 and P10.

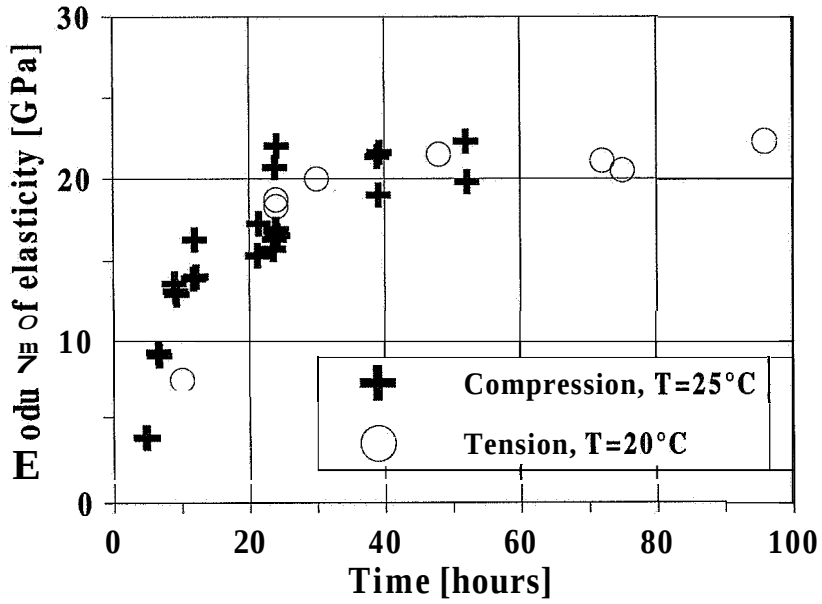

FIG. - 2 Modulus of elasticity of cement paste **P20** containing **20%** microsilica

Several other factors influence the development of eigenstresses. The stiffness of the aggregate or the sensor is as important as the stiffness of the cement paste. The stiffness of the sensor however, is complicated to determine through standard tests.

As the main part of the autogenous shrinkage of cement paste develops at early ages, the creep and relaxation has a big influence as well. Relaxation tests have been carried out during a 6 months visit at TUDelft. The results from these tests will not be presented in this paper, but reference is made to [3].

Among other important factors also the wall effect around the aggregate or sensor has to be mentioned. The interfacial transition zone (ITZ) has a higher water-cement ratio which influence the shrinkage and stiffness. It is still unknown how much the transition zone influence the stress development. However, investigations [4] have shown that the ITZ around aggregates has a significant influence on stress distributions and the overall elastic moduli of mortars.

EXPERIMENTAL OBSERVATIONS OF EIGENSTRESSES

Description of sensors and set-up

As mentioned two prototype sensors applying different methods for measurements have been developed. The first sensor is based on the use of a mercury thermometer. The mercury container of an ordinary laboratory thermometer has been shown to be a very simple and sufficiently accurate pressure sensor that can monitor the development in eigenstresses. The thermometer sensor is developed by Henrik Stang and is described thoroughly in [5]. The other sensor is based on changes in electrical resistance with changes in hydrostatic pressure.

This sensor is still under development as part of a Ph.D. project.

The basic idea of the thermometer sensor is to use a laboratory mercury thermometer as a pressure sensor for the determination of shrinkage related eigenstresses around an inhomogeneity like for instance an aggregate. A standard mercury thermometer consists of a glass container filled with mercury. The container is connected to a capillary class tube. Volume changes in the mercury due to temperature changes are then detectable as changes in position of the mercury surface in the capillary tube. Obviously, also volume changes of the glass container due to mechanical action like for instance external hydrostatic pressure can be detected as changes in mercury surface position and simultaneous changes in pressure and temperature can be measured if a second pressure independent temperature measuring device such as an electrical thermocouple is introduced in the system.

For the experiments described here a laboratory thermometer with a temperature range of 50°C and an accuracy of 0,1°C was chosen. The outer glass tube which is connected to the mercury container and which is protecting the capillary tube was removed by cutting close to the connection of the mercury container. Finally, the temperature scale which originally is connected to the outer protecting tube was fixed to the capillary tube.

The measuring device was calibrated for hydrostatic pressure in pressurised air in a small pressure chamber designed for this purpose. With this test the calibration factor relating apparent temperature change to hydrostatic pressure could be determined.

After calibration the sensors are placed in the centre of a container and cement paste is poured in. The container has a diameter of 100 mm and a height of 60 mm. Nothing was done to control the temperature during hardening. Next to the pressure sensor two electrical thermocouples are placed allowing for pressure independent temperature measurements during the hydration process as well as during long term testing. Immediately after casting the cement paste is covered with a thin layer of oil protecting the paste from evaporation of water. Thus, the cementitious matrix experiences only autogenous shrinkage and the temperature variation connected with the hydration process.

The basic observations consist of observed temperature differences between the modified mercury thermometer and the average of the two electrical thermocouples observed over a period of time after casting of the cement paste. Through the calibration factor the observed differences in temperature measured by thermocouples and thermometer can be translated to an equivalent hydrostatic stress state on the mercury container. In FIG. - 3 there is a picture showing how the outer protecting tube is removed from the mercury container of the thermometer sensor.

The other type of sensor uses a technique based on electrical measurements of resistance of a 0,05 mm manganin wire. Manganin is an alloy with an electrical resistance which depends on applied hydrostatic pressure. This property is used in the electrical sensor to

detect the hydrostatic pressure in a spherical inclusion embedded in cement paste undergoing shrinkage.

The sensor that has been used in the experiments shown in this paper consist of a solid porcelain sphere used in a ball mill. The diameter of the porcelain sphere is 20 mm. On the porcelain sphere, a 0,05 mm manganin wire is glued using the same kind of glue as that used for strain gauges. The ends are solded to a standard 1 mm copper wire and glued to the sphere. It is important to avoid leakage current in the electrical system since this will influence the measurements when placed in fresh cement paste. To reduce the risk of leakage current through the cement paste the manganin wire, the solding points as well as the copper wire was painted with a sealing paint. A calibration of the sensor gives the linear relation between pressure and resistance of the wire. The calibrations are performed in an oil filled pressure cell for pressures ranging from 0 to 300 bar. The ceramic sensor has an estimated stiffness in the range of that of granite (50-100 GPa).

The sensor was fixed in the centre of a container and cement paste was casted around it. To reduce the effects of changes in temperature in the tests with the porcelain sensor, the container was kept as small as possible. It had a diameter of 55 mm and a height of 70 mm. It is furthermore put in water at $20°C$. The temperature development was measured on a dummy without a sensor to avoid electrical noise from the thermocouple. The temperature reached a maximum of 23°C during hardening. The changes in resistance was determined with the use of an amplifier, and a datalogger saved the results on a PC. Figure 4 shows a drawing of the porcelain sensor.

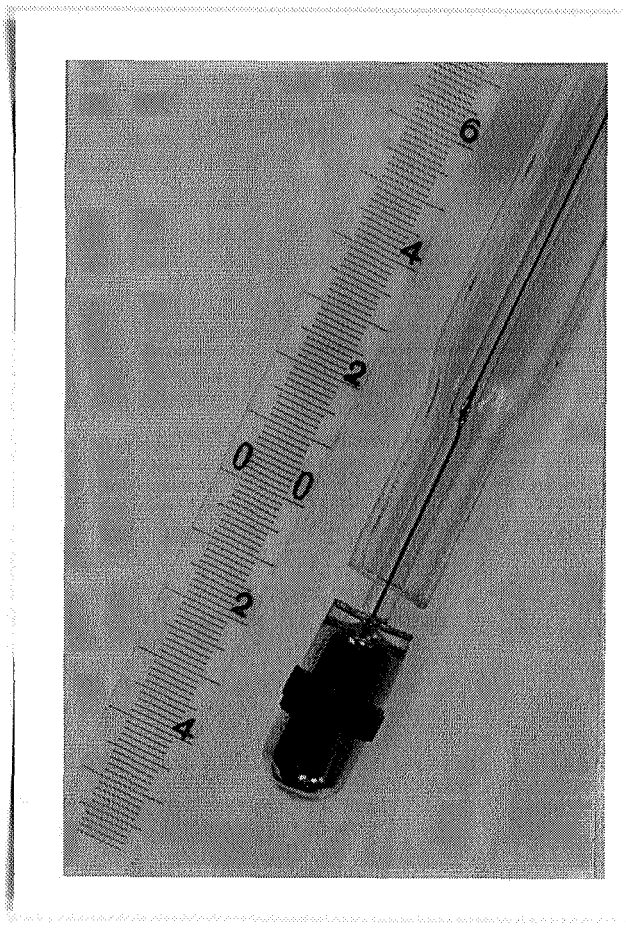

Skannad bild
Original fobot
utlånat till
Stig Dahlin
Bygg & Teknik
Box 19099
10432 STOCKHOLM
24 sept 1997

FIG. - 3 Picture of thermometer sensor

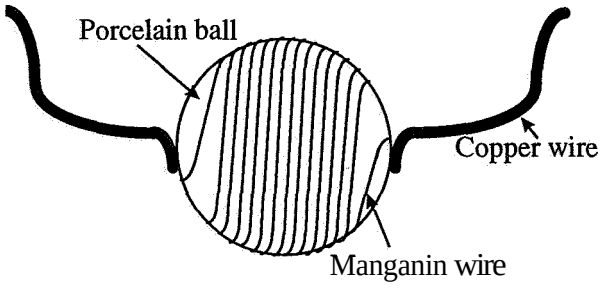

FIG. - 4 Drawing of sensor of porcelain

Test results

The tests with the thermometer sensors are carried out on paste without microsilica (P00) and with 10% microsilica (P10). The results from two independent tests with each paste type are shown in FIG. - 5. The results from the test using the porcelain sensor is shown in FIG. - 6. The paste in this case is P20.

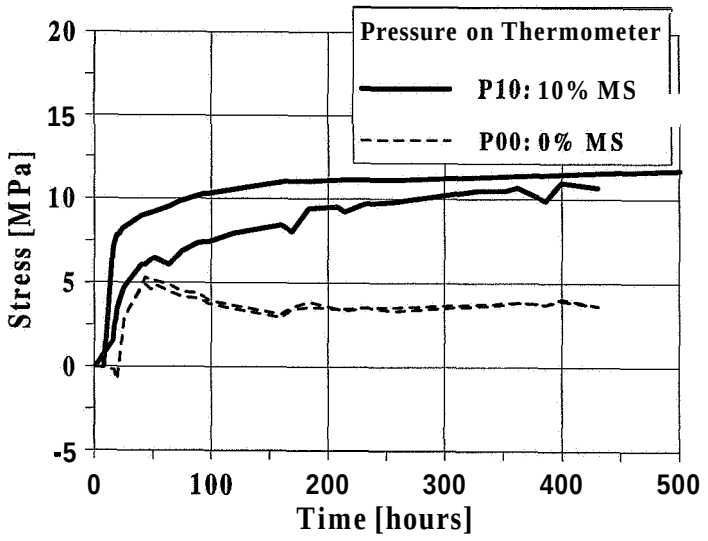

FIG. - 5 Experimentally observed eigenstresses in a thermometer sensor embedded in cement paste containing 0% microsilica and 10% microsilica. The figure shows two tests with each paste type

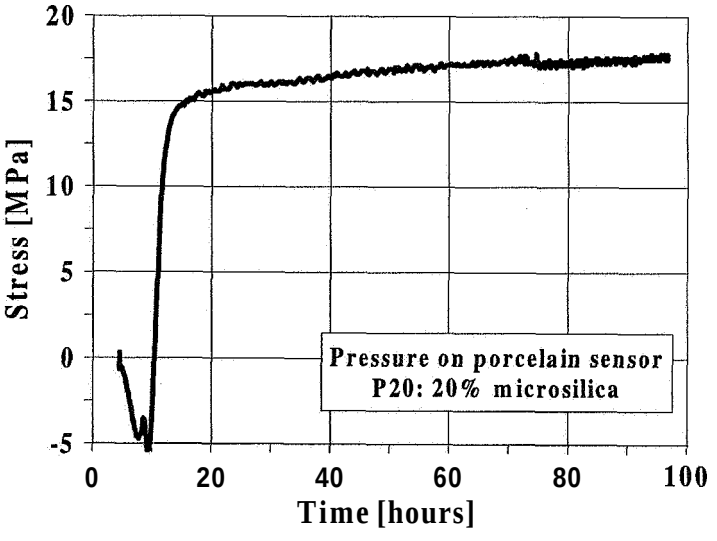

FIG. - 6 Experimentally observed eigenstresses in a spherical porcelain sensor embedded in cement paste containing 20% microsilica

DISCUSSION

The autogenous shrinkage as presented in FIG. - 1 show a clear increase in autogenous shrinkage with increase in content of microsilica. It is important to note that mix P20 is not based on the same types of materials as mix P00 and P10. Comparison should therefore be

carried out with care. The trends in the results are clear though. The paste P00 without microsilica only show autogenous shrinkage in the first 50 hours after mixing. The paste P10 and P20 both continues the autogenous shrinkage although the rate decreases with time.

The autogenous shrinkage and the development in modulus of elasticity as shown for paste P20 in FIG. - 2 gives a indication of when and how the eigenstresses develops. As the modulus of elasticity only starts to develop after setting, no stresses will be build up at this time. This means that the initial shrinkage corresponding to the steep slopes in FIG. - 1 will not have any influence on the stress development. For the paste P00 the development of eigenstresses is expected to stop before 50 hours. Due to creep and relaxation, the stresses might decrease or even disappear with time. For the pastes P10 and P20 the stresses are expected to be higher than for P00.

These expectations are clearly met by the results shown in FIG. - 5 and FIG. - 6. Obviously, the initiation of eigenstresses starts around 10-20 hours after mixing. This is clearer for the porcelain sensor whereas the results from the thermometer sensor are more ambiguous at this time. Nevertheless, the thermometer sensor show the trends as expected regarding the difference in autogenous shrinkage of paste P00 and P10. Cement paste P00 build up stresses of approximately 5 MPa at 50 hours. After this time the stresses decrease until an almost constant stress of 3-4 MPa. The drop in stresses is expected to be due to visco-elastic behaviour of the paste. There is quite some difference in the two measurements on paste P10. However, the tendencies are the same. As for P00 the stresses are mainly build up within the first 50 hours after casting, but unlike P00 the stresses continue to increase. At 500 hours the pressure on the mercury container in the paste P00 is 4 MPa, whereas it has reache d 12 MPa in paste P10.

The equivalent modulus of elasticity of the thermometer sensor which is an ellipsoidal shell of glass is estimated at 17 GPa. This is less than that estimated of the massive porcelain sensor which is 50-100 GPa. Also the shrinkage of cement paste P20 used in the tests with the porcelain sensor is higher, thus it is to be expected that the stresses measured with the porcelain sensor will be higher than those measured on paste P10 with the thermometer sensor. Figure 6 verifies the expectations with a pressure of 18 MPa at 100 hours. The measurements with the porcelain sensor are negative in the first hours. As the amplifier was balanced before pouring the cement paste the negative values in the curve can be explained by leakage current in the electrical system leading to a decrease in resistance as long as the paste is water saturated.

Leakage current in the electrical system is one of the main problems in the development of the electrical sensor. The problems will hopefully be solved with time so that more measurements on the eigenstresses can be carried out - also with the presence of neighbouring aggregates.

CONCLUDING REMARKS

The results presented in this paper can be summarised in the following concluding remarks:

- The test results presented is this paper show that it is possible to measure eigenstresses in an inclusion with the use of sensors as those presented here.
- The tests are carried out on two sensors using completely different measuring techniques which verify that the stresses measured in the tests are reliable regarding the size.
- The differences in autogenous shrinkage of the different types of paste result in different eigenstress levels.
- More work and more tests have to be carried out with the porcelain sensor to refine the measuring technique.

ACKNOWLEDGEMENT

Special thanks to Mr. F. Schilderpoort at Concrete Structures, TUDelft for his patience and good ideas when making the porcelain sensor.

REFERENCES

[1] O.M. Jensen. A dilatorneter for measuring autogenous deformation in hardening portland cement paste. Materials and Structures, 28:406–409, 1995.

[2] B. F. Dela. Shrinkage cracking in high strength concrete (in danish). Master's thesis, Building Materials Laboratory; Technical University of Denmark, July 1994.

[3] B. F. Dela, L. F. Nielsen, and H. Stang. Eigenstresses in hardening concrete. In Brittle *Matrix* Composites 5 *(BMC5)*, 1997. Under preparation.

[4] G. Ramesh, E.D. Sotelino, and W.F. Chen. Effect of transition zone on the pre-peak mechanical behavior of mortar. In Ken P. Chong and F. Asce, editors, Materials for the new millennium, pages 1238–1245, New York, USA, 1996. ASCE.

[5] S. Stang. Significance of shrinkage induced clamping pressure in fiber-matrix bonding in cementitious composite materials. Advanced Cement Based Materials, 4:106–115, 1996.

AUTOGENOUS VOLUME CHANGE OF CONCRETE AT VERY EARLY AGE MODEL AND EXPERIMENTAL DATA

ADRIAN RADOCEA
Department of Building Materials
Chalmers University of Technology
412 96 Gothenburg, Sweden

ABSTRACT

Experimental results (Sellevold et al 1994, Radocea 1996) show that high strength and high performance concrete is highly sensitive to early cracking. One of the causes of cracking is plastic shrinkage that arises when the concrete mass is exposed to early drying. It has also been reported that concrete with a low water to binder ratio can develop cracks at early ages, i.e. before thermal cracking, even when early drying is prevented (Sellevold et al 1994). There is therefore good reason to suppose that the origin of cracking in such cases is autogenous shrinkage.

The aims of this paper are to discuss the mechanism of autogenous shrinkage, to make an inquiry into the test methods and to show the influence of curing conditions on autogenous volume change at very early ages.

NOTATION

A_T	total surface (m^2)	t	time (s)
A_G	surface of gas	V	concrete volume (m^3)
A_S	surface of solids	V_G	gas volume (air and water vapour in bubbles and microcracks)
A_W	surface of water		
B	coefficient of permeability (s)	V_c	chemical shrinkage (m^3)
g	gravitational constant (m/s)	Φ	angle of internal friction
K	coefficient	ρ	density of concrete (kg/m^3)
P	water pressure (Pa)	ρ_w	density of water (kg/m^3)
P_G	gas pressure (Pa)	σ	stress on solid particles (Pa)

INTRODUCTION

Cement reactions give rise to a reduction in the volume of the cement plus water system. Autogenous volume change of concrete can then be defined as external volume change caused by this reduction.

The first step in the attempt to predict cracking or to reveal the factors resisting cracking is to understand the mechanism of volume change, that is, to investigate a possible relationship between chemical shrinkage of paste and autogenous volume change of concrete.

This paper tries to partially elucidate some of the problems involved when studying autogenous volume change of concrete at very early ages, i.e. when the paste undergoes a transition from plastic to stiff state. It is therefore quite legitimate to try to answer the following questions:

1. Are there any relationships between:
   - cement reactions and the volume reduction of cement paste
   - the volume reduction of paste and the external volume change of concrete?
2. Does the volume reduction of paste always cause an external volume reduction of concrete?
3. Are the test methods suitable for studying the above mentioned relationships?
4. Has the consistency of paste any influence on the experimental results?
5. Has a plastic paste the capacity to move a large aggregate?
6. Is there any difference between horizontal and vertical deformation?
7. Are the measurements influenced by the boundary conditions and dimensions of the sample?
8. Why is autogenous shrinkage significant only for concrete of low water to cement ratio in spite of the fact that chemical shrinkage does not depend on water to cement ratio?

DEFINITIONS

Cement related reactions:

1. ***Solution:*** the dissolved solid materials occupy less total space in solution than when in the solid condition.
2. ***Adsorption:*** the adsorbed water molecules are more densely packed than the molecules of free water.
3. ***Hydration:*** the silicates and aluminates bind water.

Chemical shrinkage denotes the contraction of the cement+water system only during hydration (chemically bound water has higher density than free water). At very early ages, solution and adsorption can also be included in chemical shrinkage.

Depending on factors such as the dimensions of the sample, boundary conditions and curing conditions, cement reactions can give rise to the following phenomena:

1. ***Autogenous shrinkage of paste*** (ASP) = External volume change of the paste.
2. ***Self-desiccation*** (SD) = Cement reactions consume the pore water. This results in development of pores filled with air and water vapour when water movement to or from the paste is prevented.
3. ***Imbibed water*** (IW) = When water movement to the paste is permitted, a part of the water consumed by cement reactions can be replaced by water coming from the water cured surface.

ASP and SD appear at the same time in sealed samples, while in water cured samples all three phenomena can appear at the same time. Actually only IW can be isolated when very small samples of paste are in contact with excess water, see TABLE-1.

TABLE-1

Phenomenon	Sealed samples	Water cured samples	
		very thin samples	large samples
autogenous shrinkage of paste	YES	NO	YES
self-desiccation	YES	NO	YES
imbibed water	NO	YES	YES

Autogenous volume change of concrete (AVCC) can be defined more precisely as external volume change caused by autogenous shrinkage of paste.

All these four phenomena have a common physical explanation, namely the decrease of pore water or capillary pressure in cement paste. This decrease in pore water pressure causes:

1. Consolidation of solid material (the distance between cement grains decreases)
2. Water movement
3. Development of gas or water filled pores.

One of the problems we must take into account when studying AVCC at very early age is that, during the period of plasticity of the paste, the pore water pressure is of the same order as the stresses due to the dead weight of concrete. Therefore, the stress conditions of a plastic concrete are influenced by dead weight, pore pressure and of course by the boundary conditions. In hardened concrete, the stresses due to the dead weight are very small in comparison with the pore pressure, and the dead weight can be neglected.

TEST METHODS

The most usual test methods are shown in FIG.-- 1.

D method, which uses the dilatometer, measures chemical shrinkage. Geiker 1983 showed that the rate of chemical shrinkage corresponds to the rate of chemical reactions when the thickness of the sample is small. In thick samples, and especially at low water

to cement ratios, dP and dx (see FIG.-1) become large and the bottom of the sample is unsaturated with water. The main problem of this test method is that it demands visual observations which are difficult to follow at very early ages.

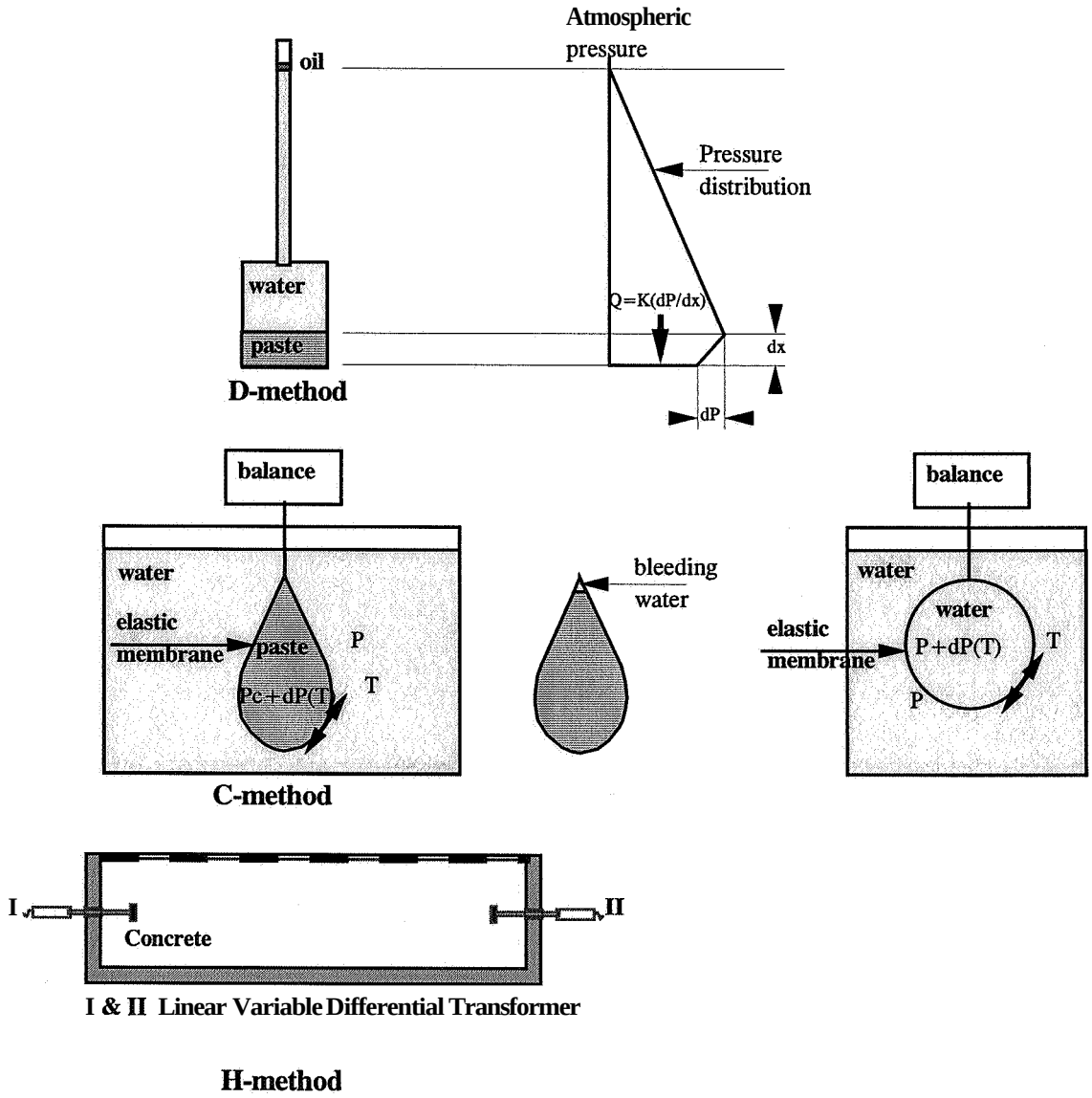

FIG.-1 Test methods

C method measures the change in weight of an elastic membrane filled with cement paste and submerged in a water bath. Sellevold et al 1994 showed that, before the formation of gas filled pores, there is good agreement between chemical shrinkage determined with the D method and the volume change of the elastic membrane. The forces involved in the process are shown in FIG.-1. It is interesting to notice that the tension T of the membrane makes a water filled elastic membrane have a spherical shape. This corresponds to the condition that in this case T must be equal at every point of the membrane. The change in volume that is measured at the movable boundary of the sample is caused by a decrease in the pore pressure Pc and dP(T). The main problem of this method is the difficulty to distinguish the imbibition of bleeding water (see FIG.-1)

from real volumetric change. Furthermore, the experimental results in FIG.-2 show that, during the first two hours, the change in volume is mainly produced by the difference in temperature between paste and water in the water bath.

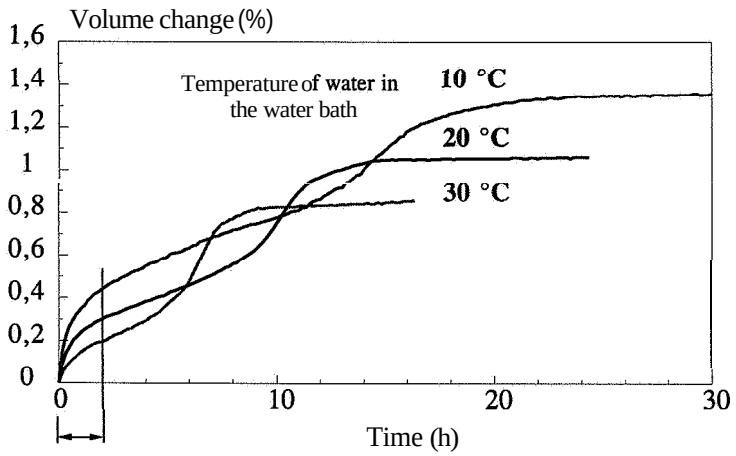

FIG.-2 Influence of the temperature of the water bath on the volume changes of paste with W/C=*.*0.24 and 8 % silica fume, SRPC cement of type Degerhamn.

H ***method*** measures the horizontal displacement of a small plate placed in a concrete sample. The dimensions of the plate are usually of the same order as those of a larger aggregate. This method gives controversial results and therefore needs a profound analysis, see next section.

INVESTIGATION OF H METHOD

The origin of controversy is the lack of agreement between the D and H methods. As can be seen in FIG.-2, the D method indicates a continuous volumetric reduction of the paste, while the H method can give results such as in FIG.-3, where the displacement of the plate indicates a horizontal swelling of the sample during the first 5 hours. It is rather obvious that the concrete sample cannot swell because the vertical walls of the container are fixed. How can we then explain that sometimes the displacement of the plate indicates swelling instead of shrinkage?

The behaviour of plastic concrete, where the solid particles have great mobility in relation to each other, is characterised by:

1. pressure against the vertical wall
2. chemical shrinkage, which is three dimensional, is partially transformed into vertical deformation

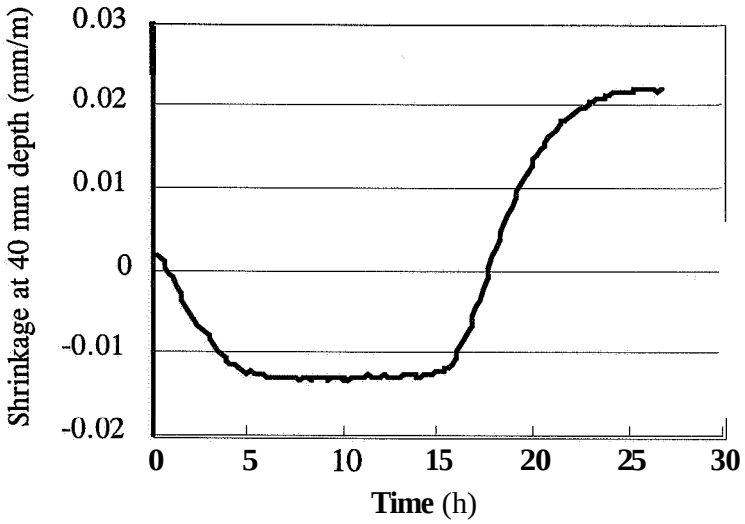

FIG.-3 Horizontal shrinkage at **40 mm** depth of a sample of high performance concrete

Pressure against the vertical wall

The stress conditions at the vertical wall of a sample container are described by the diagram in **FIG.-4.** When the vertical surface of concrete is immobile, the horizontal stress on the solid particles at a given depth is proportional to the vertical stress at this depth:

$$\sigma_x = K\sigma_z \qquad (1)$$

The coefficient K can be expressed as a function of the angle of internal friction:

$$K = 1 - \sin\Phi \qquad (2)$$

which means that the horizontal stress is dependent on the workability of concrete.

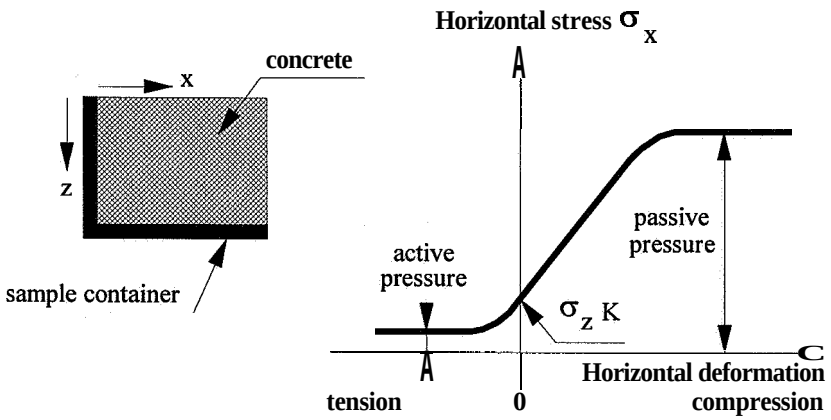

FIG.-4 Stress conditions at the vertical wall of the sample container, after Sallfors 1995.

Horizontal shrinkage can occur only if the horizontal stress on the vertical surface of concrete exceeds $\sigma_z K$. Since no external forces act on the concrete mass, we may assume that the equilibrium of stresses that produce a volume change can be described by the following equations:

$$s_z \frac{As}{At} + P\frac{Aw}{At} + P_G\frac{Ag}{At} = \rho g dz \qquad (3)$$

$$\sigma_x \frac{As}{At} + P\frac{Aw}{At} + P_G\frac{Ag}{At} = 0 \qquad (4)$$

The vertical surface of concrete at the boundary has to satisfy equation (4) only after the beginning of horizontal shrinkage.

Radocea **1997** showed that the horizontal shrinkage at a distance dz starts when the water pressure exceeds a certain value given by the following equation:

$$P > -\frac{K}{1-K}\rho g dz \frac{At}{Aw} \qquad (5)$$

Pore water pressure and pressure against the vertical wall (see FIG.-5) were determined by using the arrangement shown in FIG.-6.

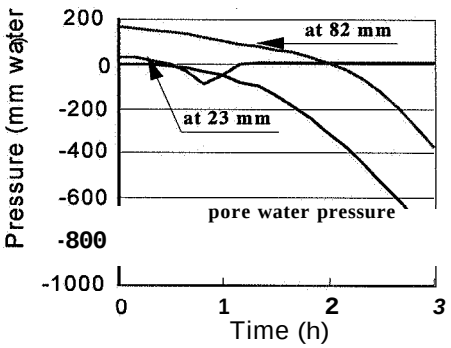

a. Indoor conditions (low rate of evaporation)

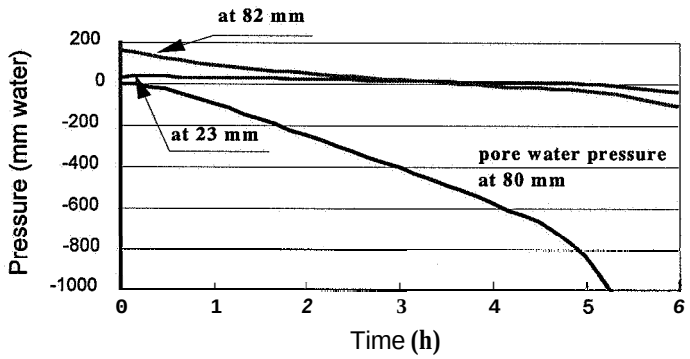

b. Sealed curing

FIG.-5 Pore water pressure and pressure against the vertical wall in a sample of high performance concrete **(w/c=0.3).**

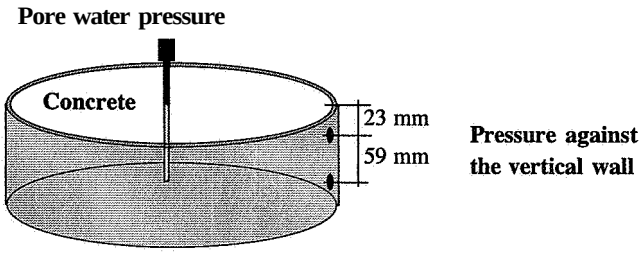

FIG.-6 Arrangement for measurements of pore water pressure and pressure against the vertical wall.

The diagrams in FIG.-5 show the following:

1. There is a proportionality between the pore pressure and the pressure against the vertical wall; this confirms equation (4).
2. When the upper surface of the sample is exposed to evaporation (approx. 0.15 kg/m^2 h), the pressure against the wall becomes zero after 40 minutes at 23 mm and after 2 hours at 82 mm. These are the times when shrinkage starts at these two levels.
3. When early drying is prevented, the pressure against the wall does not become zero for almost 5 hours, which means that the sample cannot shrink during this time.
4. The decrease in pore water pressure in the sealed sample is lower than when evaporation is permitted.
5. There is however a decrease in pore pressure of the sealed sample, and this must cause movement of water and rearrangement of the solid particles.

Rearrangement of cement grains, aggregates and other objects situated inside the sample during the period of plasticity of concrete has to fulfil two conditions:

- local vertical and horizontal displacements depend on the local stiffness of concrete, packing and size of aggregates being determining factors
- only the upper surface of the sample can move downwards.

Vertical deformation versus horizontal deformation

The diagram in FIG.-7 shows that, during the first 5 hours, chemical shrinkage is transformed into purely vertical deformation.

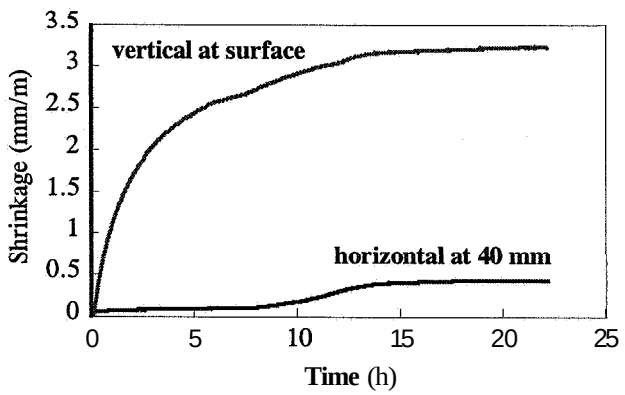

FIG.-7 Vertical and horizontal autogenous shrinkage. w/c=0.3.

After this investigation we may conclude that:

1. There is agreement between the *C* and H methods, but, in order to demonstrate this, the vertical movement of the upper surface of the sample must be determined during the period of plasticity of concrete.
2. The direction of horizontal movement of large solid particles during the period of plasticity depends on the local stiffness of concrete.

AUTOGENOUS VOLUME CHANGE OF NORMAL AND HIGH PERF'ORMANCE CONCRETE

Autogenous shrinkage and development of pore pressure in normal and high performance concrete (HPC) are shown in FIG.-8. The diagrams give a reasonable answer to the question why the autogenous shrinkage of high performance concrete is much larger than that of normal concrete.

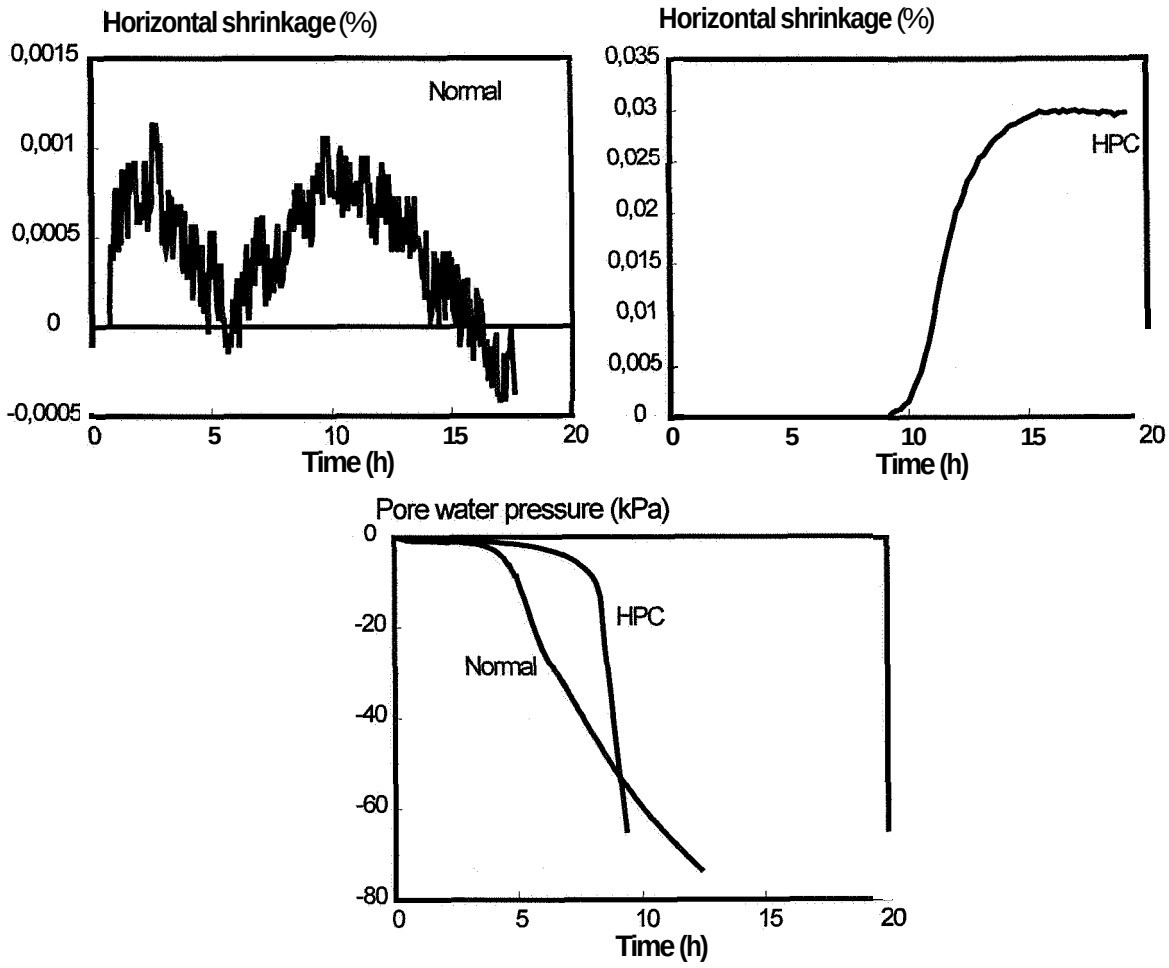

FIG.-8 Autogenous shrinkage and pore pressure in normal and high performance concrete (w/c=0.3).

The shrinkage of normal concrete is insignificant (only 2 to 3 times larger than the noise of the LVD transformer). This is due to the fact that the development of pore pressure occurs too late; the structure of concrete is strong enough to resist stresses of this order.

The development of pore pressure in high performance concrete is even later, but it is important to consider the retardation caused by a high amount of superplasticizer. In this case, when the amount of superplasticizer was 1,5 %, the concrete was still plastic after 6 hours. The pore pressure develops just in time to produce significant autogenous shrinkage.

A possible conclusion is that if high performance concrete could be mixed without superplasticizer, the autogenous shrinkage would also be insignificant.

MODEL OF AUTOGENOUS SHRINKAGE OF CONCRETE AT EARLY AGE

Radocea 1997 developed a model that describes the rate of total volumetric reduction as a function of chemical shrinkage V_K, pore pressure P and the volume of gas filled pores V_G:

$$\frac{dV}{dt} = \frac{dV_K}{dt} - \frac{1}{r_w}\frac{\partial}{\partial z}\left(B\frac{\partial P(z,t)}{\partial z}\right) - \frac{dV_G}{dt} \qquad (6)$$

V_K and V_G have to be determined for every combination of binder and superplasticizer. The C method gives both dV_K/dt and dV_G/dt.

An arrangement for measurements of pore pressure is shown in FIG.-9.

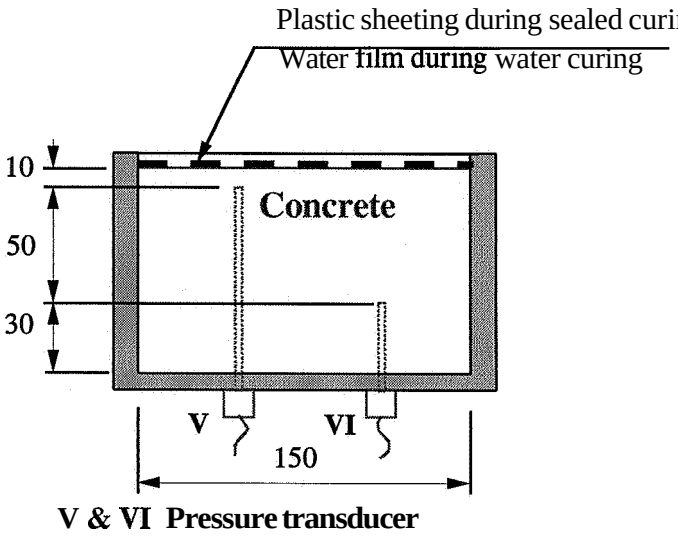

FIG.-9 Arrangement for measurements of pore water pressure in samples of concrete (PVC container 150x150x100 mm)

EXPERIMENTAL RESULTS

The development of negative water pressure and length change in sealed samples of concrete are shown in FIG.-10 and FIG.-11 respectively. An insignificant difference was detected between the water pressure at 10 and 60 mm below the concrete surface. It can be observed that the high rate of pressure change begins a little earlier than the high rate of shrinkage. This can be explained by a higher concrete temperature in the samples placed in the PVC container (see FIG.-12).

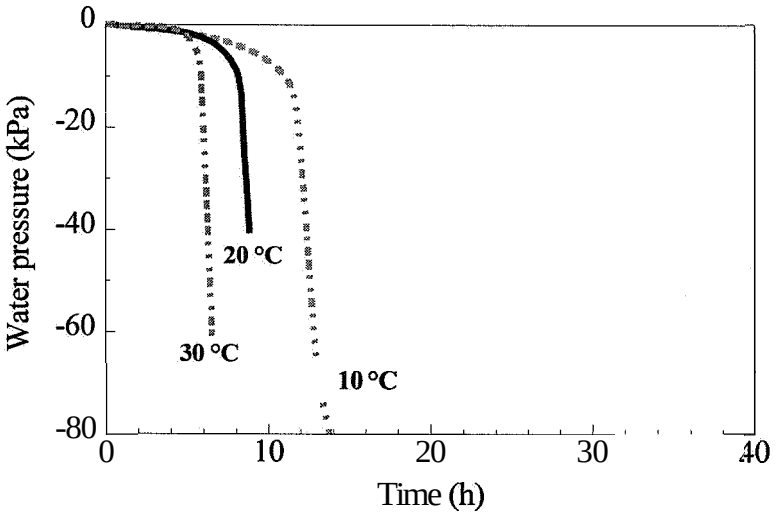

FIG.-10 Development of water pressure in sealed samples of concrete (w/c=0.3)

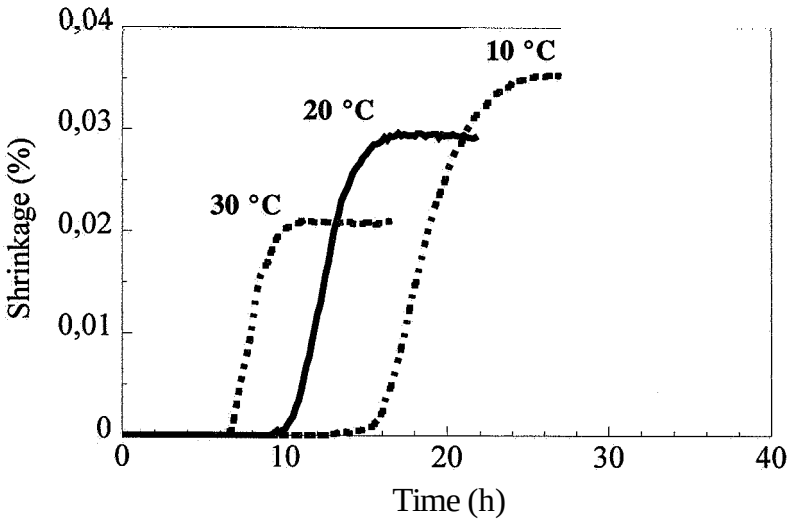

FIG.-11 Length change at 40 mm depth in sealed samples of concrete (w/c=0.3)

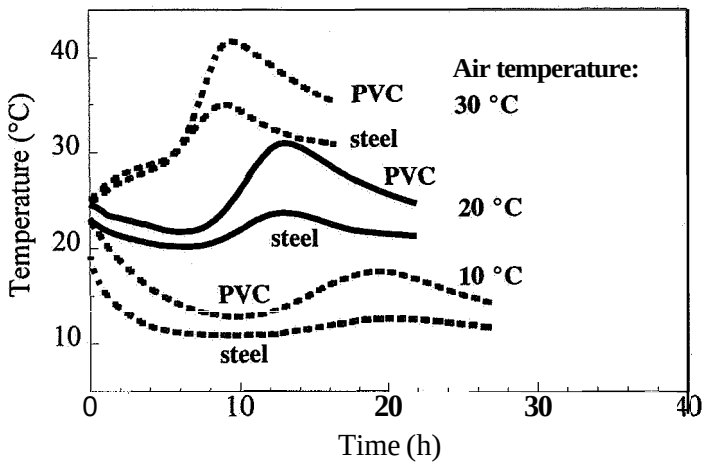

FIG.-12 Temperature development in sealed samples of concrete (w/c=0.3)

The diagram in FIG.-11 indicates that differences in temperature cause significant differences in shrinkage . It is also interesting to observe that the length reduction takes place in spite of an increase in the temperature of concrete.

If the curves in FIG.-11 are multiplied by a factor 3 (to transform the one-dimensional shrinkage into a volumetric reduction) and by a factor 0.3 (which represents the volume of paste per cubic metre of concrete), the shrinkage of concrete determined with the H method can be compared with autogenous shrinkage of paste determined with the C method. The agreement between these two methods is shown in FIG.-13.

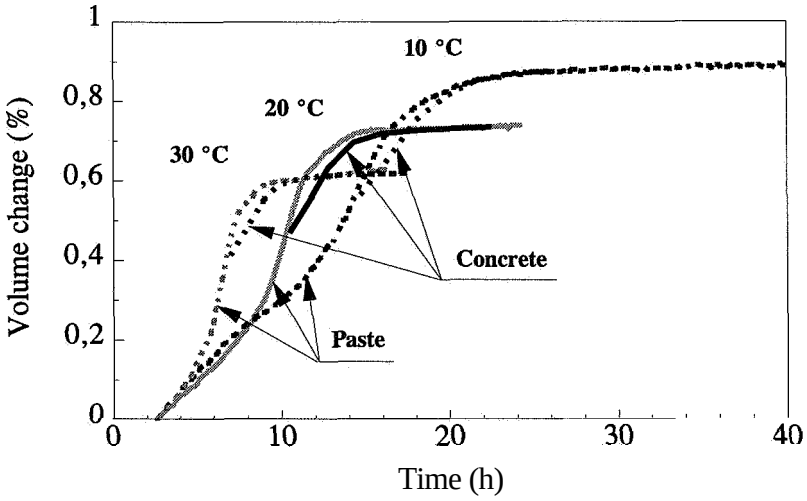

FIG.-13 Comparison between autogenous shrinkage of paste and concrete (w/c=0.3)

The development of water pressure and length change in water cured samples is quite different from that in sealed samples (see FIG.-14-16).

If the pore water pressure at the water cured surface is considered to be zero, the development of water pressure at 10 and 60 mm depth (see FIG.-14) indicates that the increase in pressure before the break through pressure at 60 mm is proportional to the distance from the water cured surface. This means that we may assume that the distribution of additional water is also proportional to the distance from the surface.

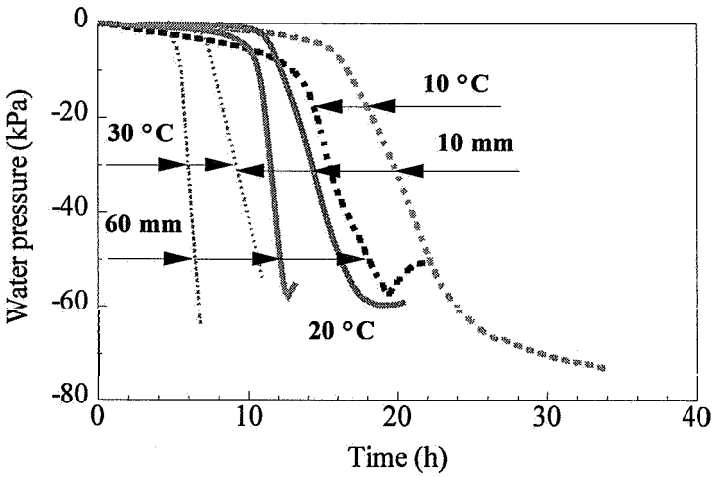

FIG.-14 Development of water pressure in water cured samples of concrete (w/c=0.3)

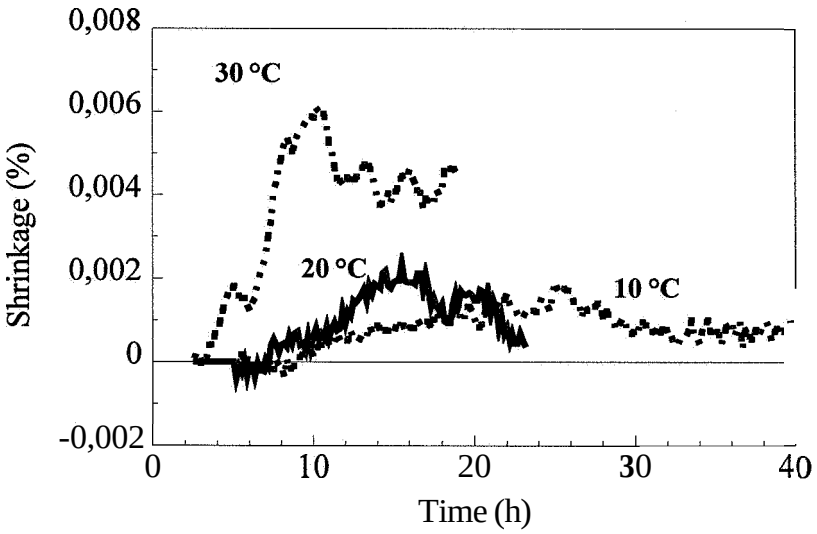

FIG.-15 Length change of water cured samples of concrete (w/c=0.3)

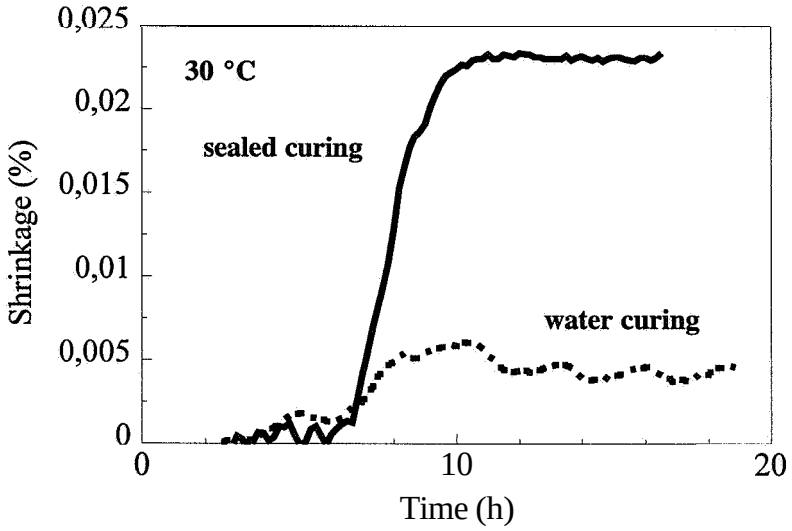

FIG.-16 Comparison between sealed and water cured samples of concrete (w/c=0.3) at 30 °C

The amount of additional water (see FIG.-17) corresponds to the development of water pressure. This, together with the fact that the length change at 40 mm diminishes when the samples are water cured, confiis the proposed model according to which autogenous shrinkage is equal to the difference between contraction and the amount of additional water before the formation of gas filled spaces.

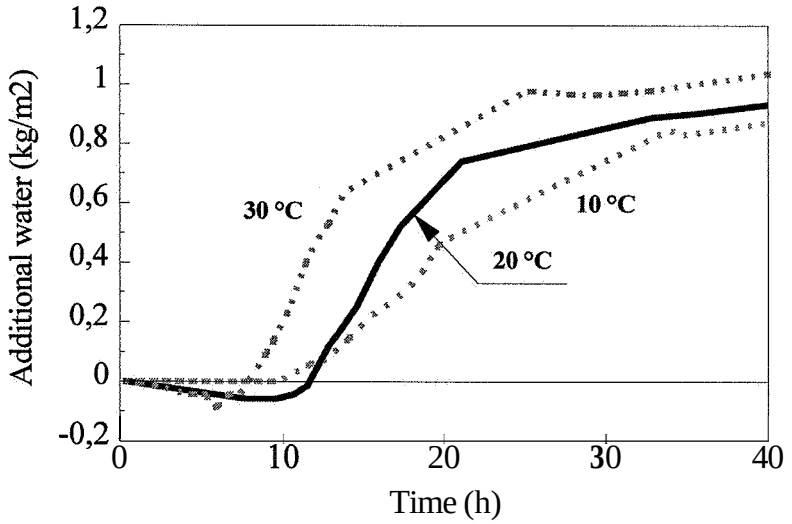

FIG.-17 Amount of additional water in concrete (w/c=0.3)

During the period of constant rate of pressure change (approximately between 10 and 60 kPa), the flow of additional water is almost constant. By using the results shown in FIG.-10-17 and equation (6), the coefficient of permeability during this period could be calculated (see TABLE-2). It was assumed that at negative pressures in the range -10 to -60 kPa, the volume change is three times the length change, i.e. shrinkage is equal in all three directions.

TABLE-2 Coefficient of permeability (10^{-11} s)

	Air temperature during curing ("C)		
Water pressure (kPa)	**30**	**20**	**10**
10	18	15	8
60	3	2.5	1.5

CONCLUSIONS

1. Equation (6) describes the relationship between autogenous shrinkage of concrete, chemical shrinkage, pore water pressure and the development of gas filled spaces.

2. At the beginning of the process of autogenous shrinkage, when concrete is plastic, chemical shrinkage causes only a vertical deformation of the sample. This behaviour implies movement of pore water and rearrangement of solid particles. During this period the direction of horizontal displacement of large solid particles inside the sample does not always correspond to a volumetric reduction. In other words, the horizontal shrinkage of a sample starts when the pressure of the concrete against the vertical wall becomes zero.

3. Experimental results obtained by using the investigated test methods are consistent.

REFERENCES

Bjontegaard O., Makro-opprissing av brudekker i fersk fase, Department of Structural Engineering, NTH, Trondheim.

Geiker M, Studies of Portland Cement Hydration, Institute of Mineral Industry, Technical University of Denmark, 1983.

Jensen O.M. and Hansen P.F., A dilatorneter for measuring autogenous deformation in hardening Portland cement paste, Materials and Structures, Vol. 181, 1995.

Kronlöf A. et al, Experimental Study on the Basic Phenomena of Shrinkage and Cracking of Fresh Mortar; Cement and Concrete Research, Vol. 25, No. 8, 1995.

Radocea A., A study on the mechanism of plastic shrinkage of cement-based materials, PhD thesis, CTH Goteborg, 1992.

Radocea A., Volume changes and cracking of high performance concrete at very early age (confidential report in Swedish), CTH Goteborg; 1996.

Radocea A, Autogenous volume change of concrete at very early age, accepted for publishing in Magazine of Concrete Research, 1997.

Sellevold E. et al, High performance concrete: early volume change and cracking tendency, Proceedings of RILEM symposium on Thermal cracking in concrete at early ages, Munich 1994.

Sallfors G., Geophysics (in Swedish), 1995.

Tazawa E. and Miyazawa S., Autogenous shrinkage caused by self desiccation in cementitious material, 9'' International Congress on the Chemistry of Cement, New Delhi, pp 712-718, 1992.

EXPERIMENTAL INVESTIGATION OF SELF-DESICCATION IN HIGH-PERFORMANCE MATERIALS - COMPARISON WITH DRYING BEHAVIOUR -

Véronique BAROGHEL-BOUNY
Laboratoire Central des Ponts et Chaussées,
58 Bd Lefebvre, F-75732 Paris cedex 15, France

ABSTRACT

This paper presents some experimental results about self-desiccation of ordinary and (very-) high-performance (HP) cement pastes and concretes. The HP materials tested in this study have a very low water-to-cement ratio and they contain silica fume and superplasticizer. Self-desiccation, occuring in hydrating materials, is here characterized by the measure of internal relative humidity and autogenous strains. High-Performance materials exihibit strong self-desiccation along their ageing. For example, the internal relative humidity reaches the value RH = 72% in the HP concrete tested here, within six months. This strong self-desiccation of HP materials is also shown by the high autogenous shrinkage measured on these materials (205.10-6, within six months for the HP concrete tested), compared to ordinary materials. A linear relationship is exhibited between internal relative humidity and autogenous shrinkage, for each mix, illustrating the range where these deformations can be considered as self-desiccation shrinkage. Drying shrinkage results of the hardened materials, as a function of relative humidity, are also presented and compared, in the high RH range, with self-desiccation shrinkage data, showing roughly similar values. In this study, a particular regard is given to point out the similarities and the differences of behaviour between ordinary and high-performance materials (mixed with silica fume).

Key-words: Cementitious Material, High-Performance Concrete, Silica Fume, Relative Humidity, Self-desiccation, Autogenous Shrinkage, Drying Shrinkage, Total Deformations, Experimental Study.

1 - INTRODUCTION

Recent researches yield to think that high-performance (HP) concretes have an enhanced durability compared to ordinary concretes, due to their compactness. Their finer pore structure and hence their reduced permeability and diffusivity (to gaseous and liquid phasis), and also their

lower calcium hydroxide content, compared to ordinary materials, offer a better resistance to water and aggressive agents ingress. Moreover, their smaller mean pore radius diminishes the freezing temperature of pore water, which can induce a better frost resistance. The low water content of these materials can also be an advantage to prevent them from alkali-reaction, for example.

But, the early and marked self-desiccation (internal drying due to cement hydration) of HP materials can have other positive or negative effects on real structures. For example, the particularly high autogenous shrinkage of these materials, when it is hindered, can generate tensile stresses which can induce micro- or macro- cracking. And early age cracking is able to affect mechanical properties and also to reduce the efficiency of durability properties of HP materials. Besides, as a result of self-desiccation and of fine pore structure, the hygral behaviour of HP hardened materials is modified, compared to ordinary materials.

Therefore, in order to be able to take into account the effects of self-desiccation in the prediction of the behaviour of concrete structures, in particular for delayed deformations, and to use suited HP mixes, it is necessary to study accurately the self-desiccation process, its origins and the mix-parameters influence.

The aim of this paper is to contribute, on the basis of a set of experimental results, to give a complete description of the self-desiccation features of high-performance materials, compared to ordinary materials. A comparison is also made with the drying behaviour of the hardened materials.

2 - MATERIALS

In this study, two cement pastes and two concretes are tested. The mix compositions of the different materials are given in table 1. The mixes CO and BO correspond to ordinary materials, while CH and BH, mixed with a low water-to-cement ratio (W/C) and which contain silica fume (SF) and superplasticizer (SP), are (very-) high-performance materials. The materials are prepared with a French type I OPC (CEM I) from Le Teil. The cement chosen (cf. table 2) is rich in C3S (57.28%) inducing high strength at early age, and has a low C_3A content (3.03%), which goes to give a good workability, despite low water-to-cement ratio (low need of water, for this cement). The cement has a Blaine fineness of 342 $m^2.kg^{-1}$. The silica fume, added as dry powder, is from Laudun (France). Its B.E.T. specific surface area is 17.6 $m^2.g^{-1}$ (measured by nitrogen adsorption). The superplasticizer is a formaldehyde-naphtalene sulfonate copolymer. Concretes are prepared with limestone aggregates (maximum size : 20 mm).

The 28-day compressive strength of the high-performance concrete BH is 115 MPa. For the ordinary concrete BO, the value is 49 MPa.

TABLE 1
Composition of mixes (mass proportions)

Mix	W/C	Additives	Aggregate/C	Sand/Gravel
CO	0.34	-	-	-
CH	0.19	SF/C=0.10 and SP/C=0.018	-	-
BO	0.48	-	5.48	0.62
BH	0.26	SF/C=0.10 and SP/C=0.018	4.55	0.51

TABLE 2
Mineral composition of the cement

C_3S	57.28 %
C_2S	23.98
C_3A	3.03
C_4AF	7.59
gypsum	4.39
$CaCO_3$	1.84
free CaO	0.53
Na_2O eq.	0.48

3 - INTERNAL RELATIVE HUMIDITY

The internal relative humidity of a material is the relative humidity (RH) of the gaseous phasis in equilibrium with the interstitial liquid phasis, in the pore network of the material.

Cement hydration processes consume water molecules. This induces a liquid water content decrease in cementitious materials while the microstructure is hardening and the pore structure is refining (development of gas/liquid menisci in the pore network and of depression in the pore water). From a given hydration degree of the cement and depending on the initial water content (more generally on the mix parameters), the material exhibits self-desiccation (internal drying). It means that the material undergoes a decrease of its internal relative humidity, when it is not in contact with an external moisture supply. However, it can be noticed that, in the case of HP materials (mixed with SF), as a result of their compactness, the core of samples can undergo self-desiccation even if the samples are under wet external conditions [1), 2)].

The internal RH decrease can be measured continuously in laboratory on hydrating samples protected from moisture exchange with the surroundings and stored at constant temperature (method first applied by Copeland and Bragg [3)]). Here, the measurement is made with samples enclosed immediately upon casting into sealed cells. Each cell contains a RH-probe (a capacitive sensor with an accuracy of ± 1% RH) previously calibrated with saturated salt solutions over the whole range of RH. And, in order to verify the validity of long-term measurements and the fiability of the RH-probes, some limited measures have been also performed and compared to continous measures [4)].

Some values of internal RH, measured continously by RH-probes at T = 21 ± 0.5 °C with the mixes CO, CH, BO and BH, are reported in table 3, as a function of the age of the materials.

TABLE 3
Internal RH-values measured continously by RH-probes at T = 21 ± 0.5 °C,
as a function of the age of the materials

	Internal RH (%)			
Age	CO	CH	BO	BH
28 days	97	88.5	97	77.5
50 days		84.5	96.5	76
2 months		83	96	75.5
3 months		81.5	95.5	74.5
6 months		80	95	72
1 year	90.5	80	94	69

Our results, for cement pastes as well as for concretes, are in very good agreement with the RH-values given in the literature.

For example, RH = 75% was found by Buil for a 50-day concrete containing silica fume and with W/C = 0.26 [5]. And for a concrete with W/C = 0.44, the value given by the author was RH = 97%. These values are to be compared with RH = 76% obtained at the same age with the concrete BH, and RH = 96.5% found for the concrete BO. Persson[2] found RH ≈ 80% at the age of 28 days and RH = 76% at the age of 3 months (values read on the published figures), for a concrete similar to BH (RH = 77.5% and RH = 74.5%, respectively). He found RH ≈ 97% at the age of 28 days and RH ≈ 95% at the age of 3 months, for a concrete not very different from BO (RH = 97% and RH = 95.5%, respectively).

For a cement paste with W/C = 0.2 and SF/(C+SF) = 0.08, Sellevold and Justnes found RH = 77% within 1 year [6]. The value found here for CH at the same age is RH = 80%. The results from Wittmann reported by Buil[7] are RH ≈ 99% and RH ≈ 94% for 28-day cement pastes with W/C of 0.4 and 0.3, respectively. The value of RH = 97% found here for the cement paste CO (W/C = 0.34) within 28 days seems therefore correct, given the likely differences in the cement used.

Self-desiccation depends on mix-parameters. First, it depends on cement type (main influence of the fineness, C3A content, alkali content [8], [4]). Furthermore, it increases with the decrease of the "efficient" initial water content (role of parameters like W/C, or effective water-to-binder ratio W/[C+k.SF], or water-to-solid ratio, ...), other paramaters (for example the cement) being constant.

In the case of classical materials (W/C ≈ 0.5), self-desiccation remains low. Thus, RH = 95% is reached within 6 months and RH = 94% is reached within 1 year with BO.

High-Performance materials (mixed with SF) exhibit intense self-desiccation. And this self-desiccation process starts very early. The RH decrease measured in CH and BH is particularly high in the two first months. For example, the RH-values reached in the concrete BH are RH = 75.5% within 2 months, RH = 72% within 6 months, and RH = 69%. within 1 year. In HP materials, at a given age, self-desiccation is increased both by lowering W/C and by increasing SF/C. The effect of each of these parameters has been widely studied by Jensen and Hansen (see for example [9], [10]) and also by other authors (see for example [11], [4], [2]). In particular, the marked effect of SF probably includes :

- filler effect of the fine SF particles : addition of SF gives a finer mixture and afterwards, a finer pore structure, generating lower internal RH according to Kelvin-Laplace law (and higher depression in the pore water). The pozzolanic reaction increases this effect. It refines the pore structure still further (calcium hydroxide crystals replaced by C-S-H gel) and consumes a lot of water molecules at least by adsorption (C-S-H have a high specific surface area and an intrinsic porosity of 28% [4], [12]), thus reducing the free water content available for chemical reactions.
  The central role of the pozzolanic reaction on the internal RH decrease is pointed out in [9],
- the fine SF particles act as nucleation sites for crystallization, inducing acceleration of hydration reactions of the cement, at early ages and in particular with high W/C [4], [9].

For all of the mixes and more particularly for the ordinary materials, the experimental results show that self-desiccation continues along several months.

For durability of reinforced concrete concerns, it is necessary to mention that strong self-desiccation can favorize penetration of fluids, from the environment through the possible cracks but also through the pore network (capillary suction effect, for example). These agents can be aggressive for concrete or rebars (water containing chloride ions, for example). Nevertheless, only the surface layer of the structure is concerned if there is no macrocracking and if intrinsinc porosity and permeability of the material are low (inducing very slow transfer processes), which is the case with the most HP concretes.

Besides, as a result of their strong self-desiccation, which drives their internal RH to a value close to the average RH of common environmental media, and of their fine pore structure (low diffusivity), HP materials are fairly insensitive to environmental hygral variations over a wide range of RH.

It is necessary also to keep in mind that the internal RH depends on the composition of the interstitial liquid phasis. The internal RH is influenced by dissolved salts. Thus for example, as previously said, the alkali content of usual cements induces RH ≈ 97% instead of RH = 100% at saturated state, due to dissolution of alkalies in the interstitial liquid phasis. And depending on their concentration in the liquid phasis, different ions can induce still further lower RH-values in concrete [13), 4)]. It can be given, as an illustration, the internal RH-values measured (in the experimental conditions previously described) with hydrating samples of paste CO mixed with different NaCl contents (0, 1.5 and 3% NaCl by mass of cement). The results obtained, as a function of the age of the materials, are reported in table 4.

TABLE 4

Internal RH-values measured with CO mixed with different NaCl contents, as a function of the age of the materials (NaCl is expressed in %, by mass of cement)

	Internal RH (%)		
Age	CO	CO+ 1.5% NaCl	CO+ 3% NaCl
7 days	100	97.5	96
28 days	97	86	82
3 months	95	82	78.5
6 months	93	80.5	76
1 year	90.5	< 79	≈ 75

Likewise, the internal RH measured with the concrete BO mixed with 3% NaCl by mass of cement is RH = 92% at 7 days (RH = 100%, without NaCl) and RH = 86% at 6 months (RH = 95%, without NaCl).

The moisture properties of cementitious materials are therefore modified by the presence of NaCl [14)]. And this effect increases with the ion concentration, all of the other parameters being constant. This point is of importance towards the behaviour of concrete structures exposed to marine environment or to deicing salts. Thus, for example, ingress of NaCl into concrete decreases the internal RH of the material. And hence increases the suction effect previously described (areas of low internal RH make easier water and ions penetration from the environment into the material). In some cases, this phenomenon can increase concrete or reinforcement degradations.

Not only the cement, but also the other components of the material influence the chemical composition of the interstitial liquid phasis, like SF or admixtures. Thus, although the specific

influence of admixtures on internal RH is not studied here, it can be noticed that their composition (see for example the alkali and chloride contents given in table 5 for the superplasticizer used in this study) gives to think that admixtures, when used in non-negligible amounts, can decrease the internal RH of the material.

TABLE 5
Alkali and chloride contents (in %) of the superplasticizer used

Content (in %)	
Chlorides	Na_2O eq.
0.22	13.49

4 - AUTOGENOUS SHRINKAGE

In order to assess one-dimensional autogenous shrinkage of the materials tested here, length change is measured on samples, demoulded at the age of 1 day, wrapped in two adhesive aluminium foil sheets (to avoid moisture exchange [4), 15)]) and stored at the constant room temperature T = 21 ± 0.5 °C. The measurement is performed with classical dial gauges (with an accuracy of 10 μm/m) on 4x4x16cm samples for cement pastes and on 7x7x28cm samples for concretes. The absence of evaporation is checked by weighing the samples.

The values of one-dimensional autogenous shrinkage (mean values of three samples) measured as a function of the age of the materials are given in FIG.-1, for the mixes CO, CH, BO and BH.

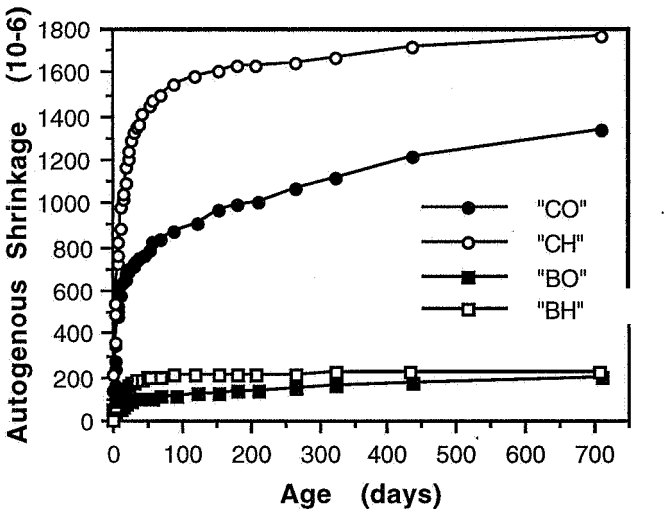

FIG.-1. One-dimensional autogenous shrinkage measured at T = 21 ± 0.5 "C, versus the age of the materials

The strong self-desiccation of HP materials is here pointed out by the early and high autogenous shrinkage measured on these materials (205.10-6, within 6 months for the HP concrete tested), compared to ordinary materials.

The autogenous shrinkage values measured with the HP concrete can be compared to those given by Persson for a similar concrete [16)]. The comparison shows a good agreement on the results obtained (cf. table 6).

TABLE 6
Experimental values of autogenous shrinkage compared to'values obtained by Persson[16] (read on the published figures)

	Autogenous shrinkage (10^{-6})	
Age	Exp. data	*Persson[16]*
28 days	170	≈ 150 - 200
3 months	205	≈ 250
1 year	220	≈ 250 - 300

Our results are also included in the range 130 - 250.10-6 reported in [17] for long-term autogenous shrinkage values of HP concretes with silica fume.

As a result of the presence of aggregate particles, strains measured on concretes are smaller than strains of cement pastes, as for drying shrinkage (cf. § 6). This is due to the reduction of the cement paste content (where the strains are originated) and to the stiffness of the aggregates which restrain shrinkage. A complex stress-state is generated in concrete. Therefore, it is difficult to exhibit a direct relationship between deformations in concrete and in cement paste. But, modelling based on the composite rule (assuming concrete as a two-phasis model where aggregates are dispersed as inclusions in a cement paste matrix) has been proposed by different authors to calculate long-term autogenous shrinkage of concrete from that of the matrix (see for example [18]).

5 - CORRELATION BETWEEN INTERNAL RELATIVE HUMIDITY AND AUTOGENOUS SHRINKAGE

Autogenous strains of cement pastes and concretes are originated by physical and chemical processes linked to hydration reactions. Free external autogenous strains have different components : Le Chatelier contraction due to the smaller volume of hydration products (C-S-H, calcium hydroxide, ...) compared to those of the reactants water and anhydrous phasis, thermal deformation due to the exothermal hydration of the cement, swelling strains induced by the crystallization of ettringite and calcium hydroxide, and self-desiccation shrinkage which occurs when capillary pores begin to empty.

With the mixes tested here, no swelling is exhibited from the initial time (1 day). And, the self-desiccation shrinkage becomes after a given time the main component of autogenous strains, the other components being efficient only at early age. This is proved in particular by the very good correlation which is pointed out in a given range between the autogenous shrinkage and the internal RH of the materials tested. FIG.-2 (respectively FIG.-3) illustrates for the pastes CO and CH (respectively for the concretes BO and BH), the linear relationship existing between autogenous shrinkage and internal RH, measured as previously described, from 28 days until around 6 months.

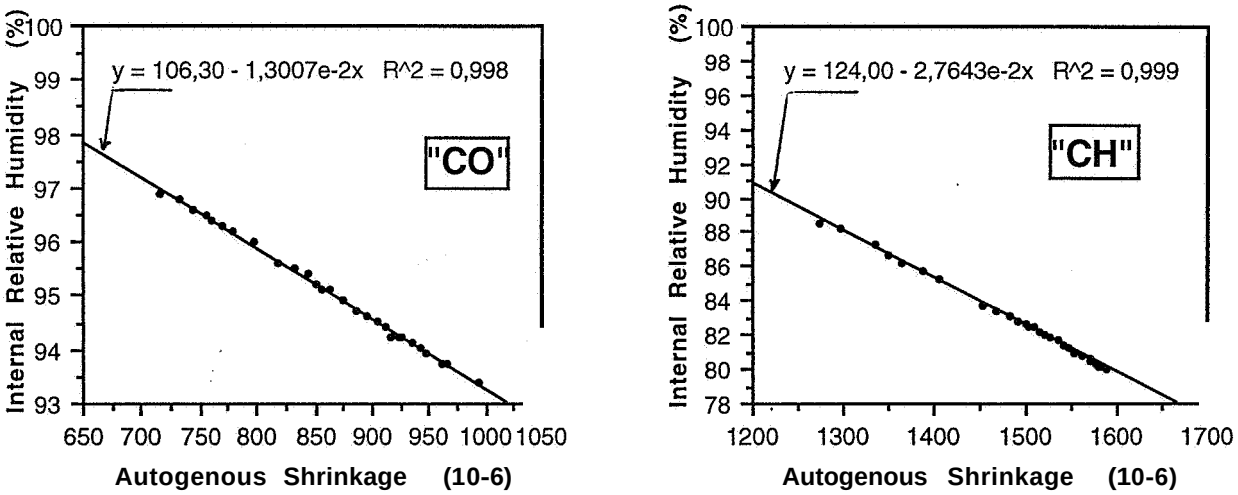

FIG.-2. Correlation between the autogenous shrinkage and the internal RH of the cement pastes, measured at T = 21 ± 0.5 "C, from 28 days

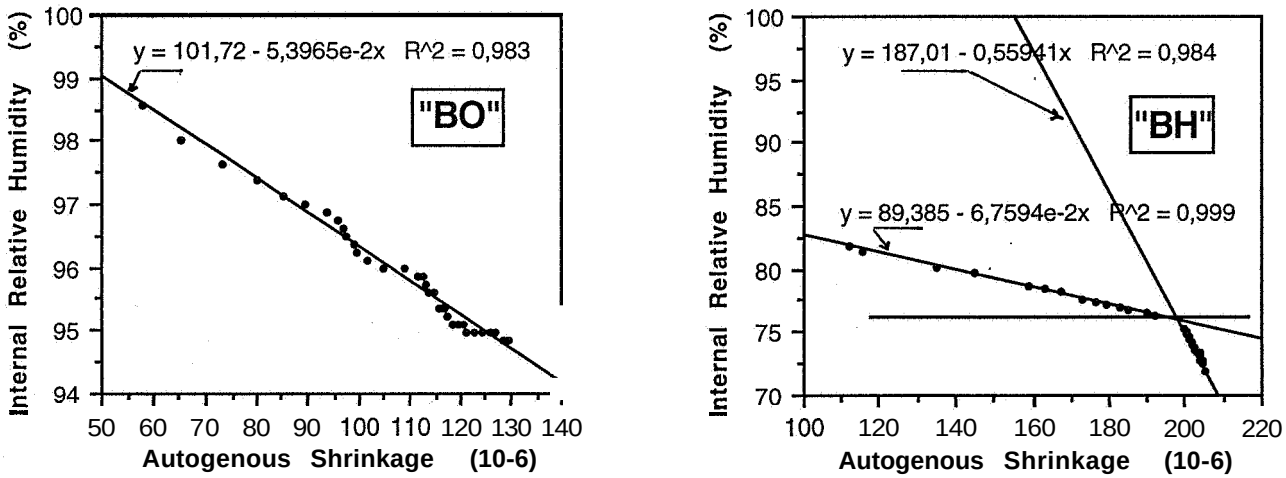

FIG.-3. Correlation between the autogenous shrinkage and the internal RH of the concretes, measured at T = 21 ± 0.5 "C, from 28 days

The decrease of internal RH (self-desiccation), inducing for example capillary tension variations, is therefore in the range where the linear relationship exists (for example from 28 days), directly at the origine of the measured long-term autogenous strains. This gives the range where autogenous strains are only due to the transformation of the liquid pore water into chemically bound water and can be considered as self-desiccation shrinkage.

Given the linear relationship existing between self-desiccation shrinkage and internal RH, same influence of mix-parameters is expected on this skrinkage as on internal RH (cf. § 3). In particular, both lowering W/C and increasing SF/C induces higher self-desiccation shrinkage. Thus, for example, the self-desiccation shrinkage measured on BO represents 55% of the value measured on BH (at a given age, between 28 and 90 days).

With the concrete BH, a sharp change of the slope of the straight correlation line occurs at RH = 76%. Since equilibrium at RH = 76% means that pores with $r_p > 50$ Å are empty, and since the value $r_p = 50$ Å corresponds to the beginning of the C-S-H gel pores [4), 12)], therefore, below RH = 76%, the RH decrease results in the removal of water adsorbed on C-S-H hydrate. In this low

RH range, with low "capillary" water content, it is difficult to assume that capillary tension variation is the main origin of the measured deformations. Other mechanisms become probably prominent. Nevertheless, deformations remain correlated to RH change.

Moreover, the self-desiccation results obtained for BH show that the limiting RH-value which indicates a stop of hydration reactions, whatever the amount of unreacted cement, is lower than what it was previously thought (RH ≈ 80% for Powers and Brownyard[19] in 1948, RH ≈ 75% for Atlassi [8] in 1991 and Jensen[20] in 1995). Nevertheless, the value of RH ≈ 75% proposed in the literature corresponds very well to the change of slope of the straight line on our graph. This means that the self-desiccation process can go on, even when "capillary" pores are empty. When "capillary" water is lacking, the chemical reactions are probably slowed down, but unreacted cement particles (or the unreacted core of cement particles), more hydrophilic than hydrate, use adsorbed water from hydrate (or hydrated ring of the cement particles) to continue their hydration 4).

6 - DRYING SHRINKAGE

Besides the "internal" drying of hydrating cementitious materials, let us consider now the "external" drying process of hardened materials, in order to make a comparison.

"External" drying occurs in hardened cement paste (hcp) or concrete when the material is submitted to a lower environmental RH than its internal RH. This phenomenon occurs at the surface zone of a lot of civil engineering concrete structures. Water movement (evaporation at the surface) induces deformations of the material (drying shrinkage). The relationship between RH and this volume change is well established for a long time. It was first formulated mathematically by Powers[21), 22)]. But, although drying shrinkage of hcp has been extensively studied for several years and though a lot of models have been proposed (for the last ten years 1987-1997, see for example [23), 24), 25), 26), 27), 28)]), this property is not yet well understood and remains not easy to predict.

Since Powers, three major mechanisms have been proposed to explain the experimental behaviour of hcp : capillary tension (in pores where menisci are formed due to loss of water), surface free energy (which depends on the amount of adsorbed water) [29)], and disjoining pressure (developed in a narrow place where adsorption is hindered) [30), 29), 31)]. Besides, Feldman and Sereda showed the importance of the movement of interlayer water in C-S-H on drying-wetting deformations [32)]. However, how each of these basic mechanisms is involved in the process and what are the combined effects of the different mechanisms over the entire RH range are not well known at the present time.

In order to assess one-dimensional drying shrinkage of the hardened materials tested here, diameter-length change is measured, as a function of RH, on l-year-old thin (2-3 mm thick, 10 mm diameter) specimens, during water vapour desorption experiments performed at the constant temperature T = 23°C. There are not many such data on cement-based materials reported in the literature. Some of the first results on hardened cement pastes were published by Feldman[33)] in 1968.

The diameter-length of the discs is here measured by means of dial gauges which have an accuracy of one micrometer. A gauge is put on each disc at the begining of the test and is no more displaced for the whole duration of the experiment.

"Equilibrium" values of the deformations can be calculated by taking as reference the diameter-length measured at RH = 100% or at RH = 90.4%, for each RH step along the desorption process until RH = 12% or RH = 3%, depending on the progress of the experiment.

RH = 90.4% can appear to be more relevant as reference than RH = 100% in order to limit possible self-desiccation effects on first drying shrinkage. Moreover, there is big difficulty to obtain accurate experimental values at RH = 100%, given the great influence of temperature and the possible occurence of sudden and massive water condensation.

The values of one-dimensional drying shrinkage (mean values of experimental data measured on the same set of three specimens) calculated by taking the diameter-length at RH = 90.4% as reference are reported in table 7 and in FIG.-4, for the four mixes CO, CH, BO and BH.

It has to be noted that, due to the small deformations of the concretes and to the capability of the gauge, it was difficult to have a good accuracy in the measures for these last materials, especially below RH = 53.5%.

TABLE 7

One-dimensional drying shrinkage as a function of RH, obtained by desorption at T = 23 °C on the hardened materials, and calculated by taking the diameter-length at RH = 90.4% as reference

	Drying shrinkage (10^{-6})			
RH (%)	CO	CH	BO	BH
90.4	0	0	0	0
80.1	733	500	157	186
71.5	1170	818	297	231
63.2	-	1249	419	-
53.5	2118	1635	663	351
44	-	2241	-	-
33	2810	2528	644	417
22.8	-	2820	-	-
12	3690	3399	679	496
3	4237	-	-	706

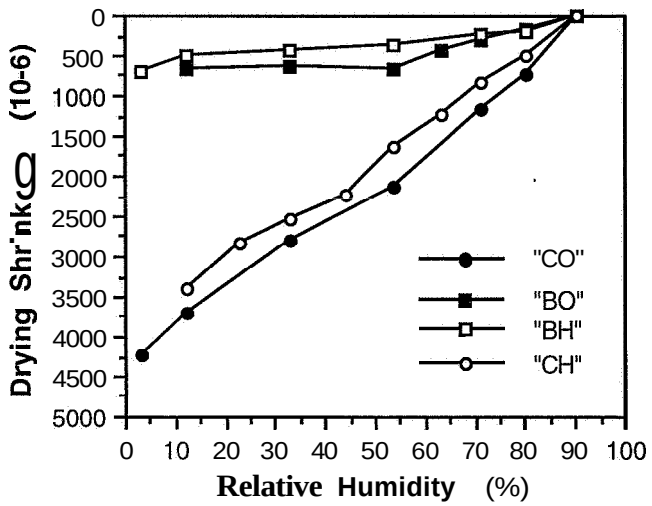

FIG.-4. One-dimensional drying shrinkage versus RH, obtained by desorption at T = 23 °C on the hardened materials, and calculated by taking the diameter-length at RH = 90.4% as reference

Measuring strains relative to small RH steps on thin specimens presents some advantages. First, it is possible to obtain "equilibrium" values at a given RH with reasonable kinetics. Secondly, the conditions of this test are close to stress-free deformations and therefore to the "real" fiee deformations of the material, at a given RH. These "real" fiee deformations are greater than the strains measured on samples exhibiting surface cracking as a result of high moisture gradients due to the large dimensions of the samples or to the width of the imposed RH steps.

It is interesting to compare the experimental results obtained on hcp CO with the results published by Ferraris and Wittmann in 1987, about the drying shrinkage of a 28-day-old cement paste with W/C = 0.3, measured at T = 20°C [31]. The length changes measured by Ferraris and Wittmann are reported in table 8. The values reported are read on the published figures.

TABLE 8
One-dimensional drying shrinkage as a function of RH, obtained by desorption at T = 20°C on a 28-day-old cement paste with W/C = 0.3 [31]

RH (%)	Drying shrinkage (10^{-6})
90.4	0
80.1	1500
53.5	2000
33	3000
12	3500

A very good agreement is pointed out with these values, below RH = 80.1%. The higher value registered by Ferraris and Wittmann at RH = 80.1% can be perhaps attributed to the young age of the paste, and to the different W/C. In this range of RH, the strains measured can result of both self-desiccation and external drying.

Likewise, Feldman[33] found with a l-year-old hcp (W/C = 0.5) a drying shrinkage value around 5500.10-6 (read on the published figures), between RH ≈ 90% and RH ≈ 0%, which is consistent with the value around 4200.10-6 found here with CO (W/C = 0.34) in the same range.

FIG.-4 shows that drying shrinkage of HP materials is lower than drying shrinkage of ordinary materials. The first is about 70% of the last, when the reference is taken at RH = 90.4%. However, this result is due to a different behaviour restricted to the high RH range. Thus, if deformations are calculated by taking the diameter-length at RH = 12% as reference, it can be seen, for example for the hcp CO and CH, that drying shrinkage versus RH is roughly linear and identical for the two hcp, at least for RH ≤ 80.1% (this value corresponds to the internal RH measured in sealed conditions at the age of 1 year for CH) (cf. FIG.-5).

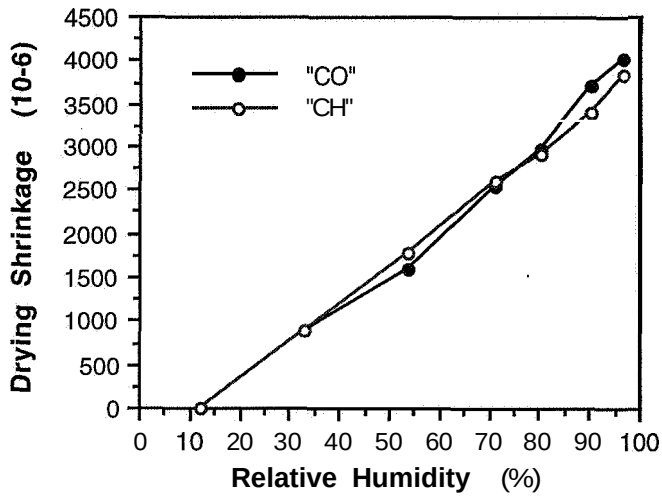

FIG.-5. One-dimensional drying shrinkage versus RH, obtained by desorption at T = 23 °C on the hcp CO and CH, and calculated by taking the diameter-length at RH = 12% as reference

7 - COMPARISON BETWEEN SELF-DESICCATION SHRINKAGE AND DRYING SHRINKAGE

Autogenous shrinkage data can be plotted versus RH, on the same graph as drying shrinkage data. Of course this comparison is only possible in the range where self-desiccation occurs in a given material, and therefore in the high RH range. Moreover, this range is wider in the case of HP materials.

In order to compare the two kinds of shrinkage, the values are calculated by taking, for each mix, the reference-length at the same RH for both autogenous and drying shrinkage (it corresponds to the higher value experimentally available in both cases). The results are presented in FIG.-6, where the solid lines express autogenous shrinkage, whereas the dotted lines express drying shrinkage, for the four mixes CO, CH, BO and BH.

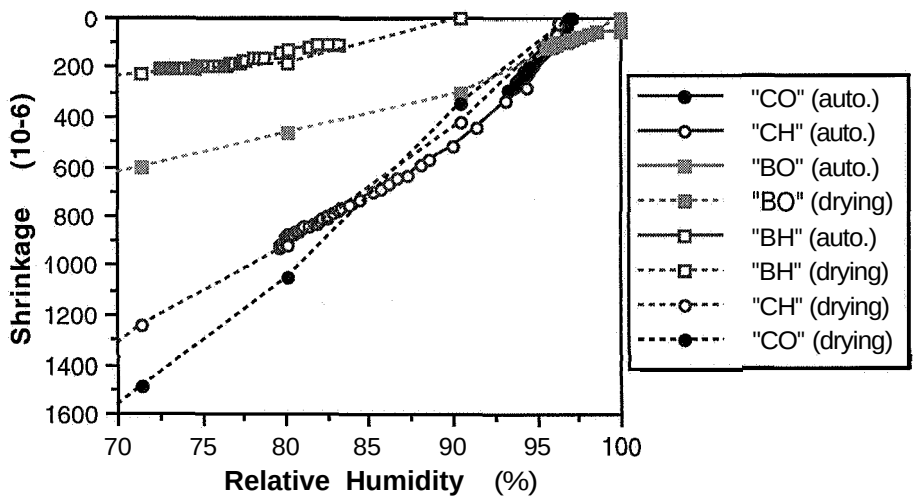

FIG.-6. One-dimensional autogenous and drying shrinkages versus RH, calculated by taking, for each mix, the reference-length at the same RH for both shrinkages

For each mix, the autogenous and drying shrinkage curves seem to roughly correspond. Furthermore, autogenous shrinkage can be assumed here to be self-desiccation shrinkage (cf. § 5). Therefore, similar relationship between RH and self-desiccation shrinkage or drying shrinkage is experimentally obtained.

Self-desiccation shrinkage data (cf. § 4 and 5) can be compared more precisely to drying shrinkage data (cf. § 6) obtained in the same RH range and with the same mix. "Estimated" values (*) of self-desiccation shrinkage of ordinary mixes can be given to complete the comparison until RH = 80.1% where experimental values can't be obtained. These "estimated" values are calculated from the linear relationship existing between self-desiccation shrinkage and internal RH (cf. § 5) for each mix. The results are given in table 9 for the four mixes CO, CH, BO and BH.

TABLE 9
Comparison between self-desiccation shrinkage and drying shrinkage

	Shrinkage (10^{-6})			
Mix	$\varepsilon_{self.}$ 97% --> 90.4%	ε_{drying} 97% --> 90.4%	$\varepsilon_{self.}$ 90.4% --> 80.1%	ε_{drying} 90.4% --> 80.1%
CO	400 (28d/1y)	345	792 (*)	733
CH	440 (6d/21.5d)	422	500 (21.5d/1y)	500
BO	>110 (28d/2y)	≈200	191 (*)	157
BH		-	140 (1d/15d)	186

(*) : "estimated" values (cf. § 5)

In a given RH range, the values of self-desiccation shrinkage and drying shrinkage then obtained are roughly similar, though there were differences in the samples, in the temperature and the accuracy of the measure. Same driving forces and same basic mechanisms can therefore be expected to explain self-desiccation shrinkage, as in the case of drying shrinkage, in the RH ranges considered. Hence, modelling of autogenous shrinkage and numerical simulations have been developed by different authors, based on the mechanisms proposed for drying shrinkage (cf. § 6), like capillary tension [34], or surface fi-ee energy [35].

8 - SHRINKAGE OF CONCRETE STRUCTURES IN FIELD CONDITIONS

All of these experimental results point out that self-desiccation shrinkage, drying shrinkage and therefore total (hygral) deformations of concrete are drived by the internal RH of the material. And in real structures, the internal RH value, at a given time and in a given area, results fi-om both internal chemical effects (self-desiccation) and environmental conditions.

Hence, in field conditions, total deformations at a given RH are not the sum of self-desiccation shrinkage and exogenous hygral strains. Total shrinkage at a given $RH_{ext.}$ ($< RH_{int.}$) has rather to be considered, in particular for HP materials, as drying shrinkage accelerated at early age by self-desiccation. The long-term equilibrium value, at this given $RH_{ext.}$, is not modified.

The higher autogenous shrinkage of HP concretes, compared to ordinary concretes, usually induces higher total shrinkage but only at early age. Thus, long-term total shrinkage of HP concretes is usually similar [17), 36)], or lower [37)] than for ordinary concretes. This is first due to the fact that the drying shrinkage potential of HP materials decreases as a function of time because the difference between $RH_{int.}$ and $RH_{ext.}$ decreases as self-desiccation proceeds.

Secondly, water diffusion between the surroundings and the material is slow due to the fine pore structure.

Furthermore, it has to be added that deformations of concrete structures include also size-effects.

9 - CONCLUSIONS

Some experimental results about self-desiccation of a set of cement pastes and concretes have been reported in this paper.

The results highlight the peculiarities induced by very low water-to-cement ratio and use of silica fume for the high-performance materials tested in this study. These materials exihibit strong self-desiccation along their ageing (RH = 72% is measured in the HP concrete, within six months). This strong self-desiccation of HP materials is also shown by the high autogenous shrinkage measured on these materials (205.10-6, within six months for the HP concrete tested), compared to ordinary materials.

A linear relationship is exhibited between internal relative humidity and autogenous shrinkage, for each mix, illustrating the range where these deformations can be considered as self-desiccation shrinkage.

Drying shrinkage of the hardened materials has also been studied as a function of relative humidity and compared with self-desiccation shrinkage data in the high RH range. The values measured for both shrinkages were roughly similar.

As a result of their strong self-desiccation, which drives the internal RH of these materials to a value close to the average RH of common environmental media, and of their fine pore structure (low diffusivity), HP materials can be insensitive to environmental hygral variations over a wide range of relative humidities.

10 - REFERENCES

1) Miyazawa, S. and Monteiro, P.J.M., 'Volume change of high-strength concrete in moist conditions', Cem. and Conc. Research, 26(4)(1996) 567-572.
2) Persson, B., 'Hydration and strength of high performance concrete', ACBM, **3,** 1996, pp 107-123.
3) Copeland, L.E. and Bragg, G.H., 'Self-desiccation in Portland cement paste', Bull. Portland Cem. Association, 52(1955) 1-11.
4) Baroghel Bouny, V., 'Characterization of cement pastes and concretes - Methods, analysis, interpretations' (in french), (Laboratoire Central des Ponts et Chaussées, Paris, 1994) 468 p.
5) Buil, M., 'Comportement physico-chimique du système ciment-fs', Annales de l'ITBTP, 483(série Béton 271)(1990) 19-29.
6) Sellevold, E.J. and Justnes, H., 'High strength concrete binders. Part B: non evaporable water, self-desiccation and porosity of cement pastes with and without condensed silica fume', Proceedings of the 4th ACI/CANMET Int. Conf. on fly ash, silica fume, slag and natural pozzolans in concrete, Istanbul, Turkey, (1992) ACI SP 132-52, vol. 2, pp. 887-902.
7) Buil, M., 'Contribution a l'étude du retrait de la pâte de ciment durcissante', LCPC report n° 92, 1979, 72 p.
8) Atlassi, E., 'Influence of cement type on the desorption isotherm of mortar', Nordic Concrete Research, 10, 1991, pp 25-36.

9) Jensen, O. M. and Hansen, P.F., 'Autogenous relative humidity change in silica fume-modified cement paste', Advances in Cement Research, 1995, 7, n" 25, pp 33-38.
10) Jensen, O. M. and Hansen, P.F., 'Autogenous deformation and change of the relative humidity in silica he-modified cement paste', ACI Materials Journal, 1996, 95, n° 6, pp 539-543.
11) MacGrath, P. and Hooton, R.D., 'Self-desiccation of Portland cement and silica fume modified mortars', Ceramic Transactions, Advances in cementitious materials, Edited by S. Mindess, vol. 16 (Am. Ceram. Soc., 1990), pp 489-500.
12) Baroghel Bouny, V. and Chaussadent, T., 'Pore structure and moisture properties of cement-based systems from water vapour sorption isotherms', Proceedings of MRS 1994 Fall Meeting, Boston (Materials Research Society, 1995) vol. 370, pp. 245-254.
13) Hedenblad, G., 'Moisture permeability of mature concrete, cement mortar and cement paste', (pH D Thesis, University of Lund, 1993), Lund, Sweden, 1993,250 p.
14) Baroghel Bouny, V., Chaussadent, T. and Raharinaivo, A., 'Experimental investigations on binding of chloride and combined effects of moisture and chloride in cementitious materials', Proceedings of the International RILEM Workshop "Chloride penetration into concrete", oct. 15-18 1995, Saint-Rémy-lès-Chevreuse, France (Edited by L.O. Nilsson and J.P. Ollivier, RILEM, 1997) pp 290-301.
15) Toutlemonde, F. and Le Maou, F, 'Protection des kprouvettes de béton vis-à-vis de la dessiccation. Le point sur quelques techniques de laboratoire', Bul. Labo. P.C., 203, mai-juin 1966, pp 105-119.
16) Persson, B., 'Early basic creep of high-performance concrete', Proceedings of the 4th International Symposium on Utilization of High-strength/High-performance concrete BHP 96, 29-31 may 1996, Paris, France (LCPC, Presses de l'ENPC, 1996), pp 405-414.
17) Le Roy, R. and de Larrard, F., 'Creep and shrinkage of high-performance concrete: the LCPC experience', Proceedings of the 5th Int. RILEM Symposium in Barcelona, RILEM 93 (E. & F.N. SPON, London, 1993) pp 500-508.
18) de Larrard, F. and Le Roy, R., 'The influence of mix composition on the mechanical properties of silica fume high-performance concrete', Proceedings of the 4th ACI/CANMET Int. Conf. on fly ash, silica fume, slag and natural pozzolans in concrete, Istanbul, Turkey, (1992) ACI SP 132-52, vol. 2, pp. 965-986.
19) Powers, T.C. and Brownyard, T.L., 'Studies of the physical properties of hardened Portland cement pastes', Bull. Portland Cem. Association, 22(1948) 276-287.
20) Jensen, O. M., 'Thermodynamic limitation of self-desiccation', Cement and Concrete Research, 1995, 25, n° 1, pp 157-164.
21) Powers, T.C., 'Mechanisms of shrinkage and reversible creep of hardened cement paste', Proceedings of the International Symposium of the Structure of Concrete and its behaviour under load, London (Cement and Concrete Association, London, 1965) pp 319-344.
22) Powers, T.C., 'The thermodynamics of volume change and creep', Materials and structures, 1(6)(1968) 487-507.
23) Hansen, W., 'Drying shrinkage mechanisms in Portland cement paste', J. Am. Ceram. Soc., 70(5)(1987) 323-328.
24) Almudaiheem, J.A., 'An improved model to predict the ultimate drying shrinkage of concrete', Magazine of concrete research, 44(159)(1992) 81-85.
25) Lassabatère, T., 'Couplages hydro-mécaniques en milieu poreux non saturé avec changement de phase: application au retrait de dessiccation', Ph. D. thesis, Ecole Nationale des Ponts et Chaussées, oct. 1994,215 p.
26) Han, M.Y. and Lytton, R.L., 'Theoretical prediction of drying shrinkage of concrete', J. of materials in civil engineering, 7(4)(1995) 204-207.

27) Bentz, D.P., Quenard, D., Baroghel-Bouny, V., Garboczi, E.J. and Jennings, H.M., 'Modelling drying shrinkage of cement paste and mortar. Part 1 : Structural models from nanometers to millimeters', Materials and Structures, 1995, 28, 450-458.
28) Granger, L, Torrenti, J.M. and Acker, P., 'Thoughts about drying shrinkage: scale effects and modelling', Materials and structures, 30(1997) 96-105.
29) Wittmann, F.H., 'Interaction of hardened cement paste and water, J. Am. Ceram. Soc., 56(8)(1973) 409-415.
30) Bazant, Z.P., 'Thermodynamics of hindered adsorption and its implications for hardened cement paste and concrete', Cem. and Conc. Research, 2(1)(1972) 1-16.
31) Ferraris, C.F. and Wittmann, F.H., 'Retrait de la pâte de ciment durcie', Chantiers, 4(1987) 289-292.
32) Feldman, R.F. and Sereda, P.J., 'A model for hydrated Portland cement paste as deduced from sorption-length change and mechanical properties', Materials and structures, 1(6)(1968) 509-520.
33) Feldman, R.F., 'Sorption and length-change scanning isotherms of methanol and water on hydrated Portland cement', Proceedings of the 5th International Congress on the Chemistry of Cement (Cement Association of Japan, Tokyo, 1968), vol. 3, pp. 53-66.
34) Hua, C., Acker, P. and Ehrlacher, A., 'Analyses and models of the autogenous shrinkage of hardening cement paste - I. Modelling at macroscopic scale', Cem. and Conc. Research, 2(1)(1972) 1-16.
35) van Breugel, K., 'Simulation of microstructural development and its potential to serve engineering purposes', in *Advances in Building Materials Science - Research and Applications.* Edited by A. Gerdes, AEDIFICATIO Publishers, 1996, pp 243-258.
36) Baroghel Bouny, V., Mazounie, S., Gawsewitch, J., Chaussadent, T., Caré, S. and Roussel, P., 'Etude comparative de la durabilité des bétons B30 et B80 utilises pour la realisation des ouvrages jumeaux de la DDE du Cher', Projet National BHP 2000 - Thème 1 : Durabilité - Sous-thème : Etude expérimentale sur ouvrages jumeaux, LCPC Report, may 1997, 51 p.
37) Baroghel Bouny, V., Godin, J. and Gawsewitch, J., 'Microstructure and moisture properties of high-performance concrete', Proceedings of the 4th International Symposium on Utilization of High-strength/High-performance concrete BHP 96, 29-31 may 1996, Paris, France (LCPC, Presses de l'ENPC, 1996), pp 451-461.

AUTOGENOUS VOLUME CHANGES AT EARLY AGES

Markku Leivo*
Erika Holt**

* VTT Building tehnology, Technical Research Centre of Finland,
PO Box 1805, FIN-02044 VTT, FINLAND
** Department of Civil Engineering, University of Washington,
PO Box 352700, Seattle, WA 98195, USA

ABSTRACT

Concrete shrinkage is of increasing concern when making durable structures. Over time, the shrinkage induces cracking can severely decrease the concrete life expectancy. These volume changes are often attributed to drying of the concrete, in which the particles are drawn closer together with the moisture loss to the surrounding environment. It is generally expected to occur over a long time period, though recent observations have focused on early age or plastic drying problems. In this phase the concrete is still moist after mixing. Difficulties in measuring have prevented extensive understanding of the influences on plastic shrinkage. The most common solution is to avoid drying by proper curing methods occurring soon after placement of the concrete.

A supplementary problem to the drying shrinkage at early ages is the changes that occur when no moisture transfer is permitted with the environment. This volume reduction is called autogenous shrinkage, which is attributed to chemistry and internal structural changes. At 100% RH, a specimen will still undergo a horizontal and vertical shrinkage. The vertical shrinkage is settlement occurring as a result of excess bleed water migrating to the concrete surface and the aggregates settling. The horizontal autogenous shrinkage is of concern and interest, as it can result in unpreventable cracks. It is this problem which needs further investigation in order to improve the durability of concrete.

BACKGROUND

Autogenous shrinkage of cement paste and concrete is defined as a volume change occurring with no moisture transfer to the surrounding environment. It is a results of physical and chemical changes affiliated with the hydration of cement particles. The exact breakdown of the influencing factors on the shrinkage magnitude are well disputed. It cannot be prevented by casting, placing or curing methods, but must be addressed when designing the concrete

mixture. The internal components or ingredients have the most significant influence. This volume change has been given a variety of labels, some of which include: autogenous deformation, chemical shrinkage (both total and external), volume contraction, Le Chatelier shrinkage, bulk shrinkage, indigenous shrinkage, self-desiccation shrinkage, and autogenous volume change. In detailed analyses, it may be necessary to further define and classify each of these various terms for consistency.

Autogenous shrinkage has only recently been documented and accurately measured. It was first described in the 1950's, as a contributing factor to the total shrinkage that was difficult to assess. Total shrinkage is usually reported over a long period of time, as a combination of drying and autogenous shrinkage. The exact proportion of these two factors to the total shrinkage is still disputed in some cases, especially at early ages. But again, the actual definition of "early age" had varied from a few hours to a couple days or weeks.

When taking measurements over a long period of time, autogenous shrinkage is measured in the same manner as drying shrinkage. The length change of a prism is measured from the time of decanting at approximately 24 hours after casting until no further volume reduction can be detected. The specimen is maintained in a moist or sealed environment for the duration of observation.

The primary influence on autogenous shrinkage is the water to cement (wlc) ratio of the composite. Baroghel Bouny [1] has shown that with a decreasing w/c ratio the autogenous shrinkage of cement paste increases, as shown in Fig. 1. Tazawa and Miyazawa [2] attribute this to the denser cement microstructure.

FIG.-1
Correlation between autogenous strain and wlc ratio.'

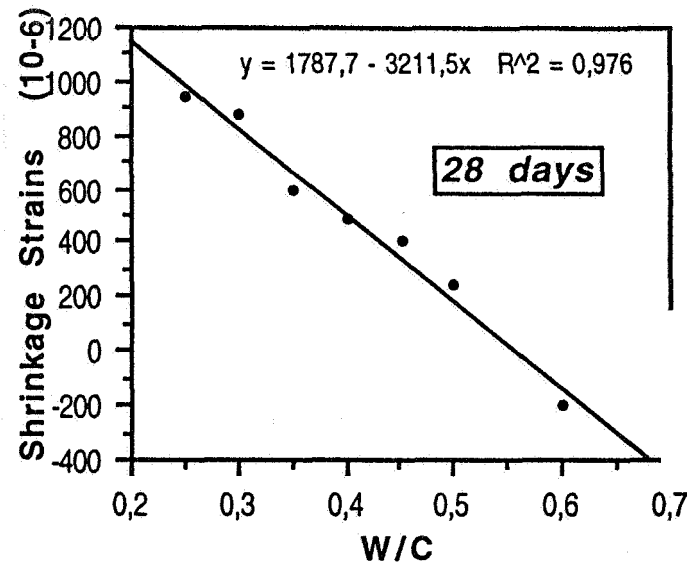

It has also been reported [3] that the autogenous shrinkage becomes equal to the drying shrinkage as the w/c ratio becomes smaller (Fig. 2). For instance, at a w/c ratio of 0.40 the autogenous shrinkage attributes 40% to the total drying shrinkage magnitude, while at a w/c ratio of 0.30 the contribution is 50%.

FIG.-2

Relationship between wlc and contribution of autogenous shrinkage strain to total drying shrinkage strain.[3]

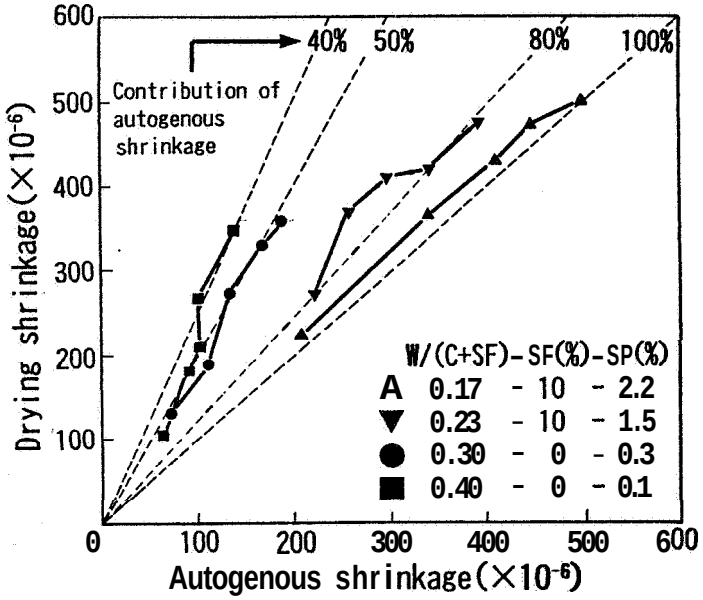

Within the concrete, the cement chemistry is the primary contributing factor to the shrinkage magnitude differences between various concretes. By adjusting the cement composition, the anticipated reactions can be altered. Paulini has accurately modelled (Fig. **3)** the specific cement components which influence the autogenous shrinkage based on Boyles equation.[4]

FIG.-3

Influence of cement composites on shrinkage.[4]

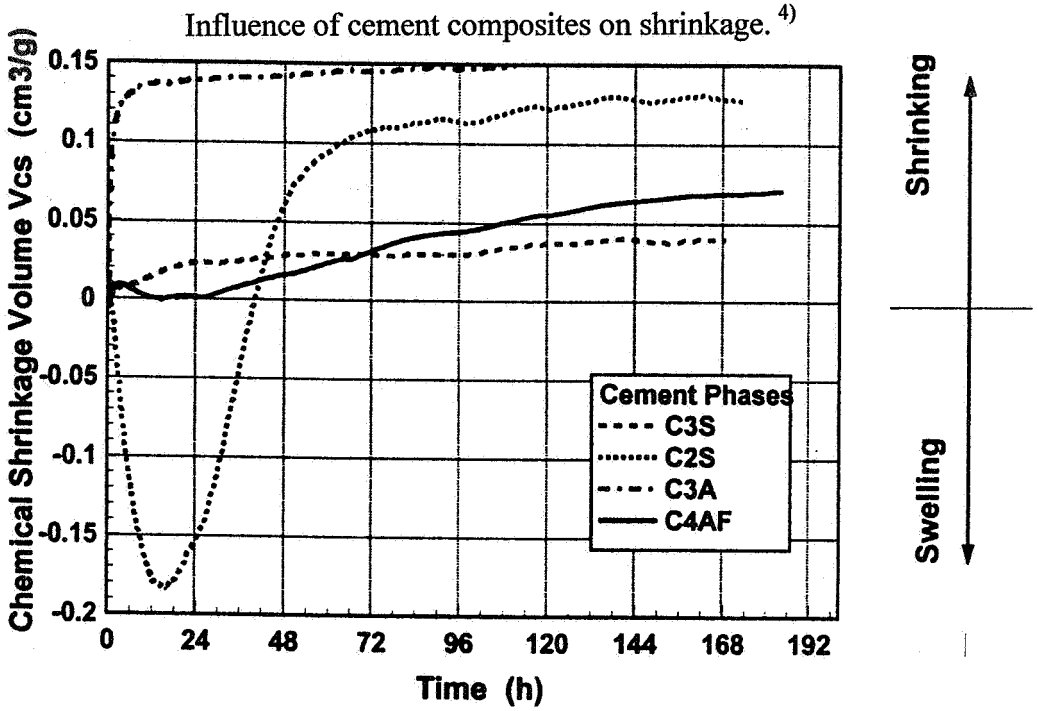

In measurements of autogenous shrinkage over a long period of time, the internal relative humidity plays an important role. The voids, or capillary pores, retain moisture from the cement paste. **A** good correlation exists between the internal relative humidity and the free autogenous shrinkage of cement paste, as shown in Fig. 4 [1] (w/c = 034).

FIG.-4
Correlation between free autogenous shrinkage strains and internal RH of the materials, measured at T=21°C, from 28 days. [1]

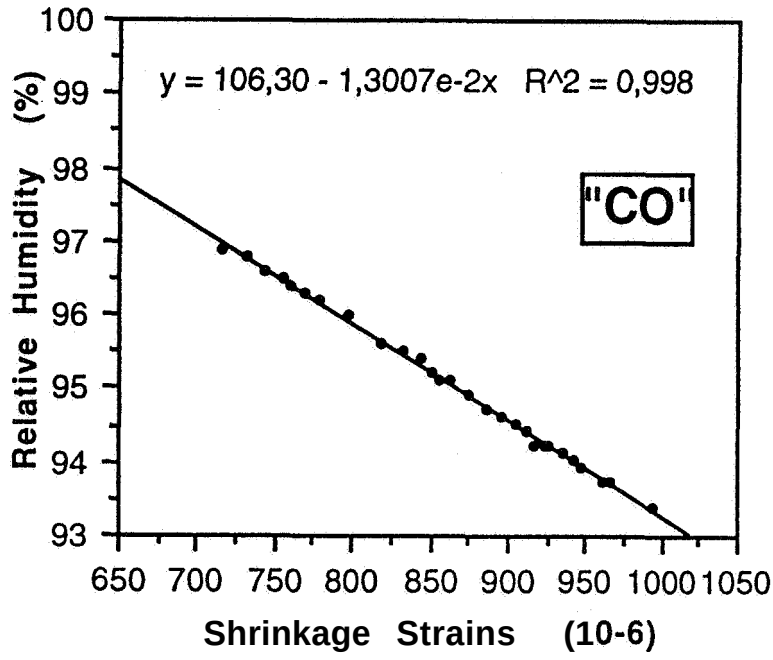

Early age autogenous shrinkage measurements provide more of a challenge, due to the difficulty in making accurate measurements of the concrete prior to demoulding. The shrinkage must be measured immediately after casting in a mould which permits constant readings without disturbing the concrete. The same factors influence the early age shrinkage as compared to the long term shrinkage previously described. Within the first hours after casting, the concrete is the most sensitive to internal stresses. Kasai has shown that the concrete has the lowest tensile strain capacity in these early hours, as shown in Fig. 5 [5]. It is at this time that the concrete is most likely to crack when the internal stresses exceed the strain capacity. Even if these cracks are internal and microscopic, drying at a later age will merely open the existing deformations and cause problems.

FIG.-5
Tensile strain capacity at early ages [5].

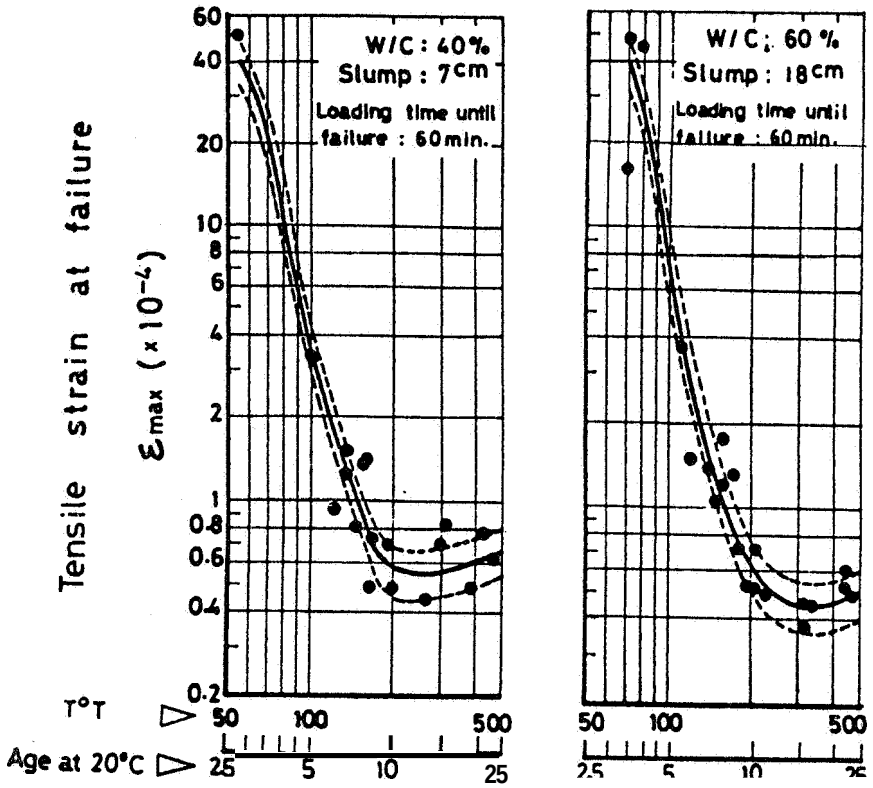

EXPERIMENTAL METHODS

Research was carried out at the Technical Research Centre of Finland regarding both drying and autogenous shrinkage at early ages. The project was aimed at investigating shrinkage of pre-cast facade elements manufactured from rapid setting cements.

The plastic shrinkage measurements employed a prior test arrangement [6], as shown in Fig. 6. Specimen dimensions are 270 x 270 x 100 mm. Plastic shrinkage was measured with respect to evaporation, settlement, setting time, and the development of internal capillary pressure. Testing began approximately 30 minutes after water addition during the mixing process. The samples were observed during the first 12 hours following casting, while exposed to ambient air conditions (T = 20°C and RH 40%). In some specific cases the specimens were exposed to wind (velocity 4 m/s) to facilitate rapid evaporation and more pronounced shrinkage. Autogenous shrinkage measurements were done along side the drying specimen, with the slab being covered with a hood and an enclosed moisture source to maintain 100% RH. Setting time was measured by a penetration test arrangement.

FIG.-6
Early age shrinkage measuring test arrangement. [6]

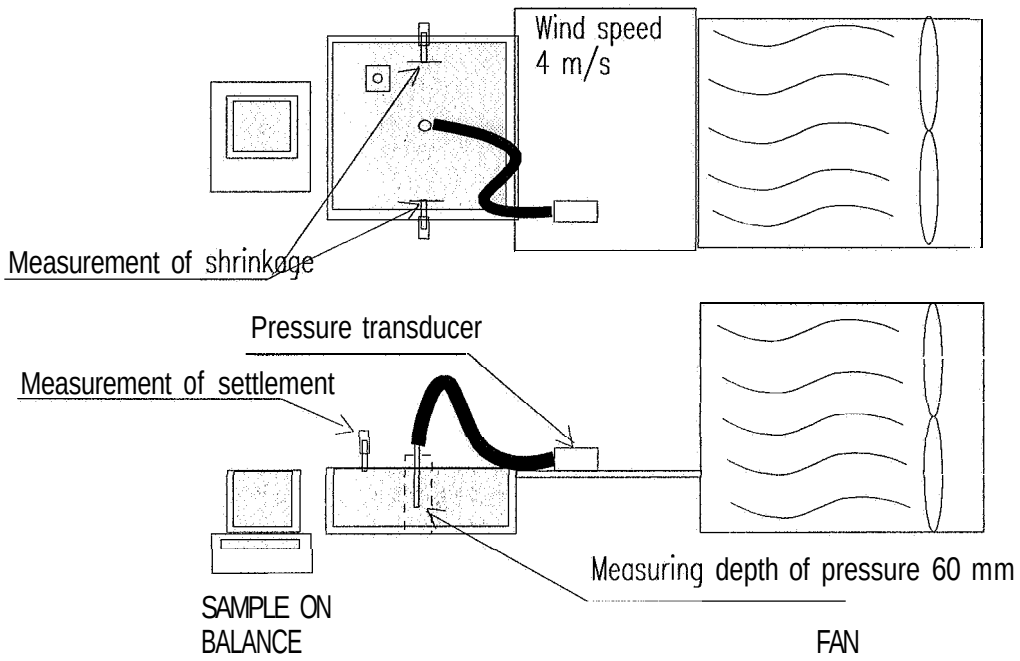

All data measurements were logged into a computer

Plastic shrinkage involves the formation of water menisci at the concrete surface, with the uppermost particles being driven downward by compression forces. Combined with the rising bleed water from internal capillary pressure, three dimensional shrinkage will occur. [7] For drying shrinkage applications, monitoring of the evaporation and settlement amount allows one to determine the concrete volume change. As shown in Fig. 7, drying occurs when evaporation exceeds bleeding (shown by the settlement curve). At this point, the capillary pressure will build up and facilitate shrinkage. Approximately 2 hours after the concrete final set point is reached, the majority of plastic shrinkage is complete due to the formation of the internal skeleton resisting further deformations [6].

In consideration of the autogenous shrinkage, no evaporation is experienced though the other pressure, settlement and shrinkage lines of the above figure are still documented. Additional ways of measuring autogenous and chemical shrinkage have also been recently developed, such as the immersion weight and volumetric change methods.

Long term concrete shrinkage measurements were done in accordance with RILEM CPC 9 recommendations, with minor adjustments. Measurements were performed until at least 28 days to allow for observation of unrestrained length change. Three prism specimens were stored at 40% RH upon decanting at 24 hours, while another three specimens were continuously stored at >95% RH.

FIG.-7
Typical concrete plastic shrinkage test curves.

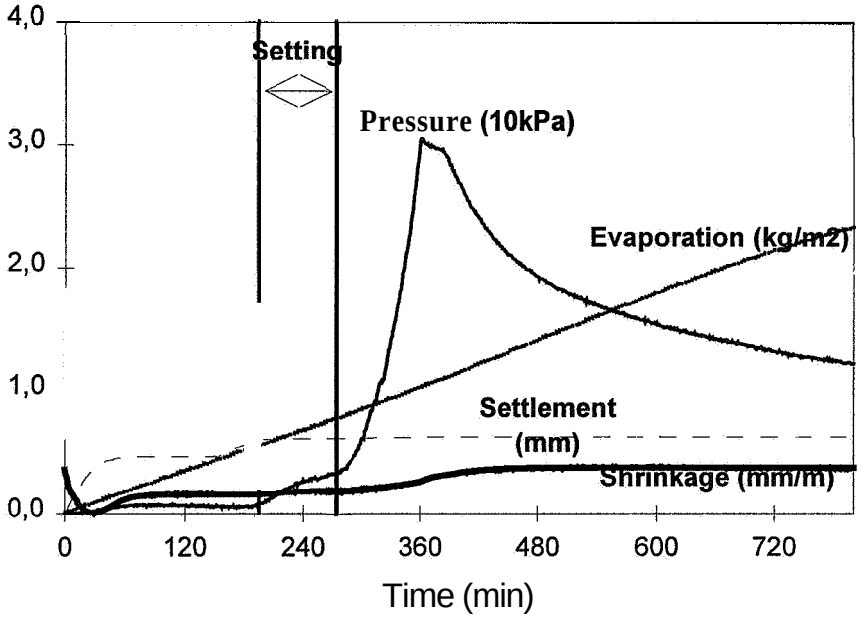

MATERIALS

Aggregate consisted of clean natural granite, with a maximum size of 10 mm. Both white and grey rapid hardened cements were used, Valkosementti and Rapid (Lappeenranta), respectively. Three additional Finnish grey cements, Rapid (Parainen) and Pika (Lappeenranta and Parainen) were evaluated in one test series. In the results used in forthcoming analyses, the water-to-cement (w/c) ratio was 0.45 with 400 kg/m^3 of cement. The only exception is in the test series of increasing superplasticizer dose, where the water amount was changed to maintain workability. This also required the cement amount to be slightly adjusted (w/c=0.45).

Chemical admixtures included an air entraining agent, Parmix L, and two superplasticizers. These high range water reducers were melamine based, Melment and naphalene based, Super-Parmix. Air entraining was used in some cases. The target fresh concrete mix properties were a slump of 100 mrn and air content of 5.0% in specific cases of needing air entraining.

RESULTS AND DISCUSSION

The experiments yielded results providing insight into the magnitude of concrete autogenous shrinkage within the first hours. Early tests revealed autogenous shrinkage that was nearly 50% of the total drying shrinkage measured in the first 8 hours (Fig. 8). The magnitude of autogenous shrinkage significantly contributes to the overall shrinkage which was previously explained merely by drying phenomena. Knowing that the autogenous deformations cannot be prevented by casting procedures, the shrinkage is already at a risk of exceeding the tensile strain capacity of concrete, and therefore visible cracking can occur.

FIG.-8
Magnitude comparison of drying shrinkage and autogenous shrinkage.

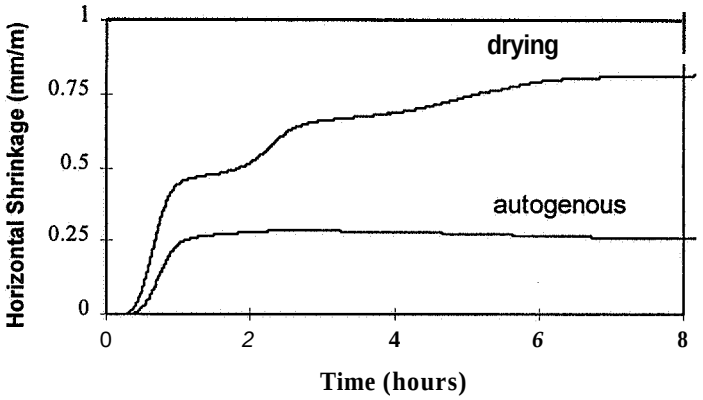

Another test series involved the comparison of various rapid setting cements, as previously described in Materials section. The results showed a variety in the magnitude of the autogenous shrinkage between the cement types (Fig. 9). This variance in shrinkage magnitudes is even more pronounced when comparing basic Portland cements to rapid hardening or high early strength cements.

FIG.-9
Autogenous shrinkage of various rapid hardening cements.

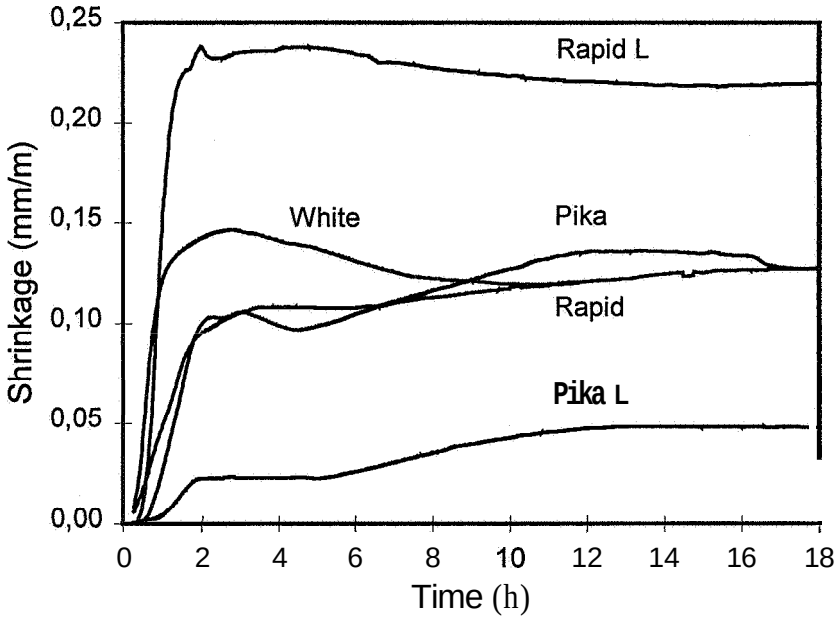

The effect of superplasticizer type and dose were investigated in a few test series. Both melamine and naphalene based superplasticizers were used from 0 to 1.5 percent. The results of increasing superplasticizer dose on the drying shrinkage at early ages are shown in Fig. 10.

FIG.-10
Effect of superplasticizer dose on early age drying shrinkage. Cement and water contents were changed to maintain constant w/c-ratio and workability.

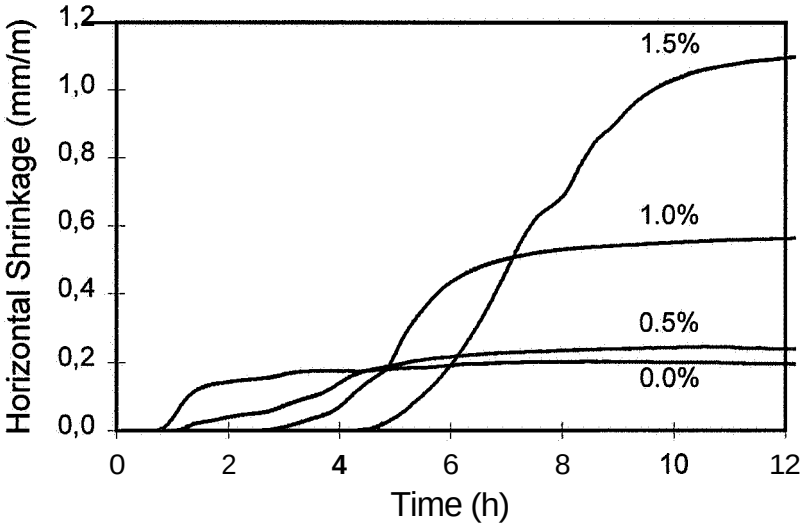

It is believed that the trend for the effect of such superplasticizer on the autogenous shrinkage magnitude would be the same. Although the chemical dosage effects the setting time because of the secondary retarding effects, the superplasticizers also change the chemical composition and internal pore structure. The change in development of capillary pressure and shrinkage tendencies if of concern when the magnitude is excessive and again approaching the concrete's tensile strength capacity.

Comparisons were also made between the early age and long term magnitude of autogenous shrinkage. In standard shrinkage observations of prisms, the measurements do not begin until demoulding, which prevents and early age changes to be accounted. When comparing the shrinkage recorded in the first 12 hours to that which is measured at 28 days, it is seen that the early age shrinkage contributes significantly. In Fig. 11, the autogenous shrinkage magnitudes are graphed for 3 different mixes at 12 hours and 28 days.

Fig. 11 shows the importance of the early age shrinkage, which is often not measured or accounted for. But it is at this time when the tensile strain capacity is a minimum and the concrete is most likely to crack. Even if microcracks are initially formed internally, with ageing the cracks will merely expand. It is inaccurate to fully attribute the cracking problems to drying shrinkage tendencies that occur at early or late stages of the concrete's life.

CONCLUSIONS

Autogenous deformations are a significant contributor to the total concrete shrinkage measured in early and later ages. It has been documented, though not fully understood. The difference in chemical versus structural changes is not well defined, as well as the possibility of other internal alterations. Early age shrinkage challenges the material's tensile strength and

poses a risk to cracking within the first hours after casting. In both the drying and moist conditions, the immediate shrinkage should not be overlooked.

FIG.-11
Comparison of 12 how to 28 day autogenous shrinkage measurements of 3 various concretes.

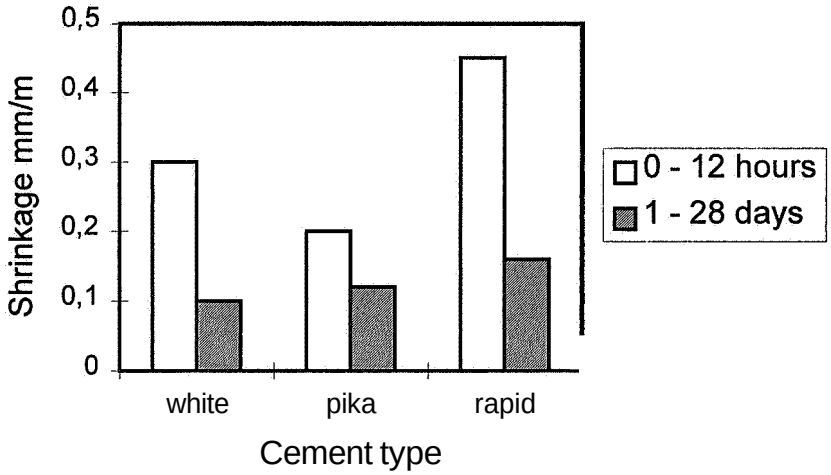

The mix composition is the most critical factor affecting the autogenous shrinkage magnitude. Chemical admixtures, cement amount and type, and the water-to-cement ratio are all items which can directly adjust the anticipated shrinkage tendencies. The combination of such concrete compositions makes it difficult to assess which items are truly contributing to the volume change.

Autogenous shrinkage can be a large portion of the measured total shrinkage, which is often attributed to drying over a long period of time. It is important to establish these two types of shrinkage separately in order to determine their contribution to cracking. Early age autogenous shrinkage can create microcracks which later propagate and expand to be more of a problem. The phenomena which control the autogenous shrinkage need to be well understood and documented. Further research is needed to achieve this. After this we will be able to prolong the life of our concrete.

REFERENCES

1) Baroghel Bouny, V., "Texture and Moisture Properties of Ordinary and High-Performance Cementitious Materials," Proceedings of Seminaire RILEM 'Benton: du Materiau a la Structure', September 1996, Arles, France.

2) Tazawa, E., Miyazawa, S., "Influences of Cement and Admixtures on Autogenous Shrinkage of Cement Paste," Cement and Concrete Research, Vol. 25, No. 2, 1995, pp. 281-287.

3) Tazawa, E., Miyazawa, S., "Experimental Study on Mechanisms of Autogenous Shrinkage of Concrete," Cement and Concrete Research, Vol. 25, No. 8, 1995, pp. 1633-1638.

4) Paulini, P., Outlines of Hydraulic Hardening - an Energetic Approach. Workshop NTNU/SINTEF - Trondheim, Early Volume Change and Reactions in Paste - Mortar - Concrete. 28-29 Nov. 1996.

5) Kasai, Y., Yokoyama, K., Matsui, I. & Tobinai, K. "Tensile Properties of Early-Age Concrete," Mechanical Behavior of Materials, The Society of Materials Science, Japan, Vol. 2, 1974, pp. 433-441.

6) Kronlof, **A.,** Leivo, M., & Sipari, P., "Experimental Study on the Basic Phenomena of Shrinkage and Cracking of Fresh Mortar," Cement and Concrete Research, Vol. 25, No. 8, 1995, pp. 1747-1754.

7) Radocea, A., "A Model of Plastic Shrinkage," Magazine of Concrete Research, Vol. 46, No. 167, June 1994, pp. 125-132.

EXPERIMENTAL DETERMINATION AND ANALYSIS OF STRESS AND STRAIN DISTRIBUTION OF REINFORCED HIGH-STRENGTH CONCRETE COLUMN CAUSED BY SELF-DESICCATION AND HEAT OF HYDRATION

F.TOMOSAWA, T.NOGUCHI and K.B.PARK

The University of Tokyo, Faculty of Engineering, Dept.of Architecture,
7-3-1, Hongo, Bunkyo-ku, Tokyo, 113, Japan

HSANO

Housing and Urban Development Corporation,
2683-3, Ishikawa-cho, Hachiohji-shi, Tokyo, 192, Japan

N.YAMAZAKI, H.HASHIDA and Y.KURODA

Shimizu Corporation,
3-4-17, Etchujima, Koto-ku, Tokyo, 135, Japan

INTRODUCTION

High-rise reinforced concrete buildings made using high strength concrete with a design strength of more than 60 N/mm^2 have been increasing in recent years. High strength concrete is known to entail a large temperature rise due to hydration heat even from a volume of as small as a beam/column member. It is also known to undergo shrinkage due to self-desiccation, i.e., autogenous shrinkage. The resulting thermal strain and autogenous shrinkage restraint may cause composite stress, increasing the risk of concrete cracking. However, actual strain and stress within high strength reinforced concrete rigid frames have not been clarified, as there have been few examples of measuring such strain and stress.

In this study, the authors measured the strain of column and beam concrete and reinforcement in an actual concrete building under construction, as well as the strain of real-scale models with and without reinforcement, to grasp their actual behavior. The mechanical properties of concrete were also measured using specimens to elucidate the development of mechanical properties of concrete subjected to temperature changes.
These mechanical property parameters were then used for the analysis of the temperature and

shrinkage of actual concrete columns incorporating the creep. Based on the results of these measurements and this analysis, the authors investigated the strain and stress distribution in high strength reinforced concrete rigid frames, as well as the risk of cracking.

OUTLINE OF CONCRETE AND CONSTRUCTION

MATERIALS AND COMPOSITION

The materials and mixture proportions of concrete used in the construction are given in Table 1 and 2. Two types of concrete were investigated: concrete containing normal portland cement (OPC) and concrete containing belite-rich portland cement (BPC), which has been increasingly used for massive concrete and high strength concrete member, due to its low hydration heat generation and low water-reducer demand.

Table 1 Materials of concrete

Materials	Kind / Characteristics
Cement	Ordinary Portland cement Specific gravity = 3.16, Specific surface (Blain) = 0.340 m^2/g
	Belite-rich Portland cement Specific gravity = 3.16, Specific surface (Blain) = 0.417 m^2/g
Water	Potable
Fine aggregate	Crushed sand and land sand / Specific gravity = 2.62 Absorption = 1.52, Fineness modulus = 2.78
Coarse aggregate	Crushed stone (sandstone) / Maximum size = 20mm, Specific gravity = 2.68, Absorption = 0.72, Fineness modulus = 6.58
Chemical admixtures	Air entraining and high-range water reducing agents

Table 2 Mix proportions

Description			OPC	BPC
Water-cement ratio	W/C	(%)	28.0	27.0
Sand-coarse aggregate ratio	s/a	(%)	44.4	47.0
Air content		(%)	3.0	3.0
Water	W	(kg/m^3)	165	170
Cement	C	(kg/m^3)	589	630
Fine aggregate	S	(kg/m^3)	719	741
Coarse aggregate	G	(kg/m^3)	922	854

OUTLINE OF CONSTRUCTION

High strength concrete was experimentally placed in a 3-storey reinforced concrete building having a basement floor with a building area and total floor area of 615 m^2 and 1,353 m^2,

respectively. The concrete and main reinforcement strain behavior was observed at columns (cross section: **550** × **600** mm) on the second and third floors (floor height: **3.5** m and **3.75** m) and beams (cross section: **600** × **600** m, span: **6** m) on the third floor and roof. Second floor columns and a third floor beam were placed with OPC on September **18, 1996,** and third floor columns and a roof beam were placed with BPC on October **12, 1996.** Along with this construction, part of the concretes was taken to prepare specimens and full-scale models. The properties of fresh concrete at the time of placing are given in Table **3.**

Table **3** Characteristics of fresh concrete

	OPC	BPC
Slump	**24.0** cm	**26.0** cm
Slump flow	**47.5** cm	**55.5** cm
Air content	**1.5** %	**1.7** %
Concrete temp	**30.0** ℃	**24.0** ℃
Specific gravity	**2.44** t/m^3	**2.42** t/m^3

EXPERIMENTS

SPECIMENS

Experiments were carried out on concrete specimens to grasp their mechanical properties. The measurement items included autogenous shrinkage strain, compressive strength gains, and elasticity modulus gains. Setting tests were conducted as well. Autogenous shrinkage strain of **100** × **100** × **400** mm prisms was measured with embedment strain transducer. The temperature change in the centers of beams were monitored using thermocouples (Fig.1). The compressive strength and elasticity modulus of cylinders **100** mm in diameter and **200** mm in length were measured from the earliest testable age up to **28** days. These specimens were cured in a thermostatic chamber at **20** ℃ or a water tank simulating the temperature histroy of a full-scale member from immediately after placing. The specimens immersed in water were sealed with plastic sheets so that they were not impregnated with water. Concrete for setting tests was made into prismatic specimens **150** × **150** × **150** mm in size and was cured in the same manner.

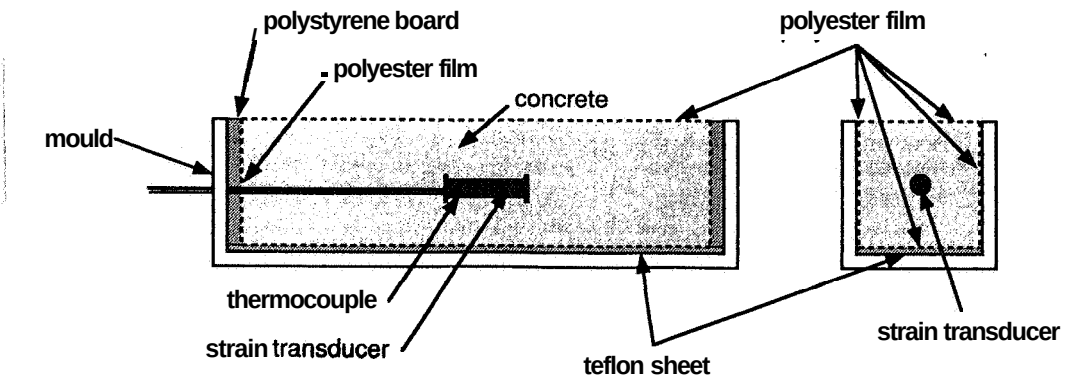

FIG.1 Test specimen

COLUMN MODEL MEMBERS

Column models 1.5 m in height having the same cross section as actual columns were prepared with or without the same reinforcement as actual columns. Where as unreinforced model columns were used for measuring the free shrinkage strain of concrete, reinforced models were used for measuring the actual strain of the main reinforcement and concrete under restraint of the reinforcement. To minimize the effect of drying, the exposed surfaces of the wooden forms were covered with curing sheets made of polyethylene. The placing surface of OPC were exposed similarly to actual columns, while those of BPC were covered with curing sheets from immediately after placing.

The strains of concrete and the main reinforcement were measured with embedded strain gauges and foil strain gauges (the 4 gauge method), respectively. The measuring points for strain and temperature are as shown in the cross sectional view in Fig. 2. Measurements were made at **3** heights, but this paper deals with only the central measuring point readings.

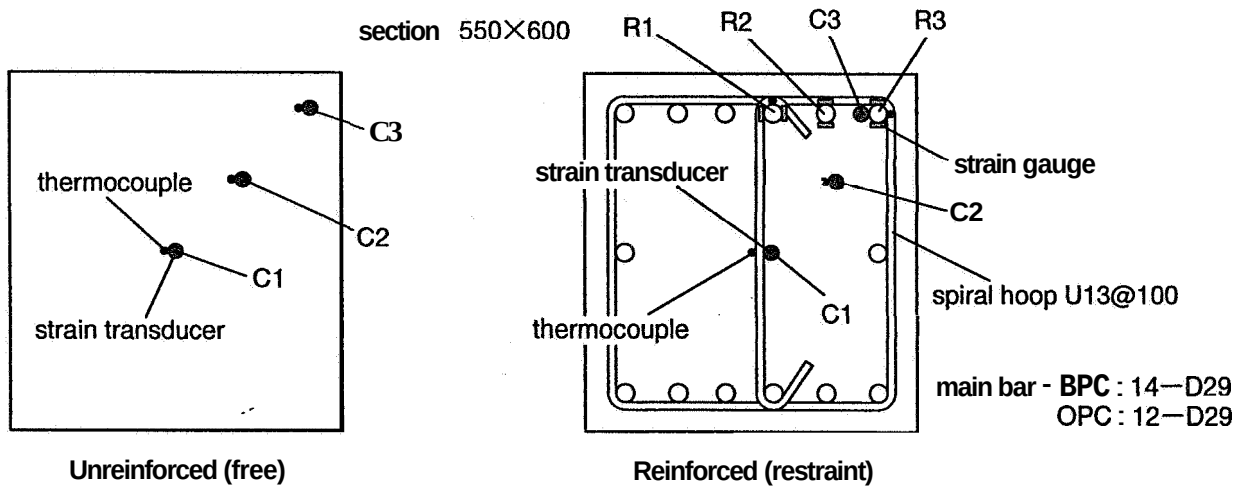

FIG.2 Cross section of model members

ACTUAL COLUMNS AND BEAMS

The concrete and main reinforcement strains of actual columns and beams were measured with embedded strain gauges and foil strain gauges, respectively. The measuring points are as shown in the cross-sectional view in Fig. **3.**

The numbers of main reinforcement of second floor columns (OPC) and third floor columns (BPC) were 12 and 14, respectively. Measurements were made at three heights of the columns, but only the readings of the mid-length gauges are reported in this paper. Regarding beams as well, only the mid-span measurements are reported, though measurements were also made at both ends.

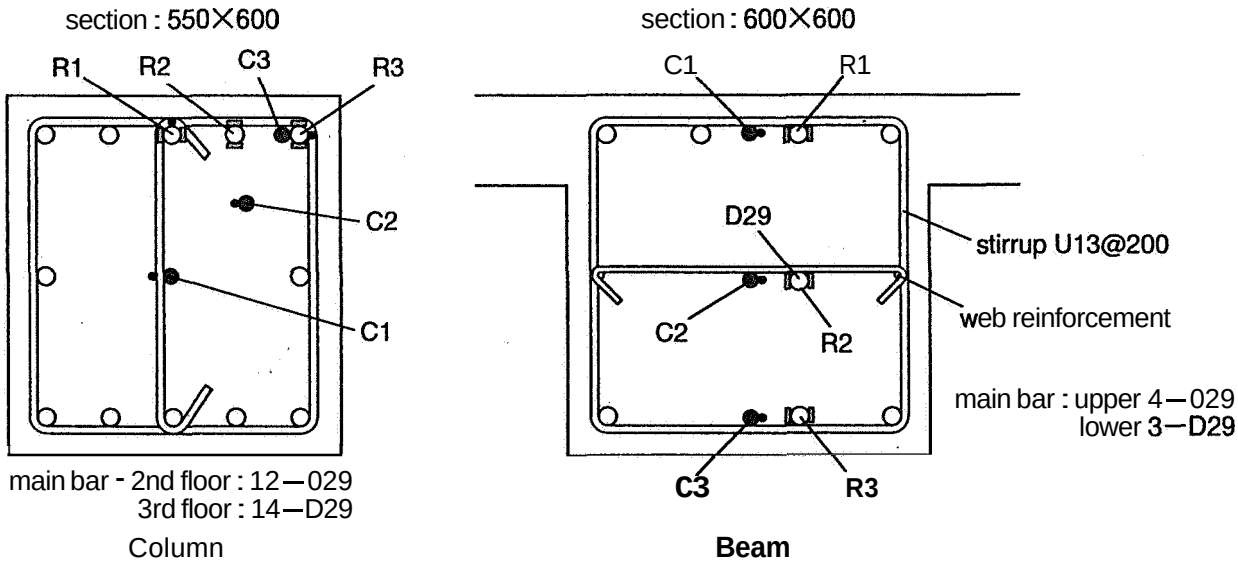

FIG.3 Cross section of column and beam

RESULTS AND DISCUSSION

MECHANICAL PROPERTIES OF CONCRETE

TEMPERATURE HISTORY AND MODIFIED AGE

Fig. 4 shows the changes in temperature of OPC and BPC specimens (100 × 100 × 400 mm) for autogenous shrinkage. The temperature changes imparted to the specimens were programmed to simulate the temperature histories of actual members. Due to its low hydration heat, BPC showed a lower temperature rise than OPC.

Concrete maturity should be taken into account to consistently express the development of mechanical properties of concrete subjected to temperature changes.

The modified age specified in the CEB-FIP model code[1]) [Eq.(1)] was used as the maturity in the present discussion.

$$t_T = \sum_{i=1}^{n} \mathrm{At};\ \exp\left[13.65 - \frac{4000}{273 + T(\Delta t_i)/T_0}\right] \qquad (1)$$

where t_T =modified age in (days);
$T(\Delta t_i)$ =temperature in ("C) during the time period At;;
At; =time period in (days) where the temperature T prevails;
T_0 =1℃

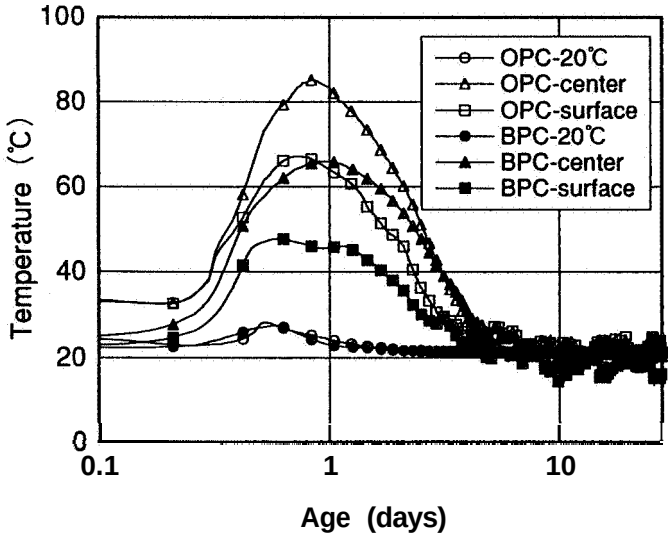

FIG.4 Temperature histories of specimens

AUTOGENOUS SHRINKAGE STRAIN

Fig. 5 shows the autogenous shrinkage strain measurements of OPC and BPC specimens (with the linear expansion coefficient assumed to be $10 \times 10^{-6}/℃$ and the thermal strain canceled). The origin of the strain measurements is set at the initial setting time. This applies to all other strain measurements. When arranged in terms of the modified age, early autogenous shrinkage strain was nearly the same for all temperature histories. However, a high member temperature tended to lead to rapid convergence of autogenous shrinkage.

In this experiment, the shrinkage no longer increased after the temperature began to drop. In the case where the maximum temperature exceeded 60 ℃, the strain appeared to turn to expansion, and then converged to a certain value. On the other hand, the shrinkage of specimens maintained constantly at 20 ℃ increased for a long time, which was larger than that of specimens subjected to temperature changes. The autogenous shrinkage strain of BPC is smaller than that of OPC. The strain of members subjected to temperature changes was closed to that value, suggesting weak effects of temperature.

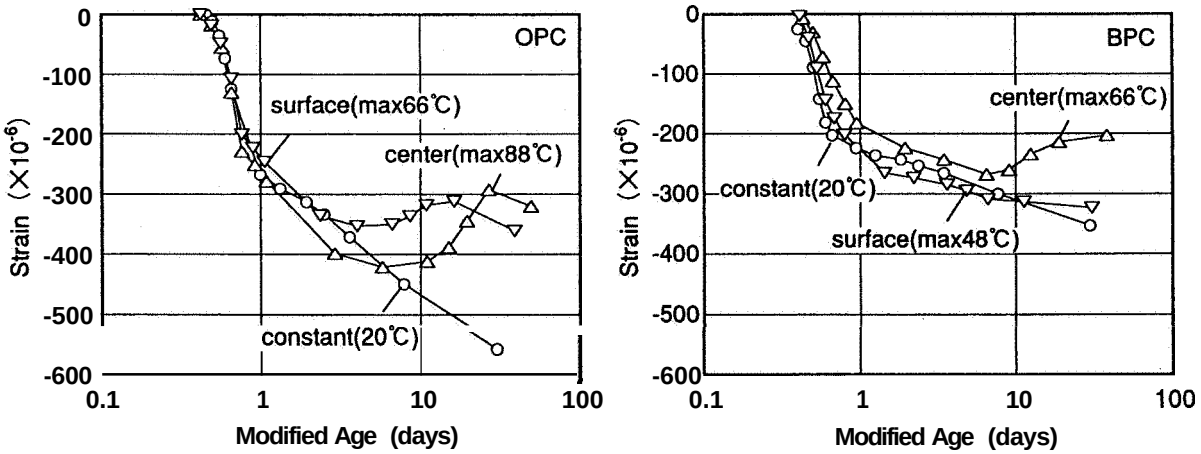

FIG.5 Autogenous shrinkage strains

COMPRESSIVE STRENGTH AND MODULUS OF ELASTICITY

Figs 6 and 7 show the compressive strength and modulus of elasticity, respectively, related with the modified age. Both can be expressed as similar development curves irrespective of the temperature histories. However, temperature changes applied to OPC after an age of 3 days led to smaller compressive strength gains than those of OPC water-cured at 20 "C. Meanwhile, temperature changes scarcely affected the strength gains of BPC, suggesting weak effects of temperature on BPC. The regression curve shown in Fig. 6 is based on a compressive strength development equation(2) derived by adding a parameter for initial setting time to the equation specified in CEB-FIP mode code 90[1].
The curve for elasticity modulus development shown in Fig. 7 is similarly derived by adding a parameter for final setting time.

Compressive strength development:

$$f_c(t) = f_c \cdot \exp\left[S_f\left(1 - \left(\frac{28 - t_{is}/t_1}{(t - t_{is})/t_1}\right)^{0.5}\right)\right] \tag{2}$$

where f_c =compressive strength in (N/mm^2) at the age of 28 days cured in water at 20 "C;
S_f =coefficient which depends on the type of cement;
t_{is} =initial setting time in (days);
t =modified age in (days);
t_1 =1 day.

Elasticity modulus development:

$$E_c(t) = E_c \cdot \exp\left[S_E\left(1 - \left(\frac{28 - t_{fs}/t_1}{(t - t_{fs})/t_1}\right)^{0.5}\right)\right] \tag{3}$$

where E_c =modulus of elasticity in (N/mm^2) at the age of 28 days cured in water at 20 "C;
S_E =coefficient which depends on the type of cement;
t_{fs} =initial setting time in (days);
t =modified age in (days);
t_1 =1 day.

Both Eq.(2) and (3) are found to adequately regress the compressive strength and elasticity modulus development including ages earlier than one day, independently of the temperature changes.
When regressing, the parameters S_f and S_E were determined by using the measured values for the case of constant 20 "C as such. However, effective regression data of OPC compressive strength were limited to those for members water-cured at 20 "C, as the compressive strength development of OPC subjected to temperature changes slowed down after 3 days.

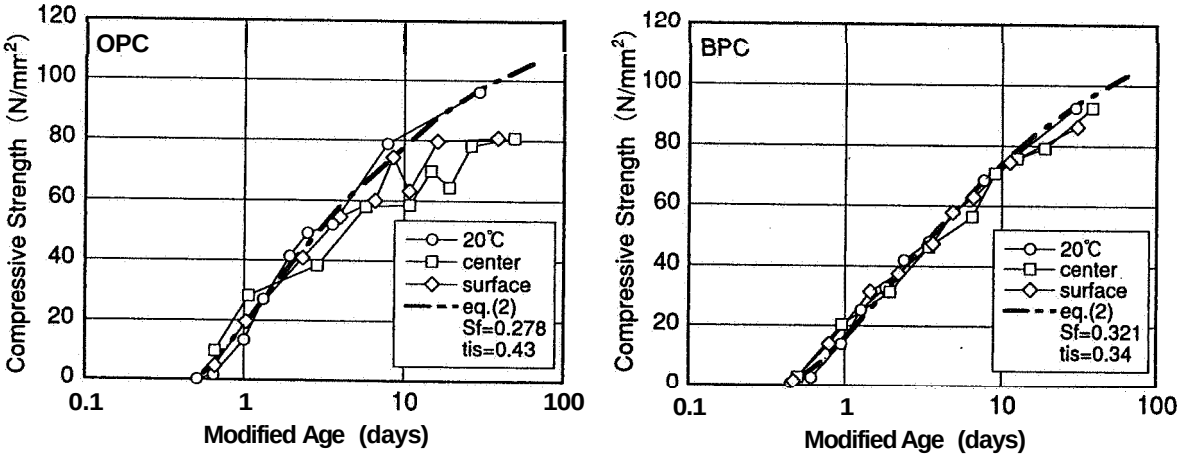

FIG.6 Developments of compressive strength

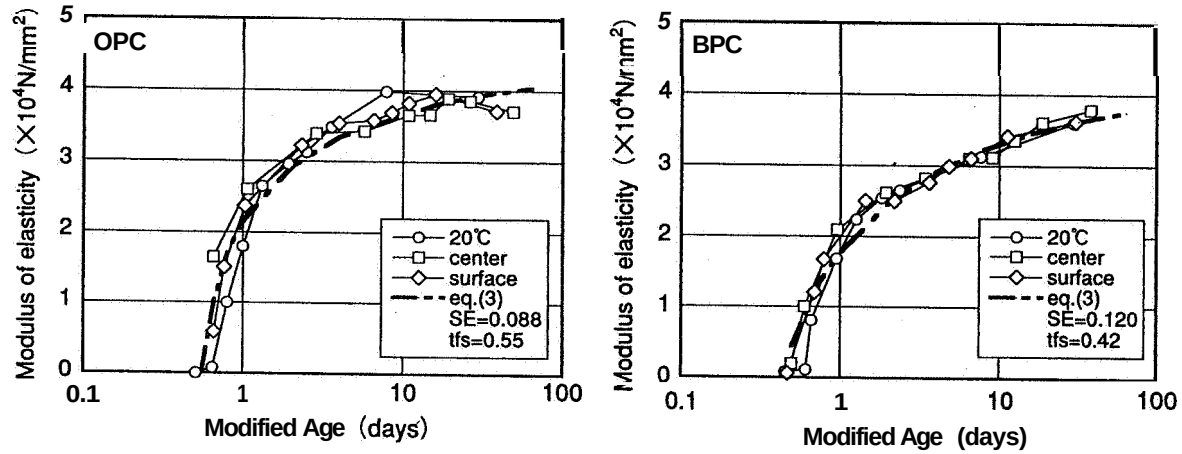

FIG.7 Developments of modulus of elasticity

STRAIN BEHAVIOR OF MODEL MEMBERS

Fig. 8 shows the temperature history of the free shrinkage model members. Fig. 9 shows the concrete shrinkage strain measurements of the free shrinkage model members (with the thermal strain canceled) along with the measurements of specimens.

Measurements of model members indicate the averages of strain measurements at the mid-height measuring points, C1 and C2. The changes in the shrinkage of model members ought to be similar to those of specimens subjected to similar temperature histories. However, **OPC** model members had larger early shrinkages than specimens, while BPC models and specimens showed similar patterns. One reason for the difference may be, though not clear, that the placing surfaces of **OPC** model members were not covered by curing sheets, while **BPC** model members were covered. This may have increased the water evaporation from **OPC** model members, causing the plastic shinkage to increase.

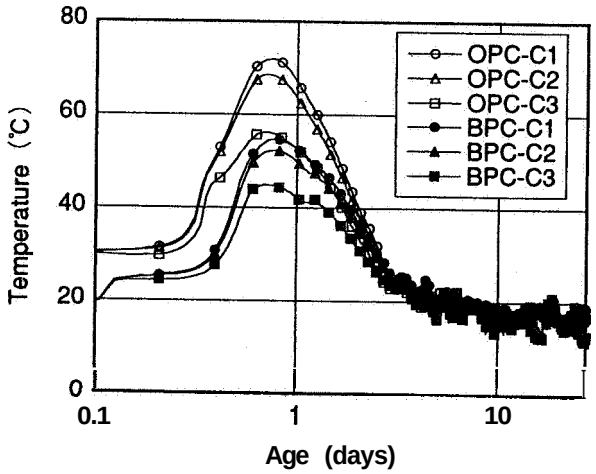

FIG.8 Temperature histories of model members

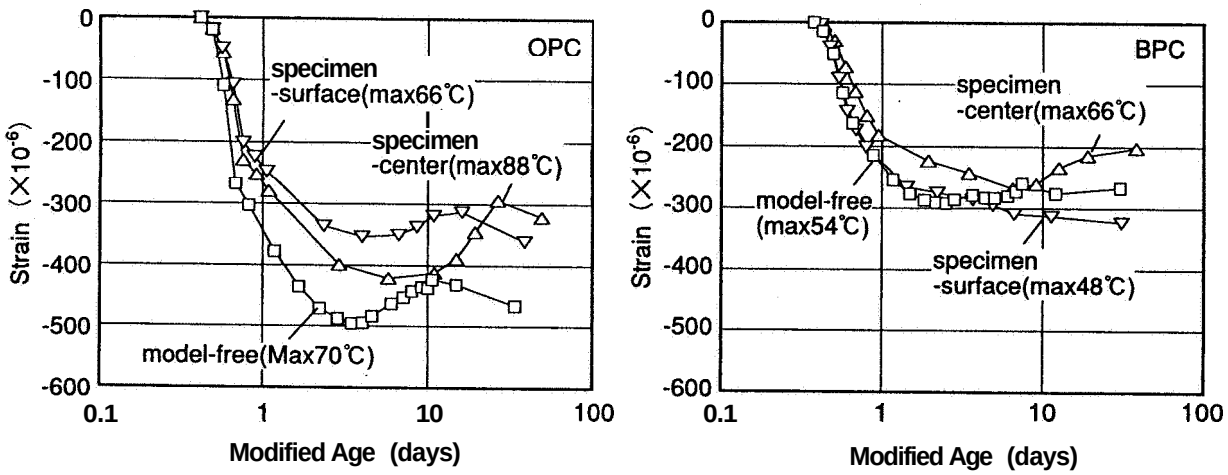

FIG.9 Shrinkage strains of model member and specimens

Figure 10 compares the measurements of concrete strain induced by autogenous shrinkage (with the thermal strain canceled) of free shrinkage model members with reinforcement similar to actual columns. The temperature history of restraining model members was nearly the same as that of the free shrinkage model members in Fig. 8. The strain of OPC and BPC restraining model members was lower by 260×10^{-6} and 170×10^{-6}, respectively, than free shrikage model members. These differences can be regarded as the tensile strain in concrete due to the restraint by the reinforcement.

Fig. 11 shows the actual strain results (including thermal strain) of concrete and reinforcement (with the linear expansion coefficient assumed to be $11.5 \times 10^{-6}/℃$ of reinforcement). The strain behaviors of concrete and reinforcement nearly agreed except immediately after the initial setting time. This suggests that the tensile force generated on the entire cross section of concrete balanced with the compressive force generated in the reinforcement, resulting in the integrated deformation. It should be noted that the reinforcement strain at R1 in OPC is found to tend to relax, presumably due to microcracks or bond slip between concrete and reinforcement.

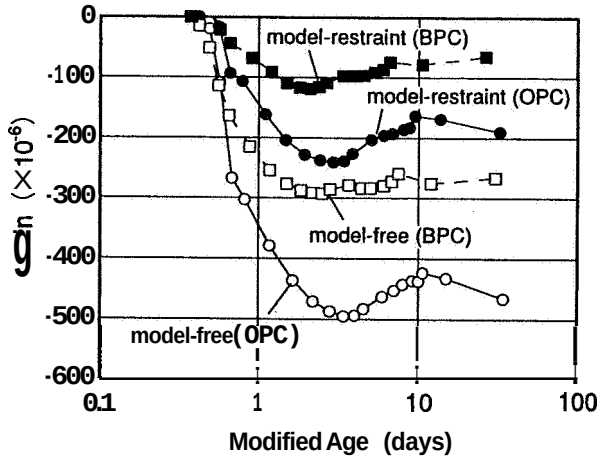

FIG.10 Shrinkage strains of free and restrained model members

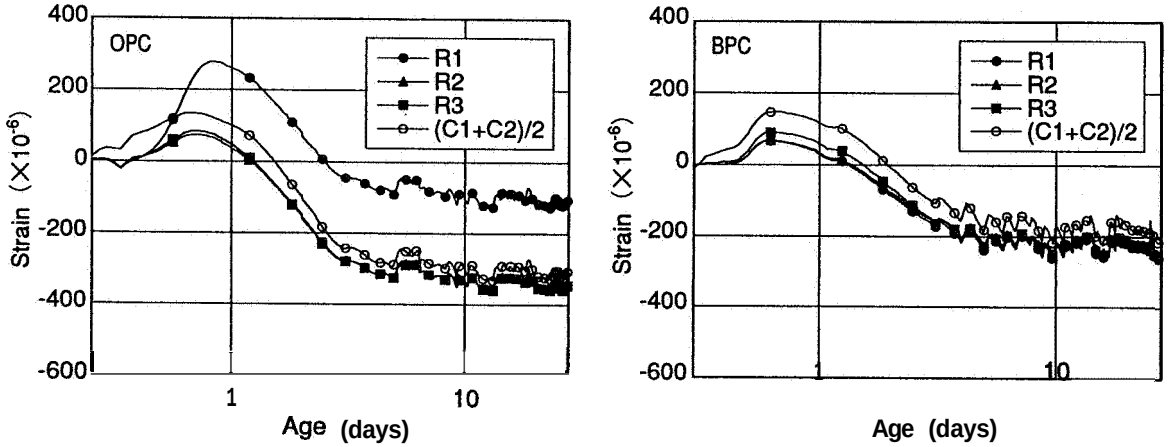

FIG.11 Actual (shrinkage+thermal) strains of main reinforcements and concrete of restrained model member

STRAIN BEHAVIOR OF ACTUAL RIGID FRAME MEMBERS

Figs 12 and 13 show the temperature histories of actual columns and beams. Fig. 14 shows the main reinforcement strain measurements of columns compared with a average of the reinforcement strain of restraining model members (except R1 in OPC). The strain behavior of actual columns is found to agree with that of restraining model members.
Fig. 15 shows the main reinforcement strain in measurements of beams. Release of main reinforcement strain was observed in OPC at about 0.5 days. However, no such strain release was observed in BPC.

The reinforcement strain measurements of OPC columns with a reinforcement ratio of 2.4 % indicate that an average restraining tensile stress of about 1.0 N/mm^2 was generated on a concrete cross section at an age of 0.6 days, at which the strain hit the maximum. Though the reinforced OPC model members showed a tendency towards strain relaxation at some reinforcing bars, no strain relaxation was observed at any measuring points on reinforcement in actual

columns. Accordingly, the specifications for the columns used in these tests are considered to be on the borderline microcracks or bond slip between reinforcement and concrete, due to autogenous shrinkage and thermal strain restraint. In regard to beams, the tensile stress of a concrete cross section is considered to be higher than in the columns, due to the restraint by the columns. The relaxation of reinforcement strain in OPC beams may therefore be attributed to microcracks or bond slip.

On the other hand, in BPC columns with a reinforcement ratio of 2.8 %, an average restraint tensile stress of a concrete cross section was calculated at about 0.9 N/mm^2 at an age of 0.6 days, and the value is considered to be higher in the beams. However, no relaxation of reinforcement strain was observed in either. Consequently, BPC with low hydration heat and small autogenous shrinkage is concluded as being superior for high strength reinforced concrete members from the standpoint of crack resistance.

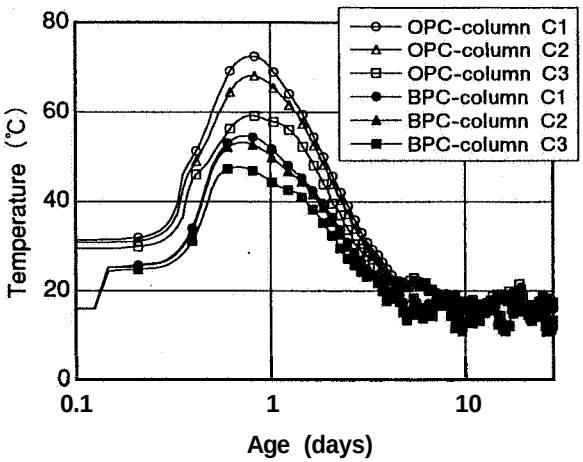

FIG.12 Temperature histories of columns

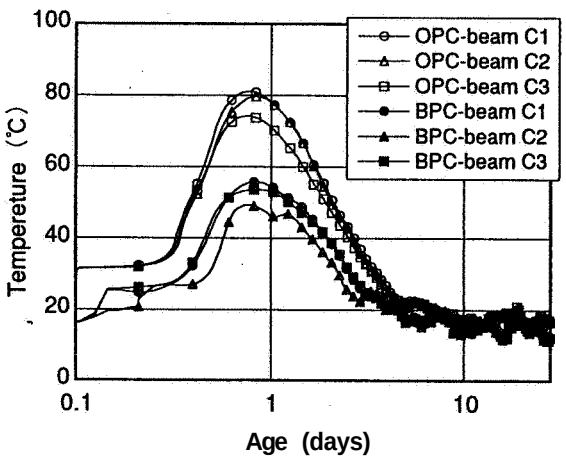

FIG.13 Temperature histories of beams

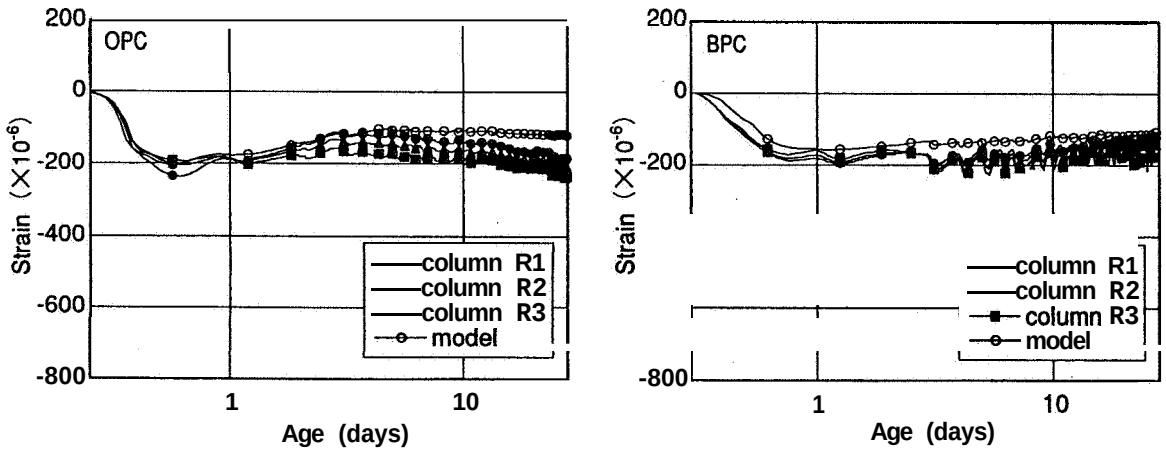

FIG.14 Strains of main reinforcements of column due to concrete shrinkage

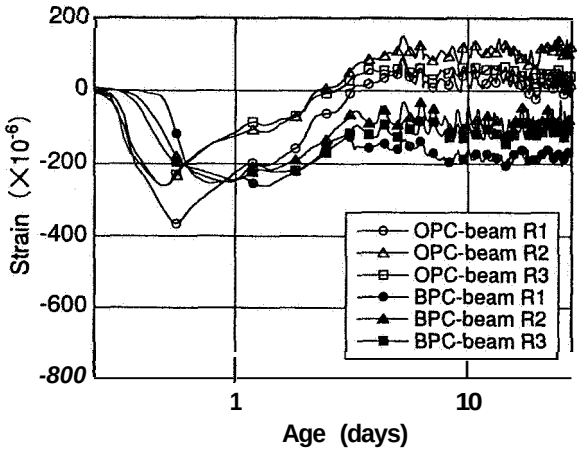

FIG.15 Strains of main reinforcements of beams due to concrete shrinkage

CREEP STRESS ANALYSIS OF COLUMN MEMBERS

ANALYSIS METHOD

The stress of column members was calculated by the step-by-step method based on the principle of creep superposition. The stress by the step-by-step method is expressed as follows:

$$\sigma(t_{i+1/2}) = \frac{1}{J(t_{i+1/2}, t_i)}\{\varepsilon_c(t_{i+1/2}) - \varepsilon_{ce}(t_{i-1/2}) - \varepsilon_{cf}(t_{i+1/2})\} \tag{4}$$

$$J(t_{i+1/2}, t_i) = \frac{1}{E(t_i)} + \frac{\phi(t_{i+1/2}, t_i)}{E_c} \tag{5}$$

$$\varepsilon_{ce}(t_{i-1/2}) = \sum_{j=1}^{i-1} \Delta\sigma(t_j) \cdot J(t_{i+1/2}, t_j) - \sigma(t_{i-1/2}) \cdot J(t_{i+1/2}, t_i) \tag{6}$$

$$\Delta\sigma(t_i) = \sigma(t_{i+1/2}) - \sigma(t_{i-1/2}) \tag{7}$$

where $\sigma(t_{i+1/2})$ =stress of concrete at time of $t_{i+1/2}$;
$\varepsilon_c(t_{i+1/2})$ =actual strain of concrete at time of $t_{i+1/2}$;
$\varepsilon_{cf}(t_{i+1/2})$ =total free strain (shrinkage+thermal) of concrete at time of $t_{i+1/2}$;
$\phi(t_{i+1/2}, t_i)$ =creep coefficient at time $t_{i+1/2}$,when concrete is loaded at time t_i;
$E(t_i)$ =modulus of elasticity at time t;;
E_c =modulus of elasticity at the age of 28 days cured in water at 20 ℃.

In the case where reinfoced concrete is assumed to be a uniaxial model, the compatibility condition under which the forces of reinforcement and concrete balance each other and their strains are equivalent is expressed as follows:

$$A_c \cdot \frac{1}{J(t_{i+1/2}, t_i)}\{\varepsilon_c(t_{i+1/2}) - \varepsilon_{ce}(t_{i-1/2}) - \varepsilon_{cf}(t_{i+1/2})\} + A_s \cdot E_s\{\varepsilon_s(t_{i+1/2}) - \varepsilon_{st}(t_{i+1/2})\} = 0 \tag{8}$$

$$\varepsilon_c(t_{i+1/2}) = \varepsilon_s(t_{i+1/2}) \tag{9}$$

where A_c =sectional area of concrete;
A_s =total sectional area of main reinforcement;
E_s =modulus of elasticity of main reinforcement;
$\varepsilon_s(t_{i+1/2})$ =actual strain of main reinforcement at time of $t_{i+1/2}$;
$\varepsilon_{st}(t_{i+1/2})$ =thermal strain of main reinforcement at time of $t_{i+1/2}$.

The strain and stress of reinforced concrete members can be determined sequentially by inputting the free strain of concrete (thermal strain and autogenous shrinkage strain) and thermal strain of reinforcement to Eqs (4)—(9).

When calculating, the linear expansion coefficients of concrete and reinforcement were assumed to be $10 \times 10^{-6}/℃$ and $11.5 \times 10^{-6}/℃$, respectively. The value input as the free strain of concrete to determine the strain of column members and the average restraining tensile stress of concrete was the average of measurements at C1 and C2 on plain model members, on the assumption that the deformation behavior at these points (center of concrete cross section) nearly determines the behavior of the entire member.

The stress at C3 (in the corner) was calculated similarly based on Eqs (4)—(7) on the assumption that the restrained strain is the difference between the determined strain of the entire member and the free strain at C3. The input value of the free strain at C3 was estimated from the tendencies of the changes in autogenous shrinkage strain corresponding to the temperature conditions of the specimens based on the temperature history at C3. It was assumed that the shrinkage of OPC columns was greater than that of specimens by about $100 \times 10^{-6}/℃$ due to plastic shrinkage, similarly to plain model members.

The input autogenous shrinkage strain values are shown in Fig. 16. The elasticity modulus of concrete was determined from the modified age at each portion and the relationship indicated in Fig. 7. The creep coefficient was determined according to the concept explained below.

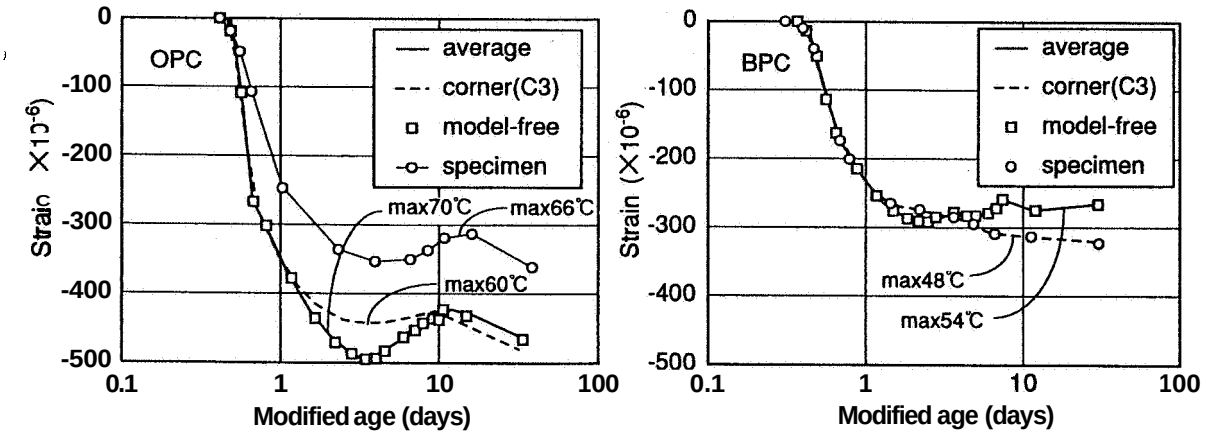

FIG.16 Free shrinkage strains of column concrete for analysis

CREEP COEFFICIENT

No measurements were made for creep coefficients in these experiments. However, the report[2]) provides the equation below as a practical relational equation for creep coefficients and elasticity modulus ratios (the ratio of the elasticity modulus at the loading age to that at 28 days) determined from the compressive creep measurements of high strength concrete (28-day compressive strength : 89.7 to 127 N/mm^2) including early ages before 1 day.

$$\phi(t,t_0) = \phi_\infty(R_E)\left[\frac{(t-t_0)/t_1}{\beta(R_E)+(t-t_0)/t_1}\right]^{0.3} \tag{10}$$

where

$$\phi_\infty(R_E) = 0.826 \cdot R_E^{-1.67} \tag{11}$$

$$\beta(R_E) = 0.0588 \cdot \exp(7.75 \cdot R_E) \tag{12}$$

where $\phi(t,t_0)$ =creep coefficient at time t,when concrete is loaded at time t_0;
t, t_0 =modified age;
R_E =$E_c(t_0)/E_c$; $E_c(t_0)$=modulus of elasticity at the age of t_0;
E, =modulus of elasticity at the age of 28 days cured in water at 20 ℃;
t_1 =1 day.

Due to begin obtained under the condition of constant 20 ℃, the consistency of these relation under temperature changes is unknown. Also, the creep under tensile stress can differ from that under compressive stress. Despite these concerns, the authors estimated the creep coefficients using Eqs (10)—(12) for numerical analysis, as these are the most effective data currently available.

An example of the estimated relationship between the creep coefficient and the modified age is shown in Fig. 17, which also shows the creep coefficient of normal-strength concrete determined from the estimation equation specified in CEB-FIP model code 90[1]).

The creep of high strength concrete tends to be high at early ages for its strength and to converge at an early age.

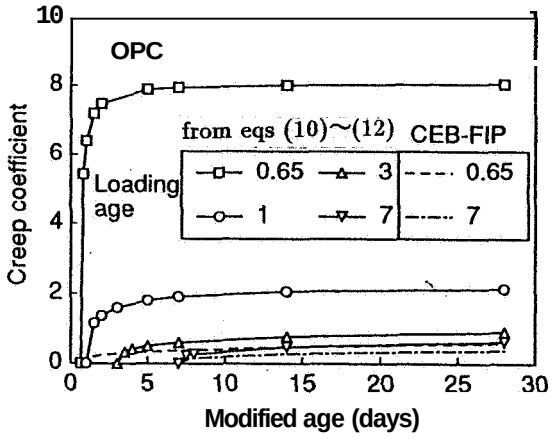

FIG.17 Creep coefficient predicted; comparison of eqs (10)—(12) with CEB-FIP

ANALYSIS RESULTS

Fig.18 shows the analyzed strain of columns compared with the measured strain (embedded strain gauge readings). Fig. 19 compares the calculated average restraining stress of concrete with the restraining stress in the corner. The analysis results for both OPC and BPC satisfactorily reproduce the actual strain behavior. This suggests that the strain behavior of high strength reinforced concrete columns entailing hydration heat can be relatively accurately traced by appropriately selecting the autogenous shrinkage (including the plastic shrinkage due to water evaporation), elastic modulus, and creep coefficient.

In regard to the absolute strain values of OPC, the analyzed and measured values agreed well, with the calculated restraining tensile stress being around 90 % of the values calculated from the measured strain of main reinfocement. On the other hand, the analyzed values for BPC differed from the measured values, with the calculated restraining tensile stress of concrete being only 60 % of the measured values. The fact that the analyzed values for both concrete were smaller than the measured values suggests that the actual tensile creep is smaller than the actual compressive creep and that the input creep coefficient is excessively large. The reason for the large gaps between the measured and analyzed values for BPC may be that actual columns may have undergo larger shrinkages than model columns, due to plastic shrinkage.

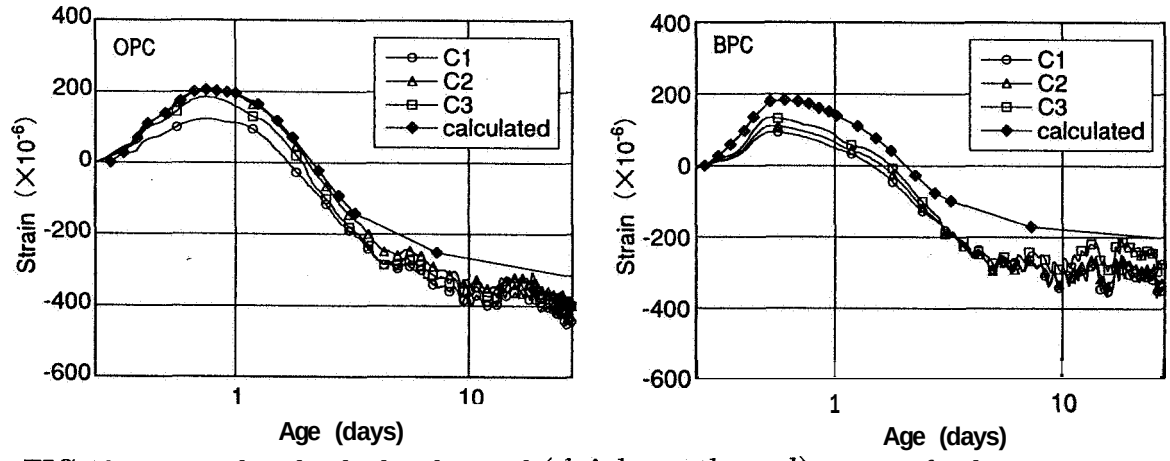

FIG.18 Measured and calculated actual (shrinkage+thermal) strains of column concrete

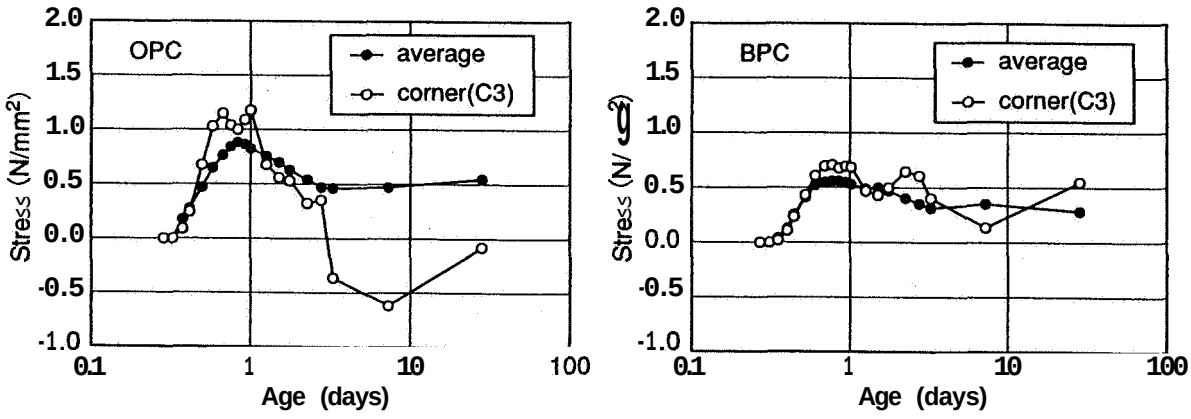

FIG.19 Calculated stresses of column concrete

The stress in the corner increased more rapidly at early ages than the average stress, particularly in OPC. The high stress in the corner is attributed mainly to internal restraining temperature stress. From these results, it is considered that if a crack occurred in a high strength concrete column, it would occur on the outer surfaces, and that such a crack can develop to a through crack, due to the significantly high stress within the concrete resulting from the restraint by the autogenous shrinkage strain.

CONCLUSIONS

The stain of column and beam concrete and main reinforcement was observed during actual construction using high strength concrete. Simultaneously, the authors measured the strain of full-scale model columns and the mechanical properties of concrete on a specimen level. These measurements and the stress analysis taking account of creep revealed the following:

1) The autogenous shrinkage of high strength concrete can be expressed by a single curve up to a modified age of 1 day. It rapidly converges thereafter, if subjected to temperature changes. On the other hand, the autogenous shrinkage of high strength concrete at a constant temperature of 20℃ increases for a long period. Concrete containing belite-rich portland cement (BPC) leads to smaller autogenous shrinkage than concrete containing normal portland cement (OPC), and the effect of temperature changes on BPC is weaker than that on OPC.

2) The elastic modulus of both OPC and BPC can be expressed as a single development curve in terms of the effective age, independently of the temperature history conditions of the members. Whereas the compressive strength development of OPC is curbed under temperature changes after an age of 3 days, BPC can be expressed as a single development curve, independently of the temperature history conditions of the members.

3) Development of the compressive strength and elastic modulus of high strength concrete including early ages before 1 day can be accurately approximated by adding the initial or final setting time as a parameter to the development equation specified in the CEB-FIP model code.

4) By the specifications for the columns in this construction, the maximum restraining stress was generated in concrete before an age of 1 day (near the peak of the member temperature) due to the reinforcement restraint of autogenous shrinkage including plastic shrinkage. The restraining stresses in OPC columns (reinforcement ratio: 2.4 %) and BPC columns (reinforcement ratio: 2.8 %) were 1.0 N/mm^2 and 0.9 N/mm^2, respectively on average over a concrete cross section.

5) The restraining stress in beams are considered to be higher than in columns. Release of main reinforcement strain was observed in OPC beams, presumably due to microcracks. However, no such strain release was observed in BPC beams. With its low hydration heat and low autogenous shrinkage strain, BPC is concluded as being excellent for high strength members from the standpoint of crack resistance.

6) The strain behavior of columns can be traced relatively accurately by a step-by-step stress analysis based on the free shrinkage strain, elastic modulus, and creep coefficient of concrete.

7) The analysis of stress generation at the inside corner compared with the average over the entire cross section revealed that the stress increased rapidly at early ages at the corner due to internal restraining temperature stress, particularly when OPC was used. If a crack occurred in high strength concrete, it would occur on the outer surface, and could develop to a through crack, as significantly high stress would have been generated within the concrete as well, due to the restraint by autogenous shrinkage strain including plastic shrikage.

8) Analyzed values for average stress over the concrete cross section were 90 % and 60 % of measured values for OPC and BPC, respectively. The gaps between the measured and calculated values may be because the creep coefficient assumed for the analysis was excessively high and because the actual free shrinkage strain of BPC concrete was higher than the value assumed in the analysis.

Acknowledgment

The research reported on this paper was carried out under the sponsorship of the committee on Practical Application Super High-strength Concrete (Chairman; Prof.F.Tomosawa). The authors would like to express their appreciation to Mr.A.Shimizu (Science Univ.of Tokyo), Prof.Y.Masuda (Utsunomiya Univ.), Dr.M.Abe (Building Research Institute), Mr.S.Arakawa (Housing and Urban Development Corp.), Hachiyo Concrete Consultant Co.,LTD.and the other committee members.

References

1) CEB-FIP model code 1990
2) Report of the research committee of the autogenous shrikage, Japanese Concrete Institute, November, 1996. [In Japanese]

EXPERIMENTAL STUDIES OF THE EFFECT OF SILICA FUME ON CHEMICAL SHRINKAGE AND SELF-DESICCATION IN PORTLAND CEMENT MORTARS

BERTIL PERSSON

Lund Institute of Technology, Division of Building Materials

Lund University, Box 118,221 00 Lund

Sweden

ABSTRACT

This article outlines an experimental and numerical study of self-desiccation and chemical shrinkage in Portland cement mortars, with or without silica fume. For this purpose 9 different cement mortars were cast in 90 pycnometers (study of chemical shrinkage and hydration) or 180 glass flasks (study of self-desiccation and hydration). Chemical shrinkage was observed for 14 days and self-desiccation for 70 days. Parallel studies were carried out on evaporable water (only cement mortar with sealed curing) and hydration. The results indicate that silica fume slightly affects the specific volume of the hydrated water. The silica fume also had a substantial (physical) effect on the self-desiccation when used in Portland cement mortars.

INTRODUCTION

Self-desiccation and strength

For normal concrete with a water-cement ratio, w/c > 0.4, sufficient water is available for the hydration of the cement to be finalised. Self-desiccation hardly effects the moisture of the concrete at all. Normally concrete is regarded as a porous material affected by the ambient climate. However, for concretes with w/c $\leq$ 0.4, the rate of hydration is decreased substantially due to self-desiccation.

The volume created in the concrete due to the chemical shrinkage that takes place when the water is attached to the cement, [1)] decreases the internal relative humidity, O_r, as low as 0.72 at low w/c. This might then affect the strength of the concrete. Furthermore, a concrete with low w/c has in any case very few capillary pores internally. The concrete might be more porous close to the surface. The few capillary pores in a concrete with low w/c probably influence the effect of water curing on both hydration and strength development in the concrete. It was thus considered important to measure the internal relative humidity of the concrete, especially at low w/c.

Effect of moisture on the durability of the concrete

Durability factors such as corrosion of reinforcement and freeze-thaw resistance are clearly affected by the moisture conditions in the concrete. The chloride diffusion is dependent on O in the concrete as well as on diffusion of gas. [2] Above a certain degree of pore saturation a substantial amount of surface concrete will spall due to ice lenses created in fieeze-thaw periods. [3), 4)] A freeze-thaw resistant concrete must be either air-entrained or contain a sufficient air-filled pore volume related to chemical shrinkage during the hydration. In this case too, knowledge of the moisture situation in the concrete is of the utmost importance.

Factors influencing the human environment

In dwelling houses the maximum ambient O is normally restricted to $O < 0.70$. For houses made of concrete it was then considered essential to estimate the time required for the drying of the concrete to this level of O. During the drying period the ventilation must be sufficient to reduce the moisture content in the house. When wood is placed directly on the concrete, the O of the concrete must not exceed 0.75, [5)] or else the moisture of the concrete will cause mould fungus between the concrete and the wood. These organisms will secondarily cause a bad smell in the house, allergic reactions etc. When $O > 0.80$ the wood starts to rot. [5)] At $O > 0.85$ fungus may also occur between the plastic carpet and the concrete. [5)] Finally, when $O > 0.90$ glued carpets may loosen from the concrete due to too high a saturation of the pores (no space for the glue resin in the concrete pores). [5)]

Self-desiccating concrete has been used in practice in Sweden since 1990 to avoid those problems in dwelling houses. [6), 7)] Until today about 1.000.000 m^2 of concrete floor have been made using concrete with $w/c < 0.4$ for the purpose of obtaining fast desiccation. Presently this method has also been used in Finland [8)] and is being introduced in Denmark.

Objectives

The main objective of this study was to determine the effect of silica fume on chemical shrinkage and on self-desiccation of Portland cement systems. Secondarily the effect of silica fume on the hydration was studied in combination with studies of the evaporable water.

CHEMICAL SHRINKAGE

Theory

When water, cement and silica fume are mixed a chemical reaction occurs at which mainly calcium hydroxide and calcium silicate hydrates are formed. After the reaction has started the water appears as chemically bound, physically bound to the inner faces of the material and as free capillary water. Both the physically bound and the free water evaporate during desiccation at 105°C. Those two types of water are denoted evaporable water, w_e. The chemically bound water is denoted non-evaporable, w_n. It can be detected by ignition at 1050°C. When the water is chemically bound a decrease of volume happens, known as chemical shrinkage. Also physically bound water (absorbed) exhibited shrinkage but normally very little.

The specific volume of physically bound water is about 0.99 cm^3/g, i.e. very close to the specific volume of free water. [9] Measurement of chemical shrinkage can be carried out by pycnometer tests where a glass flask, a rubber plug and a pipette is used, FIG.-1. The thickness of the specimen must be small, otherwise the intrusion of water on which the measurement is based is worsened, i.e. vacuum inside the specimen and a measurement fault appears. The chemical shrinkage, δw_n, is directly proportional to the development of hydration:

$$\delta w_n = k_1 \cdot w_n \qquad (1)$$

FIG.-1
Set-ups for pycnometer tests of chemical shrinkage.

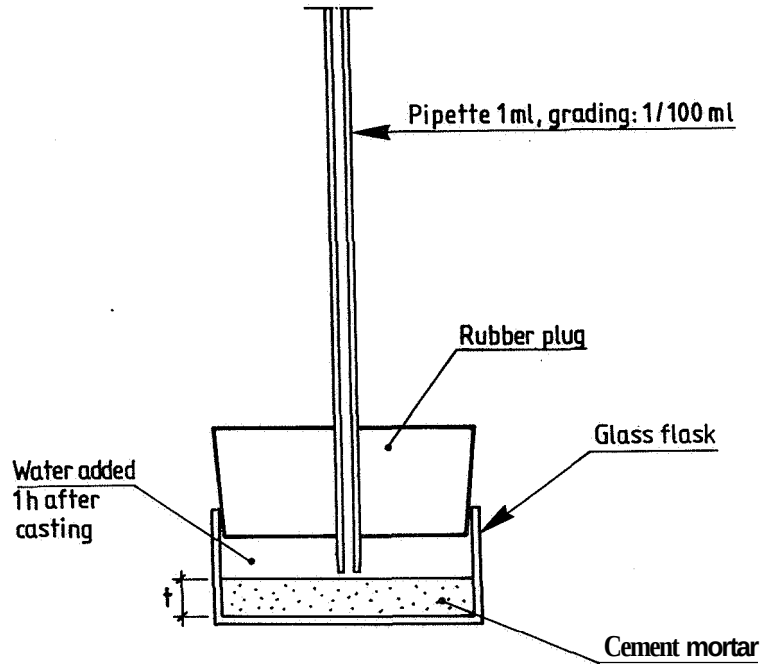

$$\alpha = (w_n/c) \cdot (1/k_2) \qquad (2)$$

k_1 ≈0.25 for Portland cement mortar with "normal" w/c
k_2 ≈0.25 for Portland cement mortar (when all cement is hydrated)
a denotes the degree of hydration

From equations (1) and **(2)** the following equation was evaluated:

$$\delta w_n = k_1 \cdot k_2 \cdot \alpha \cdot c \approx 0.063 \cdot \alpha \cdot c \qquad (3)$$

At low wlc both k_1 and k_2 may change. The value of k_1 is obtained by measurement of both chemical shrinkage and hydration in the same specimen. The degree of hydration, a, may be calculated provided that k_2 is constant and independent of w/c and presence of silica fume.

Previous research on chemical shrinkage

The average specific volume of hydrated water, k, is about 0.74 cm^3/g, i.e. $k_1 \approx 1\text{-}0.74 = 0.26$ fairly independent of the degree of hydration [9] when water was used as medium. Other liquids showed a slightly larger value of k_1. Adopting equation (3) the hydration, a, was estimated:

$$\alpha \approx (1/0.063)\cdot(\delta w_n/c) \approx 15\cdot\delta w_n/c \qquad (4)$$

Extensive studies were carried out on the chemical shrinkage of Portland cement pastes. [10] FIG.-2 shows that the chemical shrinkage is dependent on both age and thickness of the specimen. [10] The figure shows that chemical shrinkage increases with wlc and decreases with the thickness of the specimen. At w/c= 0.3 the thickness should be less than 1 cm. The chemical shrinkage was also studied versus hydration, FIG.-3, for w/c= 0.4 and w/c= 0.45 respectively. [10] According to FIG.-3 k= 0.79 and k= 0.76, i.e. slightly larger than observed by others. [9] In FIG.-3 the thickness was 3.5 and 8 cm which may be too large, causing a vacuum in the specimen. [10]

FIG.-2
Chemical shrinkage of cement paste versus age at different specimen sizes, t. [10]

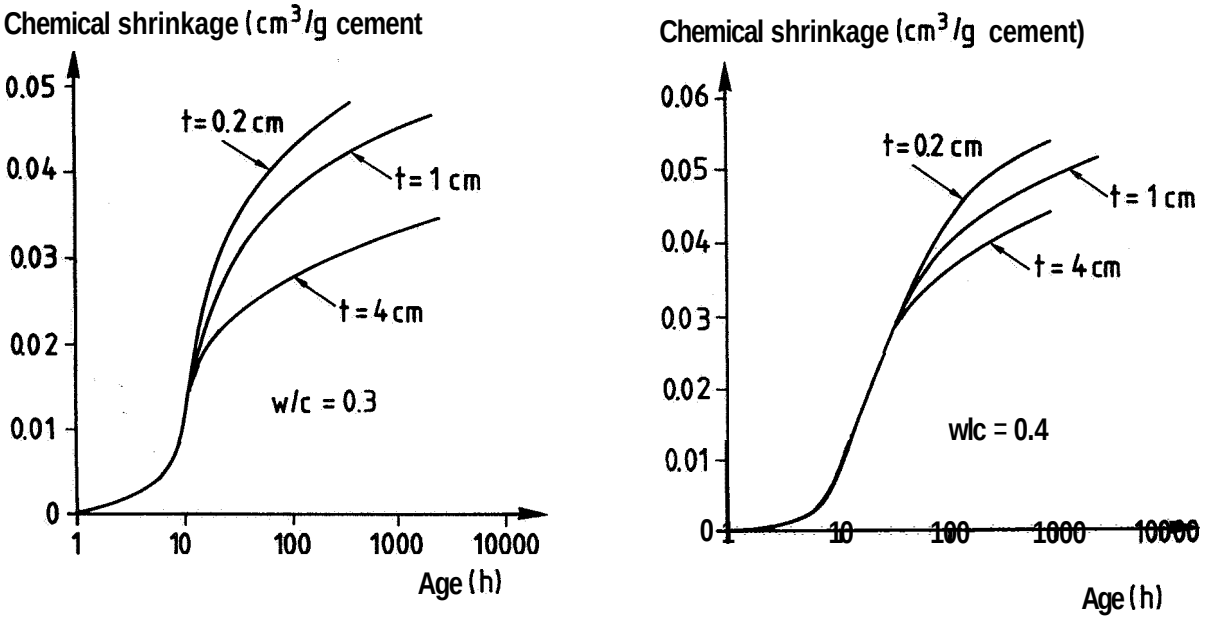

FIG.-3
Chemical shrinkage of cement paste versus ratio of non-evaporable water to cement, w_n/c. To the left: w/c= 0.4; to the right: w/c= 0.45. t denotes layer thickness (cm). [10]

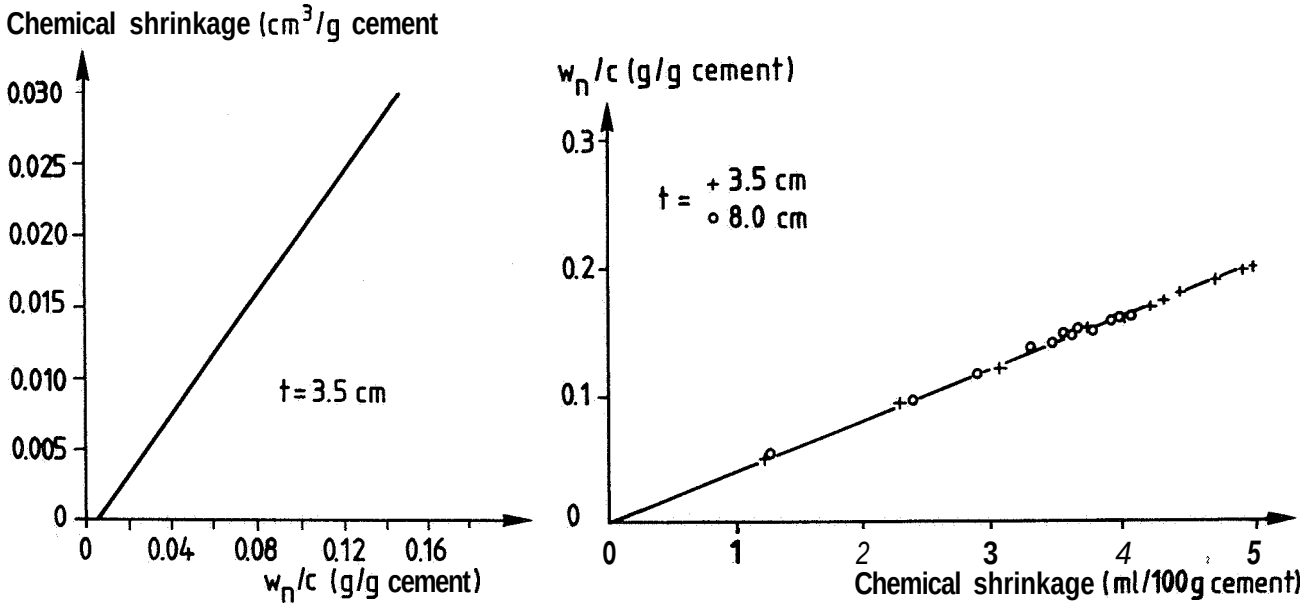

FIG.-4 shows [11] the chemical shrinkage during hydration of cement mortars with w/c varying between 0.35 and 0.55. After about 1 day the chemical shrinkage decreases with w/c. This phenomena is well-known and depends on the decreasing probability of water to reach the cement corns. FIG.-4 also shows the way to calculate the hydration from the chemical shrinkage according to equation (4) [11] provided the chemical shrinkage is 25%, i.e. k= 0.75. The chemical shrinkage of cement pastes with or without silica fume was also studied. [12] w/c exceeded 1 and the glass flasks in use were rotated for 120 days. The specific volume was found to be k= 0.74 for pure cement pastes and k= 0.72 after addition of 10% silica fume. [12]

FIG.-4
Chemical shrinkage during hydration of cement mortars with varying w/c. [11]

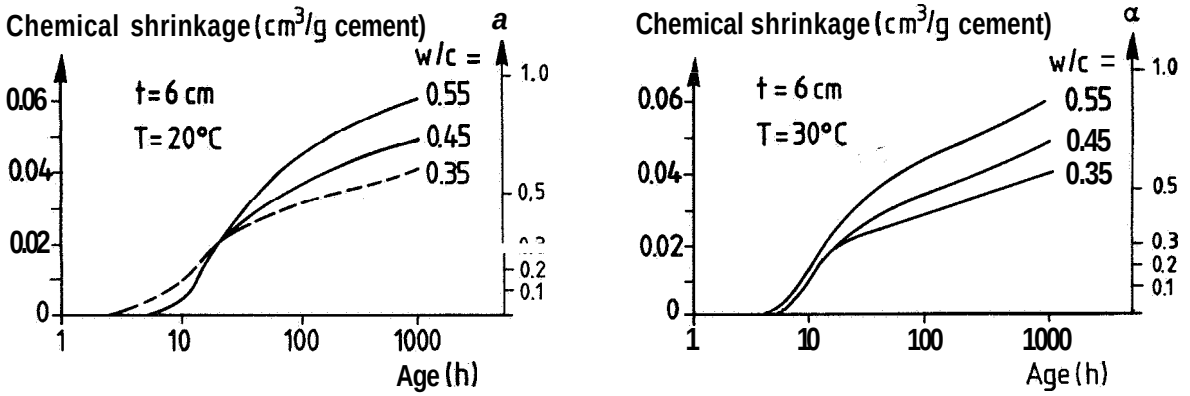

Material and experimental methods

General

The purpose of the test was to determine the chemical shrinkage and the hydration on the same specimen in order to eliminate possible faults dependent on different development of hydration. Material data is given in Tables 1 and 2. [13] Table 3 gives the mix proportion of the cement mortars. The superplasticiser was of the type naphthalene sulphonate acid/formaldehyde condensate. The amount of superplasticiser was calculated on the basis of the cement content to coincide with other parallel long-term experiments on hydration and strength of High-Performance Concrete. [14] The cement type B was chosen to observe the effect of the alkali content on the properties of the cement mortar. [15], [16]

Methods

About 30 g of each mortar was cast in 10 glass flasks each. The thickness was about 5 mm. The temperature of all the material and the equipment was held at 20°C. Cement mortar and glass-flasks were weighed before and after each stage of the test. The eleventh flask and pipette shown in FIG.-5 was filled up with the corresponding amount of sand and filled with 1.7% concentrated NaOH (in order to observe possible shrinkage or expansion of the sand or possible temperature movements). After 1 h the glass-flask and the pipette was carefully filled with water. The starting point of the pipette was set. All 99 glass-flasks were placed in a water bath in order to avoid temperature movements. The reading of the water-level were carrying out daily for 14 days. Directly after the reading the glass-flask was crushed and the cement mortar was rapidly dried out at 105°C. After the evaporable water was measured the ignition of 16 h took place.

Table 1 - Chemical composition of cements.

Analysed properties (%):	A	B
CaO	64.6	63.8
SiO_2	21.8	20.2
Al_2O_3	3.34	4.65
Fe_2O_3	4.39	2.46
MgO	0.84	3.01
K_2O	0.62	1.13
Na_2O	0.07	0.27
Alkali	0.48	1.01
SO_3	2.23	3.29
CO_2	0.14	2.0
Free CaO	1.13	0.88
C_2S	22.5	14.8
C_3S	53.0	65.8
C_3A	1.42	6.7
C_4AF	13.4	7.6
Ignition losses (%)	0.64	2.71
Fineness (m^2/kg Blaine)	325	384
Density (kg/m^3)	13180	3120

Table 2 - Properties of gravel and silica fume. [13)]

Physical properties:	Sand	Silica fume
Ignition losses (%)	0.99	2.58
Fineness (m^2/g)	-	17.5
Density (kg/m^3)	2650	550

Table 3 - Mix proportions of Portland cement mortars (dry material weight, g). [13)]

Mortar no/ material	1	2	3	4	5	6	7	8	9
Sand 0-2 mm	1528	2532	1585	3913	3315	5616	3848	4873	2585
Silica fume	333	-	319	-	252	-	198	-	319
Cement A, low-alkaline	3333	3137	3187	2698	2521	2045	1984	2027	
Cement B									3187
Superplasticiser	92	61	58.8	21.8	20.2	20.7	14.3	-	58.8
c (%)	55.4	44.7	53.8	35.9	38.7	23.7	28.4	25.3	46.1
s/c	10	0	10	0	10.0	0	9.9	0	9.9
Superplasticiser/c	2.76	1.94	1.84	0.81	0.80	1.16	0.72	-	1.84
w/c	0.218	0.246	0.241	0.333	0.352	0.463	0.469	0.556	0.239

FIG.-5
Set-ups for tests of chemical shrinkage. [13)]

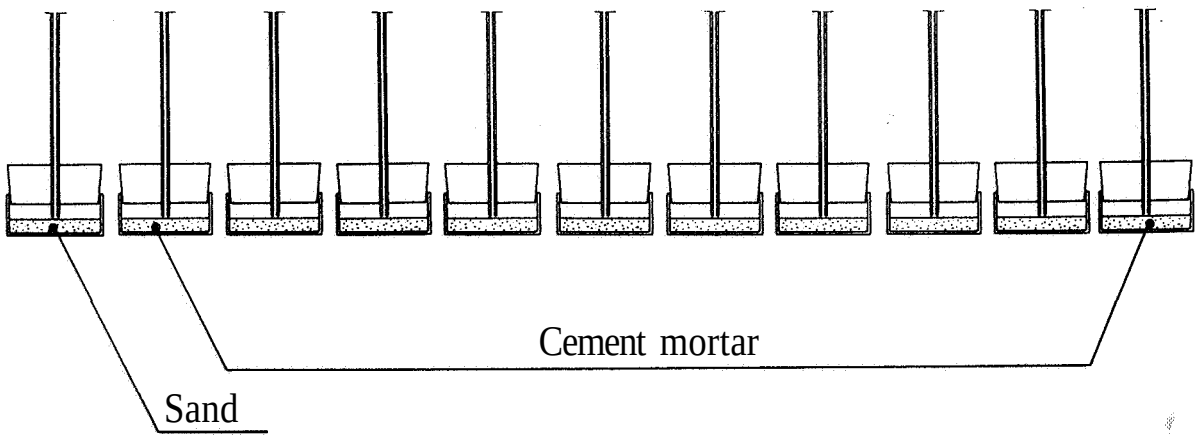

Results

Calculation of hydration

The calculation were carried out after compensation of ignition self-losses of the materials shown in Tables 1 and **2.** [17] Silica fume was considered an aggregate in the calculations. [14]

$$w_n / c = \frac{w^{105}(1-\eta) - w^{1050}}{w^{1050} - \frac{\psi \cdot \gamma}{1+\gamma} \cdot w^{105}} \quad (5)$$

$$\psi = 1-\mu_a \quad (6)$$

$$\eta = \frac{\mu_c + \gamma \cdot \mu_a}{1+\gamma} \quad (7)$$

w_{105}/c	denotes the ratio of non-evaporable water to amount of cement	(kg/kg)
w^{105}	denotes the weight after drying at 105°C	(kg)
w^{1050}	denotes the weight after ignition at 1050°C	(kg)
γ	denotes the ratio of aggregate to cement	
μ_a	denotes the ignition losses of the aggregate	(kg/kg)
μ_c	denotes the ignition losses of the cement	(kg/kg)

Hydration and chemical shrinkage

FIG.-6 shows the specific volume of chemically bound water, k, calculated by use of the measured chemical shrinkage, δw_n, and the hydration of the mortars, w_n:

$$k = 1-(\delta w_n / w_n) \quad (8)$$

The variations in FIG.-6 seem to be large mainly due to the scale. FIG.-7 shows the standard deviation and coefficient of variation of the measured specific volume of non-evaporable water.

FIG.-6
Specific volume of hydrated water versus age.

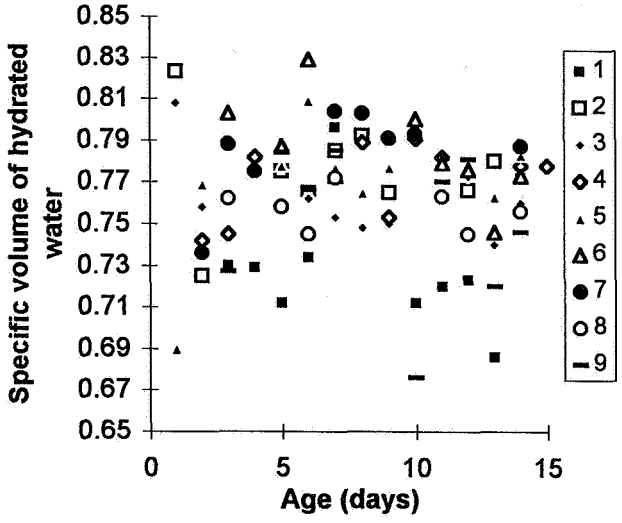

FIG.-7
Standard deviation and coefficient of variation

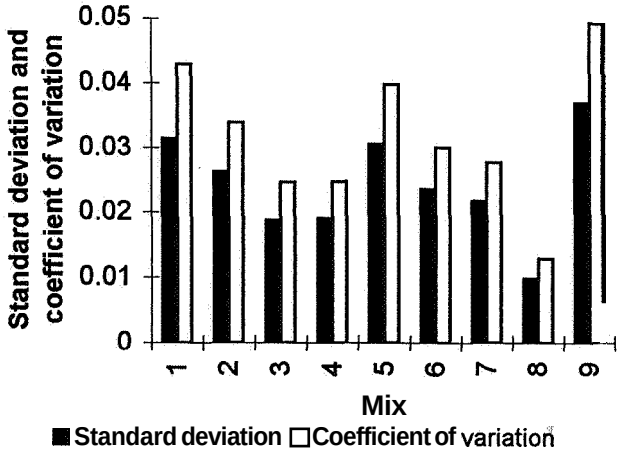

The average coefficient of variation of the measured specific volume was less than 3%, which was reasonably good taking into account that the measurements were carried out in two steps: measurement of the chemical shrinkage, δw_n, and of the hydration of the mortars, w_n.

Effect of silica fume on the specific volume of hydrated water - discussion

Both [10] and [11] showed that the thickness of the mortar had an influence on the measured specific volume of chemical shrinkage. There also seemed to be an influence of silica fume on the specific volume. [12] FIG.-8 shows the specific volume of mortar versus wlc. When w/c was held constant the specific volume was larger for mortars without silica fume than with silica fume, which partly was an effect of the cement content, c. The resistance to water penetration was larger at low wlc [18] which would have given less chemical shrinkage, i.e. a larger specific volume. This was not observed in these studies, which indicate that the thickness of the mortar was sufficiently low. FIG.-9 shows that the cement content of the mortar had an influence on the measured chemical shrinkage, especially when the mortar contained silica fume. When the cement content was low the sand probably slightly restrained the chemical shrinkage. (The cement mortar no. 8 is not shown in the Figures 8 and 9 due to bleeding.) From Figures 8 and 9 the specific volume of hydrated water in cement mortar without sand (cement paste) was estimated, FIG.-10.

FIG.-8
The specific volume of mortar versus w/c. c= cement content (by weight). B= alternative cement.

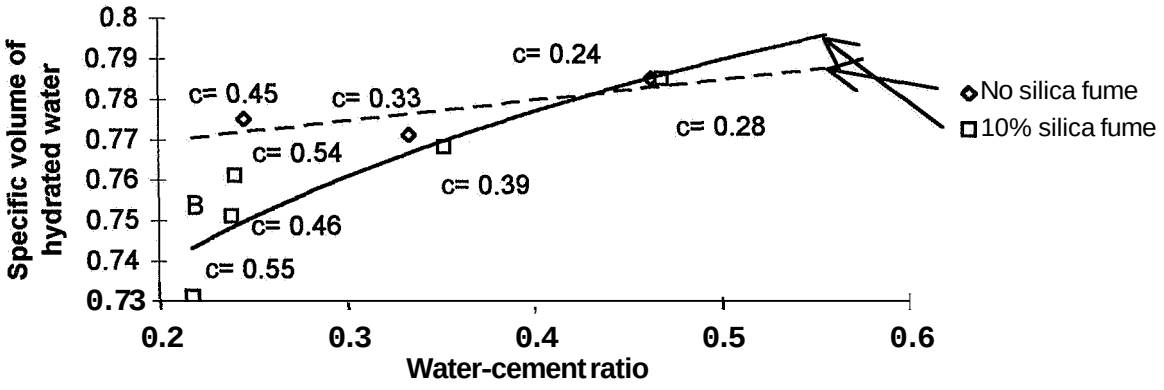

FIG.-9
Measured chemical shrinkage versus the cement content of cement mortar. B= alternative cement.

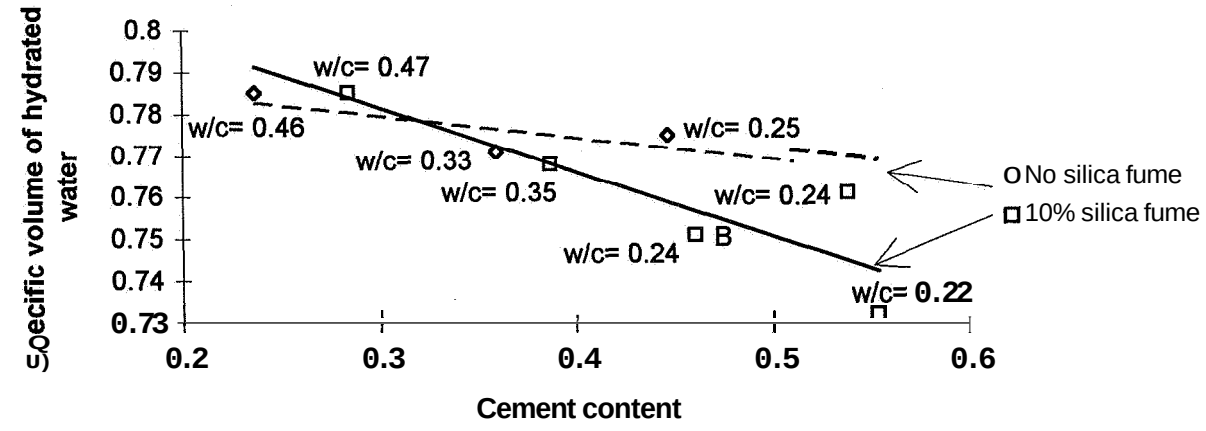

FIG.-10
Estimated specific volume of cement mortar without sand (cement paste).

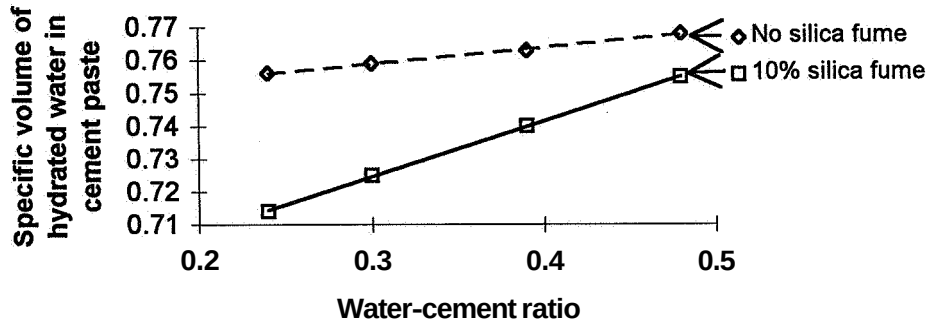

From FIG.-10 the following equations were calculated:

$$k = 0.74+0.05\cdot(w/c) \quad (9)$$

$$k_s = 0.67+0.17\cdot(w/c) \quad (10)$$

k denotes the estimated specific volume of hydrated water in cement paste
k_s denotes the specific volume of hydrated water in cement paste with 10% silica fume

SELF-DESICCATION

Theory and previous research

General

Concrete, which is regarded as a fine porous material, has great ability to bind moisture which is supplied directly from the air. The higher the relative humidity, 0 , the more water can be bound. The ability to bind moisture, hygroscopicity, depends on either adsorption, Ø< 0.45, or capillary condensation, Ø> 0.45. The physically bound and the free water evaporates during desiccation at 105°C. These two types of water are denoted evaporable water, w_e. The correlation between w_e and O is known as the isotherm which indicates that the temperature has some influence. At lower temperatures the concrete binds more water. It is of great interest to study the isotherm since it expresses the amount of water that has to be dried out from the concrete to reach a certain 0 . For example Ø= 0.85 is regarded as a safe level at which plastic carpets can be applied with adhesive compound on the concrete, cp. the text above.

Previous research

With sealed curing the concrete binds water without any excess of water. Due to chemical shrinkage, as described above, self-desiccation takes place which lower O in the concrete until the reaction ceases at about Ø= 0.72. [19), 20), 21), 22)] FIG.-11 shows the evaporable water to cement, w_e/c, of a cement paste with w/c= 0.6 at different amounts of silica fume. [19)] The results just show that the addition of silica fume increased the proportion of gel pores and small capillary pores.

FIG.-11
Evaporable water to ignited cement of cement paste with w/c= 0.6 at different amounts of silica fume. [19)]

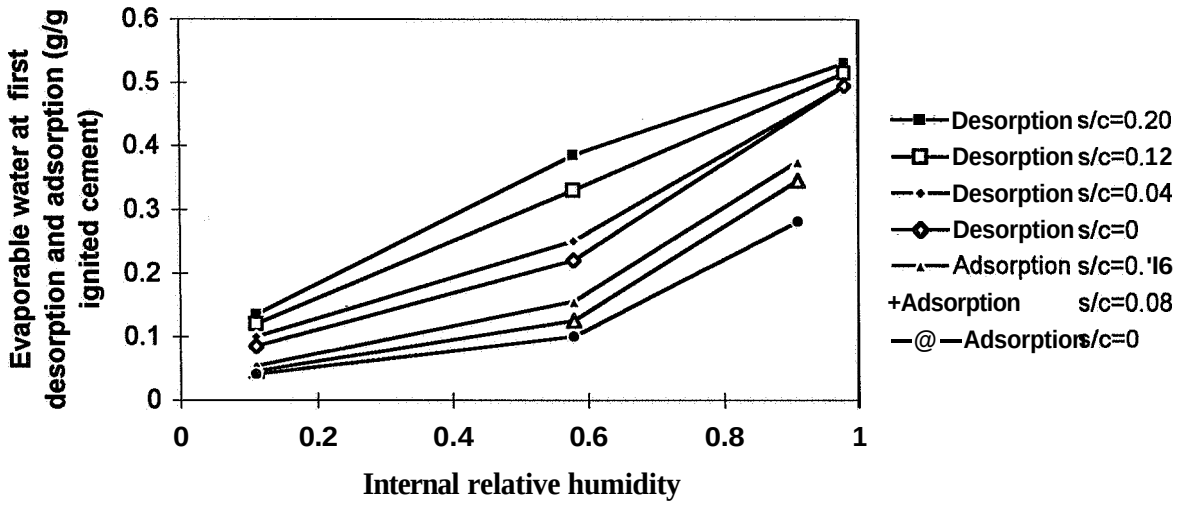

To some extent the effect was explained by the filler effect of silica fume. The filler effect had almost no effect on the gel porosity. [19)] The great effect of silica fume on the O in the isotherm was a result of the slope of the curves in FIG.-11. A small reduction of water caused a large change in O when silica fume was present. [19)] These observation also apply to sealed curing since some of the free water and capillary water then moves into the gel pores.

Hydration with sealed curing

High-Performance Concrete possesses less water than necessary for the hydration to proceed to a final state. The maximum degree of hydration, α= 1, can then only be obtained at a water-cement ratio larger than 0.39. The maximum degree of hydration, α, of a curing with a water-cement ratio less than 0.39 is then linear-dependent on the water-cement ratio. [14)]

$$\alpha_{max} = w/(0.39 \cdot c) \qquad (11)$$

α_{max} denotes the maximum degree of hydration
w denotes the mixing water of the concrete (kg/m^3)
c denotes the cement content of the concrete (kg/m^3)

The degree of hydration, α, can also be expressed as (the resisting symbols given above):

$$\alpha_{max} = w_n/(0.25 \cdot c) \qquad (12)$$

w_n denotes the non-evaporable water content of the concrete (kg/m^3)

Dividing equation (11) by equation (12) gave the maximum value of the relative hydration defined as [the symbols of Eqs (13) and (14) are given above]:

$$(w_n/w)_{max} = 0.64 \quad \{0<w/c<0.39\} \qquad (13)$$

$$(w_n/w)_{max} = 0.25 \cdot c/w \quad \{w/c>0.39\} \qquad (14)$$

Material and experimental methods

General

The purpose of the study was to determine self-desiccation and hydration on the same specimen in order to eliminate possible faults dependent on different development of hydration. Material data were given in Tables 1 and 2. [13] Table 3, above, gives the mix proportion of the cement mortars. The superplastisicer was of the type naphthalene sulphonate acid/formaldehyde condensate. The amount of superplastisicer was calculated on the basis of the cement content to coincide with other parallel long-term experiment on hydration and strength of High-Performance Concrete. [14] Cement type B was chosen to observe the effect the alkali content. [15), 16)]

Methods

From each mix of mortar 20 glass tubes were filled with about 200 ml cement mortar each and tightened with rubber plugs. The temperature of all the material and the equipment was held at 20°C. The cement mortar and the glass tubes were weighed before and after each stage of the study. Every week 2 tubes of each mix were crushed. O was measured on the mortar from one tube. The mortar from the other tube was rapidly dried at 105°C and then ignited at 1050°C for 16 h. Capacity sensors were used for 22 h to measure 0 . Calibrating of the sensors took place at Ø= 0.755, 0.851, 0.946 and 0.976 within 5 days of the time of measurement. [23] The accuracy of the sensors was within ± 0.02 O. No systematic fault was observed.

Results and discussion

Effect of silica fume on hydration and internal relative humidity, O

The ratio of non-evaporable water to cement, w_n/c, of sealed cement mortars was calculated, equation (5), and divided by w/c resulting in the parameter w_n/w, FIG.-12 [7]. FIG.-12 also shows the internal relative humidity, 0 , of cement mortars with sealed curing [13].

The maximum relative hydration was obtained at low w/c in cement mortar without silica fume, i.e. $w_n/w \approx 0.5$. In cement mortars with silica fume w_n/w became lower since some of the calcium hydroxide reacted pozzolanically. In cement mortar with cement B (normal alkaline) the O decreased more than in cement mortar with low-alkaline cement. [15), 16)] However, in cement mortar with normal alkaline cement, the O increased after 6 weeks since the alkaline effect was eliminated due the pozzolanic reaction with silica fume. [15), 16)] From FIG.-12 the following equations were calculated for the relative hydration, w_n/w, and the internal relative humidity, O:

$$w_n/w = 0.719\cdot[0.813-(w/c)]\cdot t^{0.349\cdot(w/c)-0.037} \quad \{0.2<w/c<0.6;\ 7<t<70 \text{ days}) \quad (15)$$

$$(w_n/w)_S = 0.645\cdot[0.877-(w/c)]\cdot t^{0.184\cdot(w/c)-0.020} \quad \{0.2<w/c<0.5;\ 7<t<70 \text{ days}) \quad (16)$$

$$Ø = -0.564\cdot[(w/c)^2 - 1.13\cdot(w/c)-1.43)]\cdot t^{0.0791\cdot(w/c)-0.0588} \quad \{0.2<w/c<0.6;\ 7<t<70 \text{ days}) \quad (17)$$

$$Ø_S = -1.43\cdot[(w/c)^2 - 0.838\cdot(w/c)-0.5]\cdot t^{0.208\cdot(w/c)-0.115} \quad \{0.2<w/c<0.5;\ 7<t<70 \text{ days}) \quad (18)$$

c denotes cement content (kg/m^3)
t denotes age (days)

FIG.-12
Hydration, w_n/w, and O versus age. w= mixing water; w_n = non-evaporable; S= 10% silica fume.

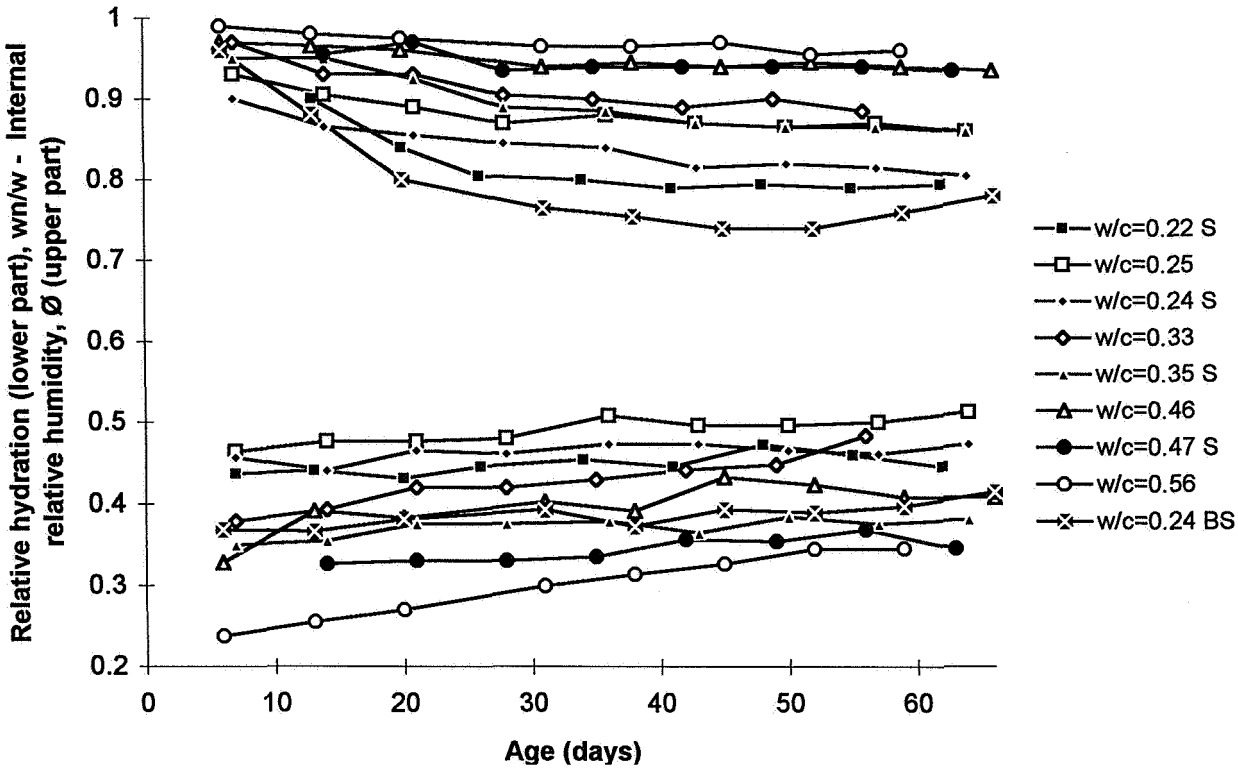

w denotes mixing water content (kg/m^3)
w_n denotes non-evaporable water (kg/m^3)
w/c denotes water-cement ratio
w_n/w denotes relative hydration
S denotes 10% silica fume
O denotes internal relative humidity

When w/c was held constant the addition of 10% silica fume to the concrete generated a substantially lower hydration and internal relative humidity in the concrete. The effect of silica fume on hydration was thus chemical since the calcium hydroxide reacted pozzolanically. The effect of the silica fume on the internal relative humidity most probably was a combined chemical effect, as mentioned above, and a filler effect according to the well-known Kelvin equation.

Internal relative humidity and hydration

A combination of the equations (15) to (18) above gave the possibility to eliminated time, t, i.e. a direct correlation between hydration and internal relative humidity, FIG.-13:

$$Ø = -1.61\cdot[(w_n/w)^2-0.48\cdot(w_n/w)-0.0552] \quad (19)$$

$$Ø_S = -0.717\cdot[(w_n/w)^2+487\cdot(w_n/w)-1.581] \quad (20)$$

w_n/w denotes relative hydration
S denotes 10% silica fume
O denotes internal relative humidity

However, the coefficient of correlation was fairly low for equations (19) and (20), 0.78 and 0.88 respectively. A coefficient of correlation above 0.9 provides a sufficient high significance. The reason for the low significance of equations (19) and (20) was probably the accuracy of the measurement of the internal relative humidity, ± 0.02 and the influence of the variation of the specific volume of chemical shrinkage. (The specific volume of chemical shrinkage was dependent on w/c especially for concrete with silica fume and was not included in relative hydration.)

Internal relative humidity and degree of saturation

One way to eliminate the influence of the variations in the specific volume of hydrated water, k, was to calculate the degree of saturation, So. From a practical point of view it was of also interest to detect the effect of silica fume on the relation between internal relative humidity, 0, and the degree of saturation, S_0. In order to calculate S_0 it was necessary to measure the evaporable water, w_e, as well Parallel to the measurements of internal relative humidity and but before ignition of the cement mortars w_e was measured for all 90 specimens. [13] Since w_e was measured for each specimen possible differences in w/c between the specimens were eliminated. The ratio of non-evaporable water and evaporable water, w_n/w_e was observed. [7] In cement mortars with silica fume the ratio w_n/w_e decreased after about 6 weeks probably due to polymerisation. [24), 25)] Finally S_0 of cement mortars with sealed curing was calculated according to the equation, FIG.-14:

$$S_0 = w_e/(w-k\cdot w_n) \qquad (21)$$

k	specific volume of non-evaporable water measured for each mix above
w	denotes mixing water content (kg/m^3)
w_e	denotes the evaporable water (kg/m^3)
w_n	denotes the non-evaporable water (kg/m^3)
S_0	denotes the degree of saturation of cement mortars with sealed curing

FIG.-13.
Internal relative humidity, 0, of cement mortar with sealed curing versus relative hydration, w_n/w.

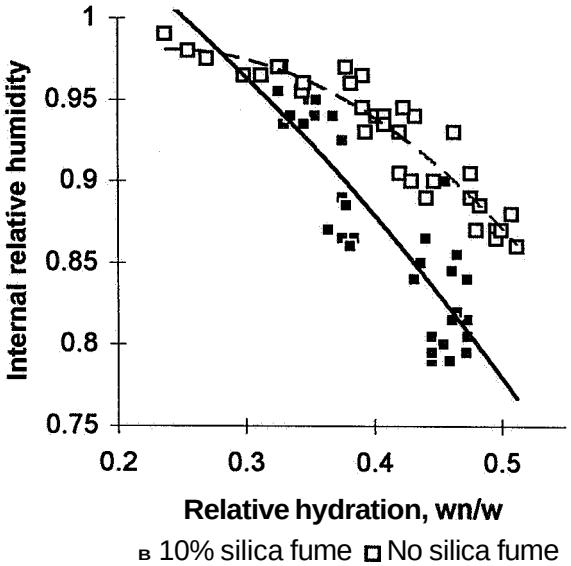

FIG.-14.
Internal relative humidity, O, of cement mortar with sealed curing versus degree of saturation, S_0.

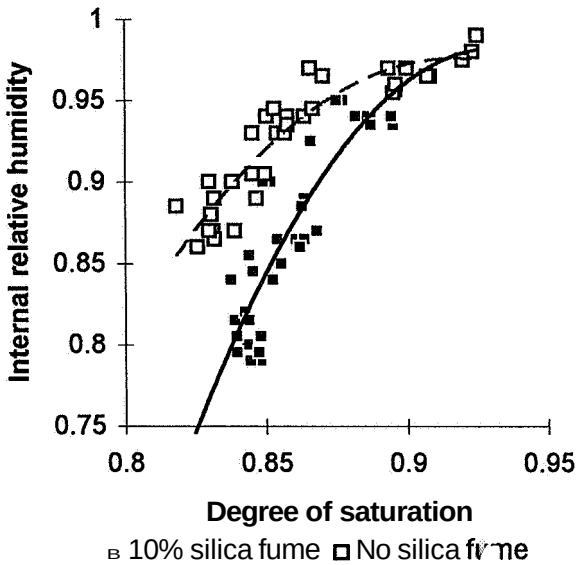

From FIG.-14 the following correlations were calculated between O and S_0:

$$Ø = -12.4 \cdot [(S_0)^2 - 1.86 \cdot S_0 + 0.821] \quad (22)$$

$$Ø_S = -20.7 \cdot [(S_0)^2 - 1.83 \cdot S_0 + 0.763] \quad (23)$$

O denotes internal relative humidity, the resisting symbols given above

The result of derivation of equations (21) and (22) indicated the sensitivity of O to changes in degree of saturation:

$$\delta Ø / \delta S_0 \approx 25 \cdot S_0 - 1.8 \quad (24)$$

$$(\delta Ø / \delta S_0) \approx 41 \cdot S_0 - 1.8 \quad (25)$$

S_0 denotes the degree of saturation of cement mortars with sealed curing

Concrete with silica fume was thus more sensitive to changes of the degree of saturation: For example, the surface of the concrete became saturated after adhesives were applied, which caused an increase of measured emissions compared with emissions from adhesives applied on normal concrete. However, noticeable emissions occurred only at high internal relative humidity, $O > 0.90$. [26] Problems related to spalling of the concrete during accidental fire also occurred in concretes with silica fume most probably due to the high sensitivity of silica fume concretes related to changes in the degree of saturation. [27), 28] (During accidental fire the relative humidity in a silica fume concrete increases more rapidly than in a concrete without silica fume.)

SUMMARY AND CONCLUSIONS

The effect of silica fume on the specific volume of hydrated water and on the internal relative humidity was studied for 9 Portland cement mortars for 14 and 70 days respectively. The following conclusions were drawn:

1) When silica fume was not added, the specific volume of hydrated water found to be around 0.75.

2) With 10% silica fume the specific volume was found to be 0.71 at low w/c and 0.75 at higher w/c.

3) Mortars with 10% silica fume exhibited around 10% lower internal relative humidity when the degree of saturation or the relative hydration was held constant.

4) The rate of self-desiccation related to desaturation increased substantially in cement mortars with silica fume compared with mortars without silica fume.

5) The measured internal relative humidity decreased more rapidly in cement mortars with normal alkaline cement than in mortars with low-alkaline cement.

6) Cement mortars with normal alkaline cement exhibited a slightly increasing of the internal relative humidity after about 6 weeks.

REFERENCES

1) T C Powers; T L Brownyard. Studies of Physical Properties of Hardened Portland Cement Paste. Research Laboratories of the Portland Cement Association. Bulletin 22. Journal of the American Concrete Institute. New Center Bldg. Detroit 2. Michigan. USA. Oct. 1946-April 1947. Proceedings. Vol. 43. 1947. Pp 984-987.
2) K Tuutti. Corrosion of steel in concrete. The Cement and Concrete Institute. Report Fo 4:82. CBI. Stockholm. Sweden. 1982. Pp 277-286, 302-303.
3) G Fagerlund. The critical degree of saturation method - a general method of estimating the frost resistance of materials and structures. The Cement and Concrete Institute. Report Fo 12:76. CBI. Stockholm. Sweden. 1976.
4) G Fagerlund. Influence of Environmental factors on the Frost Resistance of Concrete. TVBM-3059. Lund Institute of Technology. Division of Building Materials. Lund. Sweden. 1994. Pp 19-22.
5) L-O Nilsson. Moisture Problems at Concrete Floors. TVBM-3002. Lund Institute of Technology. Division of Building Materials. Lund. Sweden. 1980. Pp 36-51.
6) B Persson. Self-desiccating High-Strength Concrete slabs. Proceedings at the symposium of High-Strength Concrete in Lilleharnmer. Norway 1993. Edited by Holand and Sellevold. 1993. Pp 882-889.
7) B Persson. *"**Hogpresterande** betongs **hydratation, struktur och hållfasthet.**"* Hydration, structure and strength of High Performance Concrete. Report TVBM-1009. Lund Institute of Technology. Division of Building Materials. Lund. Sweden. 1992. Pp 225-254, 317-335. ***(In Swedish with English summary and with English captions)***
8) *V* Penttala; *T* Merikallio; L Wirtanen. Early Floor Covering of Concrete Slabs and adhesion between concrete and floor covers. Proceedings at the 5th Nordic Concrete Research Meeting. Helsinki. Edited by Norsk Betongforening. Oslo. Norway. 1996. Pp 107-108.
9) T C Powers. Physical Properties of Cement Paste. Research and Development Laboratories of the Portland Cement Association. Bulletin 54. Fourth International Symposium of the Chemistry of Cement. Washington DC. USA. Monograph 43. Volume II. Session V. Paper V-l. 1960. Pp 577-609.
10) T Knudsen. The Effect of Sample-Size on the Hydration of Water-Cured Portland Cement Pastes. Institute of Mineral Industry. The Technical University of Denmark. Lyngby. Denmark. 1987. Pp 1-4.
11) A K Christoffersen; T B Sørensen. Self-Desiccation and Chemical Shrinkage of Cement Mortar. Technical Report no 158186. The Technical University of Denmark. Department of Civil Engineering. Building Materials Laboratory. Lyngby. Denmark. 1896. Pp 56-61.
12) D Hooton. Chemical shrinkage of cement pastes with or without silica fume. Presentation at the 93rd Annual Meeting of the American Ceramic Society. Westerville. USA. 1991.
13) B Persson. *"**Hogpresterande** betongs **hydratation, struktur och - data och** beräkningar."* Hydration, structure and strength of High Performance Concrete. Laboratory data and calculations. Report TVBM-7011. Lund Institute of Technology. Division of Building Materials. Lund. Sweden. 1992. Pp 37-58. ***(In Swedish)***
14) B Persson. Hydration and Strength of High Performance Concrete. Advanced Cement Based Material. Elsevier Science Inc. New York. USA. 1996. Pp 107-123.
15) G Hedenblad; M Janz. Effect of Alkali on the Measured Internal Relative Humidity in the Concrete. Report TVBM-3057. Lund Institute of Technology. Division of Building Materials. Lund. Sweden. 1994. Pp 5-12.
16) J-E Jonasson. Modelling of Temperature, Moisture and Stresses in Young Concrete. Doctoral Thesis. Report 153D. Division of Structural Engineering. Department of Civil and Mining Engineering. Luleå University of Technology. Luleå. Sweden. 1994. Pp 129-146.

17) J Byfors. Plain Concrete at Early Ages. Doctoral thesis. Report Fo 3:80. The Cement and Concrete Institute. Stockholm. Sweden. 1980. Pp 40-43.
18) B Persson. Drying of Concrete after Different Kinds of Curing. Materials and Structures. RILEM. Paris. France. ***(Accepted for publication 1977)***
19) E Sellevold; D Bager; E Klitgaard-Jensen; T Knudsen. Silica Fume-cement pastes: hydration and pore structure. Proceedings of a Nordic Seminar on Silica Fume in Concrete. Cement and Concrete Research Institute. The Norwegian Institute of Technology. Trondheim. Norway. 1981.
20) L-O Nilsson. Desorption Isotherms for Silica-Fume/Cement Mortars. Report IF 8431. Institute of Moisture Issues on Material & Building Technology. Trelleborg. Sweden. 1984. Pp 2-11.
21) A K Christoffersen; T B Sørensen; A. Nielsen. *"Selfudtørring af betong."* Self-Desiccation of Concrete. Danish Concrete Magazine *"Beton"*. No 4, 1988. (In ***Danish)***
22) K Norling Mjörnell. Self-desiccation in concrete. Report P-94:2. Division of Building Materials. Chalmers University of Technology. Gothenburg. Sweden. 1994. Pp 21-28.
23) ASTM E 104-85. Standard Practice for Maintaining Constant Relative Humidity by Means of Aqueous Solutions. The American Society for Testing and Materials. Philadelphia. USA. 1985. Pp 33-34,637.
24) *H* Kühl. *"Der Baustoff **Zement.**"* The Building Material Concrete. Verlag fir Bauwesen. Berlin. Germany. 1967. Pp 211. ***(In German)***
25) A Durekovic; B Tkalcic-Ciboci. Cement pastes of low solid to paste ratio: An investigation of the polymerisation of silicate anions in the presence of a superplasticizer and silica fume. Cement and Concrete Research. Vol. 21. 1991. Pp 1015-1022.
26) H Gustavsson. *"Golvmaterial på olika typer av fuktiga betongunderlag - **Oversikt och kommentarer till undersokningar med inriktning på kemisk nedbrytning och emission.**"* Flooring on different types of moistured concrete - Review and comments on studies related to chemical deterioration and emissions. Report SP 1996:25. Swedish National Testing and Research Institute. Borås. Sweden. 1996. Pp 15, 21-22. ***(In Swedish)***
27) G L England; N Khoylou. Modelling of the moisture behaviour in normal and High Performance Concretes at elevated temperatures. Proceedings of the Fourth Weimar Workshop on High Performance Concrete held at Hochschule für Architektur und Bauwesen (HAB). Weimar. Germany. 1995. Pp 53-67.
28) U Diederichs. High Temperature Properties and spalling behaviour of High Strength Concrete. Proceedings of the Fourth Weimar Workshop on High Performance Concrete held at Hochschule fir Architektur und Bauwesen (HAB). Weimar. Germany. 1995. Pp 219-326.

MICROSTRUCTURAL MODELLING OF SELF-DESICCATION DURING HYDRATION

DALE P. BENTZ, KENNETH A. SNYDER and PAUL E. STUTZMAN
National Institute of Standards and Technology
Gaithersburg, MD 20899-0001
USA

ABSTRACT

A three-dimensional cellular automaton-based microstructural model has been applied to simulate the process of self-desiccation during the hydration of cement paste. As hydration occurs, the proper amount of empty pore space, corresponding to the chemical shrinkage of the cement paste, is created within the microstructure. This empty pore space in turn influences the future kinetics of the hydration process, as less water-filled space is available for the dissolution and precipitation of cement phases. Model predictions are compared with experimental data, including both SEM images of microstructure and measurements of degree of hydration based on non-evaporable water content. For water-to-cement ratios below 0.40, sealed curing conditions are seen to result in a significant decrease in the achievable hydration, relative to curing under saturated conditions. The addition of silica fume is observed to further increase the self-desiccation and decrease the achievable degree of hydration. The model can also be adapted to other curing scenarios, such as saturated curing until the capillary porosity becomes disconnected, followed by sealed curing, to assess the effects of different curing regimens on the hydration and subsequent performance of cement-based materials.

INTRODUCTION

As a concrete matures under sealed conditions, empty capillary porosity is created within its cement paste component due to the chemical shrinkage that accompanies the cement hydration reactions. This process was quantified many years ago by Powers[1], but is also the subject of much recent research[2–6]. The creation of empty capillary pore space has two major effects on the evolving cement paste system. First, the chemical shrinkage results in a reduction in the system's internal relative humidity (RH). Quantified by Gause and Tucker in 1940[7], this RH reduction can be quite substantial, with RH values as low as 70% measured for low (< 0.3) water-to-cement (w/c) ratio cement paste and concrete systems[8,9]. Based on the Kelvin-Laplace equation, this reduced RH will induce capillary pressures, $\sigma_{capillary}$, in the pore water described by:

$$\sigma_{capillary} = K\gamma = -\frac{\ln(\frac{RH}{100})RT}{V_m} \qquad (1)$$

where RH is the relative humidity expressed as a percentage, K is the average curvature of the surface of the condensed water, γ is its surface tension, R is the universal gas constant (8.314 J/(mol·K)), T is absolute temperature, and V_m is the molar volume of water. In turn, these capillary pressures will result in a measurable autogeneous shrinkage of the paste or concrete[3,5,6]. According to equation (1), the induced capillary pressures will be seven times greater in a system with an RH of 70% compared with one with an RH of 95%, which may be one reason why low w/c ratio concretes are often more susceptible to early age cracking.

The second effect of the creation of empty capillary pores is a change in the hydration kinetics of the cement paste[10,11]. Because cement hydration reactions generally proceed by a dissolution/precipitation mechanism and the empty pore space created due to self-desiccation is no longer available to be filled with hydration products, the hydration will slow down and effectively terminate at a lower degree of hydration than could be achieved under saturated conditions. The remainder of this paper will focus on this latter effect, using a combination of experimental and computer modelling techniques to quantify the effects of curing conditions on the measured degree of hydration of a variety of cement pastes with and without silica fume additions.

EXPERIMENTAL PROCEDURES

Saturated and Sealed Specimens

Composition and properties of the two ASTM Type I portland cements used in this study, Cements 115 and 116 issued in 1995 by the Cement and Concrete Reference Laboratory at NIST, can be found elsewhere[12,13]. The cement and the necessary mixing water, w/c=0.30, were conditioned at 25 °C overnight and then mixed together by hand in a sealed plastic bag for two to three minutes. Paste samples on the order of ten grams were stored in capped plastic vials at 25 °C until measuring the non-evaporable water content, typically after ages of 1, 3, 7, 14, 28, 56, and 90 days. For the saturated samples, approximately 1 mL of water was added on top of the cement paste to provide water throughout the experiment. Non-evaporable water was quantified as the mass loss between 105 °C and 950 °C, corrected for the loss on ignition of the dry cement powder, assessed in a separate measurement. These values were converted to degrees of hydration based on similar measurements performed on fully hydrated specimens (w/c=3.0, continuously rotated in a jar mill for 28 days), which yielded values of 0.226 and 0.235 g H_2O/g cement for Cements 115 and 116, respectively. 28 days in a jar mill was deemed sufficient to achieve complete hydration, as no further hydration was observed when the curing was extended to 42 days. For Cement 115, two samples, one saturated and one sealed, were removed after 94 days of curing and prepared for viewing in the scanning electron microscope (SEM).

Computer Simulations

In addition to the experimental studies, computer simulations were performed using the NIST cement paste microstructural model[12,13]. This model employs a sequence of dissolution/diffusion/reaction cycles to simulate the hydration reactions between cement particles and water. Typically, the cement paste microstructure is represented within the computer as a cubic volume 100 pixels on a side, with each pixel corresponding to a volume of 1 μm^3. Hydration is simulated using a cellular automata approach to repetitively update the phases/species present at each pixel in the microstructure[13].

In this study, for each of the two cements, initial 3-D cement particle images, based on their measured particle size distributions and the phase area and perimeter (surface) fractions measured on 2-D SEM/X-ray images[12], were created for w/c=0.30 and w/c=0.40. These 3-D systems were then "computationally hydrated" under saturated and sealed conditions. For saturated conditions, it is assumed that all capillary porosity remains water-filled throughout the hydration process. In the case of sealed (self-desiccating) conditions, the computer model creates empty pore space as the hydration occurs to account directly for the chemical shrinkage[13], which is typically on the order of 0.06 mL H_2O/g cement hydrated. This empty pore volume is computed as the difference between the total capillary porosity and the volume of water not yet incorporated into hydration products after each cycle of the simulated hydration. In an attempt to model the actual physical process, the largest pores are emptied first, and no hydration products are deposited in pores which have been emptied. A previous calibration of model cycles to real time[12,13] for hydration under saturated conditions was then applied to create model degree of hydration vs. time curves for both saturated and sealed curing conditions to compare with the experimental counterparts. In addition, two-dimensional slices from the "fully hydrated" (i.e., 5000 cycles of hydration) three-dimensional computer model microstructures were created to compare to the SEM images for the saturated and sealed curing conditions for Cement 115 with w/c=0.30.

Recently, to predict the adiabatic response of a wide variety of concretes, the NIST microstructural model has been modified to include the pozzolanic reaction between silica fume and calcium hydroxide[14], forming a pozzolanic *C-S-H* with a stoichiometry of $C_{1.1}SH_{3.9}$ and a molar volume of 101.81 cm^3/mole. The stoichiometry and molar volume were chosen to be consistent with phase composition and chemical shrinkage results presented in the literature[6,15-17]. The reaction corresponds to an additional chemical shrinkage of 0.20 mL H_2O/g silica fume reacted. Thus, systems containing silica fume, if they hydrate to the same degree, will undergo a greater amount of chemical shrinkage than those without silica fume. The effects of silica fume replacement on hydration kinetics during sealed curing were investigated using the microstructural model for Cement 116 with 5% and 10% replacement levels of silica fume, while maintaining a constant water to solids (cement plus silica fume) ratio (w/s) of 0.40.

RESULTS

FIG.-1 compares the degree of hydration achieved under saturated and sealed conditions for the two cements studied, for w/c=0.30. For both cements, the sealed conditions are observed to reduce the achieved hydration, particularly at times exceeding 7 days. At early times, the newly created empty capillary porosity has only a minor effect on the hydration kinetics as a significant volume fraction of water-filled capillary pore space still exists. For w/c=0.30, initially, about 50% of the cement paste volume is filled with water. However, as water is consumed by the hydration reactions, the fraction of empty pore space relative to that which is water-filled becomes significant, and a substantial reduction in the hydration rate is observed. The predicted results based on the NIST cement paste microstructural model are seen to closely follow the experimental values, particularly for Cement 115.

Simulations performed for the two cements with w/c=0.40 have indicated smaller differences in the hydration kinetics between curing under saturated and sealed conditions. For Cement 115, the "final" achieved degrees of hydration after 5000 cycles of the hydration model were 0.88 and 0.83 for the saturated and sealed conditions, respectively. The

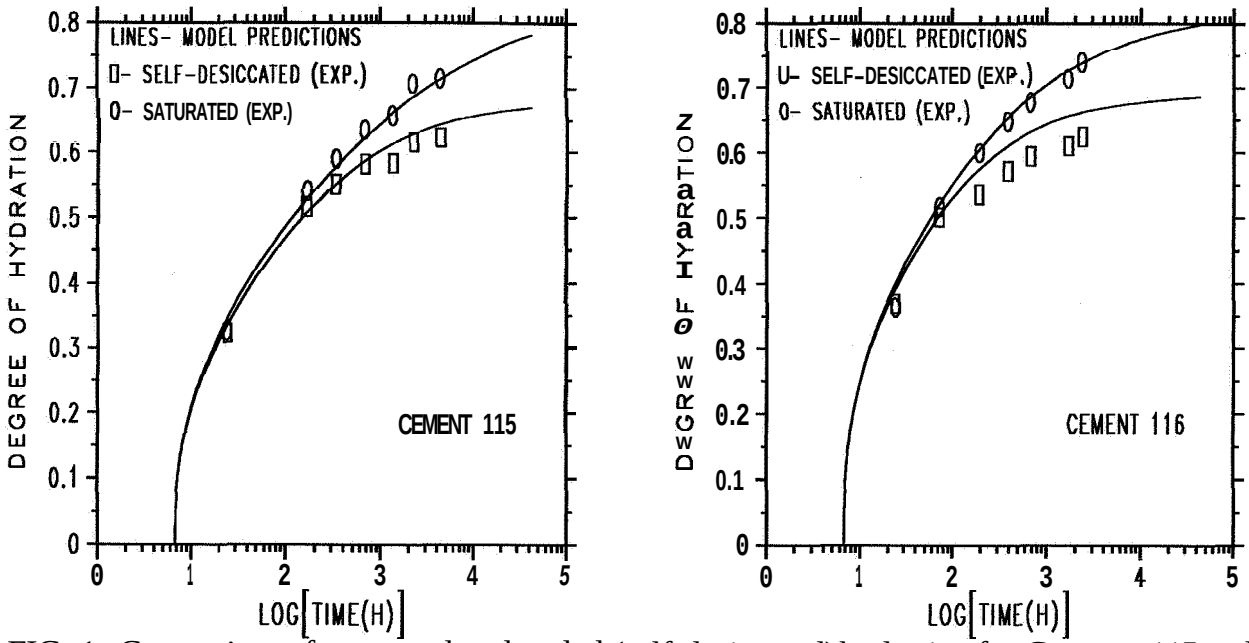

FIG.-1: Comparison of saturated and sealed (self-desiccated) hydration for Cements 115 and 116 with w/c=0.30.

corresponding values for Cement 116 were 0.90 and 0.85. These differences of 0.05 can be compared with the difference of about 0.10 for the w/c=0.30 systems as shown in FIG.-1. In addition, the differences to be expected after 28 days of curing, for example, were less than those for the w/c=0.30 systems (on the order of 0.01 for Cement 115 and 0.03 for Cement 116). Furthermore, experimental determinations have indicated basically no difference in the degrees of hydration achieved after 28 days curing for w/c=0.5 cement pastes cured under saturated and sealed conditions, in agreement with simulation results. Thus, as expected, the effects of self-desiccation on hydration kinetics are seen to definitely become more prominent at lower (< 0.4) w/c ratios.

The model can be further validated against experiment by comparing SEM micrographs of real sample microstructures to two-dimensional images from the 3-D model. Figures 2 and 3 provide such a comparison at similar scales for Cement 115 with w/c=0.30. The two most distinguishing features between the sealed and saturated specimens are the area and size of the unhydrated cement grains and the area and size of the observable capillary pores. One can clearly observe that there are more and larger unhydrated cement grains in the sealed specimens (particularly in terms of the alite grains which are surrounded by a dense layer of calcium silcate hydrate gel), in agreement with their measured lower degrees of hydration. Based on quantitative SEM measurements of the unhydrated cement area fractions, after 94 days, the saturated sample has achieved a degree of hydration of 0.79 ± 0.03 while the sealed sample has only achieved a value of 0.66 ± 0.04, based on the averages from eleven fields of view (1024 pixels $\times$800 pixels, 0.25 μm/pixel) for each sample, and expressed with an uncertainty of one standard deviation. The corresponding degrees of hydration for the two model systems shown are 0.80 and 0.69, respectively. In addition, due to the emptying of the capillary pores due to chemical shrinkage, many relatively large pores remain in the sealed specimens. Once again, the effects observed in the real specimens are duplicated reasonably well by the model, as the real and model images appear quite similar.

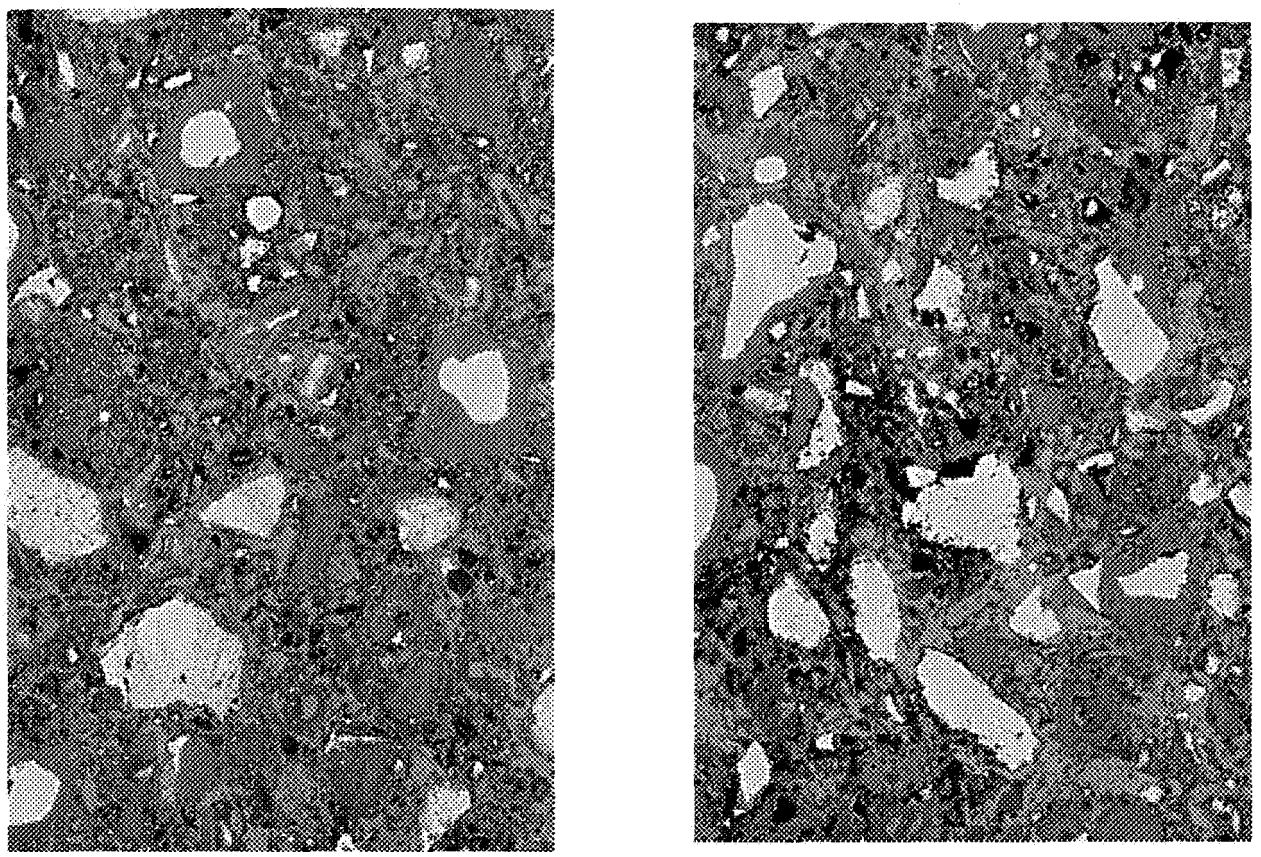

FIG.-2: Comparison of real SEM images for saturated (left) and sealed (right) hydration for Cement 115 with w/c=0.30 after 94 days of curing. Unhydrated cement is white, porosity is black, calcium hydroxide is light grey, and calcium silicate hydrate gel and other hydration products are dark grey. Areas imaged are approximately 128 pm ×190 pm.

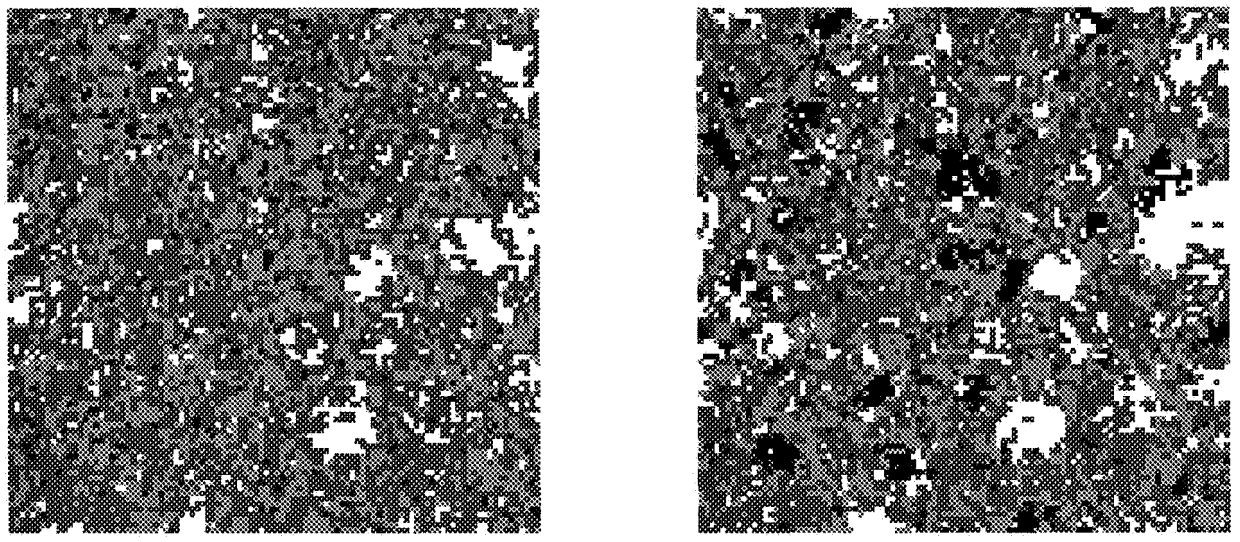

FIG.-3: Comparison of model images for saturated (left) and sealed (right) hydration for Cement 115 with w/c=0.30. Greyscale assignments are the same as those given above for the real images. Areas represented by the images are 100 pm ×100 pm.

The model can also be used to explore the effects of different curing regimens on achievable hydration. For example, many years ago, Powers[10] suggested maintaining saturated curing conditions only until the capillary porosity depercolates, as beyond this point, it may be difficult to maintain internal saturation. Analysis of microstructures generated using a monophase cement microstructural model[18] have indicated that this depercolation occurs at a capillary porosity of about 20%, for w/c ratios below 0.6, in general agreement with the earlier experimental results of Powers[19]. To explore the effect of this curing regimen on hydration, simulations were conducted for Cement 116 with w/c=0.30 in which empty capillary porosity due to chemical shrinkage was only created after the system capillary porosity had fallen below 20%, which occurs at a degree of hydration of about 0.5. FIG.-4 shows the resultant degree of hydration vs. cycles curve, in comparison with the equivalent curves for hydration under saturated and sealed curing conditions. For these simulations, 5000 cycles of hydration would correspond to approximately 4 years of curing at 25 "C. The "sealed after 20% porosity" curve is seen to most closely follow the completely saturated curve, supporting the criticality of proper early curing practices for achieving a durable concrete.

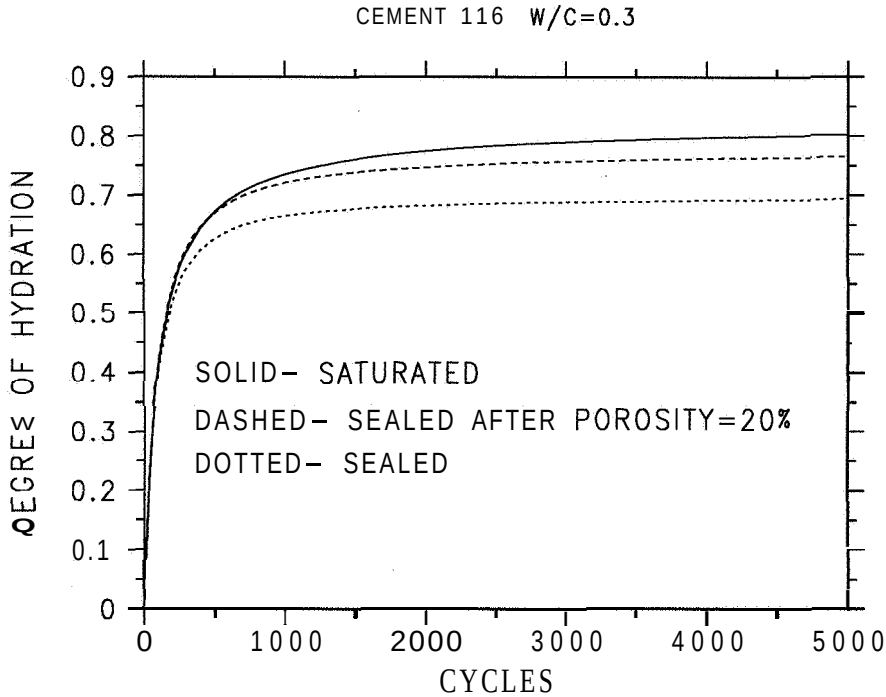

FIG.-4: Comparison of hydration under different curing regimens.

Simulations have also been performed to assess the effects of silica fume additions on the self-desiccation and achievable hydration. FIG.-5 shows the effects of 5% and 10% silica fume replacements (maintaining a constant water-to-solids, w/s, mass ratio of 0.40) on the simulated degree of hydration vs. cycles curves. The addition of silica fume has minimal effects on the early hydration kinetics but results in significantly less hydration being achieved at later ages, for curing under sealed conditions. For a w/c ratio below about 0.42, there is already insufficient water to achieve complete hydration of the cement, so that the consumption of additional water due to the pozzolanic reaction only intensifies this effect and further limits the achievable hydration.

The porosities of the cement pastes before and after hydration are summarized in TABLE-1. Because of the lower specific gravity of silica fume and the fact that the re-

placements are made on a mass basis, there is a slightly lower initial capillary porosity in the systems containing silica fume. The final total porosities of the three systems are comparable, but the water-filled porosities are reduced in the systems containing silica fume due to its increased water demand. Even though the early time hydration kinetics are similar for the three systems, there is more empty porosity in the systems containing silica fume, as the chemical shrinkage per unit mass of cement reacted is significantly increased by the pozzolanic reaction, as indicated in Table 1. In addition, as pointed out by Jensen and Hansen[6], for a given volume of chemical shrinkage, the smaller pore sizes emptied in the systems containing silica fume will result in a greater RH reduction. This will in turn lead to greater self-desiccation stresses as indicated by equation (1), perhaps making concretes containing silica fume particularly susceptible to early age cracking.

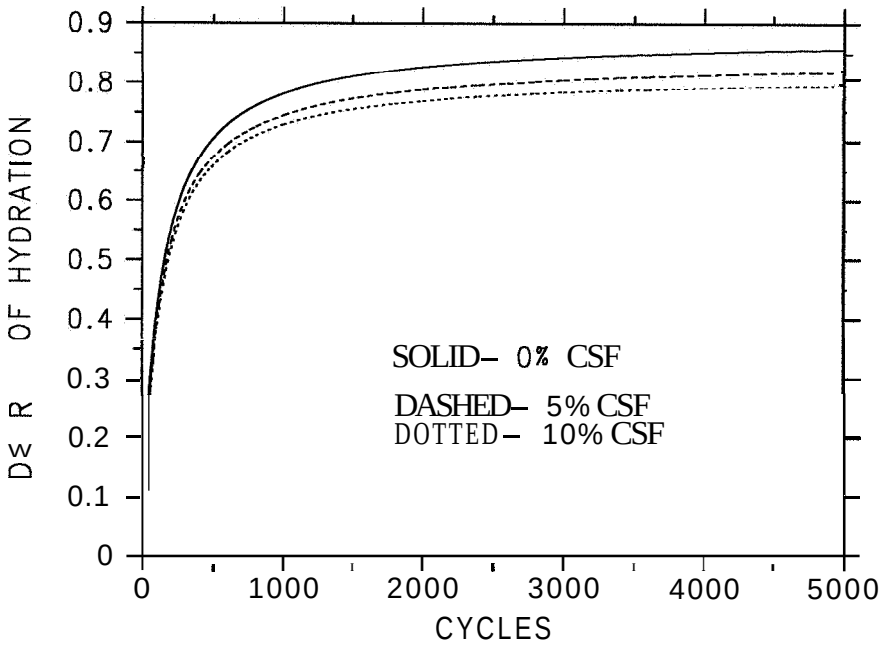

FIG.-5: Effect of silica fume (CSF) replacement on hydration under sealed conditions, Cement 116 with w/c=0.40.

TABLE-1: Capillary Porosities for Simulated Cement Pastes (w/s=0.40)

Silica Fume Replacement (%)	Initial Porosity (%)	Final Water-Filled Porosity (%)	Final Total Porosity (%)	Chemical Shrinkage per mass of cement hydrated (mL/g)
0	56.2	5.6	13.7	0.068
5	55.6	4.7	13.4	0.081
10	55.0	4.4	13.4	0.092

CONCLUSIONS

The NIST microstructural model has been applied to examine the effects of self-desiccation on the hydration kinetics of low w/c ratio cement pastes. The model successfully predicts

the observed reduction in achievable hydration at longer curing times, as the empty capillary pores eventually influence the progress of the hydration reactions. The effects of self-desiccation on hydration kinetics are more significant the lower the w/c ratio, with larger differences predicted for the w/c=0.30 than for the w/c=0.40 cement pastes. The model also indicates that the curing regimen of maintaining saturation until the capillary porosity depercolates, first suggested by Powers[10], results in long term degrees of hydration which approach those achievable under totally saturated conditions. Thus, the early time curing procedure may have a critical influence on ultimate performance. Simulations with silica fume replacements of 5% and 10% indicate that the pozzolanic reaction increases the chemical shrinkage and thus further decreases the achievable degree of hydration. This increased chemical shrinkage, coupled with the smaller pore sizes present in systems containing silica fume, may render low w/c ratio concretes containing silica fume especially susceptible to self-desiccation and subsequent early age cracking, due to the enhanced RH reduction at early ages.

REFERENCES

1) Powers, T.C., "Absorption of Water by Portland Cement Paste During the Hardening Process," Industrial and Engineering Chemistry, Vol. 27, 790-794, 1935.
2) Geiker, M., "Studies of Portland Cement Hydration: Measurements of Chemical Shrinkage and a Systematic Evaluation of Hydration Curves by Means of the Dispersion Model," Ph. D. Thesis, Technical University of Denmark, 1983.
3) Hua, C., Acker, P., and Erlacher, A., "Analyses and Models of the Autogenous Shrinkage of Hardening Cement Paste: I. Modelling at Macroscopic Scale," Cement and Concrete Research, Vol. 25 No. 7, 1457-1468, 1995.
4) Tazawa, E., Miyazawa, S., and Kasai, T., "Chemical Shrinkage and Autogenous Shrinkage of Hydrating Cement Paste," Cement and Concrete Research, Vol. 25 No. 2,288-292, 1995.
5) Justnes, H., Van Gemert, A., Verboven, F., and Sellevold, E.J., "Total and External Chemical Shrinkage of Low w/c Ratio Cement Pastes," Advances in Cement Research, Vol. 8 No. 31, 121-126, 1996.
6) Jensen, O.M., and Hansen, P.F., "Autogeneous Deformation and Change of the Relative Humidity in Silica Fume-Modified Cement Paste," ACI Materials Journal, Vol. 93 No. 6, 539-543, 1996.
7) Gause, G.R., and Tucker Jr., J., "Method for Determining the Moisture Condition in Hardened Concrete," Journal of Research of the National Bureau of Standards, Vol. 25, 403-416, 1940.
8) Mjornell, K.N., "Self-Desiccation in Concrete," Publication P-94:2, Chalrners University of Technology, Goteborg, Sweden, 1994.
9) Persson, B., "Hydration and Strength of High Performance Concrete," Advanced Cement-Based Materials, Vol. 3, 107-123, 1996.
10) Powers, T.C., "A Discussion of Cement Hydration in Relation to the Curing of Concrete," Proc. of the Highway Research Board, Vol. 27, 1947.
11) Molina, L., "On Predicting the Influence of Curing Conditions on the Degree of Hydration," CBI Report 5:92, Swedish Cement and Concrete Research Institute, Stockholm, Sweden, 1992.

12) Bentz, D.P., A Three-Dimensional Cement Hydration and Microstructure Program. I. Hydration Rate, Heat of Hydration, and Chemical Shrinkage, NISTIR 5756, U.S. Department of Commerce, November 1995.
13) Bentz, D.P., "Three-Dimensional Computer Simulation of Portland Cement Hydration and Microstructure Development," Journal of the American Ceramic Society, Vol. 80 No. 1, 3-21, 1997.
14) DeLarrard, F., Waller, V., and Bentz, D.P., "Prediction of Adiabatic Temperature Rise in Conventional and High-Performance Concretes Using a 3-D Microstructural Model," to be submitted to Cement and Concrete Research.
15) Lu, P., Sun, G.K., and Young, J.F., "Phase Composition of Hydrated DSP Cement Pastes", Journal of the American Ceramic Society, Vol. 76, 1003-1007, 1993.
16) Atlassi, E.H., "A Quantitative Thermogravimetric Study on the Nonevaporable Water in Mature Silica Fume Concrete," Ph. D. Thesis, Chalmers University of Technology, Goteborg, August 1993.
17) Jensen, O.M., "The Pozzolanic Reaction of Silica Fume," (in Danish) TR 229/90, Building Materials Laboratory, Technical University of Denmark, 1990.
18) Bentz, D.P., and Garboczi, E.J., "Percolation of Phases in a Three-Dimensional Cement Paste Microstructural Model," Cement and Concrete Research, Vol. 21, 324-344, 1991.
19) Powers, T.C., "Capillary Continuity or Discontinuity in Cement Pastes," PCA Bulletin, No. 10, 2–12, 1959.

A MODEL ON SELF-DESICCATION IN HIGH-PERF'ORMANCE CONCRETE

KRISTINA NORLING MJORNELL
Department of Building Materials, Chalmers University of Technology,
Gothenburg, Sweden

ABSTRACT

Self-desiccation is a phenomenon that has to be considered in concrete with low W/C such as High Performance Concrete. It affects the moisture condition which have an influence on many processes in the material such as transportation of gases and ions, frost, corrosion, shrinkage and even strength. The degree of self-desiccation depends on many different factors, such as W/C, cement type, silica fume and curing temperature. To be able to estimate the effect of different factors, a model has been developed. With this model it is possible to determine the reaction of cement and the decrease in relative humidity (RH) due to self-desiccation in any composition (W/C, cement type and moderate amounts of silica fume). The degree of reaction is calculated as the degree of reaction of a composition in which all cement will be hydrated times a number of reduction factors. These factors are compensating for limited space and water available for reaction products to form and the influence of curing RH and temperature on the rate of reactions. The decrease in RH is calculated from the sorption isotherm (the relation between state of moisture, RH and amount of evaporable water W,). The shape of the sorption isotherm depends on the pore structure which changes with increased degree of reaction. The empirical equation for the sorption isotherm in the calculation model is a function of W/C and degree of reaction.

The results from the model were compared to measurements of degree of hydration and RH for four compositions, SRPC type Degerhamn, W/C=0,40 and 0.25 and OPC type Slite, W/C=0.4 and there is a good correlation. The same reduction factors were used for W/C=0.4 for both types of cement. So far this model is valid for isothermal conditions. The effect of moderate amounts of silica fume (≤10%) is included. The model is still under development and in this paper the present state of the model is presented.

1. INTRODUCTION

1.1 Self-desiccation

Self-desiccation appears in cement pastes with low water cement ratios, W/C<0.5, Neville (1981), since a major part of the mixing water is bound to the cement. When cement and water reacts, water is bound chemically as hydrates and hydroxides in the reaction products. The remaining water is physically bound to the surfaces of the reaction products or in the pore spaces between the solids.

During reaction the cement paste will undergo a change of volume as a consequence of a decrease in the specific volume of water when bound to the cement. If no extra water is available the pores will gradually be emptied of water, starting with the largest pores. The water vapour pressure will decrease and so will the relative humidity. This phenomenon is usually called self-desiccation.

Self-desiccation was known already in the 1940's. Measurements show that the RH was decreasing in a sealed concrete system due to the chemical binding of water and that the decrease in RH was larger the lower the W/C ratio and to some extent depended on cement type, Gause and Tucker (1940), Powers (1947) and Copeland and Bragg (1955).

1.2 Factors influencing self-desiccation in concrete

The degree of self-desiccation depends on the W/C, see FIG.-1. The lower the W/C the larger is the effect of self-desiccation. For W/C higher than 0.7 there is almost no effect of self-desiccation. In such concrete a large proportion of the mixing water is left in the pores when the cement is hydrated and the RH will remain at a level around 100 %.

The WIC is, however, not the only factor influencing self-desiccation. Two mixes with the same W/C but different cement types may have different degree of self-desiccation. The reason is on one hand the chemical composition of the cement which influences the rate of reaction and on the other hand the size and shape of the cement particles and the hydration products formed which give different shape and size of the pores. The pore size and pore volume have an influence on the shape of the sorption isotherms.

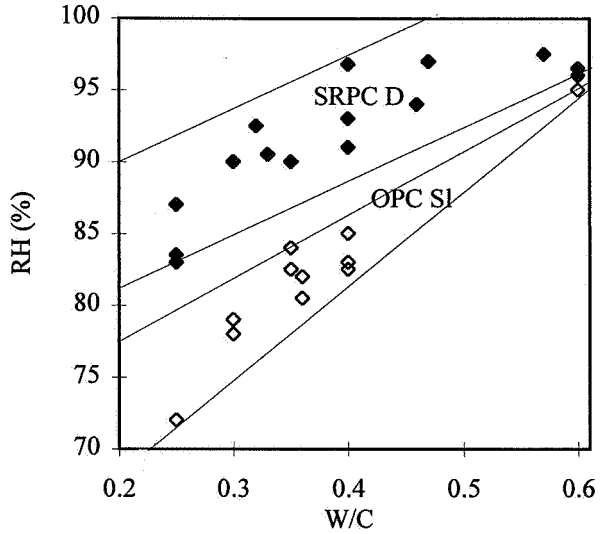

FIG.-1 The influence of W/C and cement type on self-desiccation. Measured data at an age of 28 days from Atlassi et al (1991), Persson (1992) and (1995), Norling Mjörnell (1994) and Hedlund (1995).

The shape of the sorption isotherm is also a result of the alkali content in the pore solution, which depends on the alkali content in the cement. The amount of dissolved ions in the pore solution influences the RH and in a water saturated concrete the RH may be less than 100 %, Hedenblad and Janz, (1993) and Norling Mjörnell (1994).

Silica fume is often used as an additive in concrete with low W/C. The effect of silica fume on self-desiccation has been studied by for example, Nilsson (1984), Christoffersen and Sorensen (1986), McGrath (1989), Atlassi et al (1991), Persson (1992) and (1995) and Meilhede-Jensen (1993).

The SiO_2 in the silica fume react with calcium hydroxide, CH, formed in the reactions between cement and water. In the reaction between SiO_2 and CH water is released so the amount of non evaporable water decreases. There is, however, a positive effect of silica fume on self-desiccation. This is not due to increased amount of non evaporable water but rather due to a refinement of the capillary pore structure and a change of the shape of the pores to larger pores with narrow openings, Atlassi (1992) and Atlassi (1993). The very fine silica fume particles act as a filler between the many times larger cement grains. The effect of silica fume in combination with different types of cement, is varying, see FIG.-2.

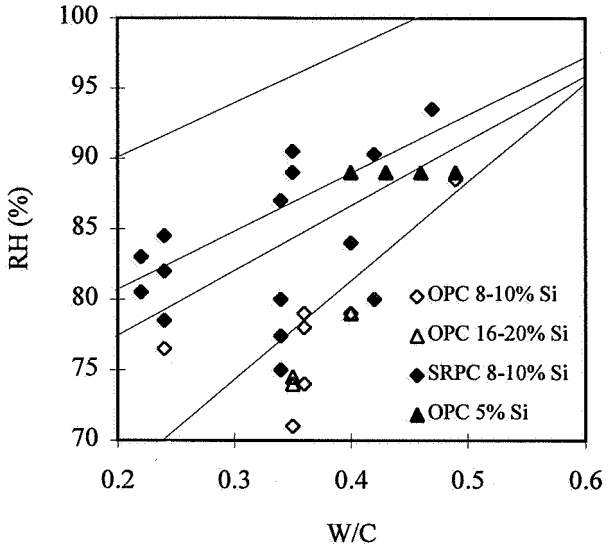

FIG.-2 The influence of silica fume on self-desiccation. Measured data at an age of 28 days from Atlassi et al (1991), Persson (1992) and (1995), Norling Mjörnell (1994), Hedlund (1995) and Hedenblad (1995).

1.3 Model formulation

The relative humidity ϕ in concrete at a specific time, t, is a function of the amount of evaporable water, W, and the pore structure, which in turn depends on W/C and degree of reaction, a, see FIG.-3.

$$\phi(t) = \phi(W_e, W/C, \alpha) \qquad (1)$$

The pore system consists of pores with different size and shape. There exist gel pores that are the voids within the gel. The gel pores contain water at low levels of RH. And there exist capillary pores that are the residue of the water filled spaces between the cement grains. The capillary pores are filled with water at levels of RH. The isotherm is the sum of water held in gel and capillary pores at different levels of RH.

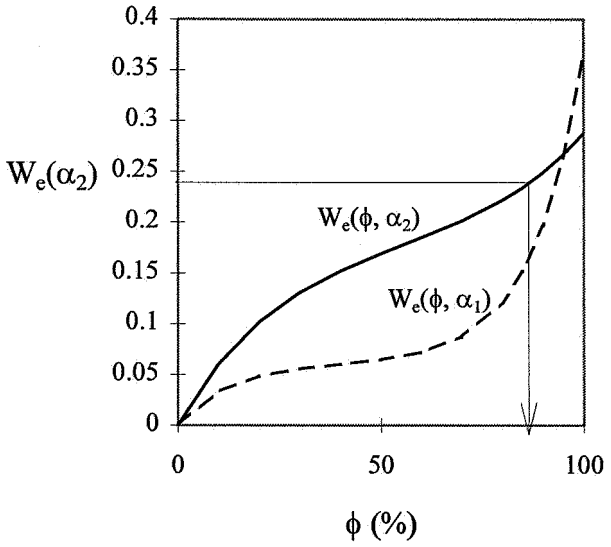

FIG.-3 The relation between evaporable water and relative humidity for a composition with W/C=0.4 at two different degrees of reaction, a, and α_2.

At a specific time, t, the concrete contains a certain amount of evaporable water which is the initial amount of water, W„ minus the amount of chemically bound, non evaporable, water, W„ for sealed cured concrete.

$$W_e(t) = W_0 - W_n(t) \qquad (2)$$

The rate with which water is bound chemically is influenced by many different factors, such as: chemical composition of cement, cement content, W/C, additives, degree of reaction of cement, temperature and RH. A way of calculating the development of RH as function of time is described in the following sections.

2. CALCULATION MODEL

2.1 Chemical binding of water

The amount of non evaporable water with only cement as a binder is proportional to the degree of reaction of cement, α_c, and the cement content, C.

$$W_n = 0.25 \cdot \alpha_c \cdot C \qquad (3)$$

For concrete with silica fume and cement the amount of non evaporable water is

$$W_n = 0.25 \cdot \alpha_C \cdot C - 0.34 \cdot \alpha_S \cdot S \qquad (4)$$

where α_{si} is the degree of reaction of silica fume and S is the amount of SiO_2 in the silica fume, Helsing-Atlassi (1993).

A way of describing the degree of reaction of cement α_c is according to Byfors (1980):

$$\alpha_c = e^{(-\lambda_1 \cdot (\ln(1+\frac{t_e}{t_1}))^{-\kappa 1})} \qquad (5)$$

where t_e is the equivalent maturity time, and h,, t, and κ, are constants obtained by fitting equation (5) to a probable development of degree of reaction of a composition in which all cement becomes hydrated. A set of constants could be obtained for each cement type. In a similar way equation (5) was used to describe the degree of reaction of silica fume as function of time.

The equivalent maturity time t_e of any composition can be calculated as:

$$t_e = \int_0^t \beta_{W/C} \cdot \beta_W \cdot \beta_\phi \cdot \beta_T \cdot dt \qquad (6)$$

In the model the rate of reaction in any composition is calculated by the rate of reaction in a fictive composition with the same type of cement and cement content which is cured at 20°C with enough water to hydrate all cement, times a number of reduction factors. The first factor is considering the limited space available for reaction products to form. The factor called $\beta_{W/C}$ varies with W/C and degree of reaction and is decreasing with increasing degree of reaction. It represents the difference between reaction of compositions with different W/C cured with full supply of water. The second reduction factor β_W is considering the amount of water available for reactions and the third factor β_ϕ is considering the state of the available water, in terms of RH. The fourth factor β_T is compensating for curing temperatures other than 20°C.

$$\beta_T = e^{(\theta \cdot (\frac{1}{293} - \frac{1}{T+273}))} \qquad (7)$$

where T is the concrete temperature in "C and

$$\theta = \theta_{ref} \cdot (\frac{30}{T+10})^{\kappa 3} \qquad (8)$$

where θ_{ref} and κ_3 are obtained from experimental adaptations, Byfors (1980).

The influence of the state of moisture (RH) on the rate of reaction is considered by a factor β_ϕ. This factor was evaluated from measurements of rate of reaction at different levels of RH. As a reference climate 100 % RH was used, Norling Mjörnell (1996a).

The relation between β_ϕ and RH has been approximated with a straight line between RH_{max} where β_ϕ =1 and RH_{min} where β_ϕ =O. Typical values are RH_{max} =100 % and RH_{min} =70 %, FIG.-4.

RH_{max} can be somewhat lower than 100 % for some types of cement due to the effect of alkali, Hedenblad and Janz (1993).

$$\beta_\phi = \frac{(\phi - 0.7)}{0.3} \quad \text{when } \phi \geq 0.7 \quad \text{and} \quad \beta_\phi = 0 \text{ for } \phi < 0.7 \qquad (9)$$

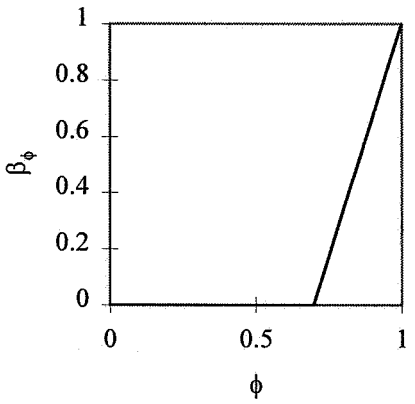

FIG.-4 Reduction factor for RH, β_ϕ.

The water reduction factor β_W is considers the decreased rate of reaction due to limited amount of water available for reactions. Since β_W and β_ϕ considers different effects of moisture, these two factors can not be evaluated separately. But without separating the effect of the amount of water available and how hard it is bound (the state of moisture), it would have been difficult to find the dependency of the degree of reaction. The factor β_W was evaluated by comparing the development of degree of reaction for seal cured and water cured cement mortar with the same composition assuming that β_ϕ can be approximated with equation (9). **A** reasonable assumption is to describe β_W as the degree of saturation of the capillary pore volume.

$$\beta_W = \left(\frac{W_e/C - k_{vg} \cdot \alpha_c}{W_0/C - 0.19 \cdot \alpha_c - k_{vg} \cdot \alpha_c} \right) \qquad (10)$$

The factor β_W for three different W/C are shown in FIG.-5. The constant k_{vg} corresponds to the amount of water held in the gel pores per amount of cement at α_c=1 and at 100 % RH. A typical value of k_{vg} is 0.25 for a concrete with W/C=0.4 and SRPC type Degerhamn.

The reduction factors β_W and β_ϕ are only evaluated for the reaction of cement. Earlier measurements indicate that reaction of silica fume also is influenced by moisture, Norling Mjörnell (1996a). However, this effect is not yet included in the model which means that β_W=1 and β_ϕ=1 for silica fume.

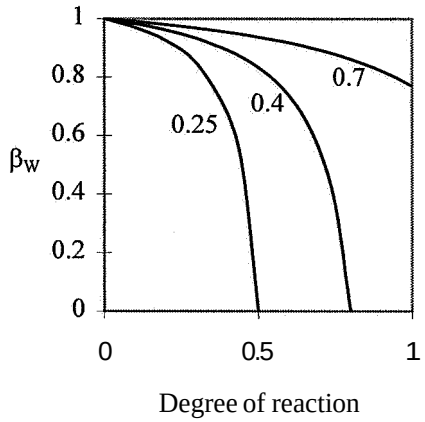

FIG.-5 The factor β_w as function of degree of reaction for seal cured cement paste with different W/C.

The product of the two factors β_ϕ and β_w is shown in FIG.-6. Factor β_w was expressed as a function of relative humidity ϕ using the relation $W_e(\phi, a)$.

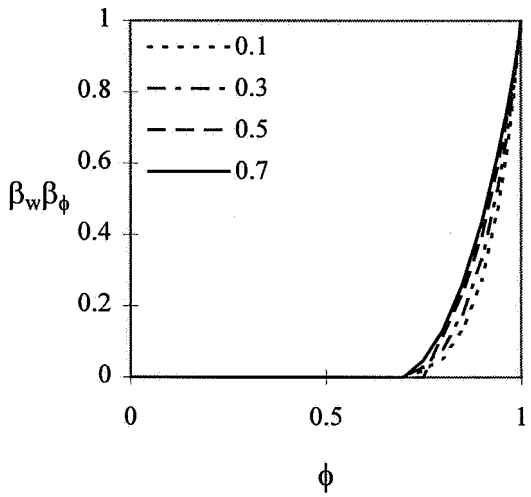

FIG.-6 The $\beta_w \cdot \beta_\phi$ factor as function of RH for various degrees of reaction, W/C=0.4.

The decreased rate of reaction due to limited space for reaction products to form is considered by the reduction factor $\beta_{W/C}$ which is a function of the maximum degree of hydration and W/C, see equation (11) and FIG.-7.

$$\beta_{W/C} = \left(\frac{\alpha_{max} - \alpha_c}{\alpha_{max}} \right)^a \qquad (11)$$

The $\beta_{W/C}$ factor was evaluated by fitting the product of the assumed development of degree of reaction for a paste with infinite W/C and $\beta_{W/C}$ to measured data on degrees of reaction of cement for water cured pastes with different W/C. The factor $\beta_{W/C}$ is assumed to be equal to 1 for silica

fume since the products formed when silica fume reacts with calcium hydroxide almost have the same volume as the reactants.

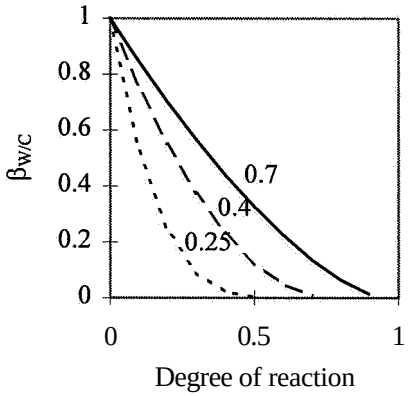

FIG.-7 Reduction factor $\beta_{w/c}$ for different W/C. Values of a_1 and a are 0.95, 1.5 for W/C=0.7, 0.77 and 2 for W/C=0.4 and 0.6 and 3.5 for W/C=0.25.

2.2 Sorption isotherms

The relation between evaporable water and RH (desorption isotherms) has been measured for compositions at different ages. The empirical expression for the desorption isotherms was originally formulated by Hedberg (1994) but it is slightly modified in the present model to include the effect of degree of reaction of the shape of the curve. The term $(b-\alpha_c \cdot 10)$ was former a constant.

$$W_e(\phi,\alpha) = G_1\left(1 - \frac{1}{e^{(b-\alpha_c \cdot 10)\phi}}\right) + K_1\left(e^{(b-\alpha_c \cdot 10)\phi} - 1\right) \qquad (12)$$

where G, is the amount of water per m^3 held in the gel pores at 100 % RH.

$$G_1 = k_{vg} \cdot \alpha_C \cdot C + 0.36 \cdot \alpha_S \cdot S \qquad (13)$$

$W_e(1, \alpha)$=P, where P is the maximum amount of water per m^3 that can fill the pores at a certain degree of reaction.

$$P(\alpha) = W_0 - 0.19 \cdot \alpha_C \cdot C + 0.36 \cdot \alpha_S \cdot S \qquad (14)$$

K, is then calculated as

$$K_1 = \frac{\left(P - G_1\left(1 - \frac{1}{e^{(b-\alpha_c \cdot 10)}}\right)\right)}{\left(e^{(b-\alpha_c \cdot 10)} - 1\right)} \qquad (15)$$

An example of empirical desorption isotherms calculated according to equations (12)-(15) are presented in FIG.-8 together with measured values for different degrees of hydration.

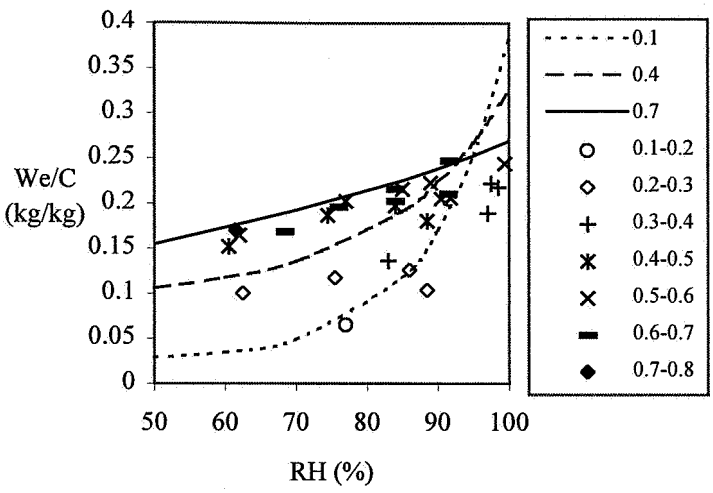

FIG.-8 Modelled age dependent sorption isotherms for SRPC D, W/C=0.40. Points are measured values for different degrees of hydration, Norling Mjörnell (1996b).

3. RESULTS

3.1 Input parameters used in the calculations

A method of finite differences is used to calculate the degree of reaction and the degree of self-desiccation in seal cured cement paste. The accuracy of this method is very much dependent on the time step used. Therefore very short time steps (0.5 hours) are used during the first day when the increase in non evaporable water is very rapid. After one day the time step is increased with half an hour per time step. This has shown to give results with good accuracy. The degree of reaction of cement and silica fume and the RH were calculated according to Equation 3 to 15 with parameters from TABLE-1 and TABLE-2 for the corresponding composition.

TABLE-1. Cement parameters used in the calculations.

Parameter	SRPC **D**	OPC Sl	Silica
λ_1	1.5	1.5	10
t_1	6	3	4
κ_1	1.4	1.6	2.2
$\theta_{ref.}$	4600	4600	4600
κ_3	0.39	0.39	0.39

TABLE-2. Other parameters used in the calculations.

W/(C+S)	Cementtype	S/(C+S)	α_{max}	a	k_{vg}	b
0.25	SRPC D	0	0.6	3.5	0.25	8
		10	0.7	2.5		8.5
0.3		5	0.72	2.4	0.26	9
0.4		0	0.77	2	0.25	10
		10	0.85	1.5	0.3	12
	OPC Sl	0	0.77	2		10
		10	0.8	1.5		12

3.2 Calculated degree of reaction

The parameters in TABLE-1 give a degree of reaction in a hypothetical cement paste in which all cement will be hydrated (W/C>1.0). With reduction factors according to equation (13) and FIG.-7 the degree of reaction for lower W/C was calculated, see FIG.-9.

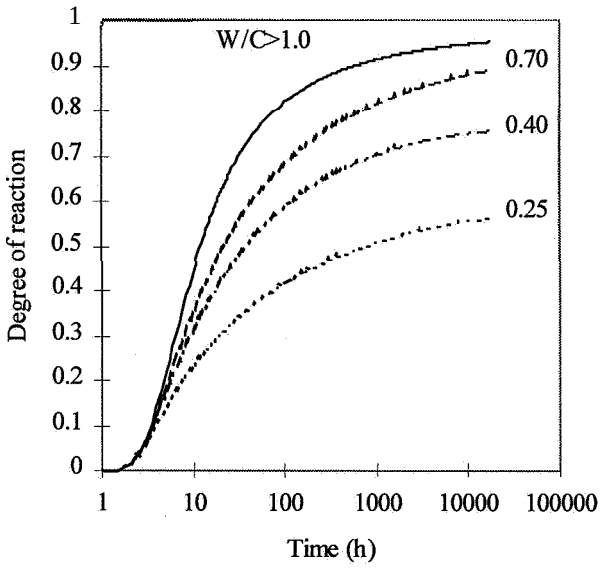

FIG.-9 Calculated degree of reaction for water cured cement paste with OPC Slite and different W/C.

A comparison between measured and calculated degree of reaction was made for water curing and sealed curing. Water curing was simulated by keeping factor β_ϕ =1 and β_W =1. For sealed curing β_ϕ and β_W were calculated according to equations (11) and (12). The results are shown in FIG.-10, FIG.-11 and FIG-12. Note that the same β_W and β_ϕ are used for the two compositions with W/C=0.4 although the type of cement is different.

For one composition the degree of reaction at a curing temperature of 5°C was calculated (β_T=0.33), see FIG.-11. When the curing temperature is not mentioned it is supposed to be 20°C.

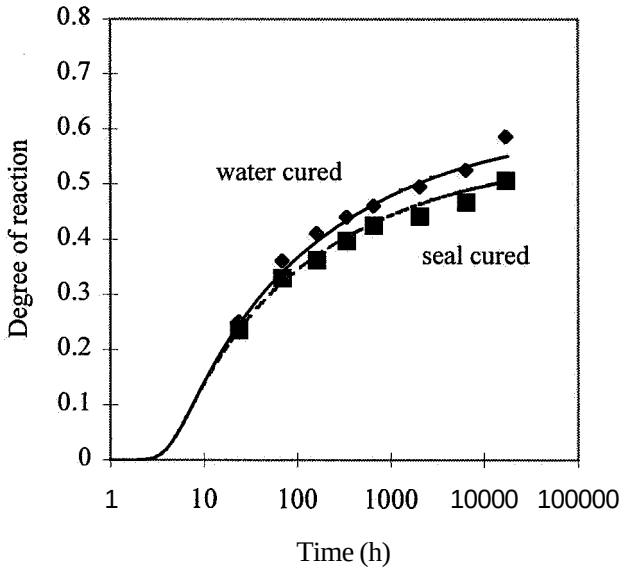

FIG.-10 Degree of reaction of seal cured and water cured cement paste, SRPC D, W/C=0.25. A comparison between measured (markers) and calculated (lines) data. Measured data from Helsing Atlassi (1996).

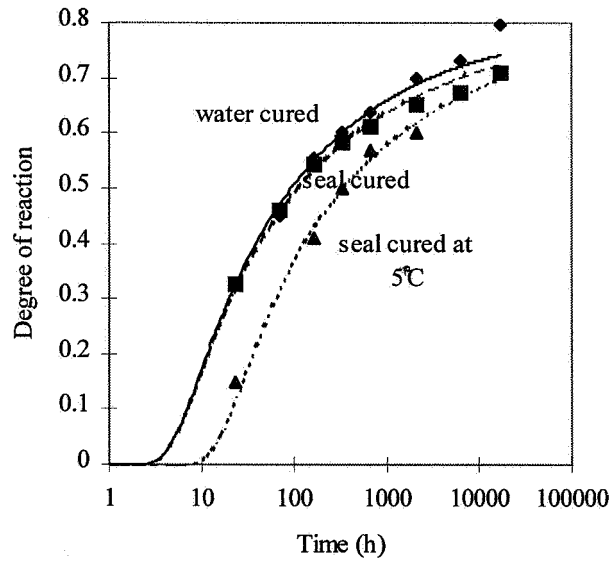

FIG.-l1 Degree of reaction of cement paste, SRPC D, W/C=0.40, A comparison between measured (markers) and calculated (lines) data for sealed cured ($\beta_w \cdot \beta_\phi < 1$), water cured ($\beta_w \cdot \beta_\phi = 1$) and seal cured at 5°C ($\beta_w \cdot \beta_\phi < 1$, $\beta_T < 1$). Measured data from Helsing Atlassi (1996) and Bengtsson et al (1996).

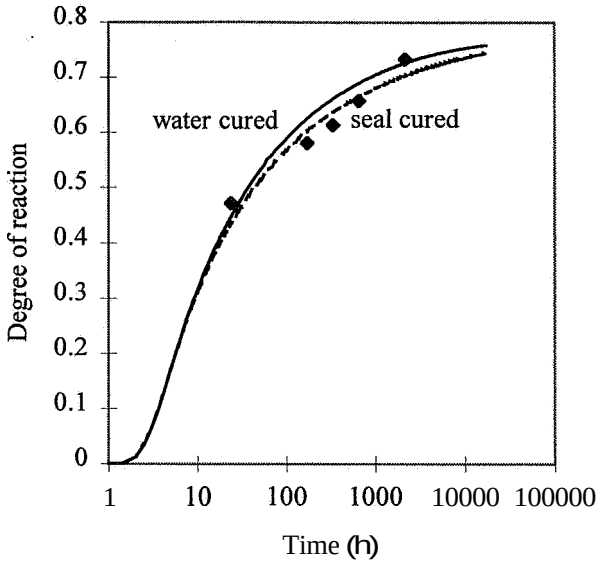

FIG.-12 Degree of reaction of cement paste, OPC Sl, W/C=0.40. Comparison between measured (markers) and calculated (lines) data. Measured data for water curing, Norling Mjörnell (1996).

3.3 Calculated relative humidity

The decrease in RH was calculated and is presented together with available measured data in FIG.-13, FIG.-14 and FIG.-15.

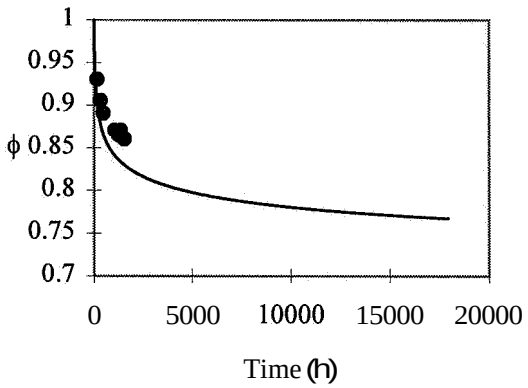

FIG.-13 Relative humidity in seal cured cement paste, SRPC D, W/C=0.25. A comparison between measured (markers) and calculated (lines) RH. Measured data from Persson (1992).

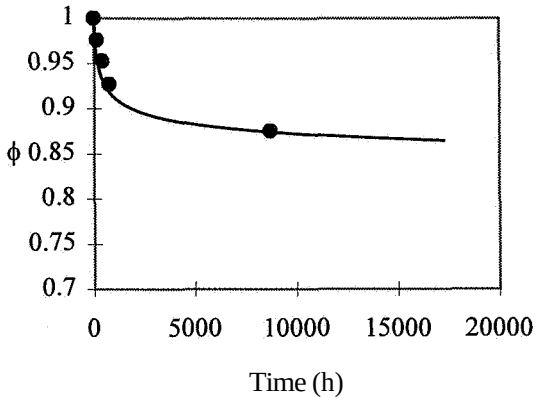

FIG.-14 Relative humidity in seal cured cement paste, SRPC D, W/C=0.40. A comparison between measured (markers) and calculated (lines) RH.

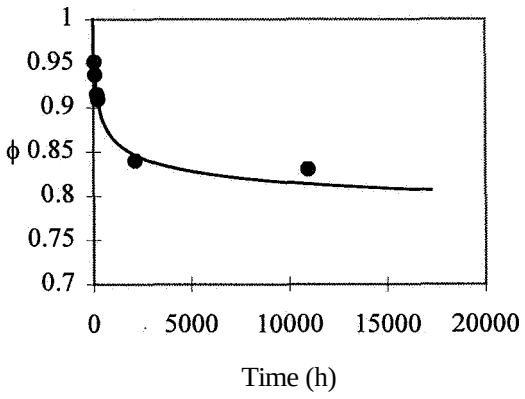

FIG.-15 Relative humidity in seal cured cement paste, OPC Sl, W/C=0.40. A comparison between measured (markers) and calculated (lines) RH.

3.4 Sensitivity analysis

The three parameters h,, κ, and t, that are influencing the development of reaction are important for the result since other parts of the model, such as $\beta_{w/c}$, β_w and RH are depending on the degree of reaction. A sensitivity analysis was made to see the effect of changing one or more of these parameters with +l-50 %. Combinations of the three parameters at three levels: initial value, (initial value)·1.5 and (initial value)·0.5 were run in the model. The results were used to evaluate the sensitivity in the degree of reaction and RH at an age of 1, 28 and 365 days. The largest difference compared to the result with the initial value of the parameters was when κ, was kept at a low level and λ_1 was kept at a high level. The degree of reaction after 365 days was 0.4 compared to 0.71 and the RH was 98 % compared to 88 %.

4. SUMMARY AND CONCLUSION

A general model of reaction of cement and decrease of RH due to self-desiccation has been developed. The results from the model correlate well with observations for SRPC Degerhamn W/C=0.4 and 0.25, and OPC Slite W/C=0.4. The same reduction factors are used for both compositions with W/C=0.4 even though the cement type is different.

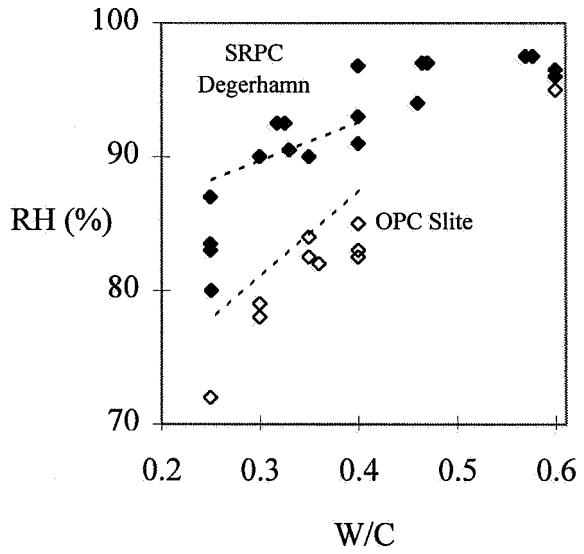

FIG.-16 RH after 28 days of sealed curing as function of W/C for two different cement types. Comparison between measured and calculated (dotted lines) values. Measured data are equal to FIG.-1.

A sensitivity analysis was carried out to study the effect of the parameters h_1, K, and t_1. These parameters are sensitive to small changes especially if one is higher and the other is lower than the "correct" values. An advantage with the model described in this paper is that only one set of parameters is required for each type of cement instead of one set of parameters for each combination of W/C and type of cement. The parameters should not be evaluated fiom heat evolution measurements during the first few days, but rather from the amount of chemically bound water. Interpolation between parameters for different compositions can be hazardous since it is the combination of the parameters that gives a specific development of degree of reaction.

ACKNOWLEDGEMENT

Financial support from theNorwegian-Swedish Consortium High Performance Concrete is gratefully acknowledged.

REFERENCES

Atlassi, E, Norling, K, Radocea, A, (1991), *Fuktfri Betong - en fråga om ratt materialkombination*, Moisture-free Concrete - a Question of Correct Combination of Materials. pp 24-26, Betong No 3. (In Swedish).

Atlassi, E, (1991), Influence of Cement Type on the Desorption Isotherm of Mortar, Nordic Concrete Research, No 10, pp 25-36.

Atlassi, E, (1992), Desorption Isotherms of Silica Fume Mortar, 9th International Congress of the Chemistry of Cement, New Delhi, India.

Bengtsson et al, (1996), Preliminary results on the influence of curing temperature on degree of hydration and RH, Project report, Chalmers University of Technology, Sweden. (In Swedish).

Byfors, J, (1980), Plain Concrete at early ages, CBI report FO 3:8, Sweden.

Copeland, L E, Bragg, R H, (1955), Self-Desiccation in Portland-Cement Pastes, ASTM Bulletin, pp 34-39.

Gause, G R and Tucker, J R, (1940), Methods for Determining the Moisture Condition in Hardened Concrete, Journal of Research, National Bureau of Standards, Vol 25, p. 403.

Hedberg, B, (1994), Application for Excel of the Model of self-desiccation in cement paste, Computer software. Department of Building Materials, Chalmers University of Technology, Sweden.

Hedenblad, G, Janz, M, (1993), *Inverkan av alkali på uppmatt RF i betong*, The Influence of Alkali on Measured RH in Concrete, Report TVBM-3057, Lunds University of Technology, Sweden. (In Swedish).

Hedenblad, G, (1995), *Uppmatta fuktfordelningar respektive viktminskningar vid uttorkning av hogpresterande betong*. Measured Moisture Distributions and Weight-losses at Drying of High-Performance Concrete, Internal report M8:1, High-Performance Concrete consortium, Sweden. (In Swedish).

Hedlund, H, (1995), Preliminary results on RH in High-Performance Concrete, Private communication, Division of Structural Engineering, The Technical University of Luleå, Sweden.

Helsing Atlassi, E, (1993), Quantitative Thermogravimetric Study on the Nonevaporable Water in Mature Silica Fume Concrete, PhD-thesis, Chalmers University of Technology, Sweden.

Helsing Atlassi, E, (1996), Internal report in M5, High-Performance Concrete consortium, Sweden.

McGrath, P, (1989), Internal Self-Desiccation of Silica Fume Concrete, MSc-thesis, University of Toronto.

Mejlhede Jensen, O, (1993), Autogen Deformation og *RF-ændring - selvuttørring* og *selvuttørringssvind*, Autogeneous Deformation and Decrease in RH- Self-desiccation and Self-desiccation Shrinkage, The Technical University of Denmark, Denmark. (In Danish)

Neville, A M, (1981), Properties of Concrete, Third edition.

Nilsson, L-0, (1984), Desorption Isotherms for Cement Mortar Containing Silica Fume, Report IF 8431, Sweden.

Norling Mjornell, K, (1994), Self-Desiccation in Concrete, Licentiate-thesis, Chalmers University of Technology, Sweden.

Norling Mjornell, K, (1996a), Kemisk bindning av *vatten* vid *olika* relativa fuktigheter, Chapter 1 in *Sammanställning* av uppmatta fuktegenskaper hos hogpresterande *betong*. A Synthesis of Measured Moisture Properties in High Performance Concrete, Internal report M8:2, High-Performance Concrete consortium, Sweden. (In Swedish).

Norling Mjornell, K, (1996b), Fuktbindning i tidig iilder, Chapter 2 in *Sammanställning* av uppmatta fuktegenskaper hos hogpresterande *betong*. A Synthesis of Measured Moisture Properties in High-Performance Concrete, Internal report M8:2, High-Performance Concrete consortium, Sweden. (In Swedish).

Persson, B, (1992), Hogpresterande *betongs* hydratation, *struktur* och *hållfasthet* - riidata och berakningar, Hydration, Structure, and Strength of High Performance Concrete - Raw Data and Calculations, Internal report TVBM-7011, Lunds University of Technology, Sweden. (In Swedish).

Persson, B, (1995), Data on Self-desiccation, Internal report M6:14, High-Performance Concrete consortium, Sweden.

Powers, T C and Brownyard, T L, (1947), Physical Properties of Hardened Portland Cement.

Sorensen, T B and Christoffersen, A K, (1986), *Selvuttørring* og kemisk svind i *mørtel*, Self-desiccation and Chemical Shrinkage in Mortar, The Technical University of Denmark, Denmark. (In Danish).

MODELLING DIMENSIONAL CHANGES IN LOW WATER/CEMENT RATIO PASTES

EDDIE A.B. KOENDERS and KLAAS VAN BREUGEL
Delft University of Technology
Delft, The Netherlands

ABSTRACT

Hardened cement paste is a porous material. Directly after mixing, all pores are considered to be completely filled with water. As hydration proceeds, pores become emptied and the relative humidity in the emptied pore space will reduce. This reduction of the relative humidity goes along with a reduction of the gas pressure in the emptied pore space. Thermodynamic equilibrium requires an increase of the surface tension in the boundary layer that develops at the inner pore wall area. Form this thermodynamical approach, autogenous deformation of a hardening cement-based material can be determined. A model will be presented which will be discussed and validated by experiments. Good agreement is reached between the simulations and the experimental results.

1. INTRODUCTION

The pore volume of cement paste is generally defined as the initial paste volume minus the volume of the solid material. The ratio between the pore volume and the initial paste volume is defined as the porosity. The total pore volume of a cement-based material is considered to be a contribution of a number of pore volumes of pores with a certain diameter. For cement paste, it is generally assumed that these pore diameters form a continuous pore size distribution [1]. For neat cement paste, the pores in the pore system consists of pores with diameters that range between 10 Å to 10^7 Å [2]. The pore diameters involved in the pore size distribution of a cement-based material can be subdivided into different categories that characterise a certain type of porosity of the cementitious material. This are: the gel pores, the capillary pores and the air voids. Several authors have proposed upper and lower boundaries for these three types of pores. However, there exists no general agreement on the boarder limits that should be applied. As an example, in Tabel 1, an overview is given on the different pore types and the range limits, as proposed by Young [2]. Each type of pores that is represented by a certain pore range, has its own properties. For the three pore classes as given before, pores within the range of the capillary pores are considered to be able to transport water or gas through the microstmcture. This is a very important property of this type of pores. On the other hand, the gel pores and enclosed air voids are not able to transport water or gas through the system. They form a closed pore system in the cementitious

material. Therefore, only the capillary pores are considered to form the "canal system" through the hardening microstructure of a cementitious material. The upper and lower boarder values of the pore diameters within which pores are classified as capillary pores are: 0.002 pm $5 \phi 5$ 10 pm, where ϕ is the pore diameter. This means that pores with a diameter smaller than 0.002 pm are assumed to be gel pores and pores with a diameter larger than 10 pm are assumed to be air voids. The porosity and the pore size distribution, generally, are assumed to be effected by several factors. These are, the degree of hydration, the waterlcement ratio, the temperature, the cement composition and the particle size distribution of the cement. Mostly, these factors effect only the total pore volume and the maximum pore diameter involved in the system. However, it will not effect the classification of the pores as given before. The porosity of cement paste consists of pores which exhibits a certain pore size distribution. In this paper, a mathematical description will be proposed that simulates this pore size distribution. With this, pore fractions of a certain diameter represent a certain pore volume in the paste. The summation of all these fractions again lead to the total pore volume. With this formulation, the moisture state in the hardening paste can be described in detail. This is necessary for modelling the volumetric changes of hardening cement paste.

It is possible to reach thermodynamic equilibrium in the capillary pore system. This is a continuously changing state of equilibrium that is driven by the degree of hydration. The model as it is proposed in this paper equilibrates the relative humidity in the emptied pore space with the thickness of the surface layer at the pore walls and with the surface tension in this layer. This equilibrium can be established iteratively.

To come to the volumetric changes of the hardening microstructure, the model originally proposed by Bangham in 1931 will be used [3]. This model relates the volumetric changes of the continuously changing microstructure to the changes of the surface tension in the surface layer that has been formed at the pore walls. This appeared to be a linear relationship.

For the determination of the evolution of the microstructure of cement-based materials, the numerical simulation program HYMOSTRUC is used. This program has the potential to simulate and predict the microstructural development as a function of the particles size distribution and chemical composition of the cement, the waterlcement ratio and the temperature [4]. The model as is discussed in this section has been implemented in the HYMOSTRUC program. The volumetric changes of experiments on cement pastes with different water cement ratios and with cement of different fineness as well as tests taken from literature are simulated with the proposed model.

Tabel 1. Classification of pores in cement paste.

Classification of pores in cement paste (after [2])			
Type	Diameter [pm]	Description	Role of water
Capillary pores	10 - 0.002	Macro pores	Accessible for water and able to transport water
Gel pores	< 0.002	Micro pores	Not accessible for water. Not able to transport water

2. PORE STRUCTURE

2.1 Modelling approach

During the hydration process, cement paste changes gradually from a viscous aqueous liquid into a hardened porous material. The total pore volume in this material is characterised by pore diameters that follow a certain distribution. The pore size distribution of a cementitious can either be measured, e.g. by mercury intrusion, or can be obtained by computer simulations. The pore size distribution relates the cumulative pore volume to a certain range of pore diameters. In this way, a relationship is known between a the pore volume that is occupied by all pores with diameters that range between certain limits. In HYMOSTRUC the pore size distribution is described mathematical by (see Fig. 1) [l]:

$$V_{por} = a \ln\left(\frac{\phi}{\phi_0}\right) \tag{1}$$

where V, is the pore volume, ϕ the diameter of the capillary pore, ϕ_0 the minimum capillary pore diameter and "a" a pore structure constant that represents the increase of the pore volume with respect to the pore diameter. The pore volume formed by pores smaller than ϕ_0=0.002μm (see Tabel l), e.g. gel porosity, is not included in this formulation. The total pore volume in a cement paste depends on the state of the hydration process, viz. the degree of hydration α. At the initial stage of the hardening process, the total pore volume is equal to the paste volume minus the volume of cement. This ratio is determined by the water/cement ratio. At that particular stage, the total pore volume is completely filled with water. After some hydration has occurred (WO), the total pore volume has decreased due to the formation of hydration products. The pores remain not completely filled with water since some part of the water volume has been used up by the reaction process with cement. From this, distinction can be made between those pores that are still completely filled with water (ϕ_{wat}) and the empty pores. The diameter of the pore that is still completely filled with water will be within the boarder limits of the capillary pores, e.g. $\phi_0 \leq \phi_{wat} \leq \phi_{por}$. The maximum pore diameter involved in the pore size distribution ϕ_{por} can be derived from equation (1). At a certain degree of hydration, the maximum pore diameter involved in the pore system can be determined by:

$$\phi_{por}(\alpha(t)) = \phi_0 \exp\left(\frac{V_{por}(\alpha(t))}{a}\right) \tag{2}$$

The actual total pore volume V, changes continuously throughout the hardening process. Pore space will reduce due to the formation of hydration products but, on the other hand, new pore space will be formed due to the volumetric reduction that is a result of the chemical reaction between the water and the cement (chemical or "Le Chatelier shrinkage). Therefore, in this equation, the total pore space $V_{por}(\alpha(t))$ is considered to be build up from two contributions. These are the actual pore volume that is occupied currently by capillary water and an additional

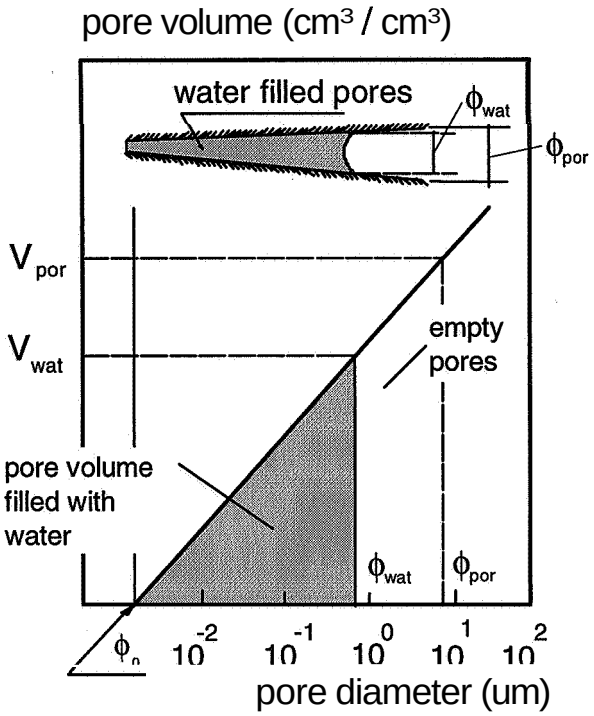

Fig. 1. Schematical representation of the pore size distribution with emphasis on the state of the pore water in the actual pore volume.

volume that is the result of the chemical shrinkage. The relative contributions of both volumes change continuously during the hydration process. Changes of the total pore volume goes along with changes of the inner pore wall area. The inner pore wall area of the hardening cement paste is considered to be covered by a thin adsorption layer of water molecules. The thickness of this layer depends mainly on the relative humidity in the pore system. Changes of the actual water volume in the system due to hydration, will change the relative humidity in the pore space and, therefore, also effect the thickness of this adsorption layer. It is assumed that the water volume that is occupied by the adsorption layer goes at the cost of the free capillary pore water volume that is available for further hydration (physically bounded water). Therefore, the diameter of the pore that is still completely filled with water will become smaller due to the existence of the adsorption at the inner pore wall area.

Adopting the modelling approach as it is proposed up till now, detailed information on the properties of pore structure of a hardening cement paste is available. The only unknown parameter in the formulation (eq. (1)) that remains unknown, is the pore structure constant "a". The value of this unknown parameter can be determined either from literature data or by using numerical models. Keeping a data base that contains information on the pore structure of different types of mixtures is a serious option to achieve an adequate prediction of the pore structure constant "a". Using a numerical model to achieve information on the pore structure constant "a" is even more convenient. However, it must be beared in mind that this is a modelling approach. Therefore, in the next section, it will elucidated how the pore structure constant can be determined form pore size distribution measurements.

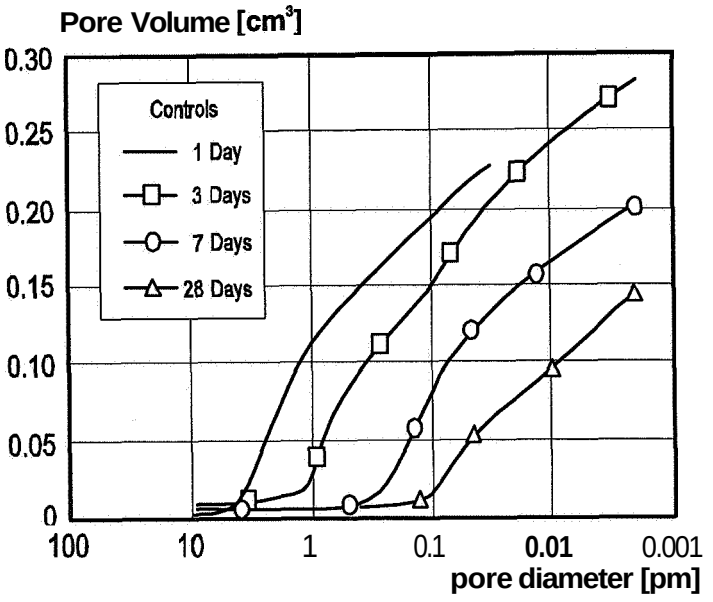

Fig. 2. Pore size distribution measured by Whiting [13].

2.2 Pore structure constant "a" determined from experiments

The dimensionless parameter "a" can be derived from measurements by dividing the intrudes pore volume by the pore range. This can be carried out with help of equation (1) and assuming the minimum capillary pore to be equal to 0.002 pm. An extended literature study turned out that this parameter ranges between 0.05 (coarse cement) and 0.11 (fine cement) depending on the type and fineness of the cement that is used.. From this information, the pore structure can be modelled in a proper way (eq. (1)). In Fig. **3,** a moddeled pore size distribution is presented which representes

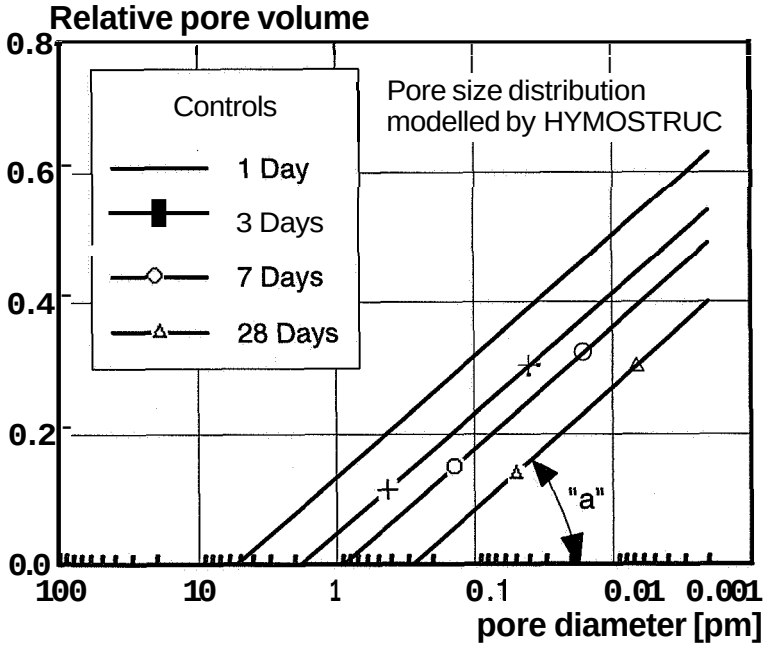

Fig. **3.** Pore size distribution according to the proposed model.

the measured pore size distribution as given in Fig. 2. From the measurements is calculated that the inclination angle "a" is about 0.08. This value was applied to the model. The agreement between the experimental and simulated results is quite good. It shows also the reduction of the average pore diameter as hydration proceeds.

2.3 Pore structure constant "a" determined from random particle structure

The pore structure constant "a", that determines the pore size distribution in a cement paste microstructure (see eq. (1)), can be derived form a random particle structure. This can be considered as the numerical way to determine the pore structure constant "a". Earlier, in section 2.2, this pore structure constant was determined from experimental results. However, in this section it will be elucidated how similar results can be obtained by application of the extended HYMOSTRUC model. In the extended version of the HYMOSTRUC model, the formation of structure is modelled by an increase of the radii of the spherical cement particles that are parked in space randomly. During hydration, the physical boundary's of the cement particle start to expand (grow) and start to form a microstructure. Some particles may become embedded in the outer product layer of larger particles. This procedure results in the formation of a load bearing framework. In Fig. 4, two stages of the progress of the hydration process are presented for a cement of medium fineness (Blaine 420 m^2/kg) and a waterlcement ratio of 0.3. Initially, if no hydration has taken place, only unhydrated cement particles (black spheres C) exist which are distributed randomly in the mixing water facing the waterlcement ratio. It is assumed that the formation of the microstructure starts, after the dormant stage has ceased. Direct after that

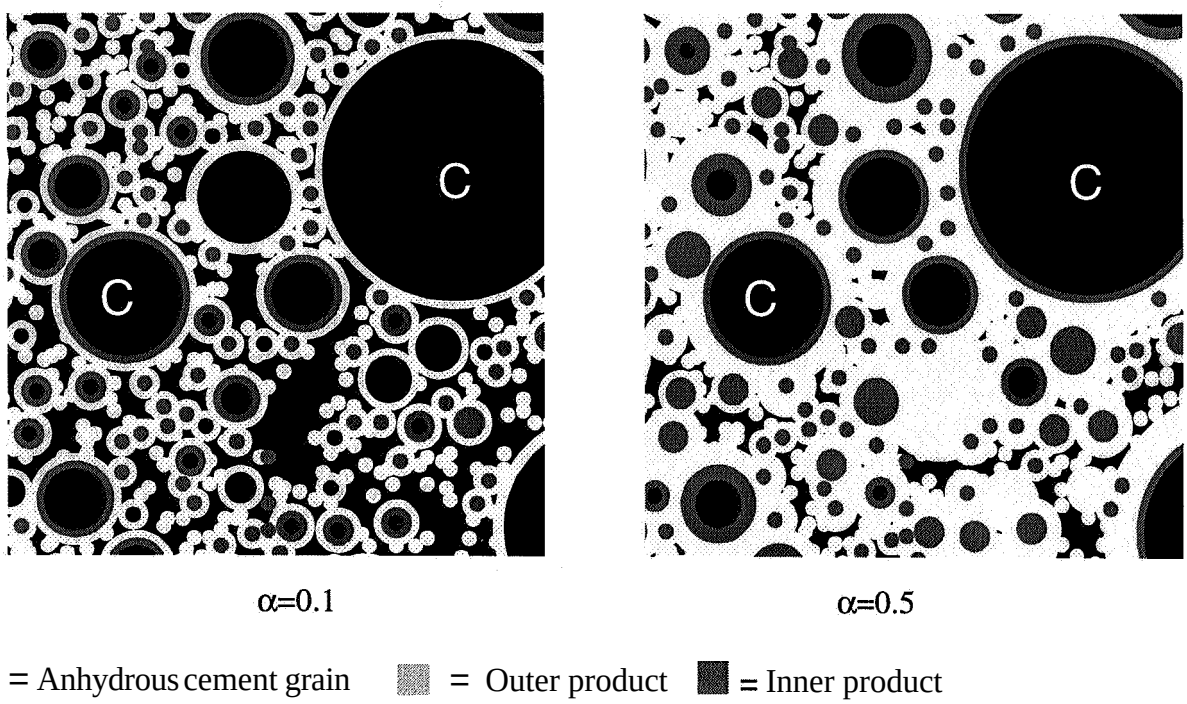

Fig. 4. Modelling Formation of structure of a cement paste with a waterlcement ratio of 0.3 and a cement fineness of (420 m^2/kg). (Background colour is black!)

particular stage, largely, a structure of unhydrated cement grains with minor formation of hydration products starts to develop. The distinction between the formed hydration products called: 'outer product' and the zone at which the mixing water has penetrated into the cement particle called: 'inner product' can be observed form the figure quite clear. At an arbitrary degree of hydration of 0.1, a microstructure with little formation of hydration products can be observed. However, at a degree of hydration of 0.5, the actually developed hydration products tend to form a dense microstructure. From this structure, the pore space can be recognised (black colour). Most of the pores are closed and surrounded by hydrating cement particles. The average dimensions of the pores that can be observed range roughly between 1 and 10 pm. However, since the shape of the pores is irregular, is it hard to determine a pore size distribution from a microstructural model that is represented by regular shaped pores. Therefore, use can be made of the weighted average of the total pore volume and total pore wall area. Among others, Setzer [6] proposed a procedure to determine the hydraulic radius from the total pore volume V, and the total pore wall area $A_{...}$. This radius is defined as follows:

$$R_{,} = \frac{V_{por}}{A_{...}} \qquad (3)$$

where R_H is the hydraulic radius. Together with the pore size distribution (eq.(1)) and the minimum diameter of the capillary pore, the hydraulic radius can be determined from the random particle structure (Fig. 5). The hydraulic radius changes continuously during hydration. It decreases with increasing degree of hydration. This appears to hold true for the three types of cement with different fineness. Densification of the microstructure due to the formation of

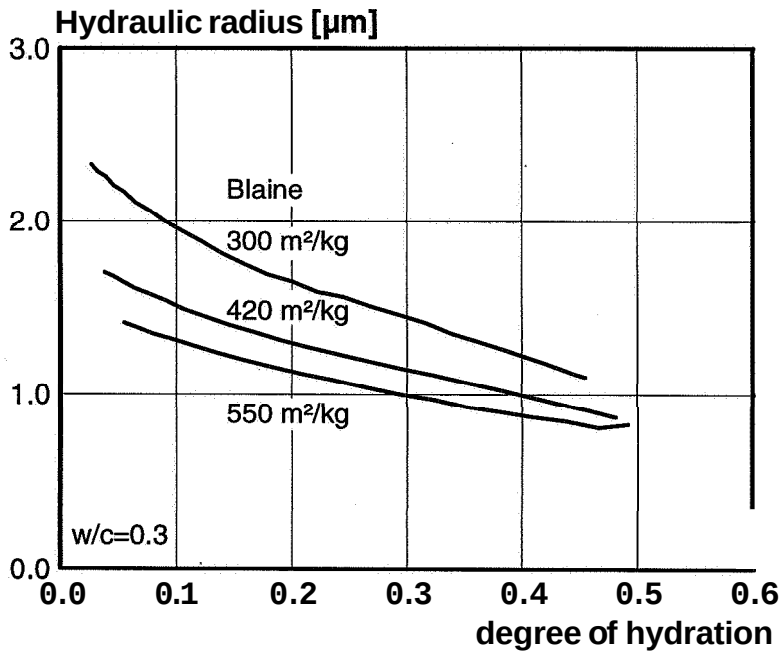

Fig. 5. Left: Hydraulic radius versus degree of hydration for three different cement pastes. The results are determined from the random particle structure.

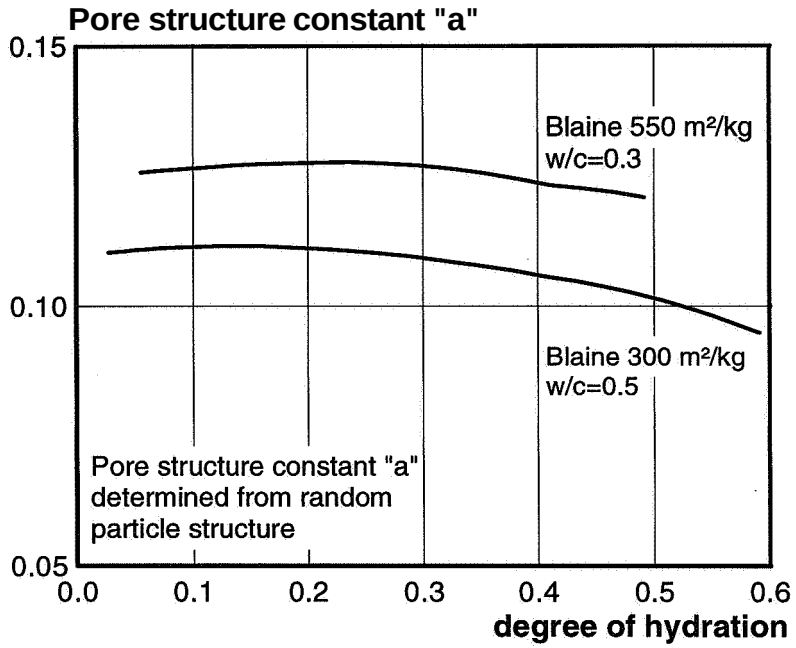

Fig. 6. Pore structure constant "a" versus degree of hydration for two different cement pastes determined from the random particle structure.

hydration products around the hydrating cement particles will reduce the initial pore volume of the hardening cement paste. On the other hand, it will enlarge the inner pore wall area, since the average pore diameter decreases. This means that if the formation hydration products proceeds, the surface area of developing microstructure will increase as well. This will also lead to an increase of the inner pore wall area. Assuming that the hydraulic radius represents the weighted pore diameter for the hardening paste, the pore constant "a" can be determined from a random particle structure. From the hydraulic radius R_H and the pore volume V_{pore} the pore structure constant "a" can be calculated. In Fig. 6, the pore structure constant is shown for two different types of cement paste. It appears that the value differs only slightly for both pastes with progress of the hydration process. It appears that the value is highest for the cement paste that contains fine cement and a low water/cement ratio. A higher value "a" in equation (1) implies that more smaller pores are involved in the microstructure. This in good agreement with what is generally found by experimental data [7].

3. THERMODYNAMIC EQUILIBRIUM IN THE PORE SPACE

In this section, a model will be derived that describes the thermodynamic equilibrium in the emptied pore space of a hardening cement-based microstructure, e.g. cement paste.
Initially, a plain cement paste consists only of a water-cement emulsion. At this particular stage of hardening, no structure has been formed by the hydrating cement grains. Cement particles are considered to be distributed randomly through the cement paste. Hydration of these particles will form a porous load bearing structure. At this moment of hardening, the pore space is considered

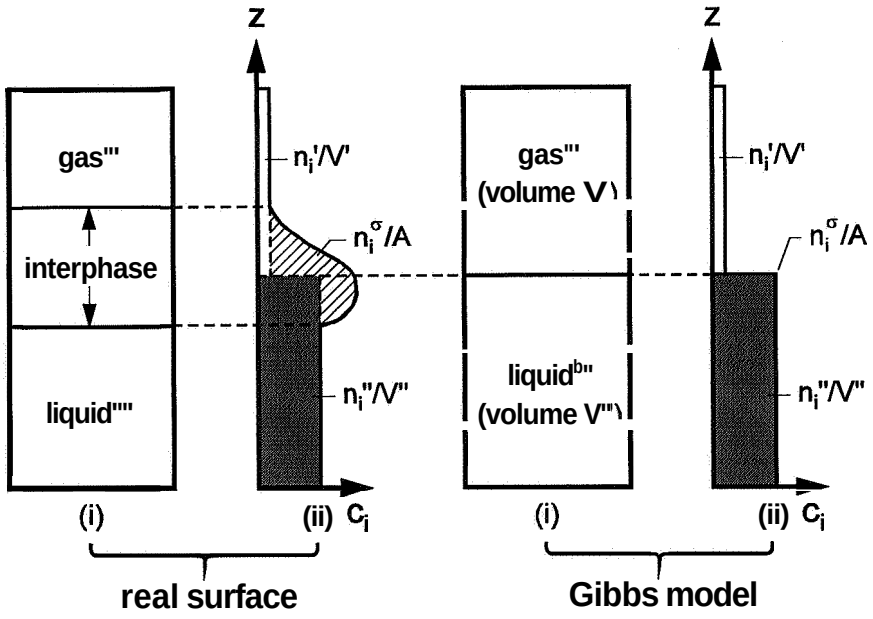

Fig. 7. Schematical representation of the liquid-interface-gas system (taken from [8]). Left: Real situation. Right: Gibbs model.

to be completely filled with water. After setting, at a certain stage of the hydration process, some pores are partly filled with fluid and partly with air. This implies that there exists a water/vapour interface layer in these pores between the fluid and the air. In general, this system can be considered as a three phase system e.g. capillary water (fluid) - interface layer - air (gas). This can also be described in terms of the bulk phases. In that case they are the free capillary water, the adsorption layer and the emptied pore space that is filled with gas, respectively. The composition of the interface volume will usually differ from the other two bulk phases. Therefore, it appeared to be useful to express the composition of the surface phase (adsorption layer) in terms of mole or weight fractions. A macroscopic definition of the adsorption volume can be derived by using the Gibbs [8] theory. This theory is based on a three phase system consisting of a dividing surface layer and two additional phases of homogenous distributed substances. The phases become inhomogenous close to the geometrical dividing surface (see Fig. 7). In the Gibbs model, initially the thickness of the interface is taken as zero whereas in a real system, this interface layer has a finite thickness. Assume c_i as the concentration of component i, in moles per unit volume. From this, the number of moles in the liquid phase and the gas (air) phase can be denoted by $n_i = c_i \cdot V_i$. Considering the capillary pore-system to be a closed system that contain n moles, conservation of mass requires for the interface:

$$n_\sigma = n - n_{liquid} - n_{gas} \tag{4}$$

where n_σ the number of molecules adsorbed to the pore wall area, n the total number of moles involved in the total system, n_{liquid} is the number of moles in the liquid phase (capillary water times its concentration c) and n_{gas} is the number of moles present in the gas phase of the system (gas in

emptied pores)). The thickness of the molecular layer per unit area that is adsorbed to the inner pore wall area can be determined by:

$$\Gamma = \frac{n_\sigma}{A_{por}(\alpha)} \tag{5}$$

where $A_{por}(\alpha)$ is the total pore wall area (see also Fig. 1). Considering the three phase system as described above, the mechanical work W that occurs after an infinitesimal phase change of the capillary system can be formulated as follows:

$$dW = d(p_g V_g) + d(\sigma A_{por}) \tag{6}$$

where p_g is the gas pressure in the system, V, the volume of the capillary gas, σ the surface tension, or often called "free surface energy", and A_{por} the surface area that is submitted to the surface tension. If dQ is the heat that is produced by an infinitesimal change of a mechanical system, then the first principal of thermodynamics leads to:

$$dQ = dU + dW \tag{7}$$

where dU is the internal energy in the system and dW the work carried out by the system. In a closed system an infinitesimal change of dQ can be written as dQ=SdT. Where dT is the absolute temperature increment of the system and S the entropy. If the temperature remains constant during a infinitesimal phase change (isothermal conditions), this latter term becomes zero. This leads to a more simplified formulation for the description of the thermodynamic equilibrium in the pore-system. Conservation of work for a closed capillary pore system leads to the following expression for the change of the surface tension with respect to a change of the gas pressure:

$$\frac{\partial \sigma}{\partial p_g} = \frac{RTn_\sigma}{p_g A_{por}(\alpha)} \tag{8}$$

with R the general gas constant and T the absolute temperature. Substitution of equation (5) in (8) and integration leads to the basic equation (9) that describes the relationship between surface tension and the relative pressure in the pore-system.

$$\sigma = RT \int_{p_g/p_0}^{p_g/p_0=1} \Gamma(p_g / p_0) d\left(\ln(p_g / p_0)\right) \tag{9}$$

This fundamental equation describes the relationship between the surface tension in the surface layer at the inner pore wall area and the relative humidity in the emptied pore space. The thickness of the adsorption layer Γ is also a function of the relative humidity in the emptied pore space. For a hardening cement paste, the relative humidity in the gradual emptying pore space will decrease as hydration proceeds. From equation (9), it can be noticed that the surface tension in the surface layer will increase if the relative humidity in the pore space decreases. This means that with this equation, thermodynamic equilibrium in the pore space can be established iteratively.

4. TOWARDS AUTOGENOUS DEFORMATION

The volumetric change of a hydrating cement paste is the result of the reduction of the relative humidity in the emptied pore space (self-desiccation). It was Bangham (1937) [9] who related the external deformation of coal to the surface tension in the adsorption layer formed at the inner pore wall area. In several papers he used the adsorption equation of Gibbs to describe this phenomenon. Bangham used his theory to point out that with solid, as opposed to liquid surfaces, the surface energy, representing the work spent for the formation of a unit of new surface, must thermodynamically be in equilibrium with the pressure. In his theory, he considered the three-phase system as discussed in the previous sections (see section 3). Next, he found that a change of the expansion of coal could be related linearly to the change of the surface energy that appears at the adsorption layer. This approach has been shown to be valid for hardened cement paste by, among others, Wittmann [10]. For hardened cement paste, the material properties are totally developed. As far as this hardening cement paste is concerned, the material properties change continuously with elapse of time. Therefore, relationship between the external deformation and the surface tension must be considered incrementally and can be formulated as follows:

$$\frac{\partial \varepsilon_a}{\partial t} = \lambda \cdot \frac{\partial \sigma}{\partial t} \tag{10}$$

where $\partial\varepsilon_a$ is the strain increment that describes the microstructural deformation of the hardening paste (autogenous deformation), $\partial\sigma$ the surface tension increment (see eq.(9)) and h a proportionality factor. In fact, this proportionality factor is the compliance modulus of the hardening material (cement paste). According to Bangham, coal would swell proportional to the decrease of the free surface energy. In general, for hardening cement paste, the opposite behaviour is observed, viz. cement paste shrinks proportional to a increase of the free surface energy.

The proportionality factor h that relates the rnicrostructural deformation to the surface tension in the adsorption layer was proposed, by several authors [11, 12, 13, 14]. Minor differences appears between the relations as proposed by these authors. According to Bangham, this constitutive relation, has the following shape:

$$\lambda = \frac{\Sigma \cdot \rho_{pa}}{3\, E_p} \tag{11}$$

where:
C = pore wall area of the empty pores
Note: $C = \Sigma(\alpha) = A_{por}(\alpha) - A_{wat}(\alpha)$
ρ_{pa} = specific mass of the cement paste
E_p = modulus of elasticity of the cement paste
Note: $E_p = E_p(\alpha)$

As can be noticed from this relation, the pore wall area, the specific mass of the cement paste and the development of the modulus of elasticity play an important role in the simulation of the volumetric changes of the microstructure (autogenous shrinkage) during the hardening phase.

5. MEASUREMENTS VERSUS NUMERICAL SIMULATIONS

In Fig. 8, the autogenous shrinkage is presented as a function of time for a cement paste that contain a cement of high fineness (Blaine 550 m²/kg). Results are shown for a waterlcement ratio of 0.3, 0.4 and 0.5. It shows a strong increase of the autogenous shrinkage for a decrease of the waterlcement ratio. The largest autogenous shrinkage, ca. 2‰, is measured after about 168 hours of hydration for the cement paste with waterlcement ratio of 0.3. The very strong increase of the autogenous shrinkage at the beginning of the hardening process can be related to fact that at this early stage of hardening process, the elastic modulus has only developed minorly. The volumetric contraction of the microstructure will then experience hardly any restraint of the stiffness of the paste. Consequently, large deformations can easily occur. For higher waterlcement ratio's, this contraction forces will be much smaller so that the volumetric contraction of the microstructure will be less pronounced at that particular stage of the hardening process. For a cement paste with a ratio of 0.4 much less shrinkage is measured. After 168 hours of hardening, a shrinkage value of about 1‰ has been reached. This is a strong reduction (50%) in comparison with the paste that has a water-cement ratio of 0.3. A further increase of the waterlcement ratio to 0.5 reduces the autogenous shrinkage again by an other 50%.
In Fig. 9, a shrinkage measurement is presented for a cement paste with a cement with a fineness

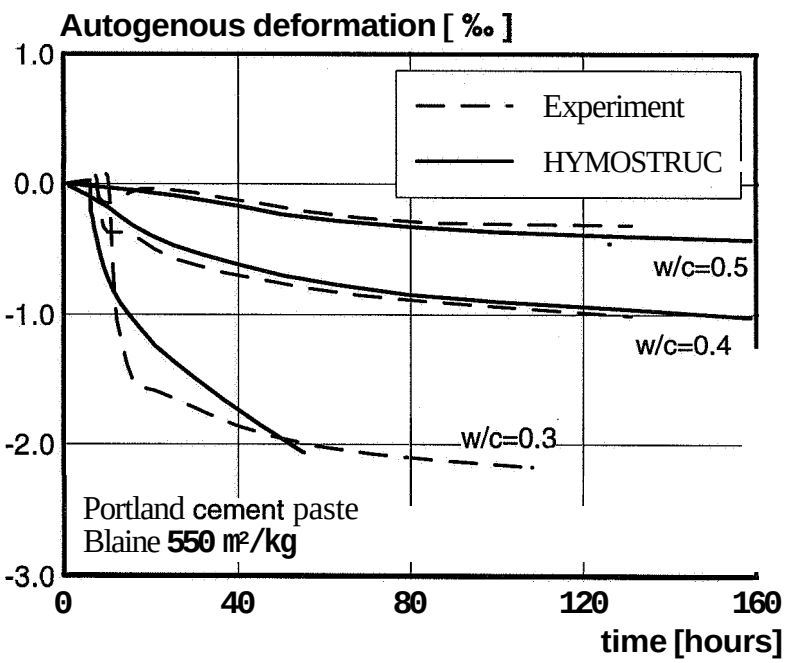

Fig. 8. Autogenous shrinkage of cement paste versus time. Left: Three different waterlcement ratio's. (Fine cement, high hydration rate)

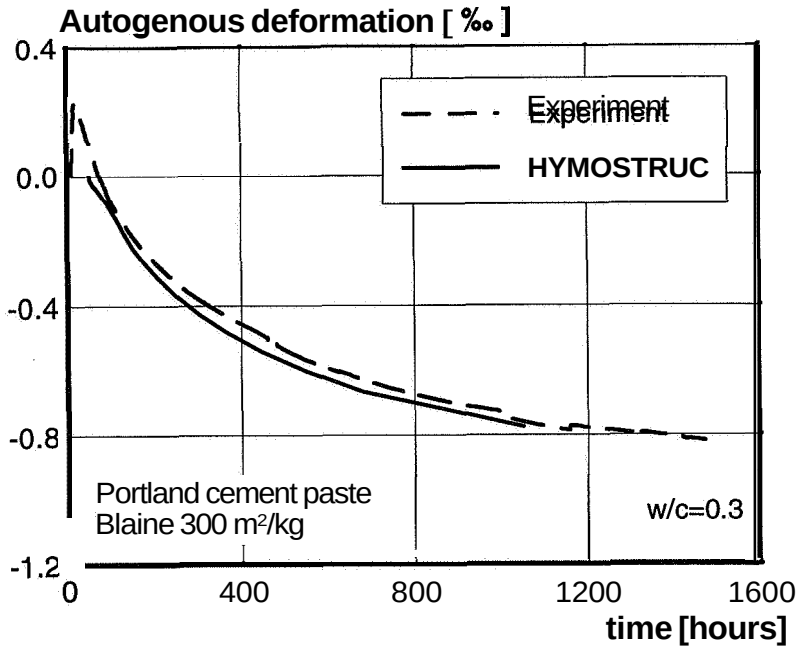

Fig. 9. Autogenous shrinkage of cement paste versus time. (Coarse cement, low hydration rate)

of 300 m^2/kg. Due to this relatively coarse type of cement, the hydration process will develop rather slow. Implicitly, the development of the autogenous shrinkage will develop slowly as well. From the figure it can be observed that the autogenous shrinkage is still increasing after about 1400 hours of hardening. This process will proceed until hydration has ceased. The measured volumetric contractions are simulated by the HYMOSTRUC. These simulations are based on the

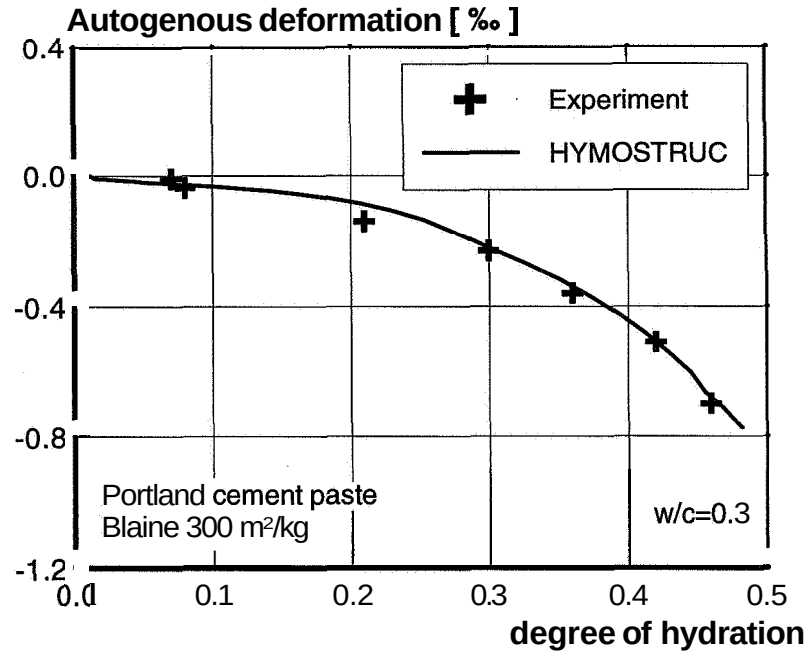

Fig. 10. Autogenous shrinkage versus degree of hydration. Portland cement paste. Water/cement ratio 0.3.

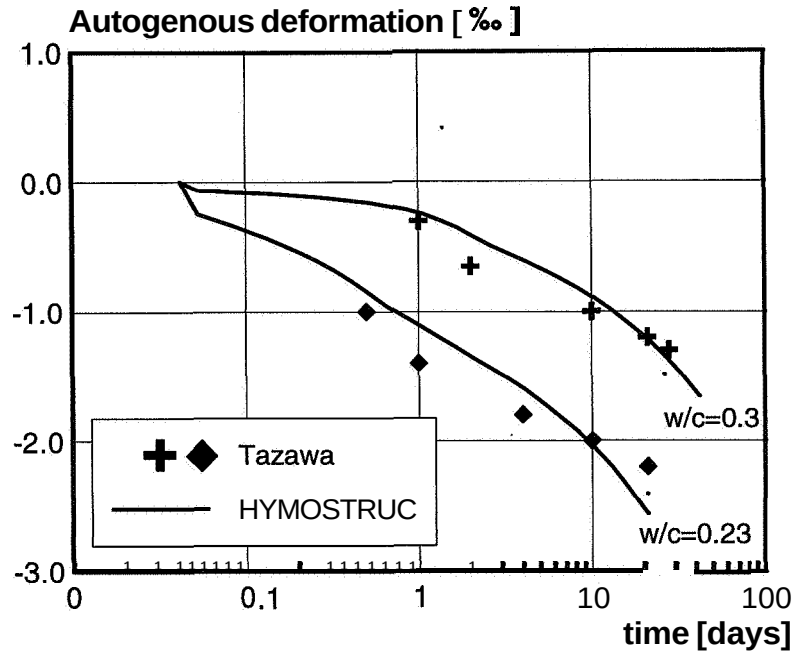

Fig. 11. Comparison between experiments on cement paste (Blaine 352 m^2/kg) carried out by Tazawa et.al. and numerical simulations by **HYMOSTRUC.**

shrinkage model as outlined in the previous sections. The results show a very good agreement.
In Fig. 10, the development of the autogenous deformation of the coarse cement paste (Blaine 300m^2/kg, wcr 0.3) is presented as a function of the degree of hydration. The numerical simulations are compared with experimental results. Also for the very coarse types of cements, the proposed model appears to be able to predict the autogenous deformation of the hardening cement paste fairly well. This holds true for the time domain as well as for the degree of hydration domain.
In [15], Tazawa has presented his results of an extended experimental study on autogenous shrinkage of cementitious material. Some of his results on plain cement pastes are simulated with the proposed shrinkage model as implemented in HYMOSTRUC. The results are shown in Fig. 11. Good agreement has been obtained between the experimental results and the numerical simulations. This holds true for both the waterlcement ratio of 0.3 and a waterlcement ratio of 0.23. The autogenous shrinkage increases to a level of about 1.5‰ for the cement paste with a waterlcernent ratio of 0.3 and for the cement paste with a waterlcement ratio of 0.23, the autogenous shrinkage reached a value of about 2.5‰. However, the volumetric contraction of the microstructure may continue as long as hydration goes on.

6. CONCLUSIONS

Describing the volumetric changes of hardening cement paste on a thermodynamical basis turned out to be quite satisfactory. The proposed model predicts the autogenous deformation of hardening cement paste quite accurately. The numerical simulations are in good agreement with the experimentally obtained results for cement pastes that contain cement of relative high fineness

as well as for pastes that contain a relative coarse type of cement. This holds true for various water cement ratios.

In addition: to come to a model to predict the volumetric changes of hardening concrete, internal restraint due to the availability of stiff aggregates has to be taken into account in the model. Reological models as proposed by Counto or Hirsch can be applied for this purpose. However, the internal restraint can also be simulated with the aid of a lattice model [16].

7. REFERENCES

[1] Breugel, K. van (1991). Simulation of hydration and formation of structure in hardening cement-based materials, Breugel K. van: 295.

[2] Young, J.F., et.al Materiaux et Construction(TC-68): pp. 377-382,.

[3] Bangham, D. H. and Fakhoury, N. (1931). "The Swelling of Charcoal." Royal Society of London CXXX(Series A): 81-89.

[4] Breugel, K. van (1995). "Numerical simulation of hydration and microstructural development in hardening cement-based materials. Theory (I) and Applications (II)." Cement and Concrete Research (I) Vol. 25, No. 2, pp. 319-331 (II) Vol. 25, No. 3, pp. 522-530.

[5] Whiting, D. and Kline, E. (1977). "Pore size distribution in epoxy impregnated hardened cement pastes." Cement and Concrete Research Vol. 7: pp 53-60.

[6] Setzer, M., J. (1978). "Einfluss des Wassergehalts auf die Eigenschaften des erharteten Betons." Deutscher Ausschuss Für Stahlbeton DAfSt Heft 280: 43-79.

[7] Feldman, R.F. and Cheng-yi, H. (1985). Cement, Silica Fume, Pastes, Porosity, Surface Properties. Cement and Concrete Research. 15: pp 766-774. 5 .

[8] Defay, R. Prigogine, I. and Bellemans, A. (1966). Surface Tension and Adsorbtion. London, Longmans London.

[9] Bangham, D.H. (1937). The Gibbs Adsorbtion Equation and Absorbtion on Solids. London, Gurney and Jackson.

[10] Wittmann, F. (1968). Physikalische Messungen an Zementstein. Miinchen, TU Miinchen.

[11] Bangham, D.H. and Maggs, F.A.P. (1944), The Strength and Elastic Constants of Coal in Relation to their Ultra-fine Structure, The British Coal Utilisation Research Association, The Royal Institution, London.

[12] Yates, D. J. C. (1954). "The Expansion of Porous Glass on the adsorption of Non-Polar Gases." Proceedings of the Royal Society of London 224(Series A. Mathematical and Physical Sciences): 526-543.

[13] Hiller, K.H. (1964). "Strength Reduction and Length Changes in Porous Glass Caused by Water Vapor Adsorption." Journal of Applied Physics 35(5): 1622-1628.

[14] Rarnachandran, V.S., Feldman, R.F. and Beaudoin, J.J. (1981). Concrete Science, Treatise on Current Research. Division of Building Research, National Research Council, Canada, Heyden.

[15] Tazawa, E. and Miyazawa, S. (1992). Autogenous shrinkage caused by self desiccation in cementitious material. 9th Int. Conf. on Chemistry of Cement, New Delhi.

[16] Breugel, K. van and Koenders, E.A.B. (1995). Numerical Simulation of the Effect of Elevated Temperature Curing on Porosity of Cement-Based Systems. MRS-FALL Conference, Boston USA.

MEASUREMENTS AND MODELLING OF VOLUME CHANGE AND REACTIONS IN HARDENING CONCRETE

HANS HEDLUND and GUSTAF WESTMAN
Luleå University of Technology
Division of Structural Engineering,
971 87 Luleå,
Sweden

ABSTRACT

The purpose of this project is to modify already existing tools and to develop new ones for crack risk estimation adopted to High Performance Concrete at early ages. In order to be able to modify known technique, it is necessary to recognise the features that characterise high performance concrete in comparison with ordinary concrete.

Two such features are shrinkage and self-desiccation in hardening concrete at early ages. The homogenous volume change (shrinkage under sealed conditions) induces additional stresses - apart from those related to temperature - in a restrained structure. Hence, investigations of shrinkage phenomena are vital for the study of early age behaviour of High Performance Concrete.

For an unrestrained structure temperature differences may cause local cracking. In such a case homogeneous shrinkage - over cross section - gives no stress contribution, and it is therefore important to distinguish between the temperature and moisture components of the non-elastic deformation. Another reason to separate moisture and thermal movements is to give a rational base for analyses of structures in general with respect to shape and restrained conditions.

To be able to calculate stresses in a satisfactory manner, it is necessary to perform stress measurements and to check the tested results with computed values. Such tests are performed here for the well defined case of fully external restraint, in which the stress state is assumed to be uniform over the cross section, see Fig. 1. If this structural member is subjected to homogeneous shrinkage and a simultaneous temperature rise followed by a cooling phase, tensile stresses will develop due to the combined effect of temperature and shrinkage. If the tensile stress level approaches the tensile strength a crack may occur. Also, lower compressive stress will be developed due to the combined effect of shrinkage and temperature.

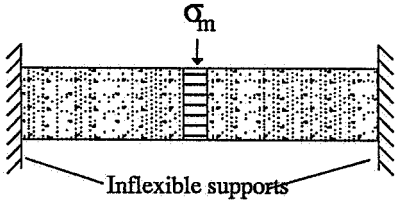

Fig. 1 Schematically picture of a fully restrained structural member.

SELF-STRESSES DURING HARDENING

If a structural member of hardening concrete is free to expand during the early age heating phase of the hydration process and later contracts without being restrained during the subsequent cooling phase evidently no stresses will be induced. However, this is rarely the case in practice as the concrete in a structure is nearly always restrained to some degree, either externally by adjoining structures or internally by temperature and moisture fields in the components of the structure itself.

For Normal Strength Concrete, NPC - water binder ratios (w_0/B) $\geq$ 0.40 and above - mainly temperature volume changes will induce stresses in the concrete due to these imposed restraint conditions. For High Performance Concrete, HPC - w_0/B below 0.40 - both temperature and moisture changes may have an influence on the stresses induced in the concrete. The issue of primary interest is whether the induced stresses will lead to cracking or not.

A very important part of the research is to calibrate the theoretical models in laboratory tests for different types of concrete mixes, cement types etc. Thus, a test method has been developed at Luleå University of Technology where the thermal stresses in concrete specimens are recorded [1].

The frame consists of rectangular hollow steel beams with profile VKR 450x250 mm (steel thickness 16 mm), see Fig. 2. The concrete specimen is a 1m long beam, 150 mm in square. In the relaxation tests the concrete is poured directly in the frame. Tensile reinforcement consisting of 8 threaded rods (6 mm in diameter, 100 mm long) at each end transmit tensile forces from the concrete to the frame during the cooling process.

A plastic foil surrounds the specimen protecting it from drying. In the frame the specimen is located in a box made of Plexiglas. Two heaters blow temperated air into the box in order to give the concrete specimen a temperature development representative to some specific concrete structure.

For the calculation of such a time-temperature curve the temperature and strength development of the concrete have to be known [2) 3) 4)]. For the calculation of the representative temperature curve a finite element program (FEM) called HETT [5)] is used in this study.

One end of the specimen is fixed in the frame, which in turn is fixed to the floor, and the other end is free to move in the longitudinal direction. When the specimen tends to expand, a servo-hydraulic cylinder (capacity ± 750 kN, cylinder stroke 150 mm) will press the free end back into position so that the length of the specimen is held constant. In the same way the servo-hydraulic cylinder will pull the free end back to its initial position when the specimen tends to contract in the cooling stage of the test. This is controlled by a displacement indicator measuring the location of the free end related to the floor (i.e. related to the free end). The force excited by the cylinder is directly proportional to the stresses occurring in the concrete specimen.

Results of one tested HPC mix and one NPC mix are shown in Fig. 3. One interesting result can be seen in the figure, for HPC 3 tensile forces starts to develop already during the heating stage. The exact reason for this is not known yet, but can possibly be related to effects of shrinkage due to self desiccation for HPC 3 with low enough water to binder ratio. The water to binder ratio for HPC 3 and for NPC are 0.31 and 0.40 respectively.

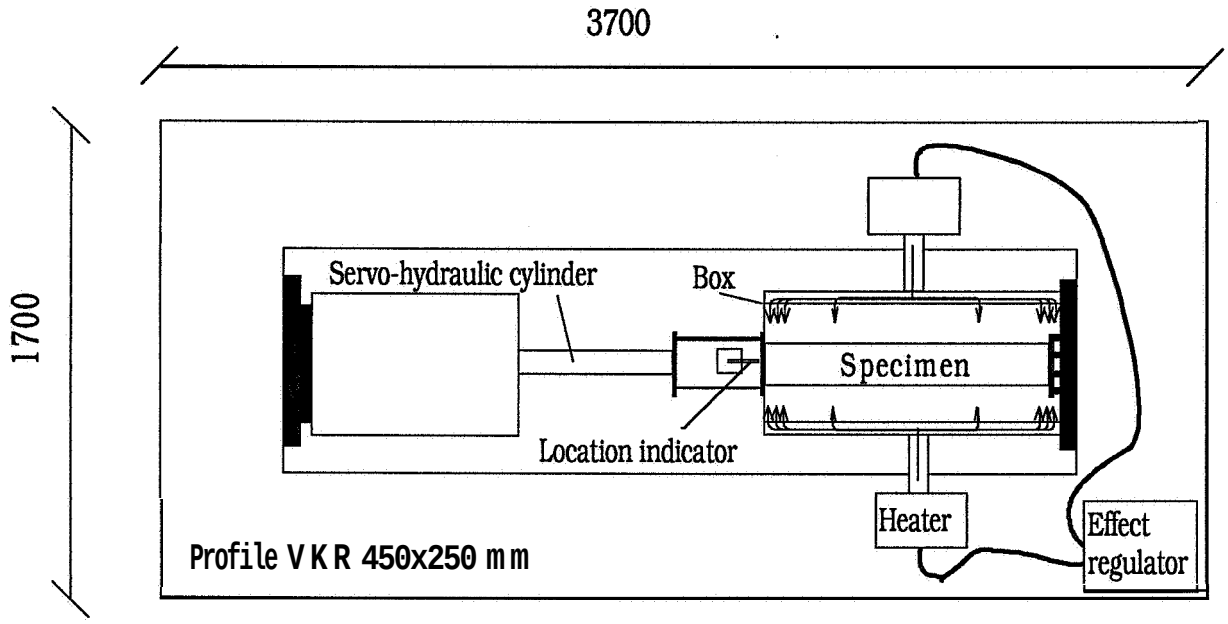

Fig. 2 Thermal stress test-frame

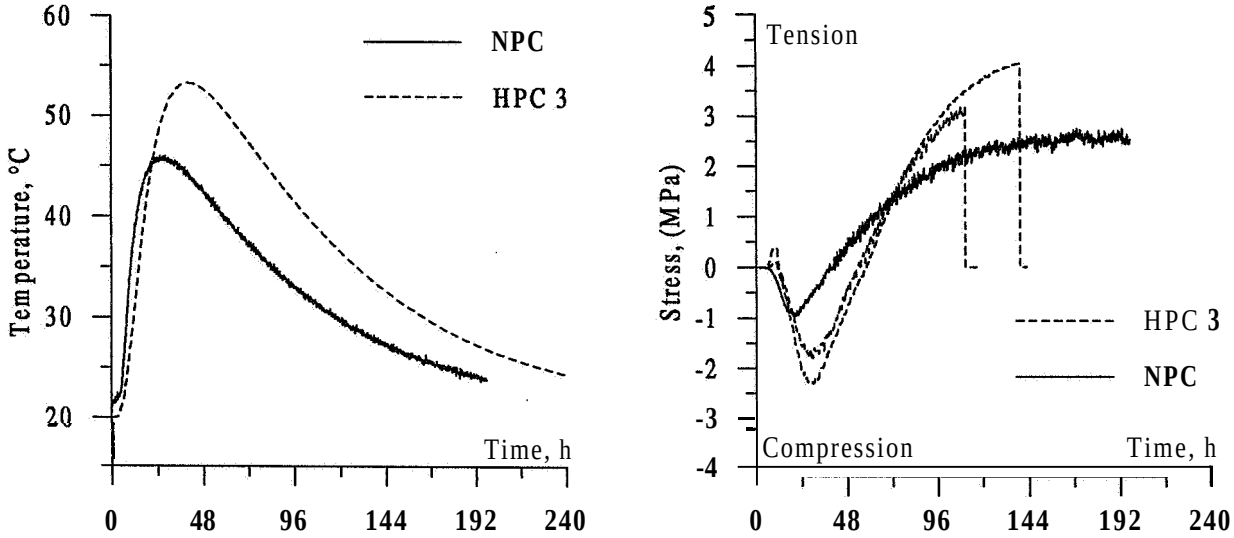

Fig. 3 Example of temperature development and test results obtained in the thermal stress test-frame.

SHRINKAGE UNDER SEALED CONDITIONS

Test specimen for concrete should have a certain height in relation to maximum aggregate size, d_{max}, in order to make possibilities for a structure in representing the concrete as an apparent homogenous material. This is often set to three times d_{max} as a minimum value. The test specimens had the dimension of 100 * 100 * 250 mm, see Fig. 4. This specimen size can be used for concrete mixes with aggregate sizes up to 32 mm, which covers most of the common concrete mixes. The standardised test specimen for shrinkage measurements on old normal concrete is a beam with the dimensions 100 * 100 * 400 mm.

For young high performance concrete there has not been any special test specimen size used as a standard. Instead, many researcher have used the same beam as for normal concrete. Measurement of self-desiccation from [6], where a specimen size of 100 * 100 * 600 mm was used, shows the similar shrinkage as our tests for the same water binder ratio. This indicates that the length of 250 mm to 600 mm does not have any influence on shrinkage at sealed conditions. One conclusion is that shrinkage at sealed conditions probably is a true material parameter.

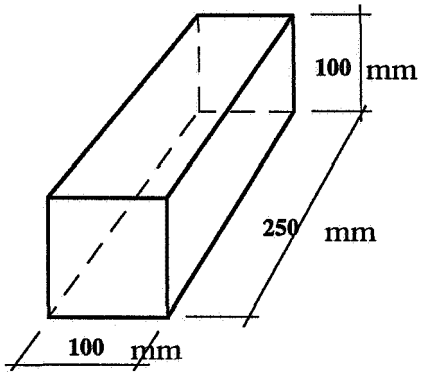

Fig. 4 Test specimen used for measurements of relative humidity and shrinkage on young HPC and NPC.

With this similar result in mind it should be possible to measure shrinkage on shorter test specimens and still have quite good accuracy of the measured result.

TEMPERATURERISE IN TEST SPECIMEN

The shrinkage of young hardening concrete competes with thermal expansion the first hours after casting. When measuring the shrinkage it is inevitable to register only the deformation (shrinkage) using manual measuring technique without possibility to regulate the temperature in the test specimen. It is therefore necessary to record the temperature changes in the hardening concrete during shrinkage measurements [7]. For a test specimen with 100 * 100 mm^2 size in this study, the temperature rise have been about 3 to 5 "C, see Fig. 5. The temperature rise may cause a swelling of the test specimen which can be noticed directly after the measurements have started.

For correction of this temperature rise the thermal strain during the expansion phase, assumed to be 10 µm/m °C, have to be excluded from the shrinkage measurements. This may be done as the temperature rise is known, and then it is possible to obtain the pure self-desiccation strain. The thermal strains represent a significant portion of the measured strains. The measured strain can be expressed as

$$\varepsilon_{tot} = \varepsilon_T + \varepsilon_{SH} \qquad (1)$$

where ε_{tot} = measured strain, µm/m
ε_T = thermal strain, µm/m
ε_{SH} = true self-desiccation shrinkage, µm/m.

If the shrinkage taken from separate tests is assumed to be ruled by the equivalent time of maturity, the values of ε_{SH} can be estimated at any temperature time development. From the measured or calculated temperature development the thermal strain is estimated by

$$\varepsilon_T = \Delta T \cdot \alpha_E \qquad (2)$$

where ε_T = thermal strain, µm/m
ΔT = temperature difference in specimen, °C
α_E = thermal expansion coefficient, µm/m°C.

The thermal distribution in the test specimens have been calculated according to how each one of them has been handled from pouring the concrete into the mould until a few days after casting, see Fig. 5. The specimens have been demoulded as early as possible, which here means at a time of 8 to 20 hours after casting. The demoulding time is determined with respect to the stiffness of the concrete to avoid damaging the concrete at preparation of the test specimen.

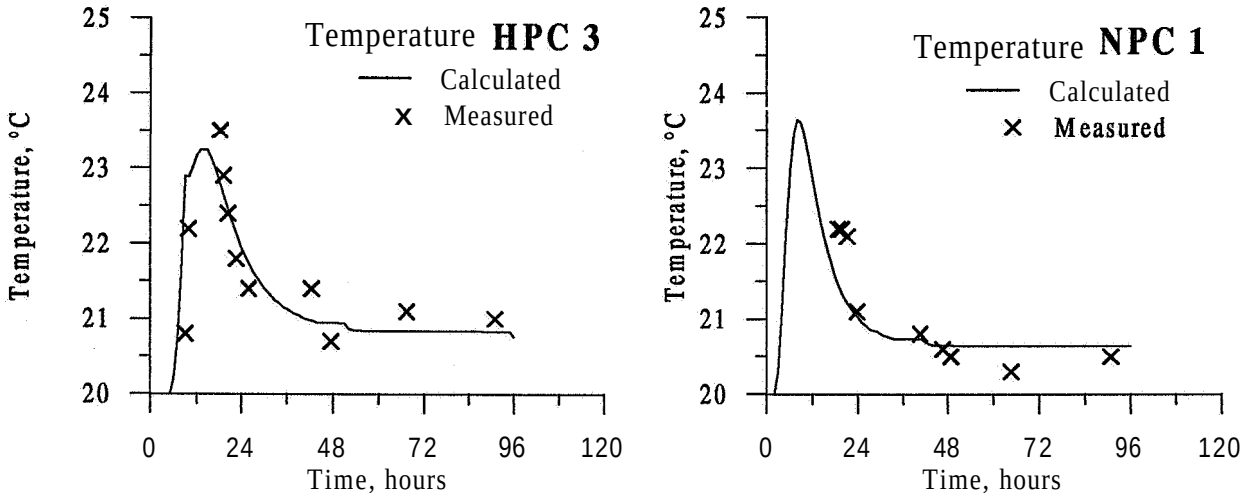

Fig. 5 Calculated and measured temperature rise of concrete specimen HPC 3 and NPC 1.

EMPIRICALLY MODELLING OF SHRINKAGE AS A FUNCTION OF TIME

When shrinkage on sealed specimens is measured there is not always measurements of the self-desiccation done in parallel tests from the same batch of concrete. If this is the case, there is still a need to be able to express the shrinkage for subsequent stress analyses.

The shrinkage as a function of time for membrane sealed concrete[7] is mainly a consequence of the self-desiccation, which is more pronounced for concrete mixtures with low water binder ratios and high binder contents, i.e. circumstances typical for HPC. Time dependence of the shrinkage is here chosen to be expressed in a similar way as may be used in describing the degree of reaction for hardening concrete by

$$\varepsilon_{SH} = \varepsilon_{ref} \cdot \exp\left(-\left[\frac{\theta_{SH}}{t_{eq} - t_{\varepsilon 0}}\right]^{\eta_{SH}}\right) \qquad (3)$$

where ε_{ref} = reference ultimate shrinkage, µm/m

θ_{SH} = empirical parameter representing the time when inclination of shrinkage changes in time, h

t_{eq} = equivalent time, h

$t_{\varepsilon 0}$ = start time of measurements, h

η_{SH} = empirical constant ruling the curvature, -

By fitting equation **(3)** with respect to the least square method, Fig. 6, the evaluation gives parameters presented in Table - 1.

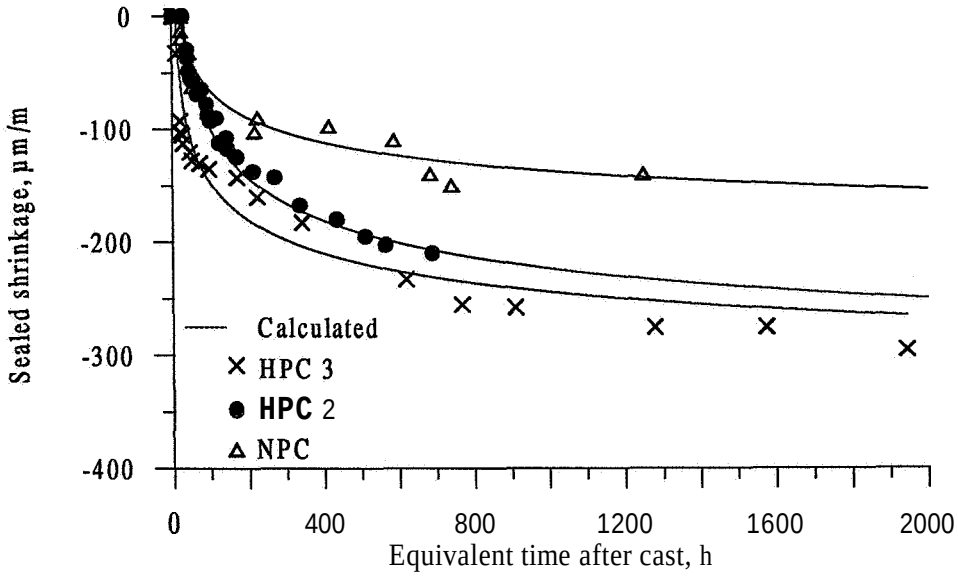

Fig. 6 Evaluated result of concrete HPC 7 according to equation **(3)**

Table - 1: Evaluated parameters using method 2 for shrinkage under sealed conditions.

Mixture	$t_{\varepsilon 0}$, h	ε_{ref}, µm/m	η_{SH}, -	θ_{SH}, h
HPC 2	26.96	-360	0.38	140
HPC 3	9.29	-370	0.33	70
NPC 1	20.56	-230	0.35	150

When using equation **(3)** no direct connection between the ultimate shrinkage and the water binder ratio has been found. One contributory reason for this may be the previous mentioned uncertainties of the shrinkage at very early ages. However, the parameter describing the curvature is in the region of 1/3 for most studied mixtures, see Table - 1.

Comparison between evaluated result for concrete HPC 2 and by Dilger [6] measured shrinkage is shown in Fig. 7, where it can be seen that the result for HPC 2 show good agreement with the measured data. Both concrete mixtures have the same water binder ratio but evaluated parameters are based on own measurements up to 28 days after casting. The calculation has been made for shrinkage starting 24 hours after casting.

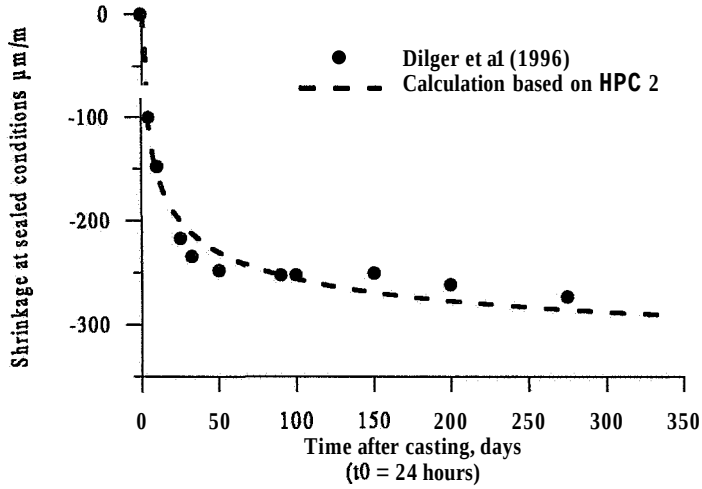

Fig. 7 Calculated self-desiccation shrinkage compared with measurements made by Dilger et al. $w_0/B = 0.30$ parameters according to Table - 1 of concrete HPC 2.

The evaluation of shrinkage using equation (3) seems to be able to predict long term sealed shrinkage from short term measurements, which could be used in the future to get fast information of sealed shrinkage based only on short term tests.

THERMAL DEFORMATION UNDER VARYING TEMPERATURE

Cylinder specimens (length 340 mm, O 80 mm) are used to determine the coefficients of free thermal dilatation of the hardening concrete. Immediately after casting the concrete specimen is placed in water with a temperature of 20 °C. 30 minutes before test the specimen is demoulded and two strain gauges are mounted on the specimen. The inductive strain gauges of type LVDT Schaevitz type 010 MRH are mounted on composite bars made of invar and graphite. With this type of gauges the deformation can be measured with an accuracy of about 0.03µm.

The two transducer gauges are placed on opposite sides of the specimen, see Fig. 8. The concrete which is controlled by the deformation gauges is located in the central part of the test specimen. Before demoulding the compressive strength is tested and has to be at least 3 MPa. Depending on the concrete it is possible to demould and apply the gauges onto the specimen about 6 - 10 hours after casting.

After the strain transducer have been mounted the specimen is placed in a water tank equipped with heating devices.

The thermal development of some chosen newly cast concrete structure is simulated. This method requires an efficient regulation of the heating device in order to follow the pre-chosen time-temperature curve with regard to the temperature in the water and consequently in the

specimen. The temperature was measured in the water just outside the specimen and inside the concrete. The regulation of the water temperature was performed in such a way that the temperature inside the concrete specimen has the same temperature development as the simulated structure. However, the temperature difference between water and specimen was found to be very small.

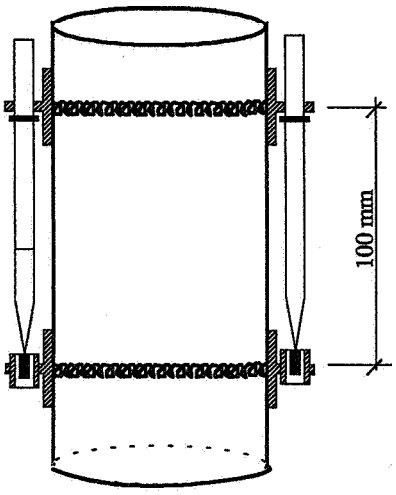

Fig. 8 Inductive strain gauge mounted on the border of the test specimen at thermal deformation tests.

Evaluating the total measured deformation without splitting of thermal and moisture movements, i.e. to directly use the total deformation from tests, will give combined "sealed" coefficients, α_E^* and α_C^*, representing the expansion phase and the contraction phase respectively. It is difficult to determine the combined expansion- and contraction coefficient with high accuracy, especially when the sealed shrinkage is very pronounced, see Fig. 9.

For High Performance Concrete the self-desiccation effect can be observed as the specimen contracts even when the temperature still is rising which gives an image of drastic changes of the deformation coefficients during hydration. However, a slight age dependence of the coefficients may be observed both for High Performance Concrete as well as for normal strength concrete.

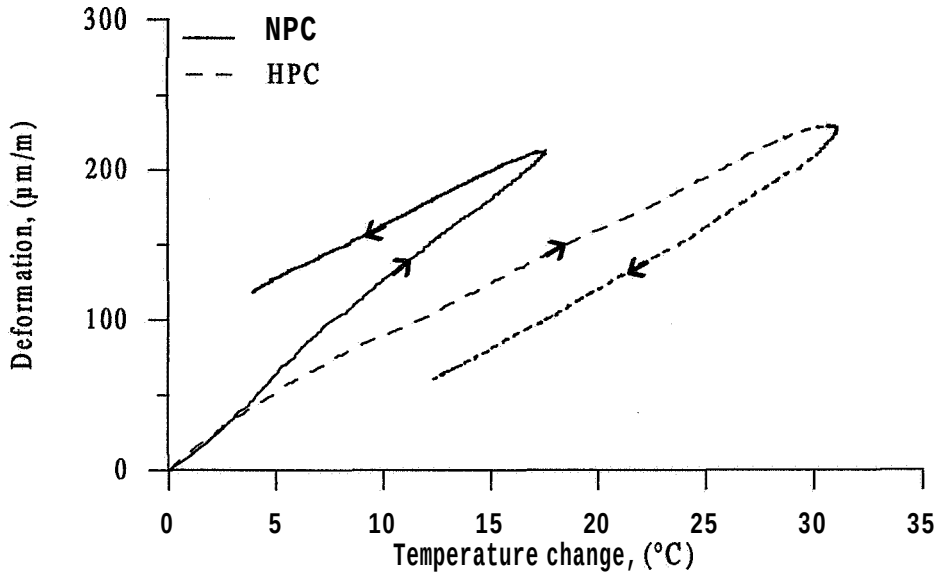

Fig. 9 Example of combined thermal and moisture movements (total deformation) for HPC and NPC.

The shrinkage measured on sealed specimens - evaluated by means of equation (1) and (2) - is expressed by equation (3). Temperature equivalent time is assumed to be ruling the shrinkage development, which is the same assumption as in Tazawa[8]. One example of measured total deformation for concrete HPC 3 is plotted together with measured shrinkage against equivalent time in Fig. 10.

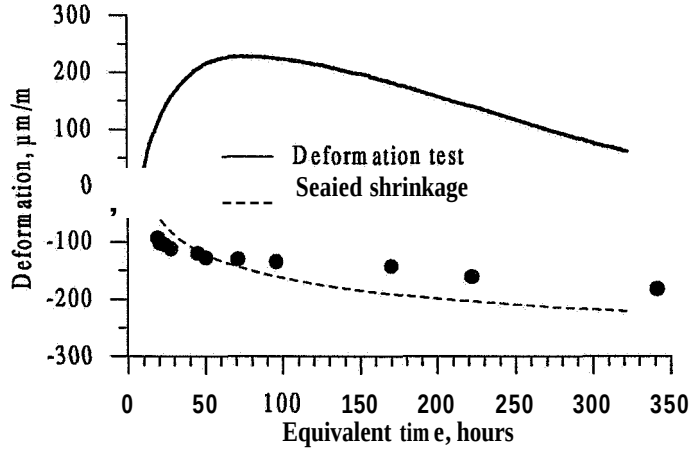

Fig. 10 Measured total deformation and sealed shrinkage for HPC 3.

The expansion coefficient, α_E, is represented by the inclination of the deformation, when the temperature is increasing, and the thermal contraction coefficient, α_C, is represented in the same way when the temperature is decreasing. The evaluation has been performed from the latest start time, see Fig. 11, of either the thermal deformation test or the start time of the shrinkage measurements. The choice of start time for separation is that both types of deformation should be valid at the same time. By subtracting the sealed shrinkage from the measured total deformation the true thermal deformation is obtained, which is shown by the solid lines in Fig. 12.

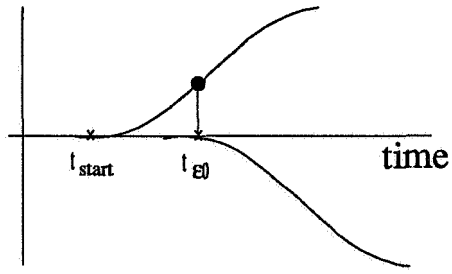

Fig. 11 Schematically picture of chosen start time for the separation of measured deformation.

The thermal expansion coefficients, α_E, is quite stabile and is in the region of about 10 - 12 µm/m °C for both High Performance Concrete and Normal Strength Concrete. The thermal contraction coefficients, α_C, show levels about 7 - 9 µm/m "C for both High Performance Concrete and Normal Performance Concrete [7)9)].

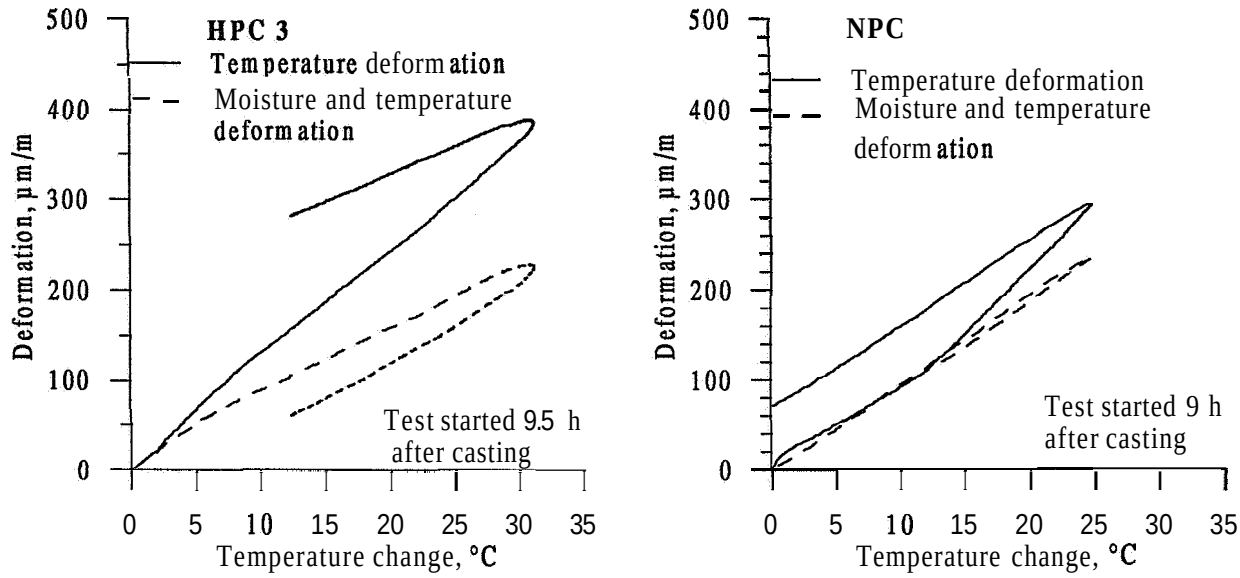

Fig. 12 Free thermal expansion and contraction test of HPC 3 and NPC.

COMMENTS CONCERNING THE EVALUATION OF THERMAL MOVEMENT COEFFICIENTS

The thermal deformation coefficients obtained may not be pure material coefficients due to the way of regulating the temperature in water with direct contact with the test specimen which may cause moisture gradients in the concrete. For high water cement ratio it may even be possible for the water to penetrate into the specimen so no moisture gradients will occur, but this could result in moisture swelling of the concrete. In the case of water cement or water binder ratios below about 0.45, it may be possible for the water to flow only into the surface layer but not through the whole specimen. If water is sucked into a certain depth, a local swelling of the specimen will occur. In this case a system property will be measured instead of an intended

material property. If a system property is measured it may reflect how the pore structure looked at that particular moment.

For High Performance Concrete the cement paste matrix is assumed to be very dense so only the very outer region of the surface layer will be affected by this swelling. Hence, the gradient will not disturb the overall deformation and the recorded deformation is therefore affected only slightly. To be sure to measure material properties it would be recommended to perform deformation tests on sealed specimens in the future.

A swelling large enough causing gradients affecting the measurements or in extreme cases an almost homogeneous swelling will lower the contraction coefficients. Similar behaviour have been reported by Ben Amor and Clement who performed thermal deformation measurements at various moisture states [10].

THERMAL AND MOISTURE STRESSES

The uniaxial constitutive law for incremental calculations of stresses for young concrete at variable humidity and temperature can be expressed [11) 12)] by

$$\Delta\sigma = E_{tot} \cdot (\Delta\varepsilon - \Delta\varepsilon^{o}_{tot}) \tag{4}$$

with

$$E_{tot} = E_c \cdot (1+\gamma_d) \tag{5}$$

and

$$\Delta\varepsilon^{o}_{tot} = \Delta\varepsilon_{rel} + \Delta\varepsilon^{o}_{\varphi} + \Delta\varepsilon^{o}_{T} \tag{6}$$

where σ = stress in the material, Pa
ε = the total strain
Δ = denotes an increment during the actual time step
E_C = fictitious elastic modulus for the time step including basic creep effects, Pa
γ_d = incremental adjustment due to non-linear stress-strain behaviour
ε_{rel} = relaxation strain
$\varepsilon^{o}_{\varphi}$ = nonelastic strain, including the stress-induced part, due to a change in humidity
ε^{o}_{T} = nonelastic strain, including the stress-induced part, due to a change in temperature

The structural condition for the stress-frame is completely restraining, which means that a relaxation test is performed and the external deformation is identically zero ($\Delta\varepsilon \equiv 0$). For this case equation (4) - (6) are reduced to

$$\Delta\sigma_{rel} = -E_{tot} \cdot \Delta\varepsilon^{o}_{tot} \tag{7}$$

where σ_{rel} = relaxation stress associated with external restraint conditions, Pa

For loading in tension the following virgin stress-strain curve is introduced

$$\frac{\sigma}{f_{ct}} = \frac{\varepsilon_m}{\varepsilon_o} \quad \text{for} \quad \frac{\sigma}{f_{ct}} \leq \alpha_{ct} \tag{8}$$

and

$$\frac{\sigma}{f_{ct}} = 1 - (1-\alpha_{ct}) \cdot \exp\left(-(\frac{\varepsilon_m}{\varepsilon_o} - \alpha_{ct}) / (1-\alpha_{ct}) \right) \quad \text{for} \quad \frac{\sigma}{f_{ct}} > \alpha_{ct} \tag{9}$$

where f_{ct} = tensile strength, Pa

ε_m = material strain (= strain related to the stress level)

α_{ct} = relative stress level ($=\sigma / f_{ct}$) at which non-linear stress-strain behaviour starts

$\varepsilon_o = f_{ct} / E_c$ = strain linearly related to the tensile strength

The non-linear stress-strain adjustment factor is formally expressed by

$$\gamma_d = \frac{d(\frac{\sigma}{f_{ct}})}{d(\frac{\varepsilon_m}{\varepsilon_o})} - 1 \tag{10}$$

which for monotonic loading gives

$$\gamma_d = \exp\left(-(\frac{\bar{\varepsilon}_m}{\varepsilon_o} - \alpha_{ct}) / (1-\alpha_{ct}) \right) - 1 \quad \text{for} \quad \frac{\sigma}{f_{ct}} > \alpha_{ct} \text{ and } \Delta\sigma > 0 \tag{11}$$

where $\bar{\varepsilon}_m$ = the average material strain during the time step in question

$\Delta\sigma$ = stress increment during the time step in question, Pa

The simplification of non-damage behaviour is here chosen for ***all*** other ***cases.*** When equation (11) is not valid $\gamma_d = 0$.

The stress-strain outlined in equation (8) - (11) is illustrated in Fig. 13.

The unrestrained movements in equation (4) - (6) are here expressed as stress-induced deformations [13] as

$$\Delta\varepsilon_T^o = \Delta\varepsilon_T^{free} \cdot (1 + \rho_T \cdot \frac{\sigma}{f_{ct}} \cdot sign(\Delta\varphi)) \tag{12}$$

$$\Delta\varepsilon_\varphi^o = \Delta\varepsilon_\varphi^{free} \cdot (1 + \rho_\varphi \cdot \frac{\sigma}{f_{ct}} \cdot sign(\Delta\varphi)) \tag{13}$$

where $\Delta\varepsilon_T^{free}$ = unrestrained and stress-free thermal strain due to thermal changes

$\Delta\varepsilon_\varphi^{free}$ = unrestrained and stress-free moisture strain due to humidity changes

ρ_T = adjustment factor for stress-induced thermal strain

ρ_φ = adjustment factor for stress-induced moisture strain

The change in relative humidity for simultaneous changes in evaporable water content can be expressed [10] by

$$\Delta\varphi = \bar{\mu}_T \cdot \Delta T + \frac{\partial\varphi}{\partial w_e} \cdot \Delta w_e \qquad (14)$$

where $\bar{\mu}_T$ = average hygrothermal coefficient during the time step in question.

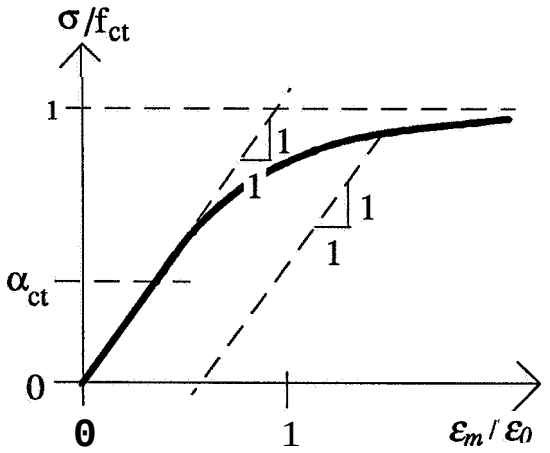

Fig. 13 Non-linear stress-strain behaviour at tension, see equation (8) - (11).

In general, equation (14) is aimed to be used to determine the term $sign(\Delta\varphi)$ in equations (12) and (13). For the calculations here, i.e. for young concrete with a considerable temperature change and a change in evaporable water content only due to self-desiccation, an assumption that temperature changes dominate equation (15) gives [11]

$$sign(\Delta\varphi) = sign(\Delta T) \qquad (15)$$

Note that equation (15) is certainly true for calculations here at the temperature cooling phase, as both AT and Δw_e are less than zero at this stage. Another simplification [11] is that stress-induced deformations according to equations (12) and (13) is not introduced until the concrete has reached an equivalent age of twelve hours. The reason for this is that at very early ages the micro-structure of the concrete is very weak, and the essential behaviour is probably caught by high creep values at this age [1].

The calculated compressive strength for each concrete mix is based on a piece by piece linear function in the logarithm of time. The tensile strength is then estimated in relation to the compressive strength as

$$f_{ct} = f_t^{ref} \cdot \left(\frac{f_{cc}}{f_c^{ref}} \right)^{\beta_1} \qquad (16)$$

where f_{ct} = tensile strength, Pa
f_{cc} = compressive strength, Pa
f_t^{ref} = reference tensile strength, Pa
f_c^{ref} = reference compressive strength, Pa
β_1 = exponent

In equation (16) f_c^{ref} can be chosen in advance (say f_c^{ref} = 10 MPa). Then f_t^{ref} is the tensile strength at that chosen reference compressive strength, and the parameter β_1 expresses the curvature of the relationship.

STRESS CALCULATIONS

The use of equations (4) - (6) with $\gamma_d = \rho_T = p, = 0$ are here called linear calculations. With γ_d according to equation (11), $\rho_T \neq 0$ and $p, \neq 0$ the calculations are here named *non-*linear. Note that to be able to use γ_d according to equation (11) in the non-linear calculations the parameters of equation (16) must be know to estimate the tensile strength.

Developed stresses have here been calculated with combined and separated (true) moisture and thermal coefficients. The results are compared with stress analyses performed in the relaxation tests, see Fig. 14. All calculations presented in these figures are non-linear with respect to the constitutive equations (4) - (6).

One general conclusion from the calculations is that to be able to follow the measured stresses within ± 0.5 MPa at every time non-linear stress calculations have to be realised. As mentioned earlier High Performance Concrete shows early tensile stresses before the temperature rise has started.

To be able to model these early tensile stresses the absolute level of the shrinkage is assumed to be linear from the time, $\tau_{\varepsilon 0}$ until the first shrinkage measurement have been recorded at the time, $t_{\varepsilon 0}$, see Fig. 15. The time for start of measured shrinkage varies in time for every concrete mixture, as the measurements are carried out manually. The starting time depends mainly on the early strength development of the concrete, which for instance is influenced by amount of admixtures (superplasticizers).

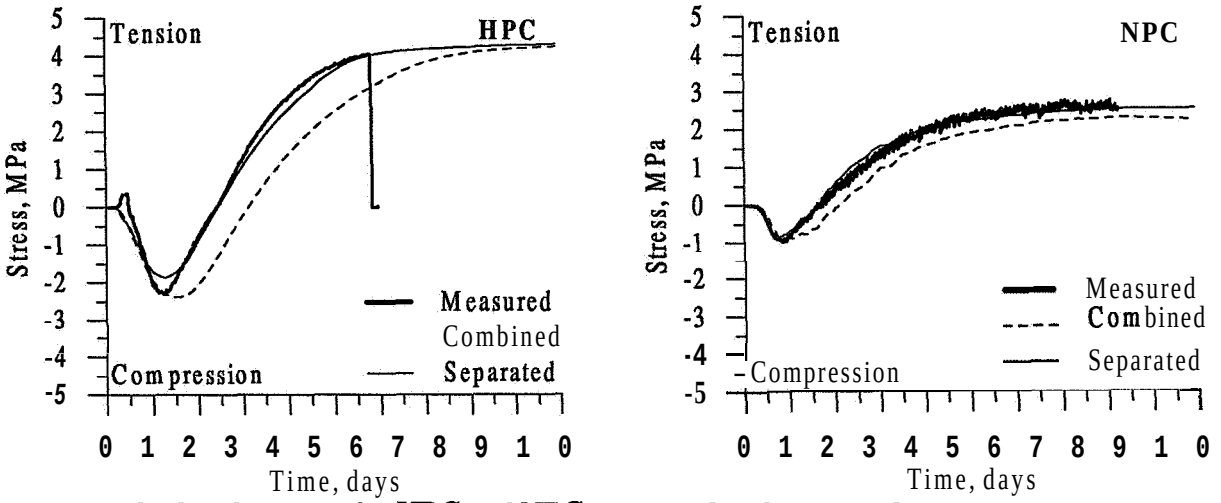

Fig. 14 Calculated stresses for HPC and NPC compared with test results.

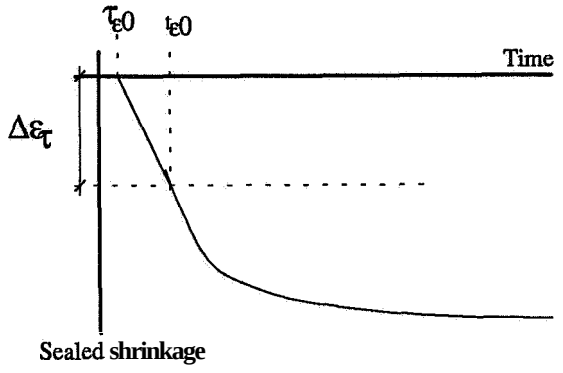

Fig. 15 Hypothetical picture of shrinkage behaviour at very early age.

For example, if concrete mixture HPC 3 is examined it can be seen that about 0.5 MPa tensile stresses are developed in the concrete specimen with start of the tensile stresses about four hours after casting. Using the hypotheses of linear shrinkage at start and measured stresses expressed by equation (3) the total shrinkage can be expressed as

$$\varepsilon_{SH} = \Delta\varepsilon_{\tau} + \varepsilon_{ref} \cdot \exp\left(-\left[\frac{\theta_{SH}}{t_{eq} - t_{\varepsilon 0}}\right]^{\eta_{SH}}\right) \qquad (17)$$

where $\Delta\varepsilon_{\tau}$ = additional shrinkage starting at very early age, μm/m

ε_{ref} = reference ultimate shrinkage, μm/m

θ_{SH} = empirical parameter representing the time when inclination of shrinkage changes in time, h

t_{eq} = equivalent time, h

$t_{\varepsilon 0}$ = start time of measurements, h

η_{SH} = empirical constant ruling the curvature, -

The very early additional shrinkage, $\Delta\varepsilon_{\tau}$, is here chosen to be 120 µm/m for HPC 3. Probably, if the measurements of sealed shrinkage would have started four hours after casting instead of eight to ten hours this early age shrinkage would have been reflected in the measurements.

If a new calculation of developed stresses is performed under assumed additional very early shrinkage the result would be as shown in Fig. 16. As can be seen in the figure, the very early age tensile stresses can be simulated, but the effect on the rest of the calculated stress development is negligible compared with Fig. 14.

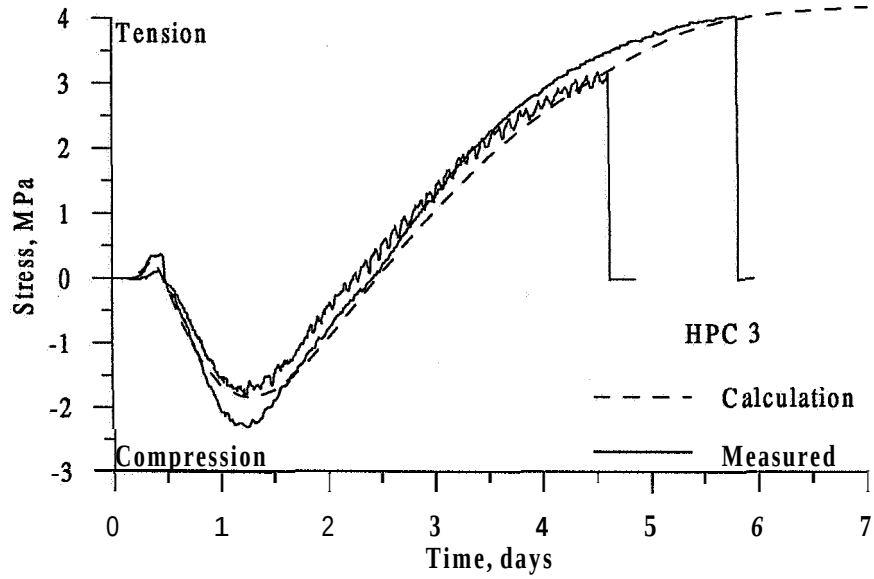

Fig. 16 Stress calculation taking early linear shrinkage into account.

Applying this way of separating the moisture and the thermal movements from each other and adopting non-linear behaviour when modelling stresses it is possible to analyse a different temperature development for the chosen structure, see Fig. 17. The result when using this method shows good agreement with test results, see Fig. 18.

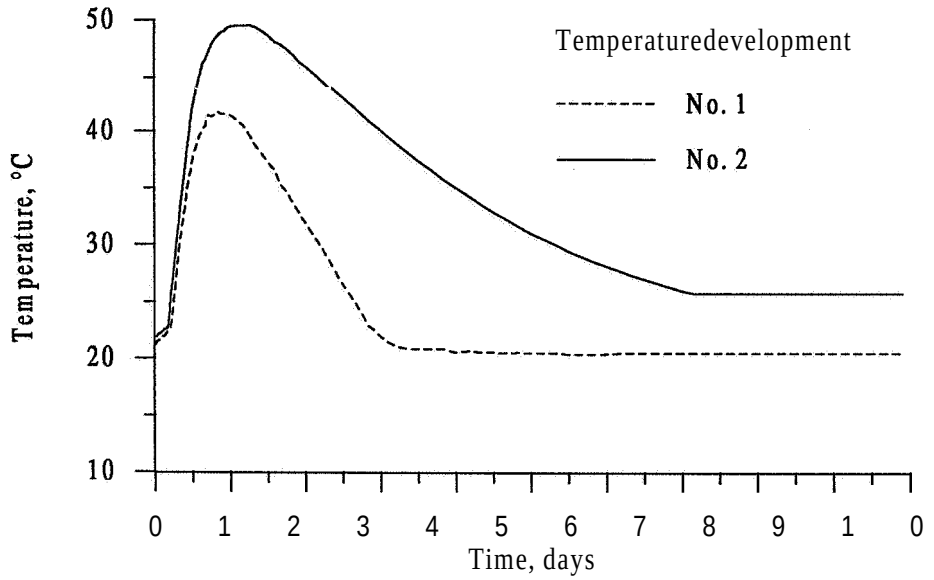

Fig. 17 Temperature development for winter (No.1) and summer (No.2) conditions for a HPC.

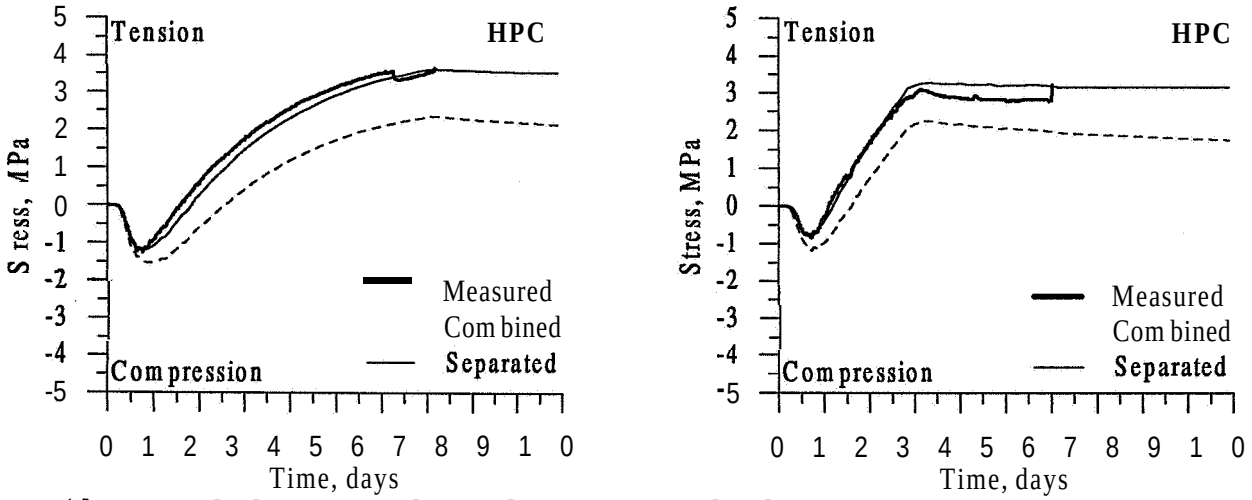

Fig. 18 Stress calculation according to the temperature development in Fig. 17.

CONCLUSIONS

Use of equation (4) based on short term measurements gives high level of accuracy for long term prediction of sealed shrinkage.

In order to get correct values of ultimate shrinkage, measurements have to start as soon as a structure has developed. An arbitrary start time of shrinkage measurements may indicate low values of ultimate shrinkage.

Very early tensile stresses have been measured in High Performance Concrete before temperature rise have started. This implies that measurements of shrinkage in High Performance Concrete should preferable start as early as four hours after casting.

It can be understood from the thermal expansion and contraction tests that shrinkage should be considered. If not, the evaluated thermal expansion and contraction coefficients will be representing both shrinkage and thermal movements. The combined coefficients may not be fit to use in other cases having another temperature development than tested.

The measured movements recorded in thermal deformation tests can be separated into true thermal movements and pure shrinkage by assuming maturity time ruling free shrinkage under sealed conditions. Then the principal of superposition may be applicable and a separation of the measured deformation can be performed.

Results, evaluating accordingly this, show stable values of the thermal expansion coefficient in the level of 10 - 12 μm/m°C and the evaluated thermal contraction coefficient indicates a level of 7 - 9 μm/m°C.

The stress development can be modelled with stress-induced deformations and non-linear behaviour. Even if the used material model is correct, the obtained result may give totally wrong information in a stress analysis if it is implemented with incorrect data of thermal and moisture behaviour of the concrete. Therefore, great care should be used in the determination of deformation behaviour.

REFERENCES

1) Westman, G., Thermal Cracking in High Performance Concrete - Viscoelastic models and laboratory tests, Division of Structural Engineering, Luleå University of Technology, Licentiate Thesis 1995:27L, (1995), 123 pp.

2) Westman, G. and Garcia, E. C., Maturity development and heat of hydration in high strength concrete, Division of Structural Engineering, Luleii University of Technology, Internal Report 93:12, (1993), 7 pp.

3) Hedlund, H., Materialparametrar for betong innehållande ultrafint cement, (Material parameters for concrete containing Ultrafine cement), Division of Structural Engineering, Luleå University of Technology, Internal Report 96:03, (1996), 26 pp.

4) Hedlund, H., Provning av betongrecept for Öresund Tunnel Contr., (Testing of concrete mixture for Öresund Tunnel Contr.), Division of Structural Engineering, Luleå University of Technology, Internal Report 96:04, (1996), 18 pp.

5) Jonasson, J-E. and Stelmarczyk, M., HETT5, (Program for computation of temperature and strength development., Tumba 1991, (1991), 135 pp.

6) Dilger, W. H., Wang, C. and Nitani, K, Experimental Study on Shrinkage and Creep of High Performance Concrete, 4th International Symposium on Utalization of High-strength/High-performance concrete, 29 - 31 May 1996, France, (1996), pp 311 - 319.

7) Hedlund H., Stresses in High Performance Concrete due to Temperature and Moisture Variations at Early Ages, Division of Structural Engineering, Luleå University of Technology, Licentiate Thesis 1996:38L, (1996), 238 p

8) Tazawa, E., Matsuoka, Y., Miyazawa, S. and Okamoto, S., Effect of Autogenous Shrinkage on Self Stress in Hardening Concrete, In Proceedings of the International Symposium on Avoidance of thermal cracking in concrete at early ages, (Edited by R. Springenschmid), International RILEM symposium on, 10 -12 October 1994, Munich, (1994), pp 221 - 228.

9) Lövqvist, B., Temperatureffekter i hårdnande betong, (Temperature effects in hardening concrete), Dissertation, Kungliga Vattenfallsstyrelsen, Tekniskt meddelande No. 22, Stockholm (1946), 1946,195 pp.

10)Ben Amor, C. and Clement, J.-L., Behaviour of HPC under Thermal and Moisture Loads, 4'' International Symposium on Utalization of High-strength / High-performance concrete, 29 - 31 May 1996, France, (1996), pp 433 - 438.

11)Jonasson, J-E., Modelling of Temperature, Moisture and Stresses in Young Concrete, Division of Structural Engineering, Luleå University of Technology, Doctoral Thesis 1994:156D, (1994), 225 pp.

12)Jonasson, J-E., ConStre - a computer package for calculations of stresses due to temperature and moisture variations, Division of Structural Engineering, Luleå University of Technology, (1996), (In progress).

13)Bazant, Z. P. and Chern, J., Concrete creep at variable humidity: constitutive law and mechanisms, Material and Structures, Vol. 18, (1985), pp 1 - 20.

MICROCRACKING IN HIGH PERFORMANCE CONCRETE - FROM MODEL TO THE EFFECT ON CONCRETE PROPERTIES

by Udo Wiens, Birgit Meng, Petra Schroeder and Peter Schiessl
Institute for Building Materials Research
Aachen University of Technology
Germany

ABSTRACT

The existence of microcracks in high performance, low w/b-concrete with silica fbme has been verified by several investigations. One of the most outstanding factors promoting the development of cracks in the microstructure of high performance silica fume-concrete is to be seen in context with the reaction characteristic of silica fbme at an early age. In order to describe the mechanisms of microcracking and their effect on durability properties of high performance concrete with silica fbme and fly ash investigations on hardened cement paste as well as concrete tests were performed with high silica fbme contents. The course of the silica fbme reaction, especially at early ages, was recorded by thermogravimetric analysis. It can be deduced from the investigations on the reaction mechanisms of silica fume at early ages that pozzolanic reactions occur with silica fbme at an early age. However, pozzolanic reactions are not the only reactions which take place: Water- rich gel phases develop very quickly within the first 12 hours, and these are accompanied by a high rate of evolution of hydration heat. These gel phases once again release a large proportion of their water relatively quickly (stage between 12 and 24 hours). This phase transition could serve as a plausible explanation for the early shrinkage and the frequent ultrafine microcracking systems which are to be found in concretes containing a high level of silica fume.

Autogenous shrinkage and water penetration experiments, as well as freeze-thaw tests with deicing salts have been carried out on concrete with Portland cement, to quantify the effect of microcracks on durability properties. With the means of thin sections from concrete specimens the crack pattern has been characterized as highly interconnected. It was found that the shrinkage under sealed conditions (autogenous shrinkage) is about 70 % of the total measured shrinkage under dry conditions. Water penetration depths of up to 20 mm within one day of water exposure were measured indicating the capillary activity of the interconnected microcracks and thus clarifying the relatively high weight losses due to freeze-thaw attack in combination with deicing salts.

Kewvords: Microcracking, Silica fbme reaction, Shrinkage, Autogenous shrinkage, Durability, Water penetration behaviour, Freeze-thaw resistance (with deicing salts)

INTRODUCTION

The positive influence of pozzolanic additions on the properties of concrete is well known from research and practice. The long term effects have been studied extensively while only a few investigations on processes at early ages (the first 3 days) exist. The known increase in early strength shows that the silica fume reaction starts at very early ages. On the other hand, effects like an increased early shrinkage (autogenous shrinkage) resulting in microcracking have been reported, when silica fume is added [1,2,3].

The investigations described in this paper were initially part of different research projects dealing with the reaction mechanisms of fly ash and silica fume in cementitious materials [4] and their influence on the alkalinity of the pore solution [5]. The phenomenon of microcracking observed in the course of these investigations were initially not the objective of these research works, but were more or less found coincidentally. The overall tests on the reaction mechansims of silica fume at early ages [4] combined with the investigations carried out with respect to the characterization of the durability properties of low w/b-concrete with silica fume [5] gave a conclusive figure of the formation and the effect of microcracks on durability properties.

MATERIALS AND MIXES

Materials

Table 1 compares some of the chemical and physical properties of the cements and the additions used in the test series. For the cement paste and concrete investigations, three Portland cements (CEM I 32.5 R) and one blast-furnace slag cement (CEM III/A 32.5 R) containing 46 wt.% of slag in compliance with the requirements of the German cement standard DIN 1164 were selected. The chemical composition of the fly ashes (FA1 and FA2) corresponds to a low-calcium class F fly ash in accordance with ASTM C 618. Both silica fumes (SF1: uncompacted powder; SF2: slurry with 50 wt.% solid content) are approved as concrete additions according to German test mark guidelines.

Table 1: Chemical Composition of Cements and Additions

Item	Unit	Cement (CEM)				Addition			
		I/1	I/2[1)]	I/3[1)]	III/A	FA1	FA2	SF1[2)]	SF2[3)]
Chemical Composition									
- SiO_2		19.7	19.2	20.4	25.9	47.1	52.0	91.1	94.8
- Al_2O_3		5.31	6.26	5.7	7.03	26.9	27.7	0.14	0.86
- Fe_2O_3		3.11	2.40	2.9	1.99	9.26	8.45	3.65	0.65
- CaO		63.9	63.6	64.0	53.6	4.26	2.58	1.09	0.37
- MgO	wt.%	1.04	1.31	1.8	3.77	2.28	1.85	1.02	0.68
- K_2O		0.71	0.89	1.3	0.74	3.31	3.64	0.60	-
- Na_2O		0.12	0.12	-	0.19	1.19	1.15	0.42	-
- Na_2O_{aquiv}		0.59	-	-	0.68	3.37	-	0.81	-
- SO_3		2.79	2.41	3.20	2.25	1.77	0.85	0.53	-
- C		0.42	-	-	-	0.80	-	1.25	-
- loss on ignition		2.06	2.71	2.30	1.89	1.93	-	1.96	-
- unsoluble residue		1.13	1.10	0.90	1.19	78.5	82.0	93.0	-
- CaO_{free}		-	0.46	-	-	0.65	0.10	-	

1) producers information

2) silica-fume: *dry*, uncompacted

3) silica-slurry: 50 wt.% solid content; chemical composition of the solid phase

Mixes and storage

The reaction behaviour of silica fume was investigated using hardened cement paste in combination with 2 different types of cement (CEM I/1 and CEM III/A, s. Table 1). All the tests were carried out on hardened cement paste specimens with a w/b value (b = total binder content = cement + silica fume = c + s) of 0.50. An extremely high dosage of silica fume in comparison with practical conditions was used (25 wt.% in relation to the total binder content), to enable clear identification of the influences on the reaction mechanisms in the hardened cement paste. After mixing, the cement pastes were poured into plastic bottles (50 ml) and sealed airtightly. To prevent segregation of the cement paste, the plastic bottles for all mixtures were rotated in the longitudinal axis for 24 h at a temperature of 20 "C. The sealed plastic bottles were then stored at a temperature of 20 "C until the date of testing.

Table 2 contains the mix composition of the concretes analysed. Since the results of these investigations originate from different research projects carried out at the Institute for Building Materials Research where overall 8 different binding components were used, it is usefull to summarize the composition of the binding materials of the 7 concrete mixes seperately (s. Table 3). Mixes 1 and 2 contain the highest level of silica fume and the lowest w/b at normal cement content. These mixes were used to study the influence of silica fume and fly ash on the alkalinity of concrete [5]. The w/b of mix 3 is somewhat higher at a lower level of silica fume and cement content.

Table 2: Composition of Concretes in the Test Series

Mix No.	Cem.	Water	Addition				w/b[1]	c/s/f	Admixture	
			Fly Ash	Silica-Fume SF	Fibre	Fibre			AEA[5]	SP[6]
	C	W	FA		PAN1[2]	PAN2[2]				
	kg/m³						-	%	kg/m³	
1	340	170	302	113[3]	-	-	0.23	45 / 40 / 15	-	13.6[7]
2	340	170	-	113[3]	-		0.34	75 / 25 / 0	-	12.9[7]
3	240	140	90	30[4]	-		0.39	67/8/25	-	7.1
4	240	140	90	30[4]	-	-	0.39	6718 / 25	1.32	5.9
5	240	144	90	30[4]	3.40	-	0.40	67 / 8 / 25	-	8.7
6	240	141	90	30[4]	-	1.20	0.39	67 / 8 / 25	-	8.6
7	300	180	-	-	-	-	0.60	-	-	-

1) w/b = w/(c+s+f) 2) polyacrylnitrile fibres 3) dry, uncompacted 4) silica fume slurry; solid content
5) AEA: air entrainment agent 6) SP = superplasticizer 7) high range water reducing agent

Table 3: Binder Composition of Concrete Mixes

Mix No.	Binder Composition
1	CEM I/1 + FA1 + SF1
2	CEM III/A + SF1
3	CEM I/2 + FA2 + SF2
4	CEM I/2 + FA2 + SF2
5	CEM I/2 + FA2 + SF2
6	CEM I/3 + FA2 + SF2
	CEM I/1

Mixes 4 to 6 have the same w/b and the same composition of the binding materials as mix 3, but are modified with two polyacrylnitrile fibres (PAN1: length l = 6 mm; O_w 104 pm; PAN2: length l = 4 mm; $O \approx 20\text{-}25$ pm) or air eintrainment agents to work out their influence on freeze-thaw resistance under action of deicing salts. Mix 7 acts as reference concrete with normal strength, (estimated strength class: C 20125 according to prEN 206-1996).

All concrete specimens with the exception of the specimens for the determination of the electrolytic resistances were stored as follows: 1 d in formwork, 6 d under water, subsequently under conditions 20 °C/65 % R.H. up to testing. For the determination of autogneous

shrinkage the concrete specimens were cast in the formwork up to 6 hours after mixing. The specimens for the measurement of time- and depth dependent electrolytic resistances were cured for 2 days in a vapour chamber and subsequently stored under conditions 20 °C/80 % R.H.

EXPERIMENTAL

Measurement of $Ca(OH)_2$ and bound water content on cement paste

The development of mineral phases in the hardened cement paste was investigated using thermogravimetric analysis (TG). At the time of testing, hydration of the cement was stopped by placing the cement in methanol. The specimen was subsequently dried at 105 °C and pulverized, prior to undergoing TG-examination. The analysis programme covered a temperature range from 30 to 894 "C. Fig. 1 shows the absolute weight losses (TG) and the appurtenant differential representation (DTG) over the entire temperature range, by reference to one representative cement paste specimen. The change in weight (TG) here represents a specific change in relation to the originally determined weight of the specimen concerned.

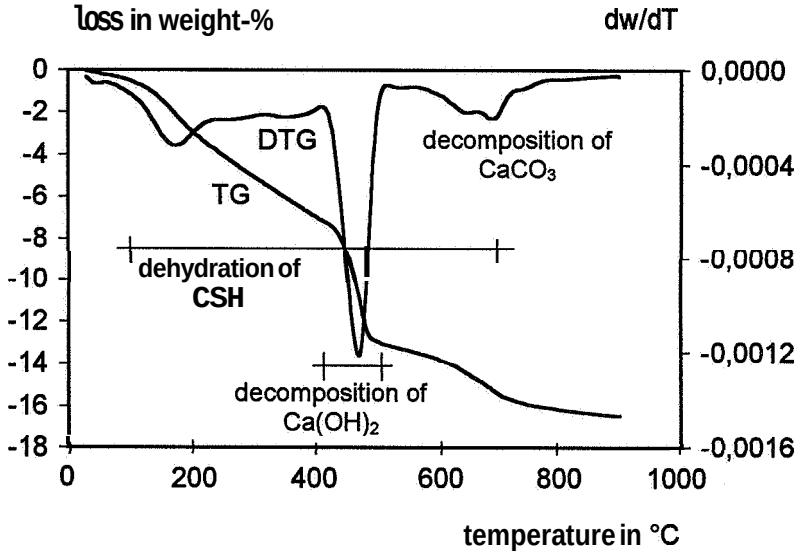

FIG.-1 TG-Analysis of hardened cement paste (100 % CEM I, age: 28 days)

The hardened cement paste consists primarily of compounds containing hydration water, together with a small fraction of inorganic compounds containing carbonates. The most important compounds, the calcium silicate hydrates and calcium aluminate hydrates, occur in cement paste in a large number of composition variants, the decomposition reactions of which overlap. The decomposition reactions can be explained by reference to Fig. 1.

In the temperature range from around 100 to 750 °C, the CSH phases dehydrate relatively continuously. Between approximately 400 and 500 "C, the water is removed from the $Ca(OH)_2$. $CaCO_3$ decomposes at a temperature of around 700 "C (separation of the CO_2). The decomposition peak of the $Ca(OH)_2$ appears relatively sharp in comparison to the continuous decomposition of the CSH phases. According to Marsh [6], the $Ca(OH)_2$ content can be calculated from the TG curve by taking due account of the CSH phases before and after the $Ca(OH)_2$ peak and, indirectly (via interpolation), during the $Ca(OH)_2$ peak. As $Ca(OH)_2$ is consumed and CSH phases are formed in the course of the pozzolanic reaction, conclusions on

the course of the pozzolanic reaction can be drawn from the results of the thermogravimetric investigation. The consumption of $Ca(OH)_2$ can be determined directly in comparison with a reference mixture. The formation of CSH phases can be determined only indirectly, via the bound water. By subtracting the water content of the $Ca(OH)_2$ from the directly measured total bound water (weight loss in the temperature range from 30 to 600 °C), the fraction of CSH phases can be deduced from the residual water, subject to several approximate assumptions. By way of approximation, the residual water is regarded as CSH water (i.e. water bound in the CSH phases), although it also contains the water bound in calcium aluminate hydrates and sulphate phases. The time-dependent development of the so-called CSH water fractions can only provide direct information on the development of the CSH phase fractions when the stoichiometry of the CSH phases remains constant.

Thin sections

Thin sections were made up from all mixes except of mix 7. In preparation for microscopy slices of the size of 100 mm · 70 mm (size of the thin section) and a thickness of 10 mm were cut. The specimens were dried as protectively as possible, taking special care to ensure that no additional changes of microstructure take place during that process. The material was then impregnated with an especially low viscosity resin. A soluble fluorescent agent was added to the resin to provide contrasting of the pore spaces and microcracks in addition to the essential fixing of the structure. Thin sections then were made up. They were subjected to microscopy, to estimate the size, the geometry and the local distribution of microcracks.

Mechanical Properties

Various strength and deformation parameters were determined in order to characterize the mechanical properties of the concrete. Cube compressive strength (150-mm cube) was tested after 2, 7, 28, 90, 180 and 360 days. The splitting tensile strength was determined using beams measuring 100 × 100 × 500 mm. The compressive and the splitting tensile strength were determined according to German standard DIN 1048 at an age of 28 days.

The direct tensile strength was determined at an age of 28 days on cylinders with a diameter of d = 150 mm and a height of h = 300 mm (load-controlled: 0.05 MPa/s). The flexural strength was determined only for the mixes 4 and 5 at an age of 28 days on beams measuring 100 × 100 × 500 mm^3 according to German standard DIN 1048 (28 days). Table 4 gives an overview of the properties of the fresh and hardened concretes.

Table 4: Fresh Concrete and Mechanical Properties of the Different Mixes

Mix No.	Fresh Concrete		$f_{c,cu}$ [1]						f_t [2]	$f_{t,sp}$ [3]	$f_{t,fl}$ [4]
	Density	Air-Void Content	2d	7d	28d	90d	180d	360d	28d	28d	28d
	kg/m³	vol.%	MPa								
1	2300	2.6	n.d.	69.2	92.7	109.0	116.5	116.8	n.d.	n.d.	n.d.
2	2370	1.9	n.d.	70.3	90.0	107.8	112.3	118.6	n.d.	n.d.	n.d.
3	2350	2.6	30.2	49.1	76.2	86.1	n.d.	87.0	2.9	4.8	n.d.
4	2290	4.7	n.d.	n.d.	58.4	n.d.	n.d.	n.d.	2.9	4.1	4.1
5	2330	3.0	n.d.	n.d.	67.1	n.d.	n.d.	n.d.	3.2	5.9	4.8
6	2360	3.0	n.d.	n.d.	n.d.	n.d.	n.d.	n.d.	n.d.	n.d.	n.d.
7	2340	1.7	n.d.	n.d.	n.d.	n.d.	n.d.	n.d.	n.d.	n.d.	n.d.

n.d. not determined

1) compressive strength, cubes 150 mm

2) direct tensile strength, cylinders 150 mm/300 mm

3) splitting tensile strength, beams 100 mm/100 mm/500 mm

5) flexural strength, beams 100 mm/100 mm/500 mm

It is evident that mixes 1, 2 and 3 containing silica fume are designated as high-strength concretes according to the RILEM/CEB/FIP classification. The addition of AEA and fibres increases the air void content of the concretes resulting in lower compressive strength values at 28 days.

Drying shrinkage

Concrete cylinders with the dimensions h = 300 mm and O = 100 mm were used as test specimens. The first measurement was taken immediately after 7 days of water immersion. The length changes were registered with 3 measuring gauges (accuracy: 111000 mm) fixed at an angle of 120 ° on the concrete surface. The shrinkage values were determined up to ≈ 170 days after the end of the dry storage.

Autogenous Shrinkage

For the autogenous shrinkage measurements cylinders with the dimensions h = 300 mm and O = 100 mm were used as test specimens. After a hydration time of *6* hours, the formwork was stripped. The measuring gauges were then installed. Subsequently, the specimens were wrapped up in aluminium foil (3 layers) to prevent the drying out of the concrete. The length changes were registered with 3 measuring gauges (accuracy: 111000 mm) which were fixed at an angle of 120 on the concrete surface. The shrinkage values were measured up to ≈ 180 days after the wrapping of the specimens.

Electrolytic resistance

A time- and depth dependent measurement of electrolytic resistances provides information about the moisture content or the permeability of the concrete surface. E.g., a decreasing water content increases the electrolytic resistance of concrete. Fig. 2 shows a possible realisation of a depth-dependent resistance measurement developed at our institute. The multi-ring-electrode

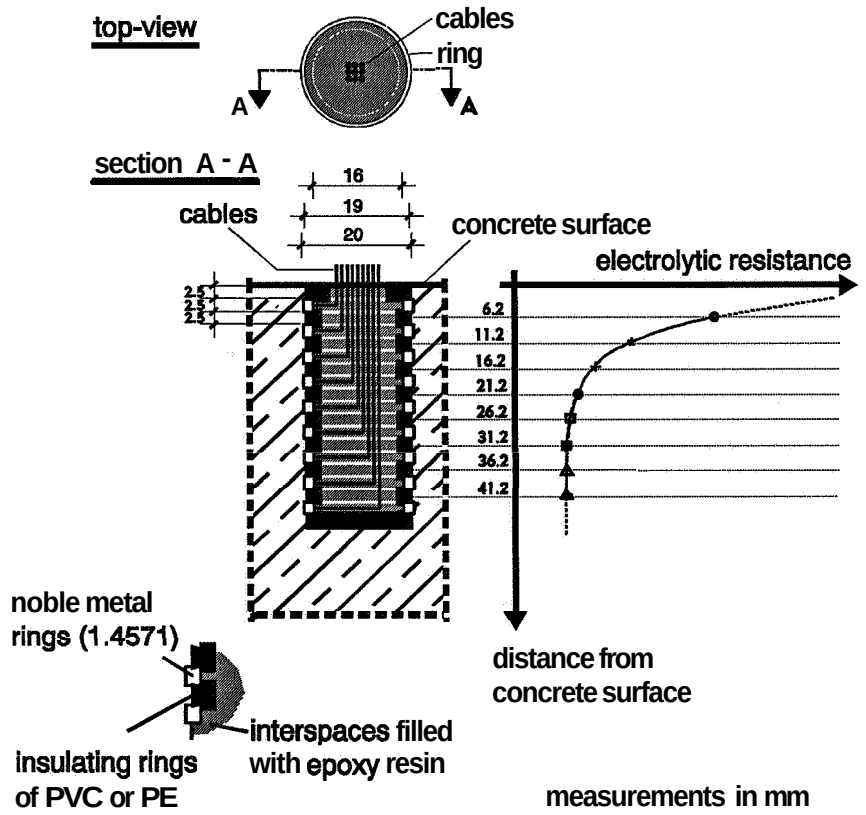

FIG.-2 Schematic representation of the multi-ring-electrode and a qualitative diagram of measured values [7]

consists of a series of alternate noble metal and insulating rings, arranged above one another. The design is modular, allowing the user to vary the number of rings according to his/her requirements. The geometrically optimized version of the sensor has a diameter of 20 mm and normally consists of nine noble metal rings, providing eight measuring points. The thickness of each ring is 2.5 mm and they are 2.5 mm apart, yielding a profile 50 mm in depth with values every five mm. The rings are connected to cables arranged inside the electrode in such a way that they do not influence the surrounding concrete (measuring area). The remaining interspaces of the electrode are filled with epoxy resin. The arrangement of the multi-ring-electrode is shown in Fig. 2.

The electrolytic resistance between neighbouring noble metal rings can be measured externally using a suitable AC ohmmeter. A profile is then inferred from the data. Fig. 2 indicates the qualitative results, e.g. an increase in resistance values due to drying processes in the concrete surface.

In principle, electrolytic resistance can be determined by AC or by DC current measurements. In this case, AC measurements are used to determine electrolytic resistance, since this virtually eliminates the effect of test electrode polarisation which could occur with DC current. The movable ions between the working electrodes are made to oscillate, preventing chemical reactions or polarisation on the working electrode (noble metal ring) surface. A hand-device designed specially for measurements with the multi-ring-electrode has been developed at the ibac. An alternative is to use a computer-controlled data logging and analysis systems [7].

Freeze-thaw resistance under action of deicing salts

Concrete cubes with a length of 100 mm were used as test specimens to determine the freeze-thaw resistance under action of deicing salts. At an age of 27 days 2 cubes were put in one container which was filled with 3% sodium-chloride solution. The quantity of solution absorption was determined after 24 hours of wetting. After that the cubes were alternatingly frozen and thawed in 3% sodium-chloride solution. The temperature in the freezer was regulated so that (0 ± 2) °C in the cubes' centre was reached after 2 hours, starting from 20 °C. After keeping the temperature at (0 ± 2) °C for another 2 hours, the specimens were cooled down to (-15 ± 2) °C within the following 12 hours. Immediately after the total cooling interval of 16 hours the storing of the containers was continued at $(+20 \pm 2)$ °C for 8 hours (1 cycle = 24 hours). The weight loss of the cubes was registered after 10, 25, 50, 75 and 100 freeze-thaw cycles.

RESULTS AND DISCUSSION

Reaction of silica fume at early ages

The development of mineral phases was investigated by TG-studies on hardened cement paste at early ages. Figs. 3 and 4 compare the $Ca(OH)_2$ and CSH water contents of mixes with and without silica fbme at ages of 12, 24 and 48 hours. It can be seen for both the CEM I and CEM III/A mixes that the $Ca(OH)_2$ contents of the specimens containing silica fbme are significantly lower than those of the reference mixes without silica fbme at all the investigated times. The reverse applies with regard to the so-called "CSH water" content. Conclusions regarding the pozzolanic reaction can be drawn from the consumption of $Ca(OH)_2$ and the bound CSH water. It can be noticed that the mixes with silica fbme contain only very minimal quantities of $Ca(OH)_2$ after 12 hours, while the reference mixes without silica fbme already reveal a high level of $Ca(OH)_2$ content. It would appear justified to assume that the quantity of $Ca(OH)_2$ corresponding to the difference involved here has already been consumed as a result of a very early reaction of the silica fume.

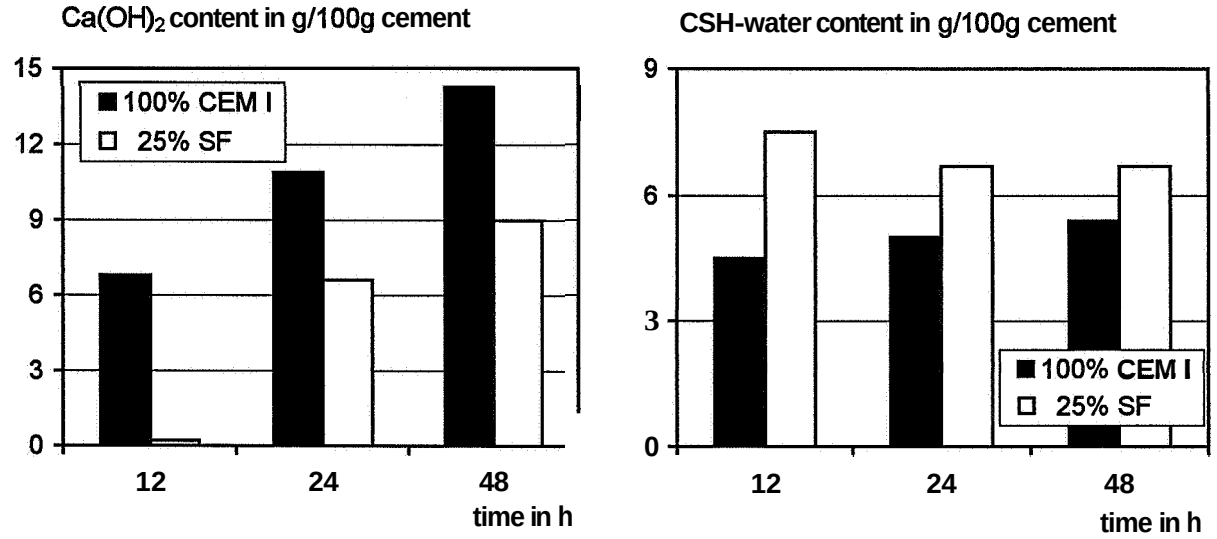

FIG.-3 Influence of silica fume on $Ca(OH)_2$ and CSH-water contents for mixes with CEM I

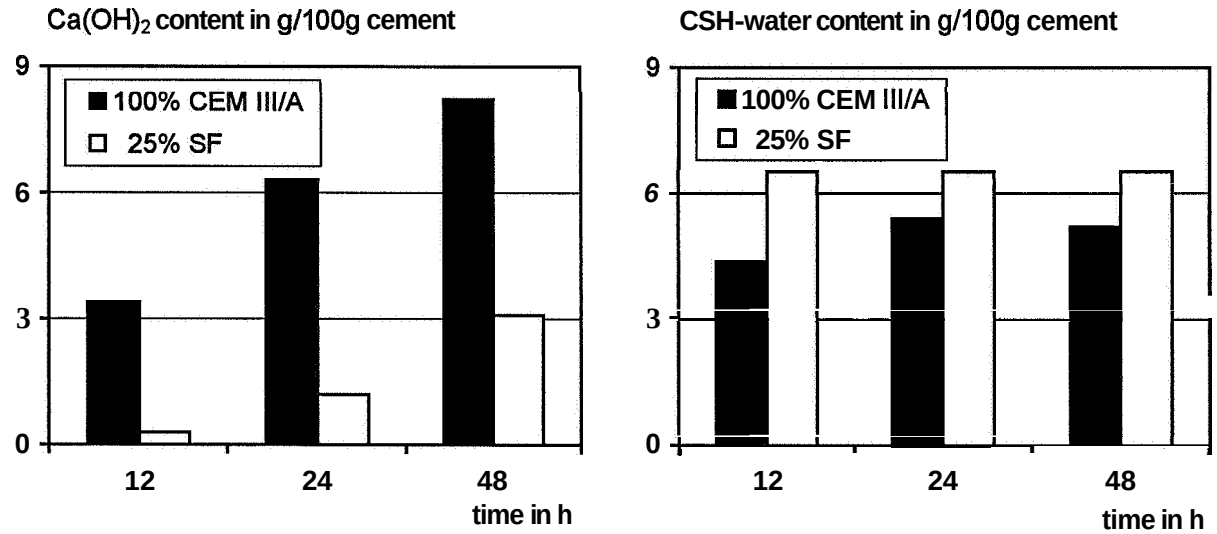

FIG.-4 Influence of silica fume on $Ca(OH)_2$ and CSH-water contents for CEM III/A mixes

Fig. 5 shows the differences in the $Ca(OH)_2$ content and in the CSH water content between the specimens with and without silica fume. If the difference between the $Ca(OH)_2$ content of the mixes containing silica fume and the mixes without silica fume is interpreted as the $Ca(OH)_2$ consumed by a pozzolanic reaction, in the case of the Portland cement this results in the paradox that the "$Ca(OH)_2$ consumption" is higher after 12 hours than after 24 hours. This can only be the case if the consumption of $Ca(OH)_2$ in the period between 12 and 24 hours is overcompensated by the new formation of $Ca(OH)_2$ (possibly accelerated cement hydration by the effect of silica fume as a nucleation substrate).

The course of development of the differences between the CSH contents of the mixes with and without silica fume, which is also presented in Fig. 5, supports the theory that a pozzolanic reaction already takes place at this stage. In all cases, the CSH water content of the mixes containing silica fume is greater than that of the mixes without silica fume.

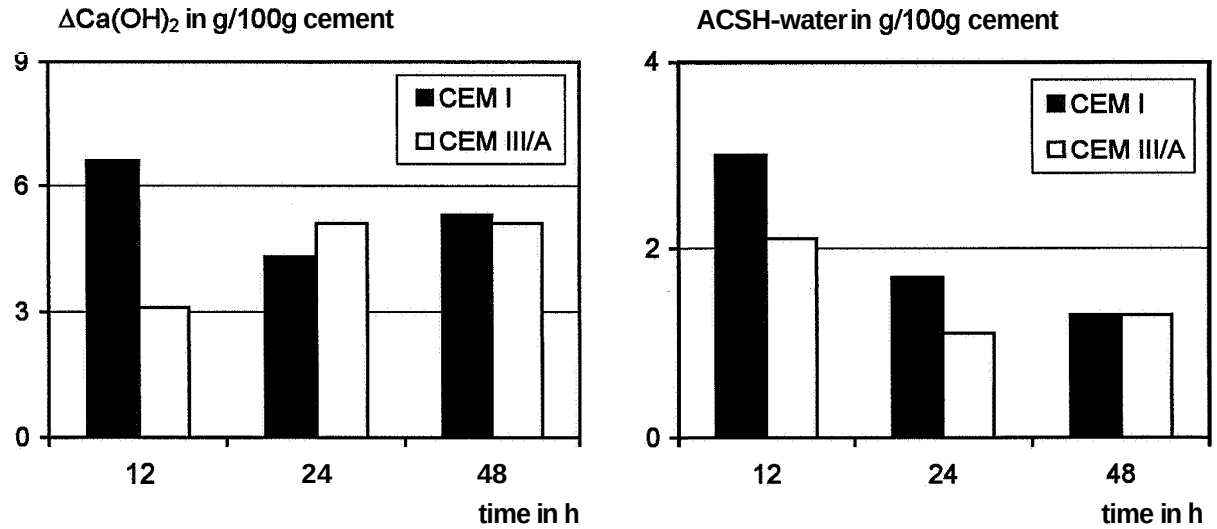

FIG.-5 Influence of silica fume on $Ca(OH)_2$ and CSH-water contents (differences between the mixes with and without silica fume)

The blends containing silica fume reveal a higher surplus CSH water content after 12 hours than after 24 hours. This can only mean that primarily water-rich hydrate phases are formed, which release part of their water content again within several hours. Such dehydration is to be found with water-rich silica gels. It is possible that this dehydration may also take place with water-rich CSH gels. Since this dehydration may be accompanied by volume changes in the already hardened cement paste structure, tensile stresses exceeding the tensile strength are implied resulting in the development of finely divided microcracks.

Specific examinations of the reaction products of silica fume in the early phase showed that CSH phases do not develop directly even when sufficient $Ca(OH)_2$ is available. Instead, a gel with high water content and low lime content is first of all formed [8]. This gel formation begins in the very first minutes after mixing. In turn, the gel then reacts to form CSH phases. This reaction takes place predominantly with $Ca(OH)_2$, but it may also occur with CSH phases containing higher levels of lime from the cement hydration process [9].

At the age of 24 and 48 hours the results can be interpreted more clearly, after initially formed water-rich gel phases have released part of their water. A substantial quantity of $Ca(OH)_2$, of approximately the same magnitude in both cases, had already been consumed in both types of cement. This is accompanied by a higher CSH water content in the mixes containing silica fume, which supports the assumption that pozzolanic reactions are already taking place here.

Influence of microcracks on concrete properties

Structure of the microcracks

When comparing the thin sections of the concretes made up from ordinary Portland cement (mix 1) and blast furnace slag cement (mix 2) in combination with the same amount of silica fume systematic differences become evident. Both mixes 1 and 2 principally show the same kind of microcrack formation. The cracks typically form an interlaced net, running along the transition zone at the aggregate surface and from one aggregate grain to another, often meeting in the middle between two grains. An obvious distinction of the two mixes manifesting by visual investigation through a microscope concerns the „meshsize“ of the microcrack net and the width of the cracks. In the CEM I concrete (mix 1) the meshsize is larger and the

cracks are smaller compared to the CEM III/A concrete. Therefore, it is to be expected, that the CEM III/A concrete (mix 2) should be more sensitive to the intrusion of fluid media by capillary suction. One reason for the unfavourable development of the microcrack system in the CEM III/A concrete may be its high silica fume content of 25 wt.% relative to the total binder content (cement + fly ash + silica fume). It seems plausible that the CEM I concrete develops a less severe microcrack system due to its smaller silica fume content (15 wt.% relative to the total binder content).

Further concrete specimens with CEM I containing less silica fume (8 wt.% related to the total binder content, mixes 3, 4, 5 and 6) were investigated. As expected the extension of the microcrack system was less severe than in the mixes rich in silica fume. At first, the investigation of the thin section of mix 3 showed, that the local distribution of the microcracks was rather inhomogeneous. For evaluation, the thin section was divided in square fields of the size of 5 mm. The evaluation was carried out scanning field by field, counting the number of microcracks visible in each field at a fixed magnification (50x). The result is shown in Fig. 6, where fields which contain nothing other than a big aggregate and therefore could not be evaluated are visualized as blank squares. Fields containing several microcracks usually represent an area with an interconnected mesh of microcracks. As demonstrated in Fig. 6, the microcracks accumulate in certain areas, while other areas are virtually free of cracks. Furthermore, Fig. 6 shows that there is no tendency of the microcracks to accumulate in the outer zone close to the concrete surface. This again supports the assumption that the development of the crack system is not introduced by the drying process but is definetely effected by autogenous shrinkage.

Such zones with accumulated and well interconnected microcrack systems will inevitably affect durability properties of the concrete, because they promote capillary suction. Theoretically different measures might be suitable to reduce this negative influence.

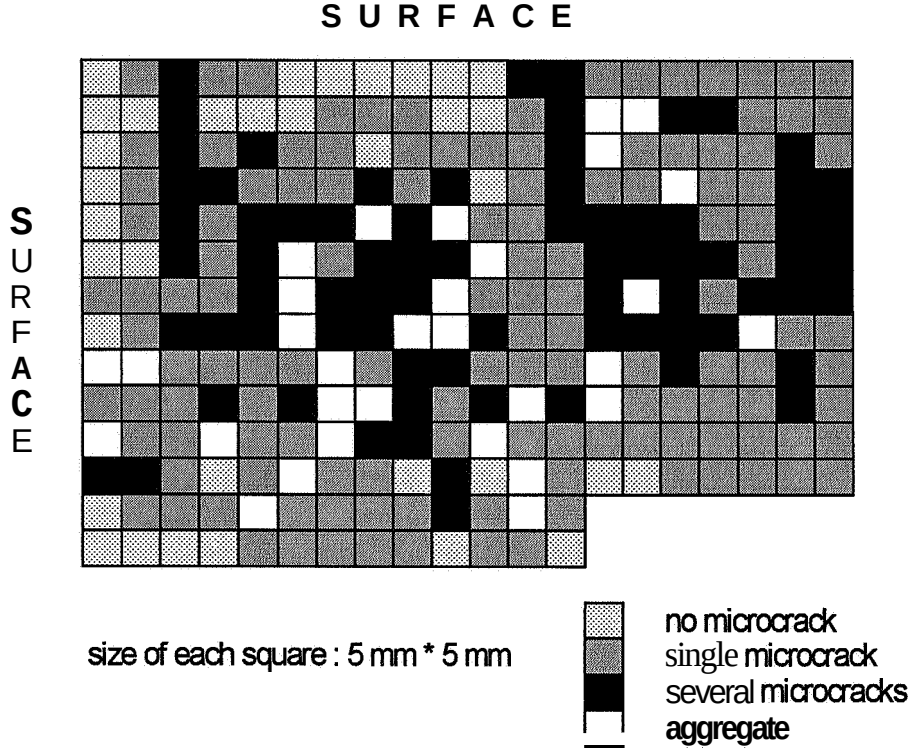

FIG.-6 Local distribution of microcracks investigated by fluorescent microscopy of a thin section of concrete mix 3

As the internal shrinkage itself seems to be immanent the only way to minimize harm is to make sure that the microcracks develop as harmlessly as possible. A favourable alteration would be achieved with shorter, finer and more homogeneously distributed cracks. Alterations in such a manner would diminish the detrimental increase of permeability. Different measures, taking this aim into account, were applied. The effect of two diierent fibre (variable: fibre size) additions and of an air entrainment agent was tested.

All three measures result in a more favourable geometry of the microcrack system. Both the fibres (independent of their size) and the air voids force the material to develop smaller and very homogeneously distributed cracks.

Shrinkage

The occurrence of high shrinkage strains at early ages (between 6 and 24 h) was reported by Wiegrink et al. [10]. When demoulding high strength concrete specimens (w/b = 0,29 - 0,40) with and without silica fume after 24 hours and continously drying the specimens at 20 °C/50% R.H. no difference in shrinkage values between the mixes was observed. Demoulding the same concretes after 6 hours an increase in strains was measured with increasing silica fume content. The shrinkage values at 90 days were more than 30 % higher for the mix with 15 % silica fume than for the corresponding reference mix without silica fume. The results from shrinkage measurements under sealed conditions (autogenous shrinkage) for the high strength concrete (mix No. 3) in Fig. 7 (left) supports the findings from Wiegrink that volume changes without evaporation processes especially at early ages must play an extraordinary role.

For the high strength concrete (mix. No. 3), an autogenous shrinkage value of 0,03 mm/m between 6 (demoulding) and 17 hours was measured corresponding to 12 % of the strain at an age of 120 days, whereas a tendency toward swelling at this time for a normal strength concrete (mix 7) without silica fume was found (Fig. 7, left). The cause of these volume changes may be related to the phase transitions described above. As is apparent from Fig. 7 (right), the proportion of autogenous shrinkage in relation to the total free shrinkage (drying + autogenous shrinkage) measured on specimens cured at 20 °C/65 % R.H. after 7 days of water storage varies between 35 % at 20 days and 70 % at 160 days after mixing. Thus, it is supposed that further phase transition reactions may occur even at later ages explaining the relatively high total shrinkage values for the high strength concrete (mix 3) to be found in the range of commonly used normal strength concrete.

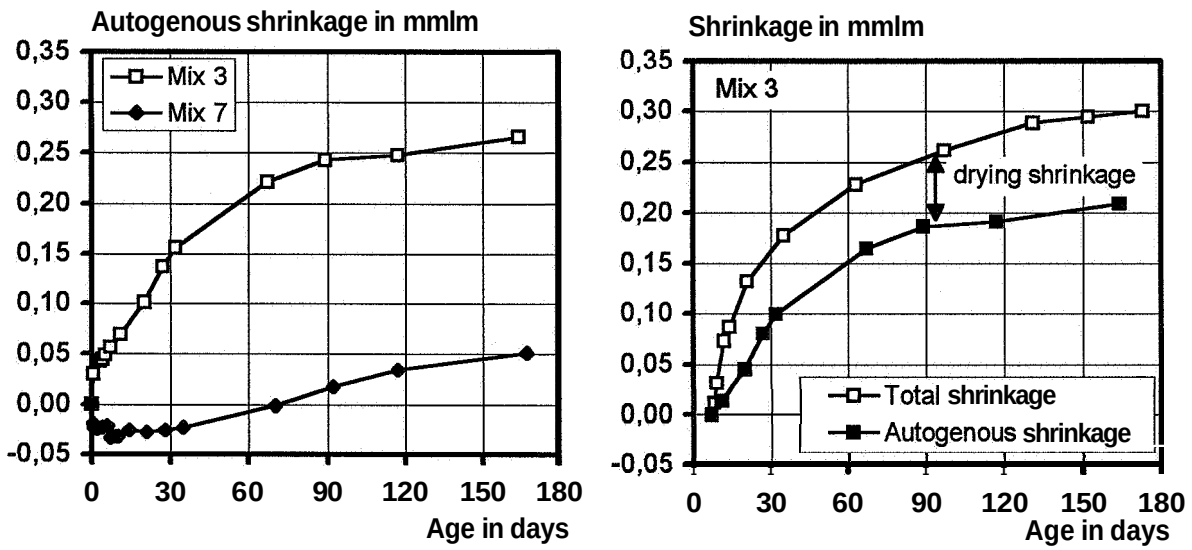

FIG.-7 Autogenous (left and right) and total (right) shrinkage of mix 3 (CEM I 32.5 R; w/(c+s+f) = 0.38; c/s/f = 67/8/25 %) and mix 7 (CEM I 32.5 R, w/c = 0.60)

Water penetration via electrolytic resistances

The degree of water saturation in the concrete cover as well as the water absorption behaviour of concrete is decisive with respect e.g. to the resistance against frost attack. By the means of measuring the depth- and time-dependence of electrolytic resistance it becomes possible to qualitatively describe the densification of the pore structure due to hydration products from the cement hydration and the pozzolanic reaction of silica fume and fly ash as well as changes of the water content in the concrete cover due to drying or wetting processes. Resistances will increase with increasing drying of concrete as well as due to the cement hydration or pozzolanic reaction of silica fume and fly ash,. The opposite is the case when concrete is exposed to water. Fig. 8 (a-c) shows the time- and depth-dependent development of electrolytic resistances for the mixes 7, 1 and 2. The concrete specimens were kept at 20 °C/80 % R.H. up to an age of 100 days. In the following 120 days, water at 20 °C was applied to the concrete surfaces, followed by a further drying period at 20 °C/80 % R.H. Starting from the normal strength concrete (mix 7) with w/c = 0.60 (Fig. 8a, left), it is apparent that a strong depth dependence of resistances due to drying processes exists, whereas for both high strength concretes (mixes 1 and 2) solely slightly increasing resistance values with decreasing concrete depth could be observed within the first 100 days of drying at 20 °C/80 % R.H. (Figs. 8b and 8c). Thus, in the case of the mixes 1 and 2, the drying velocity is very slow due to the low free water content and the reduced permeability (dense pore structure $\Rightarrow$ very high absolute resistance values). Nevertheless, the interconnected microcrack system in the pore structure of these concretes may act as a transportation path for the evaporation of free water molecules allowing a minor differentiation of resistances.

The right hand plots in Fig. 8 show the relative resistance values for the water exposure period between 100 and 220 days. The last resistant value of the drying period R_d was taken as the reference value. After different times of water-application (1, 3, 12, 34 and 42 days) the depth-dependent resistance values ($R_{w(t)}$) were taken from the resistance measurement and related to R_d. Hence, the penetration front of water into the concretes can be localized as well as structural changes in the concrete cover, e.g. due to ongoing of cement hydration.

After a hydration time of 100 days the water application of the concretes started. Consequently, a pronounced drop of the resistances occurs (Fig. 8a-c, left). The penetration behaviour of water into the concrete can clearly be extracted from the depth-dependent relative resistance values (Fig. 8, right). For the mix 7, the water-penetration front achieved a depth of 20-25 mm after 12 days of water-application. With increasing exposure time, the relative resistances fall to values between 30 and 40 % between 20 and 40 mm, indicating a relatively high degree of water saturation within this concrete layer. The penetration behaviour for the high strength concretes (mixes 1 and 2) shows some interesting effects. Due to the fine network of microcracks, high capillary forces are induced resulting in penetration depths of 20 mm after 1 day of wetting for both mixes. Despite of the rapid penetration velocity the resistance values for the high strength concretes remain at a higher level in the deeper concrete layers as compared to the normal strength concrete (mix 7). The penetration front stops at a depth of 20 mm for mix 1 and at 30 mm for mix 2, respectively, whereas penetration depths beyond the measuring range (41 mm) for the normal strength concrete (mix 7) are observable.

The resistance values for the high strength concrete with CEM I (mix 1) were shifting towards higher values in all depths with increasing time. This is a clear indication of the sealing of the microcracks due to the restart of the cement hydration and the pozzolanic reaction of the silica fume or fly ash under the action of water.

Since the crack widths in this concrete are smaller compared to the CEM III/A concrete (see evaluation of thin sections) and the reaction velocity of the additions is usually faster in CEM I mixes, a rapid refilling of microcracks with reaction products may be the case for the CEM I concrete. Thus, only a less pronounced resistance shift in the CEM III/A concrete is observable from 12 to 34 days.

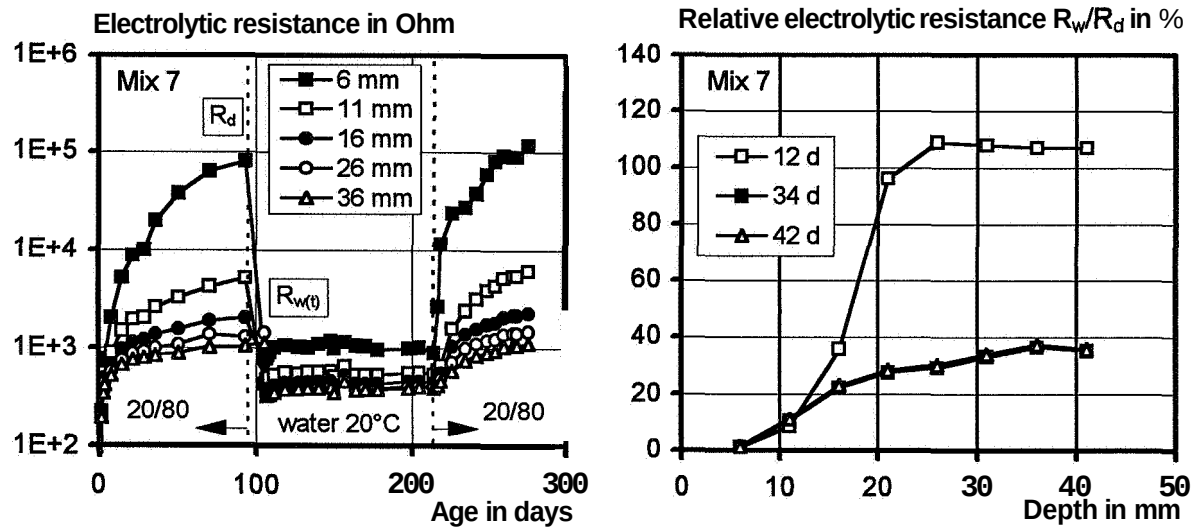

FIG.-8a Time- and depth-dependent electrolytic resistances for mix 7; CEM I; w/c = 0.60

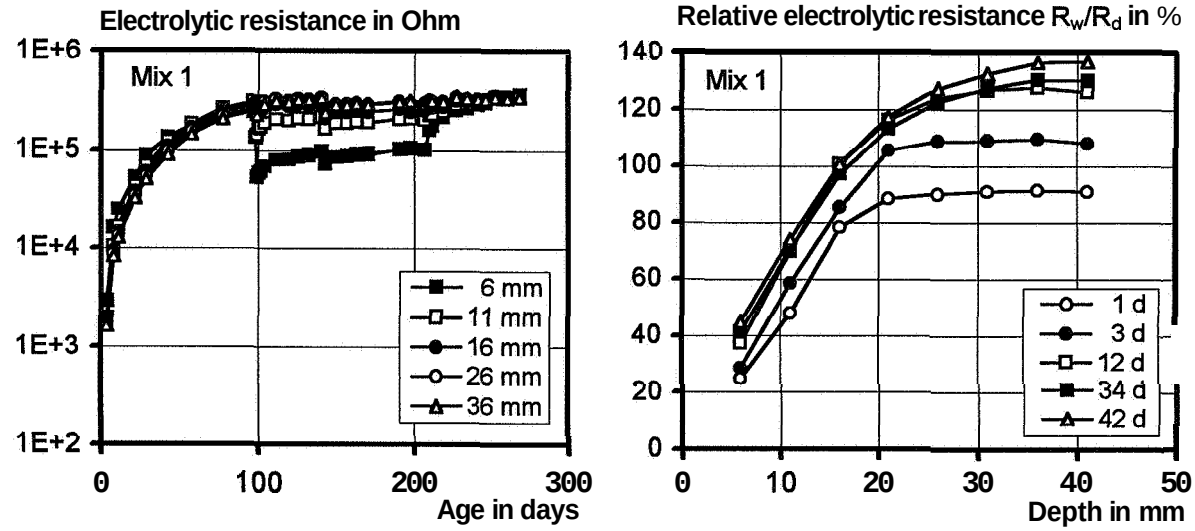

FIG.-8b Time- and depth-dependent development of electrolytic resistances for mix 1; CEM I 32.5 R; w/(c+s+f) = 0.23; c/s/f = 45/15/40 %

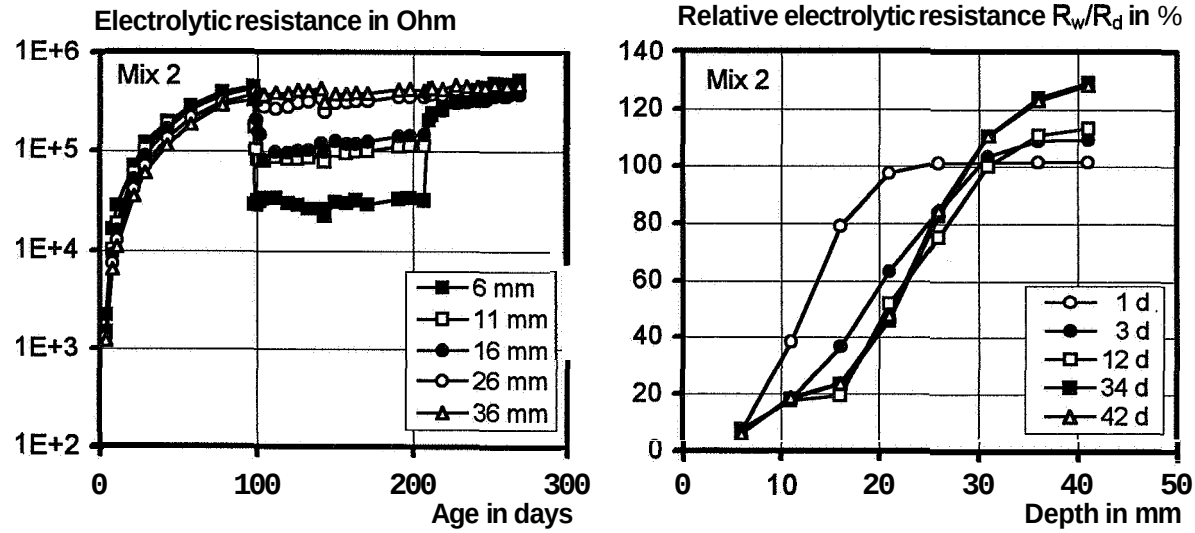

FIG.-8c Time- and depth-dependent development of electrolytic resistances for mix 2; CEM III/A 32.5 R; w/(c+s) = 0.34; c/s= 75/25 %

Freeze-thaw resistance under action of deieing salts

One of the most detrimental effects on concrete is caused by frost attack under action of deicing salts. Fig. 9 plots the scaling of mix 3after up to 100 freeze-thaw cycles. Without addition of fibres or air eintrainment agent relatively large weight losses due to the frost attack are measured for this concrete. Generally, a scaling of about 5 wt.% at 100 freeze-thaw cycles for the cube-test is recommended for concretes with high freeze-thaw resistance under action of deicing salts [11].

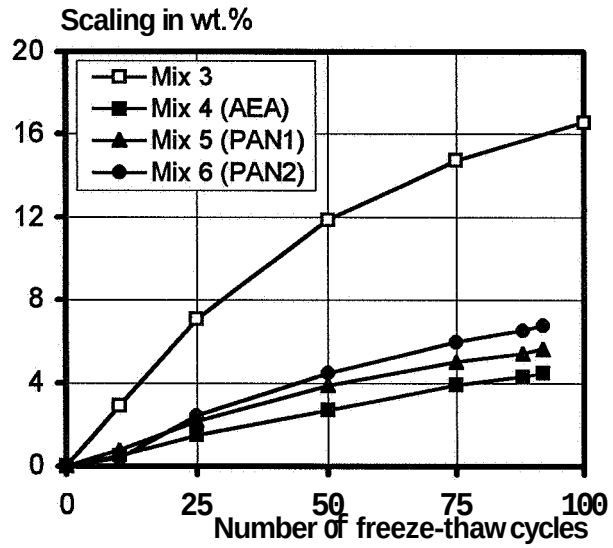

FIG.-9 Freeze-thaw resistance of mixes 3, 4, 5, 6 under action of deicing salts; CEM132.5 R, w/(c+s+f) = 0,38; c/s/f = 67/8/25 %

These concretes usually contain air entrainment agents. From the test results of water penetration behaviour (s. Fig. 8), it is evident that high strength conctretes with microcracks are supposed to be more sensitive to frost attack than normal strength concretes. However, the filling of microcracks with water occurs within one day or less due to the high capillary forces. In the areas adjacent to the microcracks no availible pore space compensating the expansion pressure exists due to the high gel-porosity (water-filled pores) in low w/b-concretes with silica fume. A tendency of microcrack sealing due to the pozzoloanic reaction of silica fume or fly ash can be deduced from the disproportionaly increment of scaling with increasing number of freeze-thaw cycles for mix 3 without modification.

By adding fibres (PAN1, PAN2, s. Table 2) or air entrainment agents (AEA, s. Table 2) to the concrete, the scaling can be reduced into the range of commonly used normal strength concretes with air eintrainment agents (mixes 4, 5, 6). The addition of microfibres (finely dispersed) leads to more homogeneously distributed microcracks with smaller crack-widths in the concrete structure (s. thin sections).

CONCLUSIONS

On the basis of the discussed mineral phase evolution in cement paste with high silica fume contents at early ages and the microcrack development in the corresponding concretes, it is possible to draw the following conclusions:

- It can be deduced from mineral phase investigations that pozzolanic reactions with silica fbme occur at an early age. Pozzolanic reactions are not the only reactions which take place, however: Water-rich gel phases develop very quickly within the first 12 hours. These gel phases release a large proportion of their water once again relatively quickly. This could serve as a plausible explanation for the early shrinkage and the frequent ultrafine microcracking systems which are to be found in concretes containing a high level of silica fbme. It is supposed that further phase transition reactions at later ages causes a further increase in autogenous shrinkage values (= shrinkage under sealed conditions). A proportion of up to 70 % of the total shrinkage values could be attributed to the autogenous shrinkage at 160 days.
- The microcracks in the structure of concretes with silica fbme and low w/b may be more or less homogeneously distributed. With an increasing silica fbme content the microcrack system is shifted from coincidentally distributed single cracks to a homogeneous network of cracks. Nevertheless, within a system of finely divided interconnected microcracks, strong capillary forces act, accelerating the water penetration. The quantity of water absorbed in a high strength concrete is usually small, but penetration depths of up to 30 mm may be measured.
- If water or solutions of deicing salts penetrate theses concretes and freeze, high tensile stresses will arise in the structure due to a lack of expansion space in the adjacent areas of the microcracks. This is a possible explanation for relatively high weight losses determined in freeze-thaw tests under the action of deicing salts. The addition of air entrainment agents or microfibres increase the freeze-thaw resistance of these concretes. In the case of fibres this may be attributed to more homogeneously distributed microcracks with smaller crack-widths.
- By the means of time- and depth-dependent measurement of electrolytic resistances it was shown that a rapid water absorption occured in the high strength concretes with an interconnected network of microcracks, but it was also evident that the water penetration front stopped at a maximum depth of 30 mm, whereas ongoing water absorbtion was measured for a normal strength concrete with increasing time. This effect together with a pronounced increase of resistance values despite of available water indicated a sealing (autogenous healing) of microcracks due to the ongoing of cement hydration and pozzolanic reaction of the additions after water application is possible. This was more pronounced for a high strength concrete with CEM I compared to a high strength concrete with CEM III/A.

Extended studies should be initiated on further parameters influencing the development of microcracks in low w/b-concretes. Systematic studies should be made on how the type of cement and, especially, the level of silica fbme addition may enhance the development of microcracks. In these investigations the level of silica fbme addition was beyond the permitted values ($s/c \leq 0{,}10$ in German approvals for silica fbme as concrete addition according to German standard DIN 1045).

REFERENCES

1. Alfes, Ch., „Modulus of Elasticity and Drying Shrinkage of High-Strength Concrete Containing Silica Fume", Detroit: American Concrete Institute, ACI SP-132, 1992.- In: „Fly Ash, Silica Fume, Slag, and Natural Pozzolans in Concrete", Proceedings 4th International Conference, Istanbul, May 1992 (Malhotra, V.m.(Ed.)), Vol. 2, 1651-1671
2. Al-Sugair, F.H., „Analysis of the Time-Dependent Volume Reduction of Concrete Containing Silica Fume", Magazine of Concrete Research 47 (1995), No. 170, 77-81

3. Cohen, M.D., Olek, J., Dolch, W.L., „Mechanism of Plastic Shrinkage Cracking in Portland Cement and Portland Cement - Silica Fume Paste and Mortar", Cement and Concrete Research 20 (1990), No. 1, 103-119

4. Meng, B., Schiessl, P., „The Reaction of Silica Fume at Early Ages". To be published in: 10th International Congress on the Chemistry of Cement, Goteborg, Schweden, 1997

5. Wiens, U., Breit, W., Schiessl, P., „Influence of High Silica Fume and High Fly Ash Contents on Alkalinity of Pore Solution and Protection of Steel against Corrosion". Detroit: American Concrete Institute, ACI SP-153, 1995. - In: Fly Ash, Silica Fume, Slag and Natural Pozzolans in Concrete (Malhotra, V.M.(Ed.)), Vol. 2, 741-761

6. Marsh, B.K., „Relationships Between Engineering Properties and Microstructural Characteristics of Hardened Cement Paste Containing Pulverized Fuel Ash as a Partial Cement Replacement", PHD Thesis, the Hatfield Polytechnic; Cement and Concrete Association, 1984

7. Schiessl, P., Breit, W., „Monitoring of the effectiveness of surface protection systems after repair measures using Multi-Ring-Electrodes". Berlin : Deutsche Gesellschaft für Zerstörungsfreie Prüfung, DGZfP, 1995. - In: International Symposium of Non-Destructive Testing in Civil Engineering (NDT- CE), Berlin, September 26-28, 1995, (Schickert, G.(Ed.)), Vol. 2, 1251-1258

8. Grutzeck, M.W., Atkinson, S., Roy, D.M., „Mechanism of Hydration of Condensed Silica Fume in Calcium Hydroxide Solutions", Detroit: American Concrete Institute, ACI SP-79, 1983. - In: Proceedings of the CANMET/ACI First International Conference on the „Use of Fly Ash, Silica Fume, Slag and Other Mineral By-products in Concrete", Vol. 2 (1983), 643-664

9. Wu, Z.-Q., Young, J.F., „The Hydration of Tricalcium Silicate in the Presence of Colloidal Silica", Journal of Materials Science 19 (1984), No. 11, 3477-3484

10. Wiegrink, K. ; Marikunte, S. ; Shah, S.P.: „Shrinkage Cracking of High-Strength Concrete". In: ACI Materials Journal 93 (1996), No. 5,409-415

11. Siebel, E., „Frost- und Frost-Tausalz-Widerstand von Beton". In: Beton 42 (1992), No. 9,496-501

DRYING OF CONCRETE WITH LOW WATER BINDER RATIO AND HIGH AIR CONTENT

VESA PENTTALA & LEIF WIRTANEN
Helsinki University of Technology
Concrete Technology
P.O.Box 2100
FIN-02015 HUT
Finland

ABSTRACT

Three material technological methods to increase the drying rate of concrete have been studied. The drying of normal strength concretes (NSC) has been compared with high strength concretes (HSC) and with concretes (AEC) produced with a normal dosage of air-entraining admixture (4-5% air content) and also with concretes (EAEC) in which excessive air contents have been introduced (8-10% air content). The air-entrained concretes and high strength concretes dry faster compared with normal strength non-air-entrained concretes. Normal air-entrainment of 4% in a 30 MPa concrete caused a faster drying rate that could be measured in a 50 MPa non-air-entrained concrete. Similarly, 30 MPa concrete having a 8% air-entrainment dries faster than a 50 MPa concrete having an air content of 4%. The drying mechanisms and their relative proportions have also been discussed in a concise manner.

The difference in the drying of non-coated specimens in different environments is very small when a concrete with a low water binder ratio but high air-content (8-10%) (EAEC) and ordinary high-strength concrete (HSC) are compared with each other. The evaporation of the EAEC-concrete is a bit faster than that of the HSC-concretes due to its larger capillary porosity volume, but the effect of self-desiccation of EAEC is on the other hand smaller because of its higher water-binder ratio. Tests have also shown that the drying of coated concrete slabs in which EAEC- concrete has been used differs from that of HSC-concrete. Concrete slabs produced from EAEC continue to dry even after the coating, whilst the drying of HSC slows down or even stops. The studied floor covering types were a plastic covering and mosaic parquet.

INTRODUCTION

The enhanced drying rate of young concrete is advantageous especially during building works at winter time in Nordic countries. According to previous investigations[1)2)] the best economic profit can be achieved by a 30 % increase in the contemporary building speed resulting in a slight increase in the cost of concrete frame but giving savings in the overall building costs. The

increased drying rate of concrete proved to be in the critical construction path and it was essential in installing the floor coverings in an adequately early phase. Present codes require the internal relative humidity of concrete to be less than 80-90% depending on the covering type before the floor covering installment.

In this paper, three methods of increasing the drying rate of concrete will be studied. High strength concretes and concretes produced with normal (4-5%) or high air content (8-10%) are compared with normal strength site concretes. The findings and test results will be dealt with in three parts. The results of the drying rate tests of plain, non-coated concretes will be presented separate from the effects of different drying temperatures. Finally, the effects of three different floor covering types on the drying rate of slabs will be studied.

DRYING OF UNCOATED CONCRETE CYLINDERS

Sample preparation, test methods and materials

The weight loss and relative humidity was determined from concrete cylinders having the diameter of 152 mm and height of 250 mm which simulated a slab of 250 mm thickness drying in both directions. The PVC-tubes used as moulds were left at their place for the entire test procedure, ensuring that the specimens would dry one-dimensionally through their non-coated end surfaces. From each test concrete three batches were cast. The batches were identical, except for the curing conditions. Six cylinders were cast from each batch. The weight loss was measured from five cylinders. Two of these five cylinders were additionally used for measuring the relative humidity. The relative humidity was measured from small plastic tubes (O= 15 mm and 1 = 100 mm) cast into the cylinders. The tubes were embedded 80 mm and located 60 mm from bottom and top surface of the cylinder i.e. 24% of the slab thickness. The bottom part of the tube contained small holes to improve the moisture transport. One cylinder was used for the manufacturing of specimens for the determination of chemically bound water and for the capillary water suction test. Drying of the concretes started at the age of two days.

The weight loss of the specimens was followed and the relative humidity of the pore structure was measured for 6 months. The relative humidity was measured using six relative humidity probes. The measuring time was 8..16 hours. The sensors were calibrated before and after every measurement, and the calibration time was 8 hours. The calibration was done with saturated salt solution of lithium chloride (LiCl) and potassium sulphonate (K_2SO_4), corresponding to a relative humidity of 11.3% and 97.6%, respectively, at a temperature of 21 "C. No calibration was made in between 11.3 and 97.6% relative humidity.

In this research project the measurement of the relative humidity was made with help of PVC-tubes cast into the concrete. This way the problems with drilling temperature and dust was avoided. The measurements can be started immediately after that the temperature in the concrete has stabilized. Between two measurements a rubber stopper was put in the tube to avoid drying. The relative humidity was measured by placing the humidity sensor in the tube and sealing the space between the sensor and the tube. When the sensor reached equilibrium the relative humidity was noted. The time required for equilibrium was assumed to be 8 hours. The measuring time for practical reasons varied between 8 and 16 hours. The drawback of this method is that the cast in tube inevitably changes the moisture flow within the specimen. The area around the tube dries therefore to some extent more than undisturbed concrete. This is

emphasized when humidity changes are followed for a longer period. The accuracy of the measurements of the internal relative humidity was estimated to vary from ±1 to ±2%.

The porosity distribution for pore radii 3.7-30000 nm was calculated from mercury intrusion porosimetry test results obtained from concrete cylinders 25 mm in diameter and 20-25 mm in height, drilled from larger test cylinders. The drilled specimens were dried in vacuum at 20° C for six weeks prior to the testing. The surface tension of mercury was assumed to be 480 N/m and the contact angle between concrete and mercury used in the calculations was 141.3". When determining the pore radii the pores were assumed cylindrical. Concrete porosity was transformed to binder porosity by volumetric calculations and by determining the amount of non-evaporable water by ignition method.

The cement type used in this research project was CEM II 42.5R and it was produced by Finnsementti Oy. Condensed silica fume in the form of powder was used in the production of high performance concretes and it was of Norwegian origin also delivered by Finnsementti Oy. Pulverized fly ash of class F was used in the production of concrete in the strength class of 30-35 MPa mainly as an filler.

A modified naphthalene sulphonate was used as a water reducing agent. The effects of three air-entraining agents were studied. The chemical compositions of the air-entraining agents were a vinsol resin, a polyglycol ether sulphonate, and a synthetic tenside. The aggregates used in the test concretes had a mineral composition of mostly granite and their shape was rounded. In the production of one test concrete also quartz fillers were used.

The mix designs of these test concretes are presented in TABLES 1-3. The maximum aggregate size in all concrete mixes was 32 mm. The workability requirements were set as 1 sVB immediately after mixing and less than 5 sVB two hours after mixing. The air content was obtained by pressure method from fresh concrete.

TABLE-1
Mix Design of the Comparison Concretes (NSC).

Test concrete	Cement content (kg/m^3)	Water amount (kg/m^3)	Fly ash amount (kg/m^3)	Silica fume amount (kg/m^3)	Aggregate amount (kg/m^3)	Air content (%)	Super-plasticizer (% of cem.)	w/ (c+sf)
C1 a	220	165	95	-	1915	0.3	-	0.75
C1 b	220	165	95	-	1911	0.5	-	0.75
C1 c	220	165	95	-	1915	0.3	-	0.75
C2 a	240	170	95	-	1883	0.4	-	0.71
C2 b	240	170	95	-	1885	0.3	-	0.71
C2 c	240	170	95	-	1883	0.4	-	0.71
C3 a	240	170	95	-	1881	0.5	-	0.71
C4 a,d,e	271	165	-	-	1974	0.8	-	0.61
C5P a	389	171	-	-	1832	1.2	2.0	0.44
C6P a,d,e	241	156	-	-	2025	0.4	1.8	0.65
C7H a,d,e	351	206	-	-	1800	0.7	-	0.59

TABLE-2
Mix Design of Normally Air-entrained Concretes (AEC).

Test concrete	Cement content (kg/m^3)	Water amount (kg/m^3)	Fly ash amount (kg/m^3)	Silica fume amount (kg/m^3)	Aggregate amount (kg/m^3)	Air content (%)	Super-plasticizer amount (% of cem.)	Air-entraining agent (% of cem.)	w/ (c+sf)
A1 a	358	153	-	-	1793	5.8	-	0.17[1]	0.43
A2 a	247	175	98	-	1726	5.3	-	0.18[1]	0.71
A2 b	245	174	97	-	1714	6.0	-	0.18[1]	0.71
A3 a,d,e	339	174	-	-	1744	6.3	-	0.07[1]	0.51
A4P a	446	188	-	19.8	1602	5.0	2.5	0.08[1]	0.40
A4P b	447	189	-	19.9	1608	4.6	2.5	0.08[1]	0.40
A4P c	447	189	-	19.9	1608	4.6	2.5	0.08[1]	0.40
A5P a	449	170	-	19.9	1658	4.2	3.6	0.08[1]	0.36
A5P b	450	170	-	20	1662	4.0	2.35	0.08[1]	0.36
A6P a,d,e	448	169	-	19.9	1657	4.4	3.3	0.08[1]	0.36
A7PM a	169	129	-	16.9	2048[2]	3.6	4.5	0.15[1]	0.69
A7PM b	167	128	-	16.7	2030[2]	4.5	4.5	0.15[1]	0.70
A7PM c	170	130	-	17	2054[2]	3.3	4.5	0.15[1]	0.70

[1] Vinsol resin [2] Includes **quartz** fillers

TABLE-3
Mix Design of the Air-entrained Concretes Having 8-10% Air Content (EAEC).

Test concrete	Cement content (kg/m^3)	Water amount (kg/m^3)	Silica fume amount (kg/m^3)	Aggregate amount (kg/m^3)	Air content (%)	Super-plasticizer amount (% of cem.)	Air-entraining agent (% of cem.)	w/ (c+sf)
AA1 a	388	169	-	1658	8.4	-	0.19[1]	0.44
AA1 b	388	169	-	1657	8.5	-	0.19[1]	0.44
AA1 c	389	170	-	1662	8.2	-	0.19[1]	0.44
AA2 a	386	168	-	1648	9.0	-	0.19[2]	0.44
AA2 b	388	169	-	1658	8.4	-	0.19[2]	0.44
AA2 c	379	165	-	1616	11.0	-	0.19[2]	0.44
AA3 a	402	175	-	1716	5.0	-	0.22[3]	0.44
AA3 b	399	174	-	1702	5.8	-	0.22[3]	0.44
AA3 c	392	171	-	1673	7.5	-	0.22[3]	0.44
AA4P a	297	139	-	1796	9.0	1.3	0.18[1]	0.47
AA4P b	299	140	-	1809	8.3	1.3	0.18[1]	0.47
AA4P c	299	139	-	1805	8.5	1.3	0.18[1]	0.46
AA5P a	454	156	20.2	1605	7.2	3.6	0.19[1]	0.33

[1] Vinsol resin [2] Polyglycol ether sulfonate [3] Synthetic tenside

Test results

TABLE-4 shows the main test results. Figures 1-6 show a comparison between the relative humidity results in the pore structure of the different test concretes with the capillary porosity values and evaporated water amount.

TABLE-4
Main Test Results of the Test Concretes.

Test concrete	RH (%) 28 d	RH (%) 168 d	Evapor. water (dm^3/m^3) 28 d	Evapor. water (dm^3/m^3) 168 d	Capillary porosity (mm^3/cm^3) 28 d	Meso porosity (mm^3/cm^3) 28 d	Throat radius (nm) 28 d	Compr. strength 28 d
C1 a	91.3	82.1	8.78	13.67	197	87	85	37.1
C2 a	92.8	84.6	8.85	13.18	241	62	85	42.7
C3 a	91.0	83.4	7.97	12.52	221	74	87	39.2
C4 a	92.5	87.0	-	-	320	151	115	39.4
C5P a	85.4	82.0	4.34	8.42	235	107	69	55.9
C6P a	93.0	87.1	-	-	288	85	100	39.3
C7H a	91.6	87.9	-	-	293	77	110	36.4
A1 a	86.8	77.4	3.78	8.29	156	210	51	37.7
A2 a	92.3	80.6	10.99	17.24	186	120	70	25
A4P a	88.2	81.5	4.59	7.72	150	146	38	56.8
A5P a	86.2	80.6	3.45	6.44	102	116	37	51.5
A6P a *	86.2	77.9	-	-	176	175	42	51.7
A7PM a	90.5	81.5	9.48	14.55	223	110	35	42.9
AA1 a	86.0	79.2	4.89	9.7	168	254	67	35.8
AA2 a	85.2	79.8	5.29	9.96	157	216	54	31.8
AA3 a	84.4	79.9	4.96	9.48	187	144	67	40.3
AA4P a	86.1	77.7	5.07	10.27	157	265	49	35.7
AA5P a	83.4	75.5	2.54	5.47	93	181	47	55.2

Discussion of the test results

As can be seen from the drying results presented in Figures 1 and 2 air-entrained concretes dry faster compared with non-air-entrained comparison concretes the strength held constant. Normal air-entrainment of 4% in a 30 MPa test concrete causes a faster drying rate than in a non-air-entrained 50 MPa concrete. Similarly, 30 MPa concrete having a 8% air-entrainment dries faster than a 50 MPa concrete having a 4% air-entrainment even though this comment can be near the precision of the relative humidity measurement deviation of ±1...±2%.

There are two main mechanisms that simultaneously govern the drying phenomenon of concrete. If the surrounding environment is dryer than the relative humidity in the largest concrete pores water evaporates from the pore structure. Except for the first few weeks, the moisture transportation mechanism is regulated by the area of the threshold throats between the capillary and meso pores presented in FIG.-7 and of course by the relative humidity of the surrounding environment.

FIG.-1
Relative Humidity in Concrete Pore Structure Versus Drying age of Three Test Concretes. K35 Denotes for a Concrete Having a Compressive Strength of 35 MPa Measured by 100-mm Cubes. WRA Denotes for Water Reducing Agent.

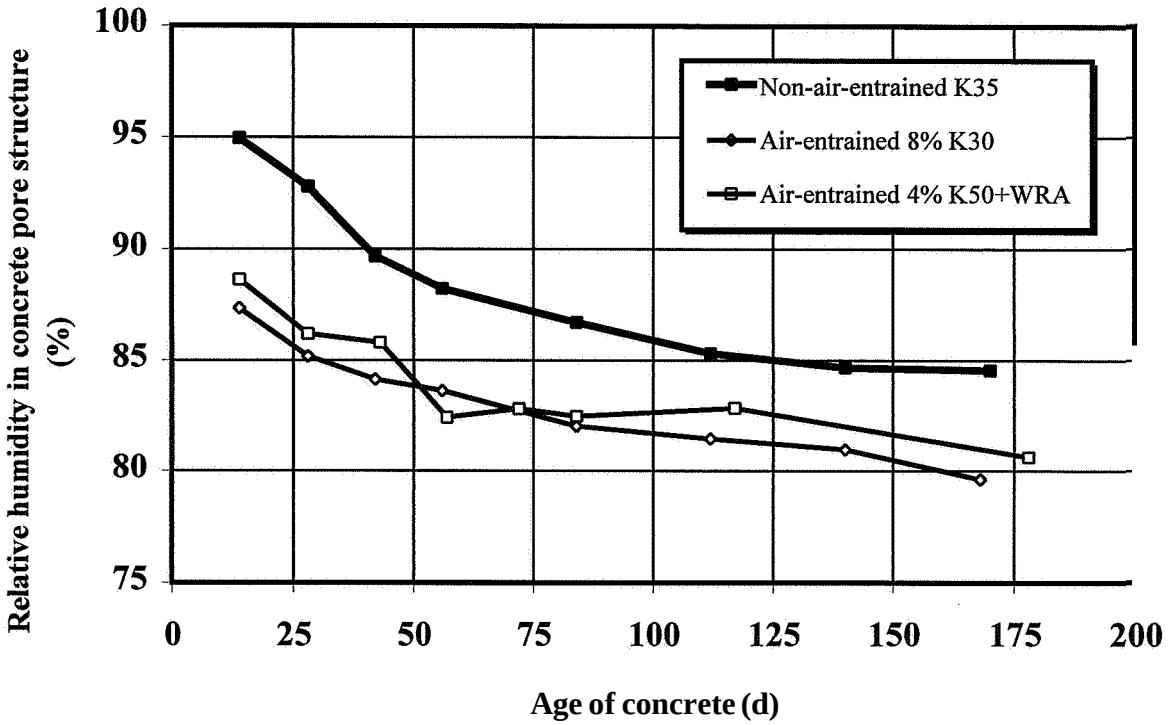

FIG.-2
Relative Humidity in Concrete Pore Structure Versus Drying Age of Three Test Concretes. K35 Denotes for Concrete Having a Compressive Strength of 35 MPa Measured by 100-mm Cubes.

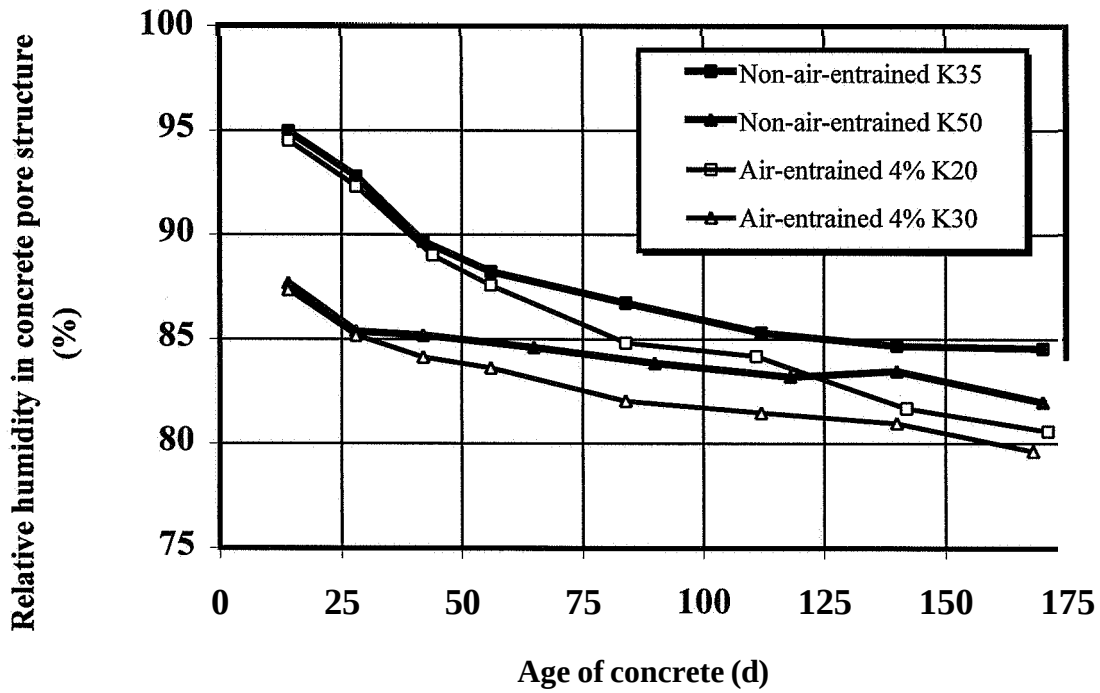

FIG.-3
The Capillary Porosity Values of the Test Concretes Versus Relative Humidity in Concrete Pore Structure at the Age of 28 Days.

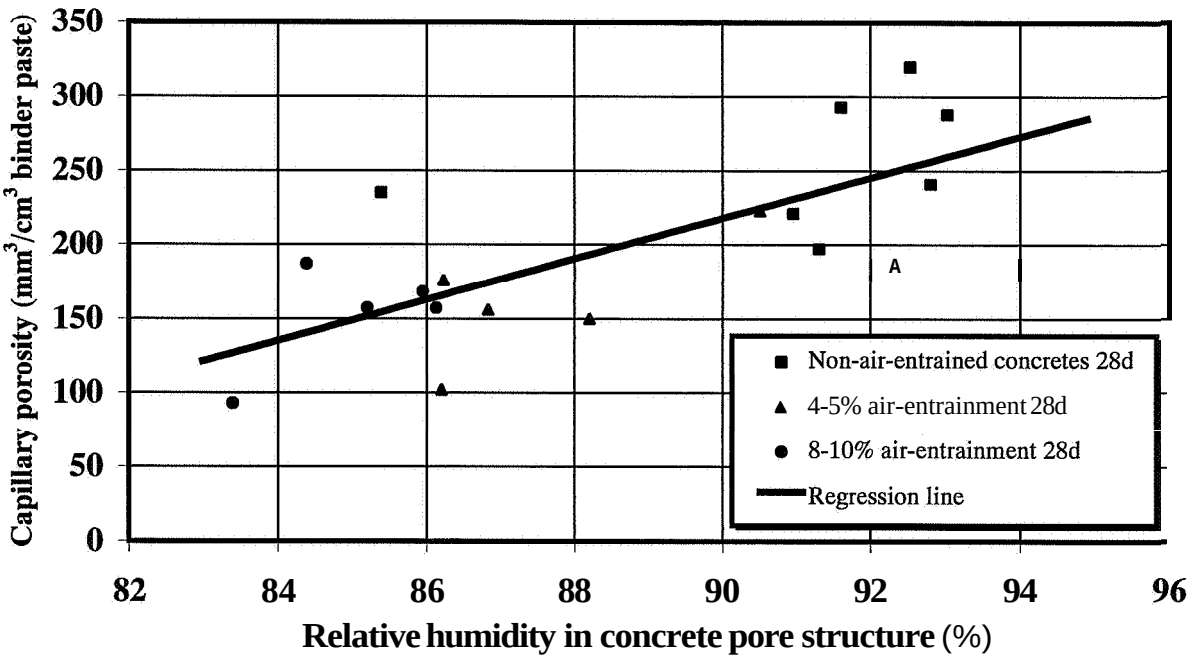

FIG.-4
The Capillary Porosity Values of the Test Concretes Versus Relative Humidity in Concrete Pore Structure at the Age of 168 Days.

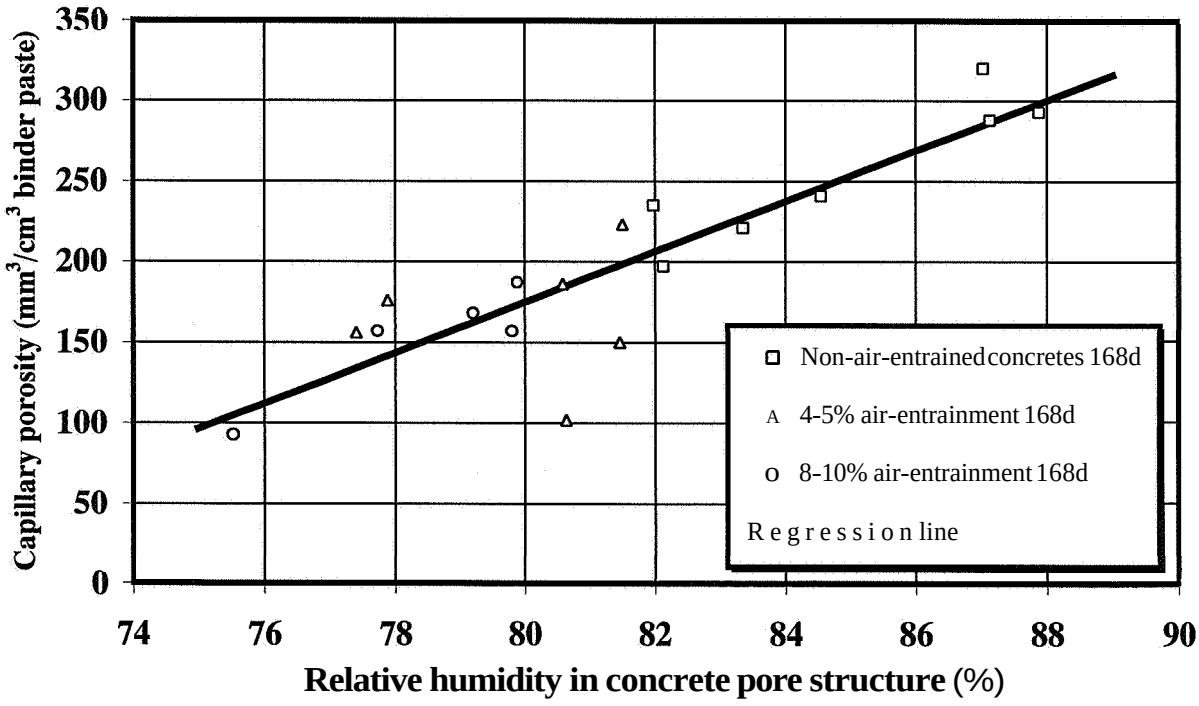

FIG.-5
Evaporated Water Amount Values of the Test Concretes Versus Capillary Porosity Values at the Age of 168 Days.

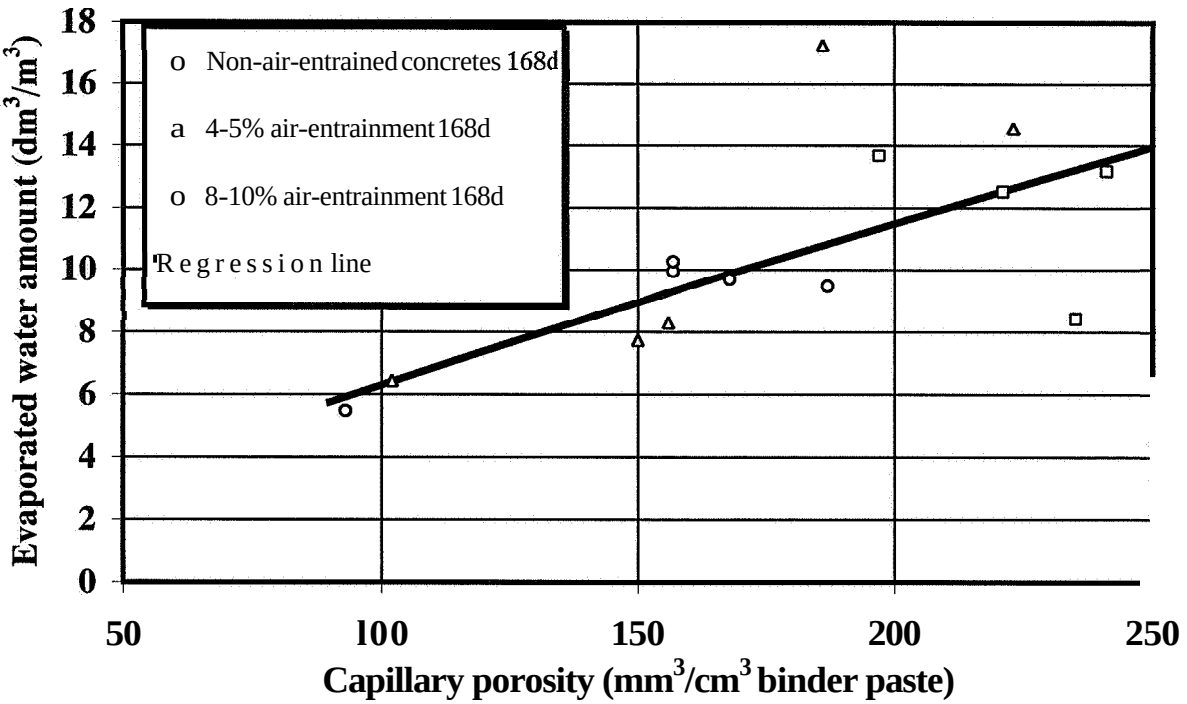

FIG.-6
Threshold Throat Areas Between Capillary and Meso Pores in the Pore Size Distributions of the Test Concretes Versus Relative Humidity in Concrete Pore Structure. The Arrows Show the Shift of the Test Results During the Aging of the Test Specimen.

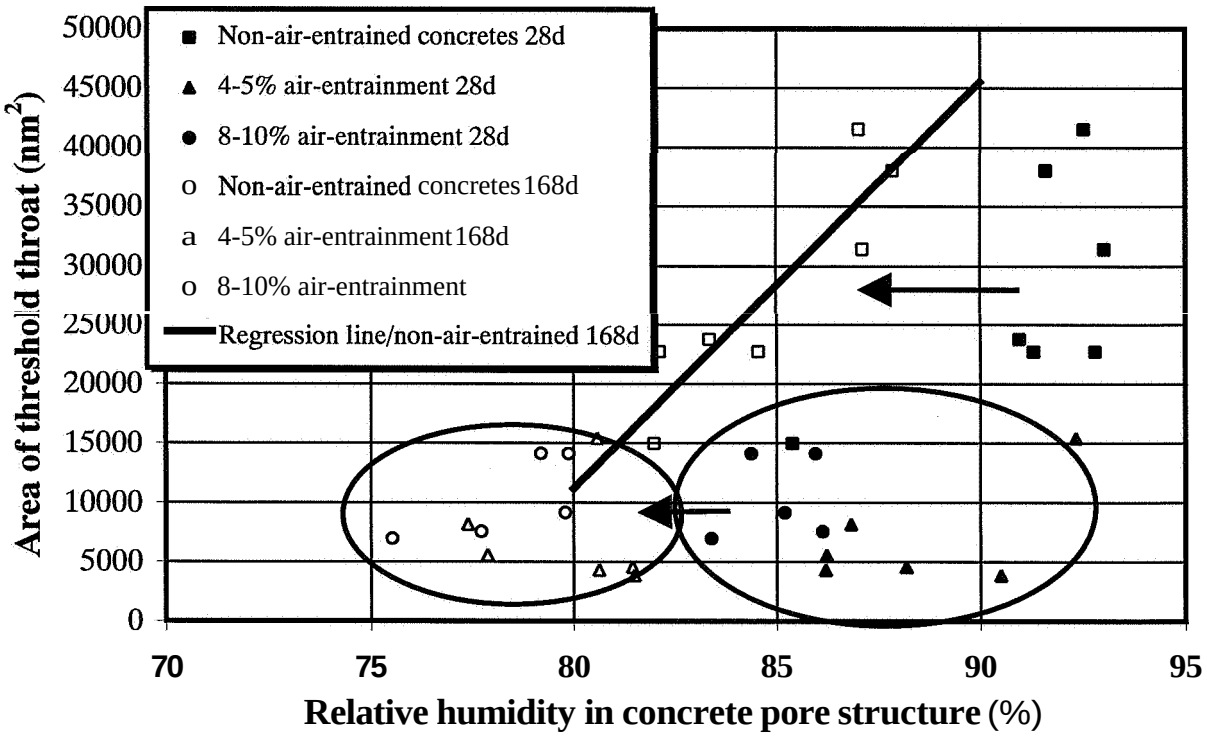

The other important drying force is the self-desiccation of the pore structure caused by the subsequent hydration of yet unhydrated binder particles. This drying process is dominating when the cement amount in the concrete is large and water-binder ratio small as is the case in high strength concretes.

Figures 3 and 4 show the relationship between capillary porosity and relative humidity in the pore system of the test concretes. Capillary porosity is directly related to the water-binder ratio and thus the relative humidity in concrete pore structure diminishes with decreasing capillary porosity due to self-desiccation. This can be also seen in the test results presented in FIG.-5 in which the evaporated water amount decreases with the diminishing capillary porosity.

FIG.-7
Schematic Presentation of the Threshold Throat Radius Between Capillary and Meso Pores. The Pore Size Distribution is Obtained from a Mercury Intrusion Porosimetry Test.

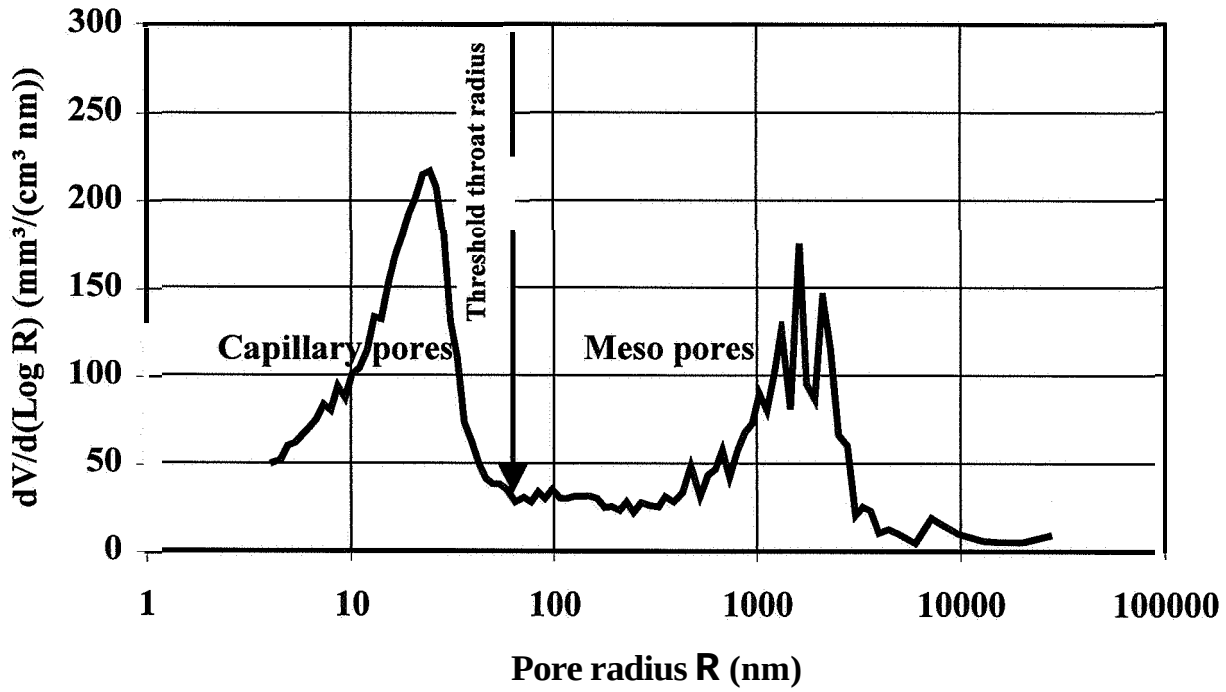

In FIG.-6 the relative humidity results of the test concretes are presented as a function of the area of the threshold throats. It can be noticed that the area of the threshold throats is rather small for all air-entrained concretes which are gathered inside two ellipsoids in the figure. The longer drying age causes merely a shift towards smaller relative humidity values. The major portion of drying in these air-entrained concretes is caused by self-desiccation due to the increased binder amount in these concretes which is needed to compensate for the weakening caused by the increased air amount.

The drying of the non-air-entrained concretes is logical in view of FIG.-6. After one months drying the relative humidity in these concretes is very similar irrespective of binder amount or threshold throat area with the exception of one high strength concrete. After six months the regression line of the non-air-entrained concretes is rather paradoxical. Those concretes that possess smallest threshold throat areas have dried most. The reason for this is again the superior

drying capability of self-desiccation compared with the drying by evaporation. The smallest threshold throat areas are in the same concretes that have the smallest capillary porosity values and hence the smallest water-binder ratios. The drying times of the test concretes to 90 and 85% relative humidity values in the concrete pore structure are summarized in TABLE-5. The drying time values are presented in two different environmental conditions. Good drying environment is considered such where temperature is 20° C and relative humidity is 45% while in a moderate drying environment these values are 10° C and 75%, respectively.

TABLE-5
The Drying Times of Test Concretes to 90 and 85% Relative Humidity in Concrete Pore Structure. WRA denotes for Water Reducing Agent.

Compressive strength/ admixture (MPa)	Air-entrainment (%)	Drying time (d)			
		Good drying environment +20° C/RH 45%		Moderate drying environment +10° C/RH 70%	
		<RH 90%	<RH 85%	<RH 90%	<RH 85%
30 and 35	-	40	130	140	>180
50+WRA	-	<14	35		
20	4	40	85		
30	8	<14	35	25	>180
30+WRA	8	<14	30	50	>180
40	4	<14	55	50	>180
50+WRA	4	<14	45	<14	>110
50+WRA	8	<14	20		

THE EFFECTS OF TEMPERATURE ON THE DRYING OF CONCRETE

Sample preparation

Three different kinds of concretes were studied. Mix proportions and properties of these test concretes are shown in TABLE-6. A modified naphthalene sulphonate was used as a water reducing agent. A polyglycol ether sulphonate was chosen as an air entraining agent. The casting was done into plastic cylinders having a height of 250 mm and a diameter of 250 mm. The curing was carried out so that the cylinders were kept under a plastic sheet for five days in the casting room. Then the bottom surfaces of the cylinders were removed in order to let the specimens dry by two surfaces.

Measuring methods and curing conditions

All the humidity measurements were carried out with Humitter 50 Y humidity and temperature transmitters. One transmitter was installed into a drill hole in the surface of each cylinder at the age of five days and the cylinders were moved to respective curing conditions which were +5° C (RH 70%), +12° C (RH 70%) and +20° C (RH 45%). New transmitters were installed into drill holes after 14 respectively 28 days of curing. All the transmitters were left in the drill holes and calibrated after the test sequence was finished. The accuracy of the measurements was ±1…±2%.

TABLE-6
Mix Proportions and Properties of the Test Concretes.

Concrete	NSC30	EAEC30	HSC70
Rapid Portland cement content (kg/m³)	200	440	475
Silica fume content (kg/m³)	-	-	28.5
Water content (kg/m³)	178	174	176
Aggregate content (kg/m³)	1969	1605	1677
Superplasticizer dosage (%)	-	0.5	1.5
Air-entraining agent dosage (%)	-	0.2	-
Water-binder ratio (w/(c+sf))	0.89	0.39	0.35
Consistency (sVb)	1.8	1.0	1.2
Air content (%)	0.9	9.5	1.6
Compressive strength 28d, (MPa)	29.6	32.3	70.6

Test results and discussion

The test results are shown in FIG.-8. The effect of the curing temperature on the drying of concrete diminishes with the decrease of the water-binder ratio in the test concretes. This means that when concrete dries mainly due to self-desiccation drying is not affected by far as much by temperature as when it dries mainly because of evaporation. Tests with supplementary curing conditions i.e. +5° C (RH 45%), +12° C (RH 45%) and +20° C (RH 70%) are being carried out for these same concretes during this spring.

THE EFFECTS OF DIFFERENT FLOOR COVERING MATERIALS ON THE DRYING OF CONCRETE SLABS

Sample preparation

Three different concrete types were studied. Mix proportions and properties of these test concretes are presented in TABLE-7. A modified naphthalene sulphonate was used as a water reducing agent and the air reducing admixture was again a polyglycol ether sulphonate. The casting was done into slabs that were 300 by 600 mm wide and 100 or 200 mm thick. The 100 mm thick slabs dried only through the upper surface, while the 200 mm slabs dried through two surfaces. Curing was carried out so that the slabs were first kept under a plastic sheet for seven days in the casting room. Then they were moved to a climate room (20° C, RH 45%). The slabs were sealed so that drying occurred only through the top surface (or both top and bottom surfaces depending on the slab). The covering was done when the relative humidity of the concrete was 90-95% at a distance of 40% of the height of the concrete slab measured from its top surface onto which the covering materials were attached. The surface of the slab was ground before the covering material was placed and the edges were sealed with silicone 24 hours after the covering works. The parquets were lacquered 5 days later.

Measuring methods

All the humidity measurements were carried out either with a Humitter 50 Y or Humichip humidity and temperature transmitters. The measurements were done both from drill holes and some transmitters were also embedded into the concrete. The measurements were done at three different heights (20, 40, and 80 mm) when 100 mm thick slabs were used and four different heights (40, 80, 120 and 160 mm) when 200 mm thick slabs were used. The humidity in the drill holes was always left to level out for a week before the readings. The readings were checked at the end of the test sequence from new drill holes. The accuracy of the measurements was similar as in the previous parts of this article.

TABLE-7
Mix Proportions and Properties of the Test Concretes. [3)]

Concrete	NSC30	EAEC30	HSC70
Rapid Portland cement content (kg/m³)	240	390	475
Silica fume content (kg/m³)	-	-	28,5
Water content (kg/m³)	180	156	170
Aggregate content (kg/m³)	1900	1638	1677
Superplasticizer dosage (%)	-	0.5	1.5
Air-entraining agent dosage (%)	-	0.2	-
Water-binder ratio	0.75	0.36	0.34
Consistency (sVb)	1.5	1.2	<1
Air content (%)	2	11	1.5
Compressive strength 28d, (MPa)	37	38	74

Results and discussion

The results are shown in Figures 9-14.

Concrete slabs made of normal strength concrete were covered when the relative humidity in the concrete pore system at 20% of the total thickness measured from the top of the slab was about 94% (Fig.-9 and 10). It can be seen that the relative humidity at the 20% thickness had increased after 20 days of curing. This can been caused by the redistribution of the humidity in the concrete after the covering works had been done or even the water in the glue can have affected the results. The humidity level had, however, decreased after three and half months curing time. It can also be seen that the humidity level measured at the 20% thickness was remarkably higher when a dense plastic cover was used than when mosaic parquet was applied. The difference in the relative humidity at 40% of the total thickness of the slab measured from the top of the slab was on the other hand very small.

The slabs made of high strength concrete had dried to a relative humidity level of 90% in less than 2 weeks at 20% of the total thickness measured from the top of the slab. Two months after the covering works the humidity level had decreased at each measuring point (Fig.-l 1 and 12). It can also be seen that the humidity level close to the surface was remarkably lower for the slab covered with mosaic parquet than for the one covered with plastic. The uncovered slab had the lowest humidity level after 88 days of curing.

FIG.-8

Humidity Evolution in the Pore Structure of the Test Concretes NSC30, EAEC30, and HSC70.[3)]

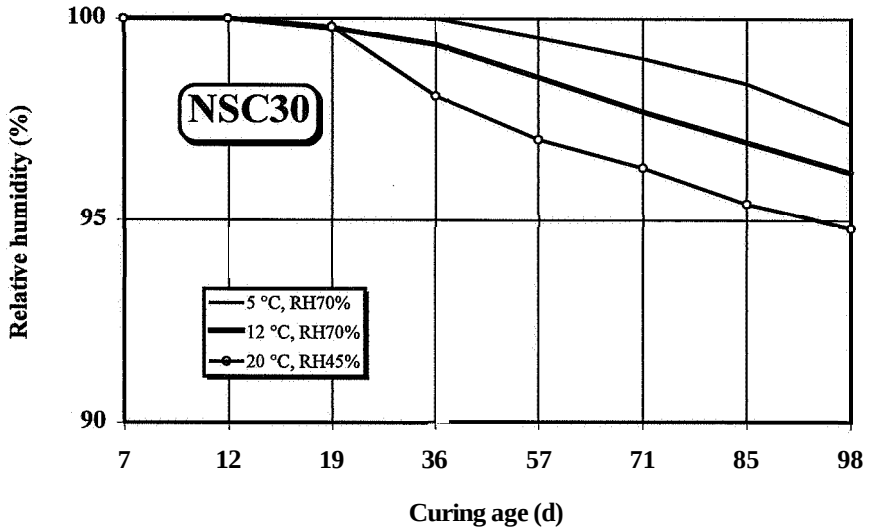

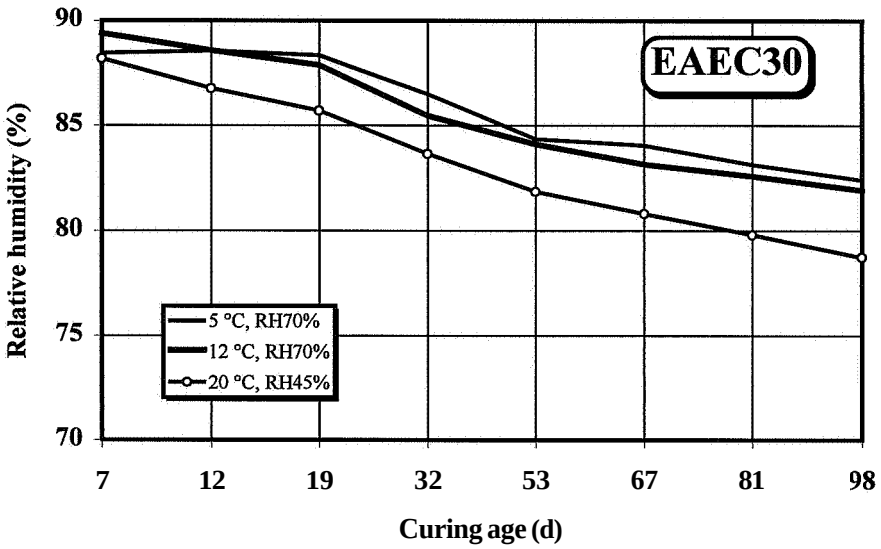

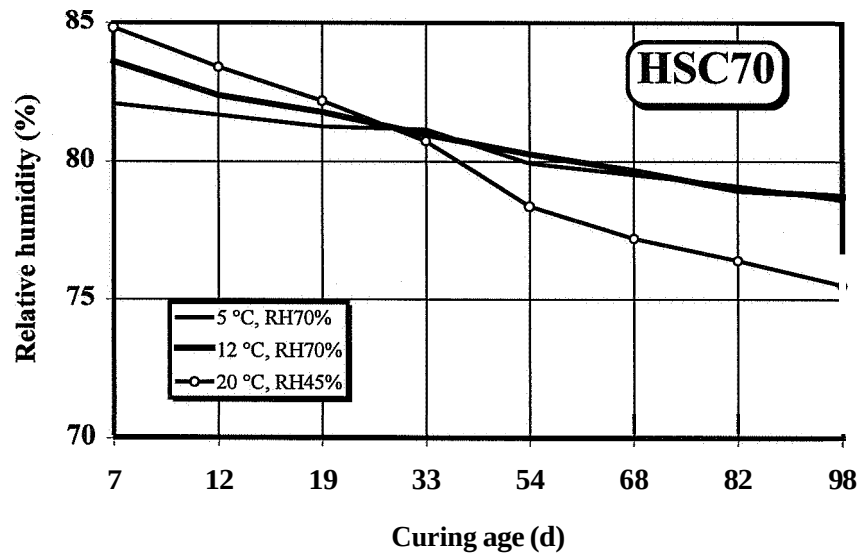

FIG.-9
Humidity Distribution of Uncovered and Covered (Plastic or Mosaic Parquet) Concrete Slabs, (Concrete Strength Class NSC30, Slab Thickness 200 mm)[3)]

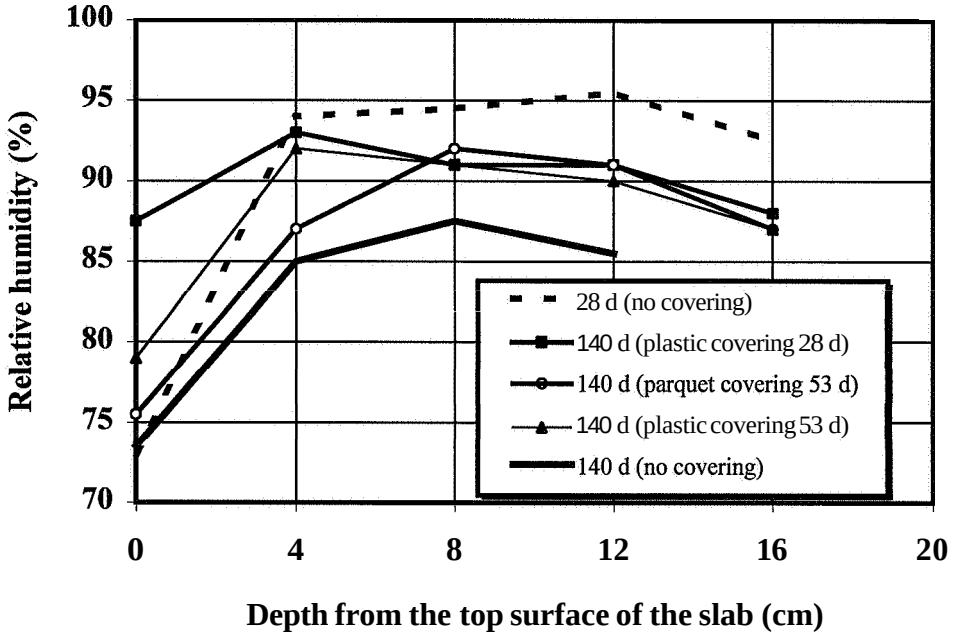

FIG.-10
Humidity Distribution of Uncovered and Covered (Plastic or Mosaic Parquet) Concrete Slabs, (Concrete Strength Class NSC30, Slab Thickness 100 mm)[3)]

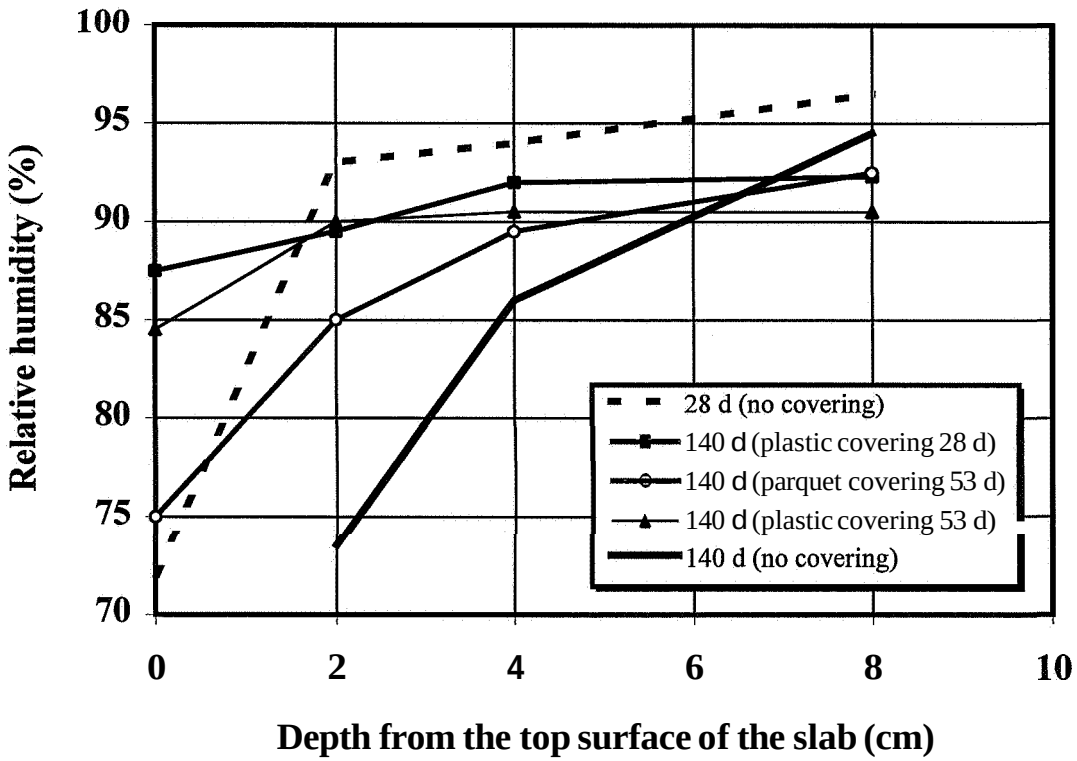

FIG.-11
Humidity Distribution of Uncovered and Covered (Plastic or Mosaic Parquet) Concrete Slabs, (Concrete Strength Class HSC70, Slab Thickness 200 mm)[3)]

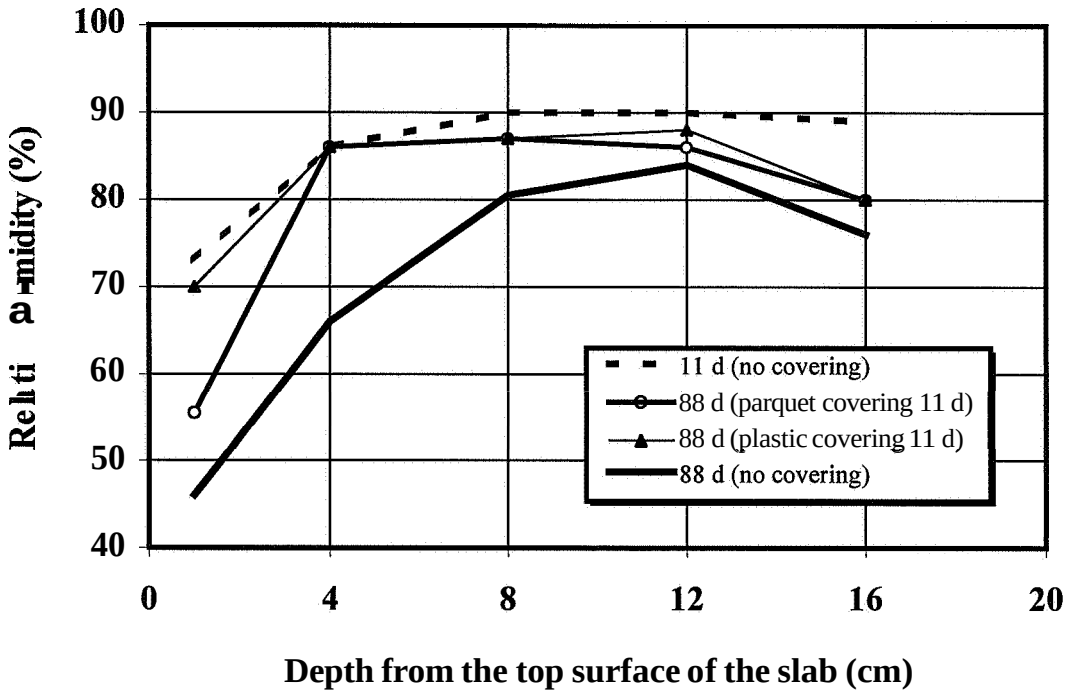

FIG.-12
Humidity Distribution of Uncovered and Covered (Plastic or Mosaic Parquet) Concrete Slabs, (Concrete Strength Class HSC70, Slab Thickness 100 mm)[3)]

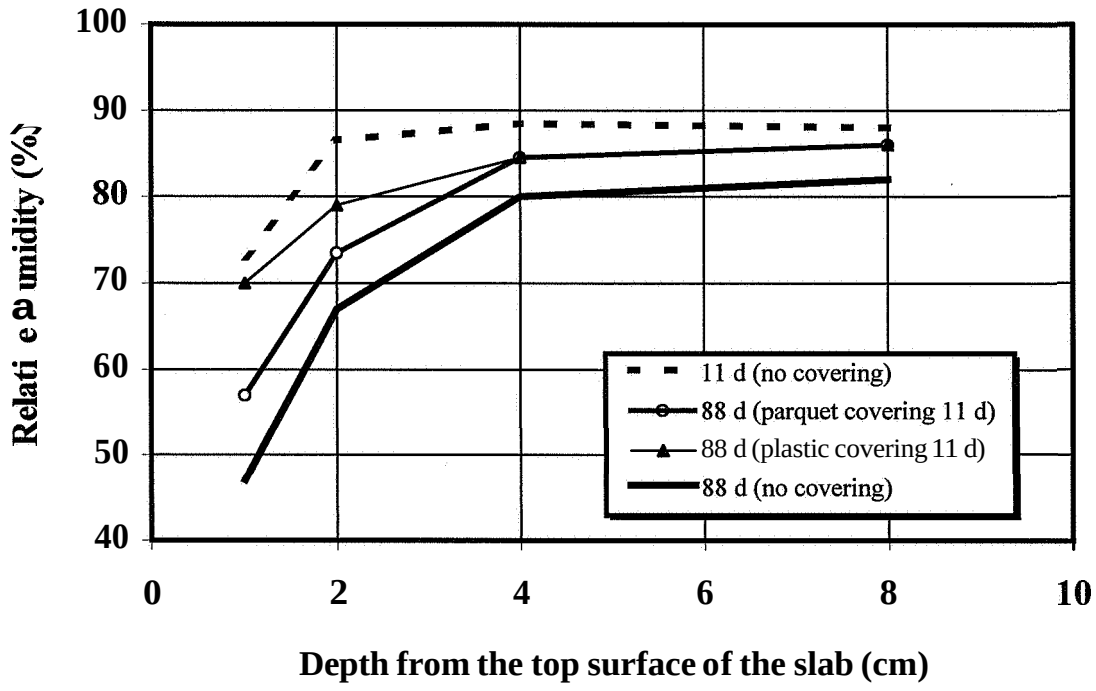

FIG.-13
Humidity Distribution of Uncovered and Covered (Plastic or Mosaic Parquet) Concrete Slabs, (Concrete Strength Class EAEC30, Slab Thickness 200 mm)[3)]

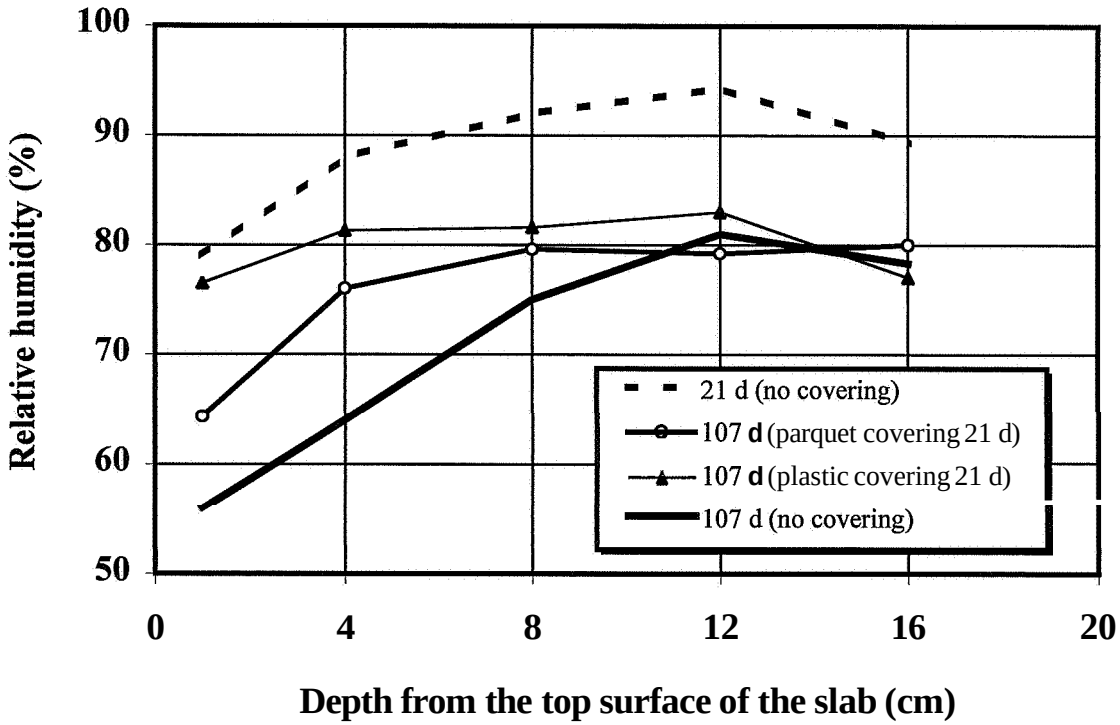

FIG.-14
Humidity Distribution of Uncovered and Covered (Plastic or Mosaic Parquet) Concrete Slabs, (Concrete Strength Class EAEC30, Slab Thickness 100 mm)[3)]

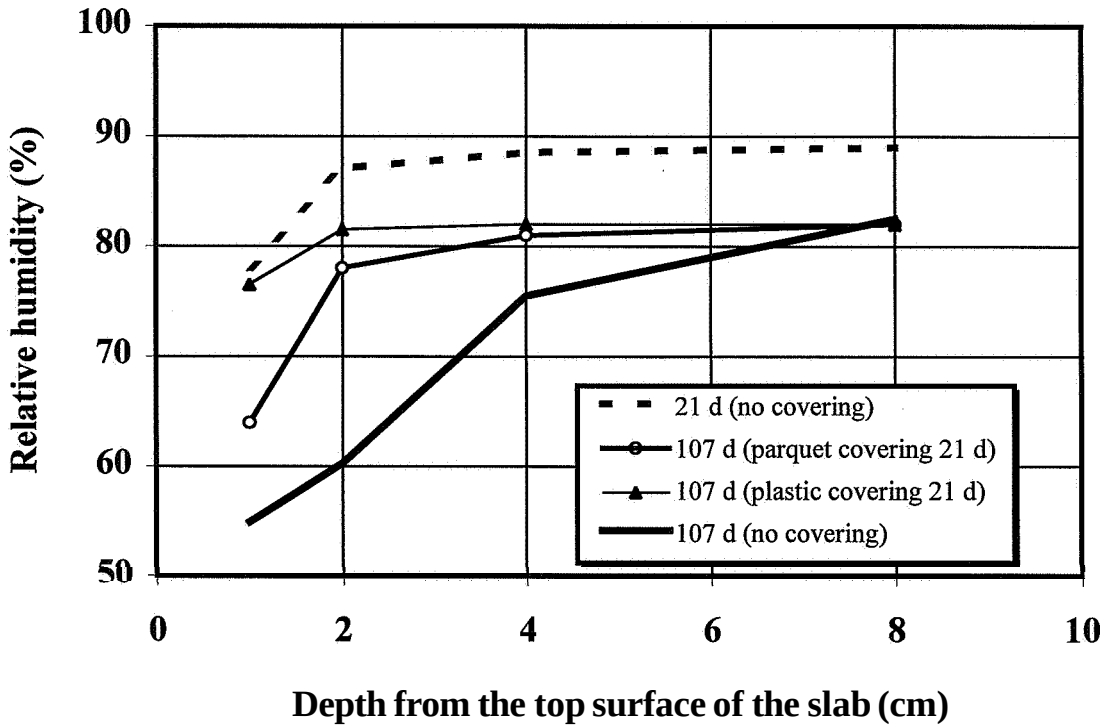

The slabs made of extra air-entrained concrete had reached a humidity level of about 90 % at 20% of the total thickness measured from the top of the slab when the covering works was carried out. It can be seen (Figures 13 and 14) that the relative humidity level after a little more than 3 months of curing was several percentage units lower than at the time of the covering work. The difference between the slab covered with plastic and the slab covered with mosaic parquet was again remarkable at 20% of the total thickness of the slab measured from the top surface. When one compares the drying of the EAEC30 concrete with the drying of HSC70 concrete it can be seen that the EAEC30 concrete had dried remarkably more after the covering works had been performed.

CONCLUSIONS

1) Air-entrained concretes dry faster compared with non-air-entrained comparison concretes the strength held constant. Normal air-entrainment of 4% in a 30 MPa test concrete causes a faster drying rate than in a non-air-entrained 50 MPa concrete. Similarly, a 30 MPa concrete having a 8% air-entrainment dries faster than a 50 MPa concrete having a 4% air-entrainment.

2) In low strength concretes in which the binder amount is small the drying of concrete is governed by the relative humidity of the surrounding environment and the threshold area of the throats between capillary and meso pores. In concretes where the water binder ratio is less than 0.5 concretes dry due to self-desiccation caused by subsequent binder hydration.

3) Capillary porosity is directly related to the water-binder ratio and thus the relative humidity in concrete pore structure diminishes with decreasing capillary porosity due to self-desiccation.

4) Concrete having a low water-binder ratio and high air content reaches lower humidity values than ordinary high strength concrete after the placing of floor coverings.

5) Concrete slab covered with a wooden parquet reaches a lower relative humidity level compared with a plastic covering material. The difference in the relative humidity levels are highest near the covered surface.

ACKNOWLEDGEMENTS

The authors wish to express their gratitude to M. Sc. (Eng.) Jussi Eronen, M. Sc. (Eng.) Kim Johansson, M. Sc. (Eng.) Pentti Lumme, and M. Sc. (Eng.) Tarja Merikallio who all have participated in some part of the research projects which have been presented in this article.

REFERENCES

1) V. Penttala, New High Performance Concretes (in Finnish), XXII Concrete Days 2.-3.11.1994 Helsinki, Suomen Betonitieto Oy, pp. 83-102.
2) T. Merikallio, P. Lumme, V. Penttala, Drying of Concrete Slabs for the Floor Covering Works (in Finnish), Betoni 1, 1995, pp. 30-35.
3) T. Merikallio, V. Penttala, Effects of Concrete Type and Floor Covering Material on the Relative Humidity Distribution Changes in Concrete Slabs after Floor Coating (in Finnish),

Research Report RBET 35, Helsinki University of Technology, Department of Structural Engineering, Laboratory of Concrete Technology, 1996, 29 p.
4) V. Penttala, , K. Johansson, J. Komonen, Fast In-Situ Concretes. Nordic Concrete Research Meeting, Espoo, Finland 1996. Nordic Concrete Federation, pp. 70-71.
5) V. Penttala, , T. Merikallio, L. Wirtanen, Early Floor Covering of Concrete Slabs and Adhesion Between Concrete and Floor Covers. Nordic Concrete Research Meeting, Espoo, Finland, August 1996. Nordic Concrete Federation, pp. 107-108.

EFFECT OF SELF-DESICCATION ON THE INTERNAL FROST RESISTANCE OF CONCRETE

GÖRAN FAGERLUND
Div. of Building Materials, Lund Institute of Technology
Box 118, S-221 00 Lund
Sweden

ABSTRACT

Frost damage occurs when the water content inside the concrete exceeds a certain critical level, which is different for different concretes. One can distinguish between two different problems: (i) freezing of the green concrete during the first hours of its life; (ii) freezing of the hardened concrete. Both problems are treated in the paper.

Frost damage of the green concrete can only be prevented if the self-desiccation dries the concrete to a level where the 9% volume expansion when water is transformed into ice can be taken care of. It is theoretically shown that this corresponds to a critical (or required) degree of hydration that is a function of the waterlcement ratio. Two expressions for the required degree of hydration are given. One is derived on basis of measurements of a relation between frost damage and the "chemical shrinkage" of chemically bound water. The other is based on measurements of the freezable water combined with an assumption concerning the critical water content. The two expressions predict similar values of the required degree of hydration. From this, the required pre-curing time can be calculated. Calculated and experimental values correspond fairly well.

Frost damage to the hardened concrete can be prevented if the self-desiccation lowers the internal RH to a level where no pore water is freezable. A relation between the freezing point and RH is given. It is shown by comparisons with experiments that the real self-desiccation in high performance concrete stored in water can reach these low RH-levels. By prolonged water storage, the self-desiccated pores might become water-filled. Test results from a large study indicate that a few years of water storage might be enough to fill the self-desiccated pores to a level where frost damage is possible. Therefore, air-entrainment is probably required also in concrete with low waterlcement ratio. So-called salt-frost scaling tests indicate that non-air-entrained high performance concrete with silica fume might be vulnerable to frost attack if the freezelthaw test is run for many cycles. This does not seem to happen in OPC-concrete with the same water/binder ratio. The reason behind this behaviour is not known. Possibly it is caused by a gradual water filling of self-desiccated pores that occurs more rapidly in concrete with silica fume. This hypothesis, however, has not been proved.

1. INTRODUCTION

There are two types of frost damage: (i) internal damage occurring when the interior of the concrete is more than critically saturated; (ii) external damage, or surface scaling, probably occurring when the surface part of concrete is more than critically saturated. Surface scaling is normally coupled to the use of deicing salts, primarily NaCl, and is, therefore, often called salt-frost scaling. This paper deals only with internal frost attack, simply because the mechanisms behind salt scaling are not very well-known. Besides, since salt scaling only affects the outmost millimetres of the concrete, it is not very plausible that self-desiccation has any long-term effect in a very moist environment.

2. FREEZING OF THE GREEN CONCRETE

2.1 Introduction

The green concrete, by which is meant concrete during the time from casting until it is set, or until a few hours after this, has a very low tensile strength. Therefore, it cannot resist the stresses occurring when the pore water freezes in completely saturated pores. It cannot even resist the hydraulic pressure occurring when excess water is expelled from the pore where water is freezing to air-pores or compaction pores. The spacing between these pores is perhaps 0.5 mm for air-entrained concrete and more than 1 mm for non-air-entrained concrete. These are too high values to secure frost resistance of a green concrete. Therefore, ordinary air-entrainment will not protect a green concrete from frost damage. The so-called critical spacing factor of green concrete is probably much less than 0.1 mm. This means that the 9% volume expansion has to be taken care of locally at the site of freezing. In principle, there should be one air-space in immediate contact with each pore in which water freezes. The only way to arrange this is to make use of the self-desiccation when sealed concrete hydrates. In this paper, a criterion will be developed for the required degree of hydration for protection of green concrete to early freezing.

2.2 Semi-empirical relation

Jung [1] studied the relation between freezing expansion of self-dessicated concrete and the degree of hydration, indirectly determined by the water uptake due to the "chemical contraction" when mixing water was bound chemically. The latter experiments were made by means of a pycnometer in which the reduction of the water level in a capillary tube could be monitored. Jung's results are shown in Fig 1.

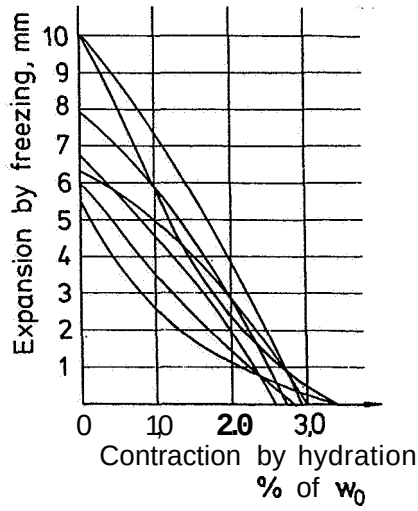

Fig 1: Experimental relation between the frost expansion of the green concrete and the chemical shrinkage; [1].

The bigger the contraction, the smaller the frost damage. It seems as if no frost damage occurs if the following criterion is fulfilled:

$$\Delta w_n/c \geq 0.03 \cdot w_o/c \quad (1)$$

where Δw_n is the volume reduction of chemically bound water [litre], c is the cement content [kg], and w_o/c is the water cement ratio. $\Delta w_n/c$ is calculated by:

$$\Delta w_n/c = (1-v_n) \cdot \alpha \cdot w_n^o/c \quad (2)$$

where v_n is the specific volume of chemically bound water [litre/kg], a is the degree of hydration and w_n^o is the amount of chemically bound water at complete hydration. For normal OPC the following values are valid: $v_n \approx 0.75$, $w_n^o \approx 0.25$. Thus, the criterion for frost resistance of the green concrete is:

$$\alpha \geq 0.03/\{(1-0.75 \cdot 0.25\} \quad (3a)$$

Or:

$$a \geq 0.48 \cdot w_o/c \quad (3b)$$

2.3 Theoretical relation

Frost damage will not occur when the effective degree of saturation of the capillary pores fulfils the following relation; see Fig 2:

$$S_{c,f} = w_f/(w_f+a_c) = w_f/(w_f+0.09 \cdot w_f) \leq 0.917 \quad (4)$$

where $S_{c,f}$ is the "effective" degree of saturation of the capillaries, w_f is the freeezable water in the capillaries [litrellitre], and a_c is the air-filled volume in the capillaries [litre/litre]. The normal air-pores and compaction pores are not considered since they could not - as said in paragraph 2.2 - serve as recipients for expelled water. Criterion (4) implies that there must be an air-filled space in the capillaries that is at least 9% of the volume of the freezable water. Self-desiccation is the only method by which such air-filled spaces can be created. The amount of air-spaces created by self-desiccation is:

$$a_c = (1-v_n) \cdot \alpha \cdot w_n^o \quad (5)$$

Therefore, the criterion for frost resistance is:

$$0.09 \cdot w_f \mathbf{I} (1-v_n) \cdot \alpha \cdot w_n^o/c \quad (6)$$

The required degree of hydration is:

$$\alpha \geq 0.09 \cdot w_f/\{(1-v_n) \cdot (w_n^o/c)\} \quad (7)$$

Or, with the values for v_n and w_n^o inserted:

$$\alpha \geq 1.44 \cdot w_f/c \quad (8)$$

The problem is to estimate the amount of freezable water of the green concrete.

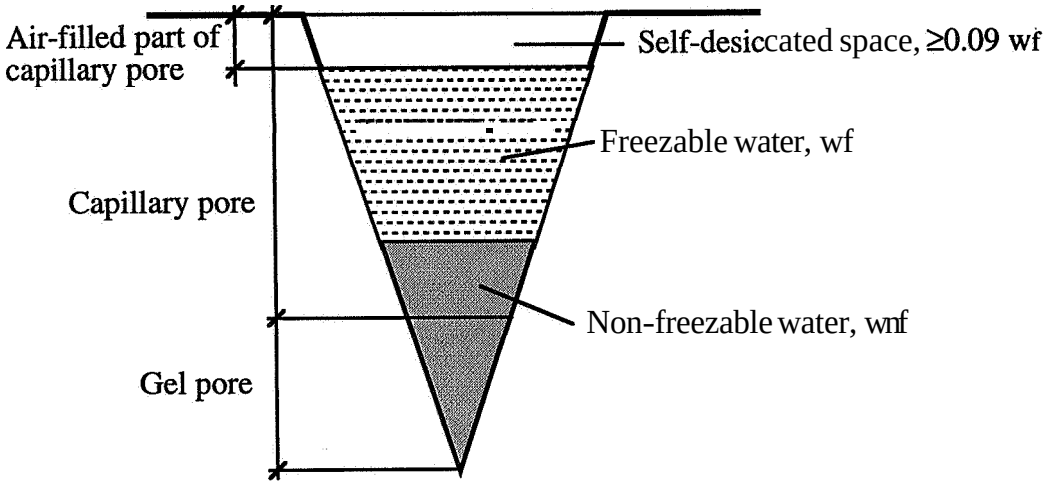

Fig 2: Schematic picture of a self-desiccated pore system at the required degree of hydration

(a) The maximum possible amount of freezable water:

The freezable water is:

$$w_f/c = w_e/c - w_{nf}/c \quad (9)$$

where w_e is the evaporable water and w_{nf} is the non-freezable water.

According to measurements by Powers and Brownyard [2] the amount of non-freezable water for completely dried, and then resaturated cement paste, is at -12°C:

$$w_{nf} = 1.04 \cdot w_n/c \quad (10)$$

where w_n is the nonevaporable water.

The evaporable water of self-desiccated concrete is.

$$w_e/c = w_o/c - w_n/c \quad (11)$$

Then, the maximum amount of freezable water is:

$$w_{f,max}/c = w_o/c - w_n/c - 1.04 \cdot w_n/c = w_o/c - 2.04 \cdot w_n/c = w_o/c - 2.04 \cdot \alpha \cdot w_n^o/c \quad (12)$$

Inserting the value 0.25 for w_n^o gives:

$$w_{f,max} = w_o/c - 0.51 \cdot \alpha \quad (13)$$

Inserting this in eq (8) gives:

$$\alpha = 1.44(w_o/c - 0.51 \cdot \alpha) \quad (14)$$

Or:

$$\alpha \geq 0.83 \cdot w_0/c \quad (15)$$

This value is much higher than that derived from Jung's experiments, eq (3b). The reason is that the amount of freezable water is exaggerated. In the real case, the green concrete has no chance to dry. Therefore, the amount of freezable water is much lower.

(b) The most probable amount offreezable water

Vuorinen made some determinations of the freezable water for virgin concrete that was never dried but completely saturated; [3]. His results can be expressed:

$$w_f/c \approx 0.65 \cdot (w_{e,max}/c)^2 \quad (16)$$

where $w_{e,max}$ corresponds to the total porosity (air-pores and compaction pores excluded) [litres/litre]. $w_{e,max}$ is:

$$w_{e,max}/c = w_0/c - v_n \cdot w_n/c = w_0/ - v_n \cdot \alpha \cdot w_n{}^0/c = w_0/c - 0.75 \cdot \alpha \cdot 0.25 = w_0/c - 0.19 \cdot \alpha \quad (17)$$

Then, the freezable water is:

$$w_f = 0.65(w_0/c - 0.19 \cdot \alpha)^2 \quad (18)$$

In reality, the amount of evaporable water is smaller than $w_{e,max}$ due to self-desiccation. The reduction corresponds to:

$$\Delta w_e/c = (1-v_n) \cdot \alpha \cdot w_n{}^0/c = (1-0.75) \cdot \alpha \cdot 0.25 = 0.0625 \cdot \alpha \quad (19)$$

Then, the freeezable water is:

$$w_f = 0.65(w_0/c - 0.19 \cdot \alpha)^2 - 0.0625 \cdot \alpha \quad (20)$$

Insertion in eq (8) gives:

$$\alpha = 1.44\{0{,}65(w_0/c - 0.19 \cdot \alpha)^2 - 0.0625 \cdot \alpha\} \quad (21)$$

An approximate solution to this equation is:

$$\alpha \geq 0.64 \cdot (w_0/c)^{1.8} \quad (22)$$

The differences between the theoretical eq (22) and the semiempirical eq (3) are comparably small, which is shown by the following examples:

w_0/c	Required α	
	eq(3b)	eq(22)
0.40	0.19	0.12
0.50	0.24	0.18
0.60	0.29	0.26
0.70	0.34	0.34
0.80	0.38	0.43
0.90	0.43	0.53

Eq (22) is based on a rather limited experimental background. Probably, a more certain relation might be derived if the freezable water of the green concrete was better known. It is therefore recommended to use eq(3b).

It can be mentioned that the semi-empirical eq (3b) should be arrived at by the theory just presented if the freezable water was:

$$w_f/c = 0.33 \cdot (w_0/c) \qquad (23)$$

This equation is obtained by making eq (3) equal to eq (8):

$$\alpha = 0.48 \cdot (w_0/c) = 1.44 \cdot (w_f/c) \qquad (24)$$

2.4. The requred pre-curing time

It takes some time to reach the required degree of hydration. This time can be calculated when the hydration-time curve is known. A suitable expression is:

$$\ln\alpha = A \cdot (\ln t)^B \qquad (25)$$

where A and B are constants that are different for different cements. For Swedish OPC A=-10 and B—2 when the time t is in hours and the hydration temperature is +20°C.

This means that the following pre-curing times at +20°C are needed when the criterion eq (22) is used.

w_0/c	required α	required time(hours)
0.40	0.12	9
0.50	0.18	11
0.60	0.26	16
0.70	0.34	21
0.80	0.43	31
0.90	0.53	53

The calculated pre-curing times correspond fairly well with the upper values determined experimentally [4] ; see Fig 3.

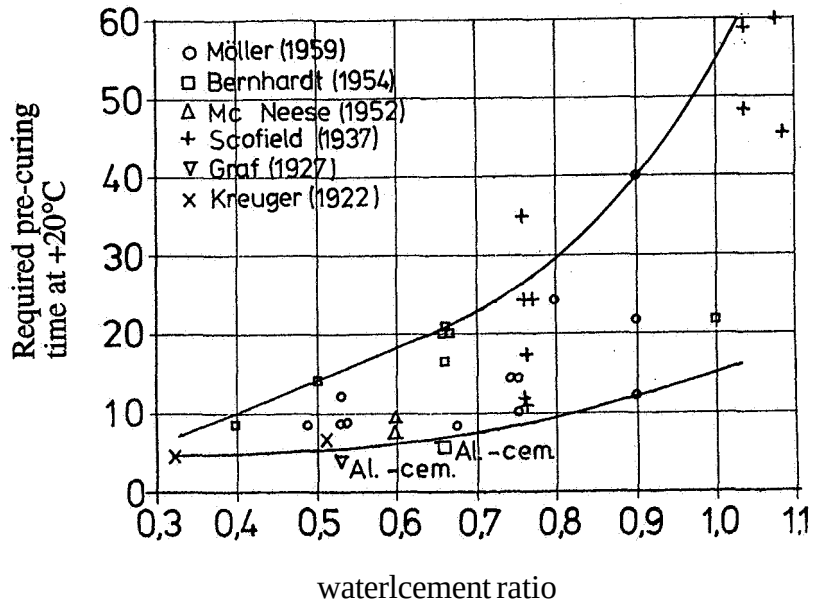

Fig **3:** Experimentally determined required pre-curing times as function of the waterlcement ratio; [4].

3. FREEZING OF THE HARDENED CONCRETE

3.1 Normal concrete

In normal concrete (water/binder-ratios above 0.40), the capillary pore system will always be completely saturated at very moist outdoor conditions. In very moist conditions, the air-pore system will also be partly filled with water. Self-desiccation plays no role in these types of concrete. Even if self-desiccation should occur, the desiccated pores would rapidly be re-saturated after a short period of exposure to water.

In order to make the concrete frost-resistant it is necessary to provide it with an air-entrained pore system of such qualities that the spacing factor will not be transgressed during natural conditions. **A** method to calculate the required air-pore volume, considering the water absorption in the finer air-pores, is given in [5].

3.2 High performance concrete

In high performance concrete (water/binder ratio well below 0.40), considerable self-desiccation will occur. The reduction in RH will depend on the shape of the desorption isotherm; the more horizontal the isotherm, the bigger the reduction in RH. Examples of the equilibrium RH of concrete stored in sealed condition are shown in Fig 4 and for concrete stored in water in Fig 5; [6]. The lower the water/binder ratio, the lower the residual RH. The effect is bigger for concrete with silica fume. For waterlcement ratios above 0.40 the effect of self-desiccation is marginal.

There is a theoretical relation between the freezing point of capillary condensed water and the RH at which capillary condensation occurs at a given temperature. For +20°C the following relation is valid (it is based on the assumption that the ice is under ordina-

ry atmospheric pressure whilst the water is exposed to an under-pressure determined by the Kelvin equation:

$$\ln\Phi = \{\Delta H/(R \cdot 293)\} \cdot \ln(T/T_0) \qquad (26)$$

where Φ is the relative humidity, AH is the molar heat of fusion [$\Delta H = M(334+2\cdot\theta)\cdot 10^3$ J/kmol where θ is the temperature in °C], T [°K] is the freezing point and T_0 [°K] is the freezing point of bulk water (273.15 °K). Examples are:

RH [%]	Freezing point [°C]
100	±0
98	-2
95	-6
92	-10
88	-15
85	-20
79	-30
74	-40

Therefore, if the internal RH can be lowered to 85% there will be no freezable water in the concrete at -20°C. Fig 5 shows that it is reasonable to believe that this reduction in RH will occur in water-stored concrete with low water/binder ratio. 85% RH might be reached in water-stored concrete after 3 months when the water/binder ratio is below 0.25 for pure OPC and below 0.33 for OPC+10% silica fume.

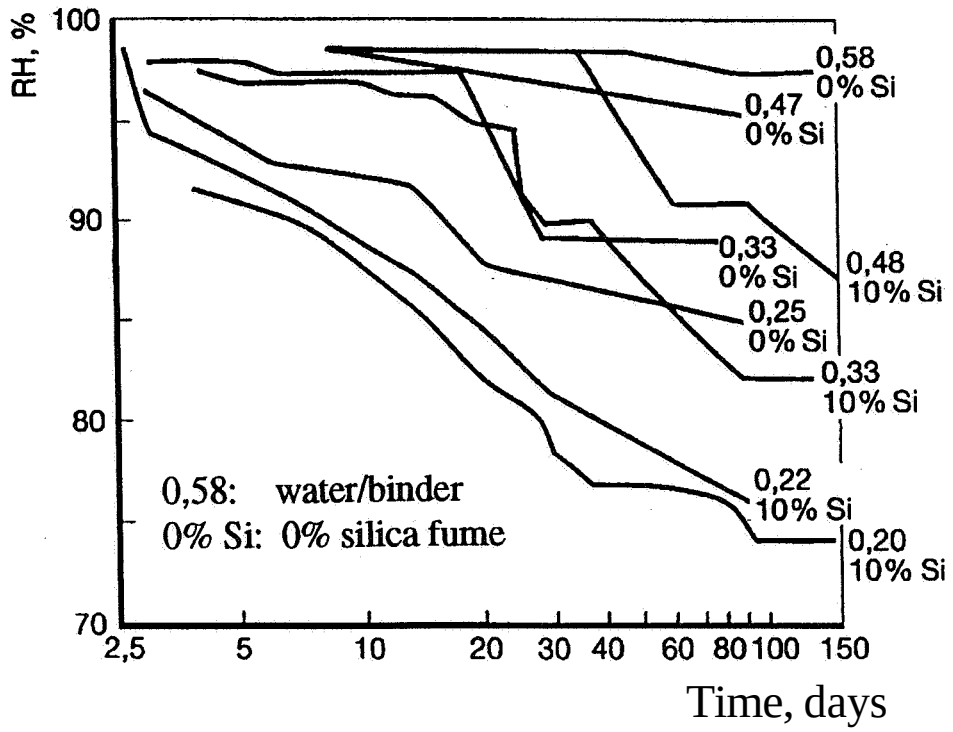

Fig 4: RH in sealed concrete; [6]

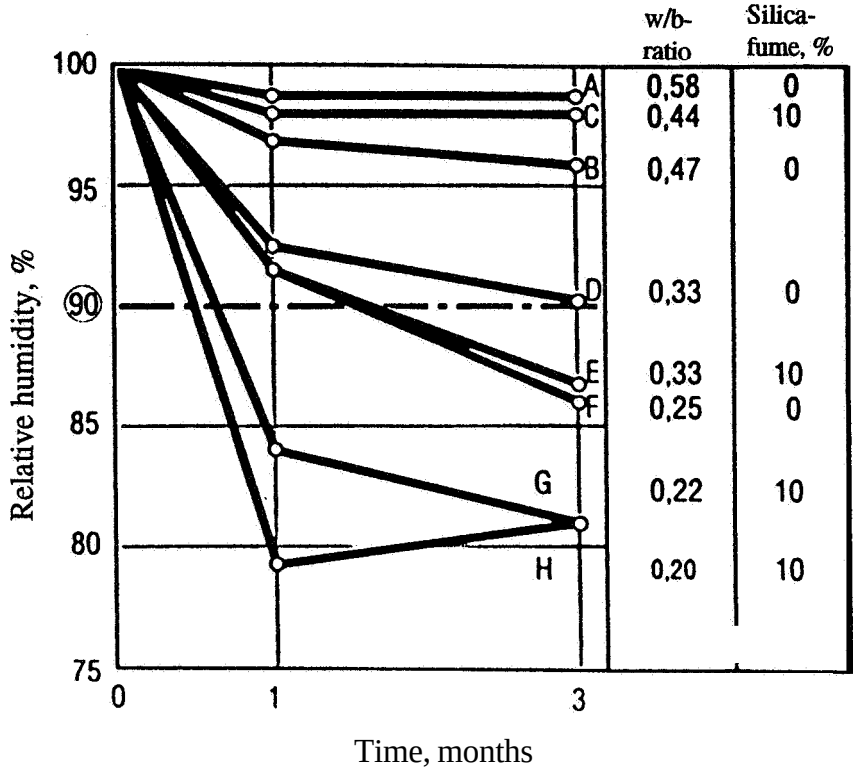

Fig 5: RH measured 5 cm from the surface of concrete immersed in water; [6].

3.2 Long-term effects

It was shown in Fig 5 that a concrete can maintain its self-desiccated state for a long period (months). Similar observations have been made on real concrete stored in sea water for a long time (decades); [7]. One cannot rule out, however, that water could enter the self-desiccated pores if the concrete had the possibility to absorb water during a very long period. Such a water absorption could perhaps be stimulated by repeated freezing and thawing cycles. Water might also enter some "defect pores" in the concrete, such as cracks, interface zones, some air-pores etc. Then some freezable water will appear in the concrete. **A** certain amount of freezable water is required if the concrete is to be frost-damaged. If all water is frozen in situ, without moisture transfer to other places during the freeezing process, a very small amount of water can severely harm the concrete. In [8] it is shown that a freezable water content as low as 15 to 20 litres/m^3 in the cement paste phase might be sufficiently high (correspond to about 5 litres/m^3 in the concrete). Therefore, one cannot rule out the posiibility that a self-desiccated concrete with no air entrainment placed in a very moist environment gradually becomes less frost-resistant.

3.3 Self-desiccation and frost-resistance testing

Self desiccation is important for frost testing. If the test is started within a few weeks after casting, as is usually the case, the concrete might be self-desiccated to such a high degree that it will not be frost-damaged. On the other hand, if the same concrete is stored for a long time in water before the test is started, it might contain so much freezable water that it becomes frost-damaged.

The same thing might happen if a moist freezelthaw test is prolonged by applying more freeze/thaw cycles than normal. Due to the repeated freezing and thawing, water absorption might become accelerated. Therefore, it might be that concrete that was judged frost-resistant after the normal number of freezelthaw cycles is judged non-resistant when the number of cycles is high. This type of behaviour has been observed by

Petersson [9] for concrete containing silica fume; see Fig 6. The test is a salt scaling test which is perhaps not quite relevant for the reasoning. The scaling is so big, however, that the interior part of the concrete is also damaged. The concretes with silica fume suffer accelerated destruction after about 25 freeze/thaw cycles, while the OPC-concretes have retarded destruction on a very low level (it must be observed that a scaling of 100 g/m^2, valid for the OPC-concretes, corresponds to a scaling depth of only 0.05 mm. Therefore, the difference between the concretes with silica fume and the OPC-concretes is very great). It is not clear what the reason is behind the observed behaviour. It might be due to a water absorption that turns a self-desiccated and therefore frost-resistant concrete into a saturated and therefore frost-sensitive concrete. It is quite clear that a non-air-entrained concrete with a water/binder ratio of 0.35 containing silica fume is not automatically frost resistant.

In the same report [9] it was also shown that a concrete with a waterhinder ratio as low as 0.25, and with 5% silica fume, had a scaling of 5.5 kg/m^2 after 56 cycles, which corresponds to a scaling depth of almost 3 mm.

At our laboratory we are now performing a test in which 26 different air-entrained and non-air-entrained concretes with water/binder ratio from 0.40 to 0.27 and with 0%, 5% and 10% silica fume are exposed to single freeze/thaw cycles or 10 repeated cycles, after water storage up to 3 years. Some of the specimens have been exposed to an cial ageing consisting of 3 repeated cycles of drying at +40°C and resaturation in water. The freeze/thaw test is based on measurements of the length changes during freezing. So far, specimens stored in water for 3 months and 1 1/2 years have been tested; [10] and [11].

Results for non-air-entrained concrete with watericement ratio 0.30 and no silica fume are shown in Fig 7 and 8. The test performed after 3 months of water storage - Fig 7 - indicates no frost dilation, neither at freezing temperatures, nor after complete thawing. The test performed after 1 1/2 years of water storage - Fig 8 - indicates a dilation of about 10 µm corresponding to a strain of 0.04‰ or about 30% of the tensile strain capacity. The specimens will be stored for another 1 1/2 years in water before they are freeze-tested again.

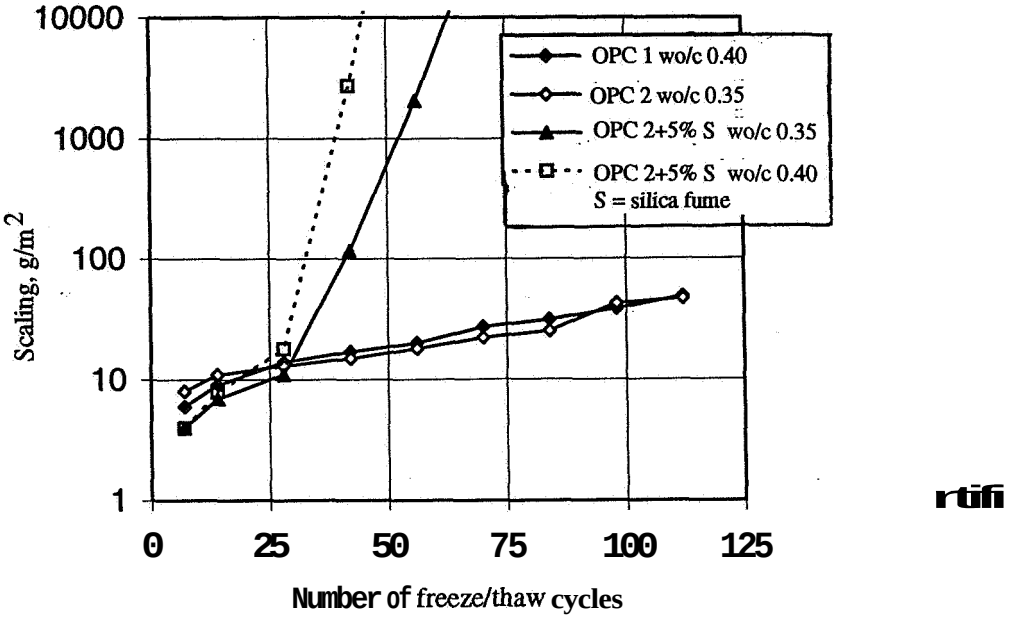

Fig 6: Salt-frost scaling of concretes with pure OPC and with OPC+5% silica fume; [9].

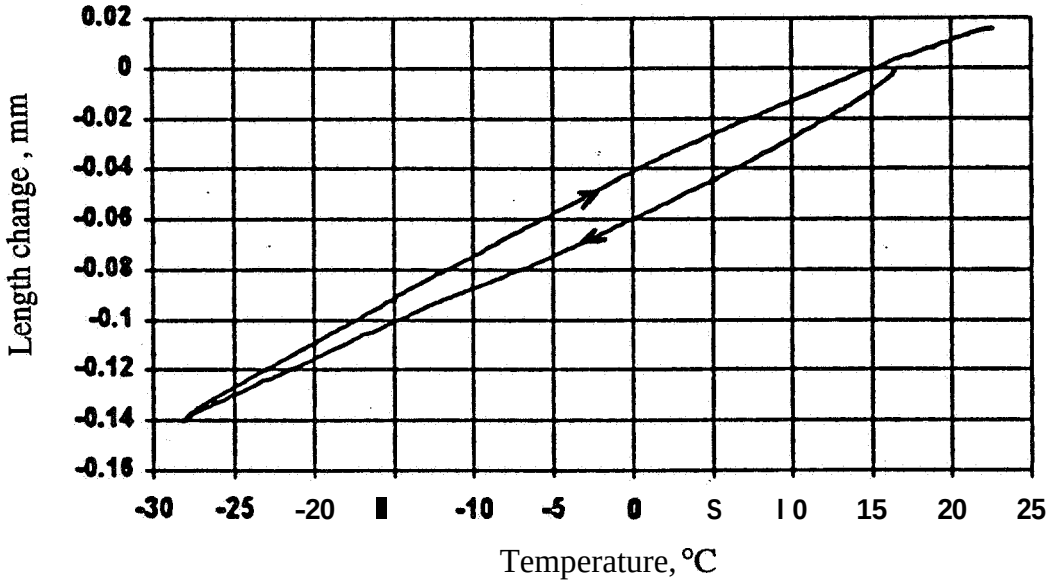

Fig 7: Measurements of the length change of concrete (w_0/c=0,30, no air-entrainment, no silica fume) during a freeze/thaw cycle to -28°C. Continuous water storage 3 months before the test; [10] (Note: The hysteresis between the freezing curve and the melting curve is due to a very rapid temperature cycle. There is no dilation during the freezing phase and no permanent dilation.)

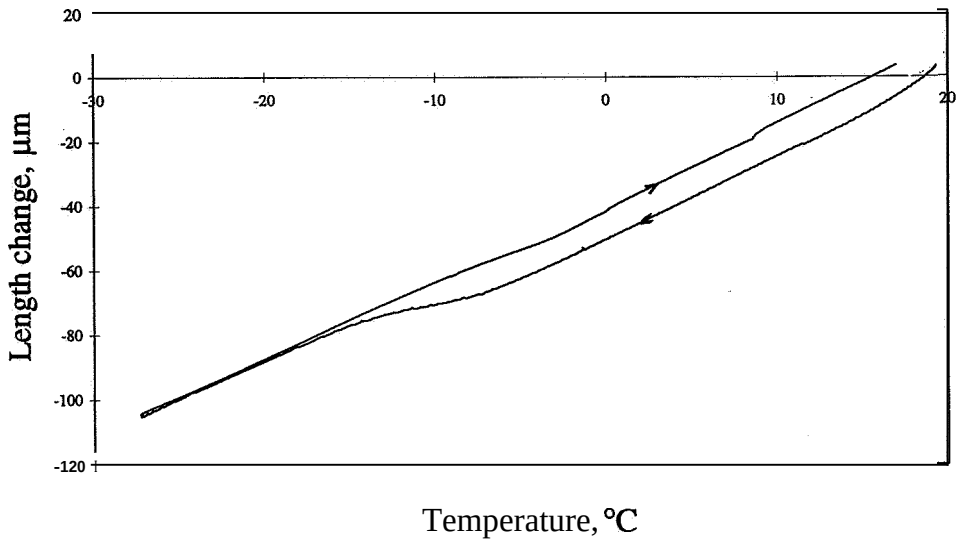

Fig 8: Measurements of the length change of concrete (w_0/c=0,30, no air-entrainment, no silica fume) during a freeze/thaw cycle to -28°C. Continuous water storage 11/2 years before the test; [11] (Note: There is a small dilation during the freezing phase, and a small permanent expansion after melting.)

REFERENCES

1. Jung, F. (1967) Über die Frostbeständigkeit des jungen Betons, Zement-Kalk-Gips, Nr 3
2. Powers, T.C. and Brownyard, T.L. (1948) Physical properties of cement paste, Research Laboratories of the Portland Cement Association, Bulletin 22, Chicago.
3. Vuorinen, J. (1973) On determination of effective degree of saturation of concrete, Concrete and Soils Laboratory, Oulu, Finland.
4. Möller, G (1962) Early freezing of concrete, Swedish Cement and Concrete Research Institute, Applied Studies No 5, Stockholm.
5. Fagerlund, G (1996) The required air content of concrete, In Frost Resistance of Building Materials (ed. S. Lindmark), Div. of Building Materials, Lund Institute of Technology, Report TVBM-3072, Lund.
6. Persson, B. (1992) Hydration, structure and strength of high performance concrete, Div. of Building Materials, Lund Institute of Technology, Report TVBM-1009, Lund. (In Swedish with English summary)
7. Hedenblad, G. (1997) Private communication concerning a field investigation of a marine concrete structure exposed to sea water at the Norwegian coast, Div. of Building Materials, Lund Institute of Technology, Lund.
8. Fagerlund, G. (1995) Frost resistance of high performance concrete - some theoretical considerations. In Durability of High Performance Concrete (ed. H. Sommer), RILEM, Cachan.
9. Petersson, P-E (1995) The salt-frost resistance of concrete - field tests, Swedish National Testing and Research Institute, SP Report 1995:73, Borås. (In Swedish with English summary)
10. Svensson, T. (1997) Frost resistance of high performance concrete, Div. of Building Materials, Lund Institute of Technology, Report TVBM-5032, Lund. (In Swedish with English summary)
11. Nordstrom, K. (1997) Private communication concerning an ongoing experimental study, Div. of Building Materials, Lund Institute of Technology, Lund.

SURFACE CRACKING OF HIGH STRENGTH CONCRETE - REDUCTION BY OPTIMIZATION OF CURING REGIMES

U. GUSE, H.K. HILSDORF
Institut für Massivbau und Baustofftechnologie
University of Karlsruhe
Germany

ABSTRACT

In an experimental investigation the extent of cracking was determined for High Strength Concretes cast with different waterlcement ratios with and without silica fume. The crack length per unit area increased with decreasing waterlcement ratio and was most pronounced at the surface. Such cracks may be harmful for the durability of a structure since they significantly increase the permeability of a concrete. The extent of cracking may be reduced by means of a special curing method which allows the addition of water to the concrete surfaces while the concrete is still in the mould.

THE PROBLEM

High Strength Concrete (HSC) with water/cement ratios < 0.4 is also considered a highly durable material and, therefore, often is also referred to as High Performance Concrete (HPC). Nevertheless, HSC is brittle and rather vulnerable to cracking, particularly at an early stage of hydration. This has been shown in various experimental investigations including studies on unrestrained and restrained shrinkage of HSC [1, 2, 3, 4]. The authors generally attribute early cracking to self-desiccation and subsequent autogeneous shrinkage of HSC. It is also pointed out that for the prediction of shrinkage of HSC distinction has to be made between autogeneous shrinkage and drying shrinkage [5].

Preliminary studies at our laboratory have shown, that early cracking of HSC significantly increases the surface permeability of HSC and leads to substantially increased depths of carbonation in the vicinity of surface cracks. Therefore, an investigation was carried out to study the extent of surface cracking in HSC, and to optimize curing regimes such that early cracking is reduced [6].

ANALYSIS OF SURFACE CRACKING

Already after demoulding at an age of 24 hours cracks with a spacing of approx. 5 to 10 mm on the surface of the HSC specimens became visible after spraying the surfaces with water and subsequent drying.

The extent of microcracking was determined experimentally for the concretes listed in TABLE-1. Different types of specimens were demoulded after one day and then stored at 20 °C and 65 % r.h. either unprotected or wrapped in wet burlap and vapourproof sheets for a period of 6 days, respectively, resulting in a total curing period of 1 or 7 days.

TABLE-1
Mix proportions of the concretes

No.	w/c or w/(c+sf)[6]	C[1] CEM 142.5 R (kg/m³)	sf[2] (% by c-mass)	sp[3] (% by c-mass)	Aggregates (kg/m³)	Flow[4] (cm)	Compressive strength[5] (N/mm²)
1	0.5	350		-	1880	45	63
2	0.3	500	-	5	1760	55	92
3	0.3	450	10	5	1760	55	112
4	0.25	500	10	6	1730	42	115

[1] cement, Blaine: 3630 cm²/g
[2] silica fume (dry weight of the slurry)
[3] superplasticizer (45 % dry weight)
[4] as measured on the flow table acc. to ISO 4103
[5] cubes a = 150 mm, age 56 days (7 days moist, subsequently 20 "C, 65 % r.h.)
[6] taking into account the water in the superplasticizer and in the silica fume slurry

For the microscopic analysis, samples have been taken from concrete cubes, side length 100 mm, after 2 years of storage at 20 °C and 65 % r.h. directly from a concrete surface, which was in contact with the formwork, and from a section perpendicular to the concrete surface (peripheral zone, distance from the surface: 1 … 20 mm). Prior to the microscopic evaluation the samples were ground and polished.

It has been found that the HSC samples showed a typical crack pattern. The cracks, with widths up to 25 pm, followed the aggregate-matrix interfaces, indicating that these cracks have been formed at a very early stage of hydration i.e. at a concrete age not exceeding 1 day. A another observation was, that cracks run through the matrix at locations where the distance between two aggregate particles was small.

The results of the crack analysis are summarized in FIG.-1. This figure shows, the crack length per unit area, the density of cracks (mm/cm²), for concrete surfaces and for sections perpendicular to the concrete surfaces, respectively. From this it follows, that the extent of cracking of the concretes with $w/c < 0.5$ is substantially higher than that of conventional concrete. In particular, a reduction of $w/(c+sf)$ from 0.30 to 0.25 led to a marked increase of cracking. Also an increase of the duration of curing from 1 to 7 days resulted in a substantial increase of the extent of cracking particularly at the concrete surfaces. It is likely, that this is due

to the increased restraint of drying shrinkage of the outer layers of the concrete cubes by the core of the specimens which has attained a higher stiffness due to the longer duration of curing prior to the commencement of drying. No significant difference in density of cracks seems to exist between concretes with or without silica fume for a given w/c or w/(c+sf).

In all cases the total crack length per unit area (density of cracks) in the peripheral zone of the section perpendicular to a concrete surface was less than the corresponding values of the concrete surfaces. From this it follows, that the extent of cracking decreased with increasing distance from the concrete surface.

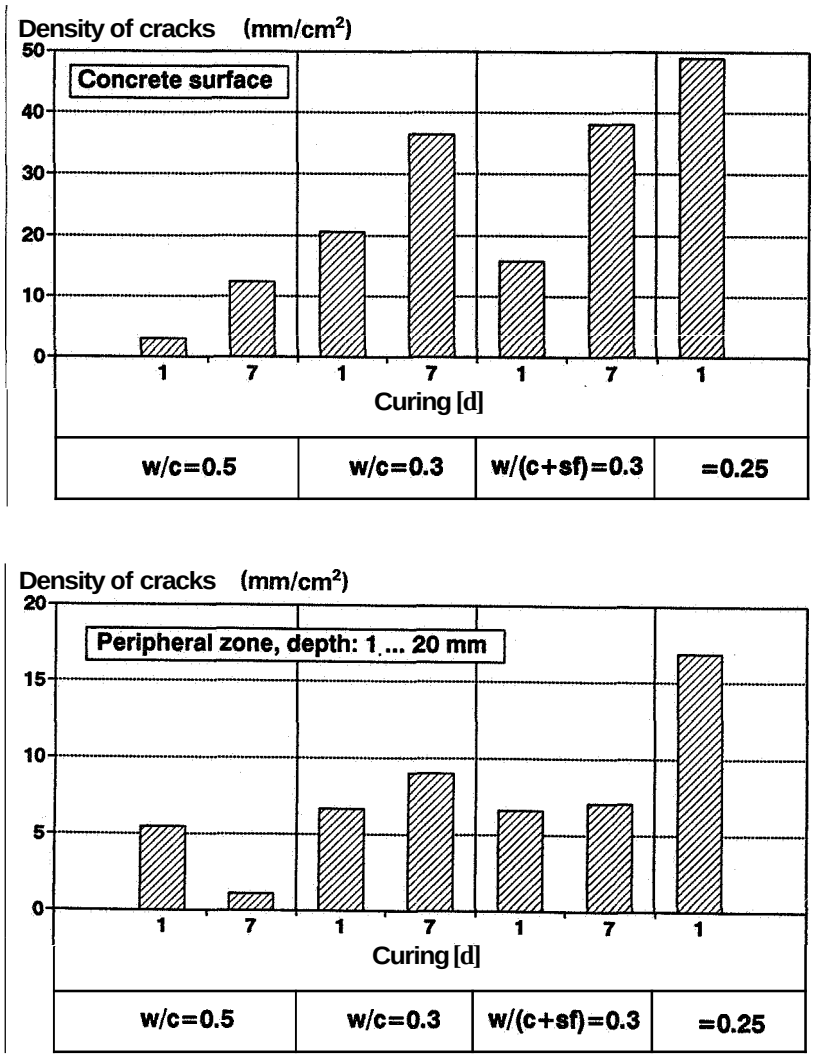

FIG.-1
Results of crack analysis

EXPERIMENTS TO REDUCE SURFACE CRACKING

Based on the results given in the preceding section, curing paramaters have been varied with the objective to reduce the extent of surface cracking. For these experiments the concrete with the highest crack length per unit area has been chosen i.e. concrete No. 4 acc. to TABLE-1 with $w/(c+sf) = 0.25$.

The experiments were based on the observation, that a significant part of the cracks had developed during the early stage of hydration, i.e. during the initial 24 hours after casting, and that these initial cracks were caused by self-dessication and autogeneous shrinkage as will be dealt with in more detail in the section "discussion" of this paper. Therefore, it should be possible to reduce such cracks by providing additional water to the concrete as soon as possible. For this two approaches appeared to be feasible:

- demoulding as soon as possible after initial set and immediate water curing of the concrete surfaces;
- continuous water curing of all concrete surfaces soon after casting while the concrete is still in the mould.

In preliminary experiments it became apparent that demoulding HSC specimens 8 hours after casting and subsequent curing with wet burlap and vapour-proof sheets resulted in a reduction of the surface permeability, indicating that such an approach can be effective in reducing surface cracking. However, there are obvious practical limitations to such methods under site conditions.

Therefore, the second alternative given above has been studied in more detail. The necessary equipment and materials are commercially available and had already been tested under site conditions though with another objective:

Plastic fleeces which can absorb a considerable amount of water are attached to the surfaces of the formwork facing the concrete. After placing a fresh concrete with a waterlcement ratio in the normal range of 0.5 to 0.6 into the form work the fleece absorbs a significant amount of water from the fresh concrete. The corresponding reduction of the water/cement ratio of the surface layers leads to a signifcant improvement of the resistance of the concrete to carbonation, abrasion, freezing and thawing and deicing salts [8, 9].

The objective of our investigation was to reverse the action of such fleeces in so far as they may provide additional water for early curing of the concrete rather than to reduce its water content in the fresh state. The set-up of this special curing method is shown in FIG.-2.

The fleece used in the experiments is a porous polypropylene (PP) sheet which intially is hydrophobic. Since this particular property could have been disadvantageous for the intended application of the fleece, some of the fleeces were made hydrophylic by treating them with an anionic tenside.

Also a combination with another fleece consisting of a polyester-wood fibre composite has been included in the study since this combination increased the water storage capacity. The various parameters studied are summarized in TABLE-2.

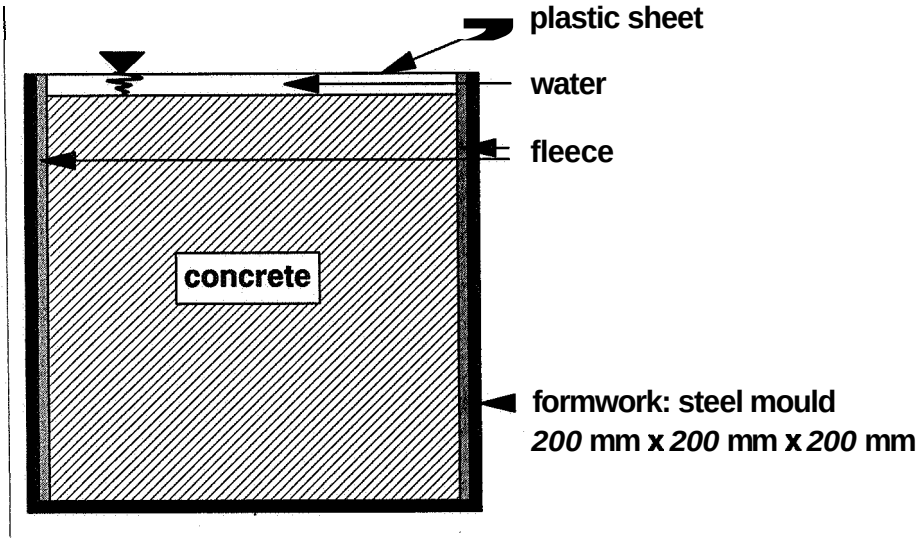

FIG.-2
Set-up to cure HSC by means of a water saturated fleece

TABLE-2
Parameter combinations investigated for the curing of HSC

No.	Description
1	- untreated steel mould, no addition of water
2	- fleece on steel mould, no addition of water
3	- fleece on steel mould, addition of water after casting
4	- hydrophylic fleece on steel mould, no addition of water
5	- hydrophylic fleece on steel mould, water saturated prior to casting, addition of water after casting
6	- hydrophylic fleece + polyester-wood fibre composite on steel mould, water saturated prior to casting, addition of water after casting

In the study concrete cubes, a = 200 mm, have been cast into steel moulds whose inner surfaces were lined with a fleece. For comparison also specimens without a fleece were manufactured. After casting, all specimens were covered with vapourproof polyethylene sheets. Water was added to the top of the specimens 1 hour after casting as shown in FIG.-2. It became apparent, that the hydrophylic fleece transported water much more rapidly than the untreated fleece. The specimens were demoulded 24 hours or 3 days after casting, respectively.

Immediately after demoulding the pemeability of concrete surfaces was determined acc. to [10]. The values obtained serve as a preliminary indicator of the extent of surface cracking.

After performing the surface permeability measurements the specimens were stored in a constant environment of 20 "C, 65 % r.h. up to an age of 56 days. At this time the surface permeability was measured again at locations differing from those where the measurements had been taken after demoulding. The measurements at an age of 56 days were taken without preconditioning the specimens by drying them with hot air as specified in [10]. The results achieved are summarized in FIG.-3.

From this it follows, that at the end of curing all specimens which had been cast in moulds containing a fleece (No. 2 - 6 acc. to TABLE-2) had a surface permeability which was significantly less than that of specimens cast in moulds without a fleece. At this stage there is no significant difference in the surface permeability of specimens cured for 1 day or for 3 days, respectively.

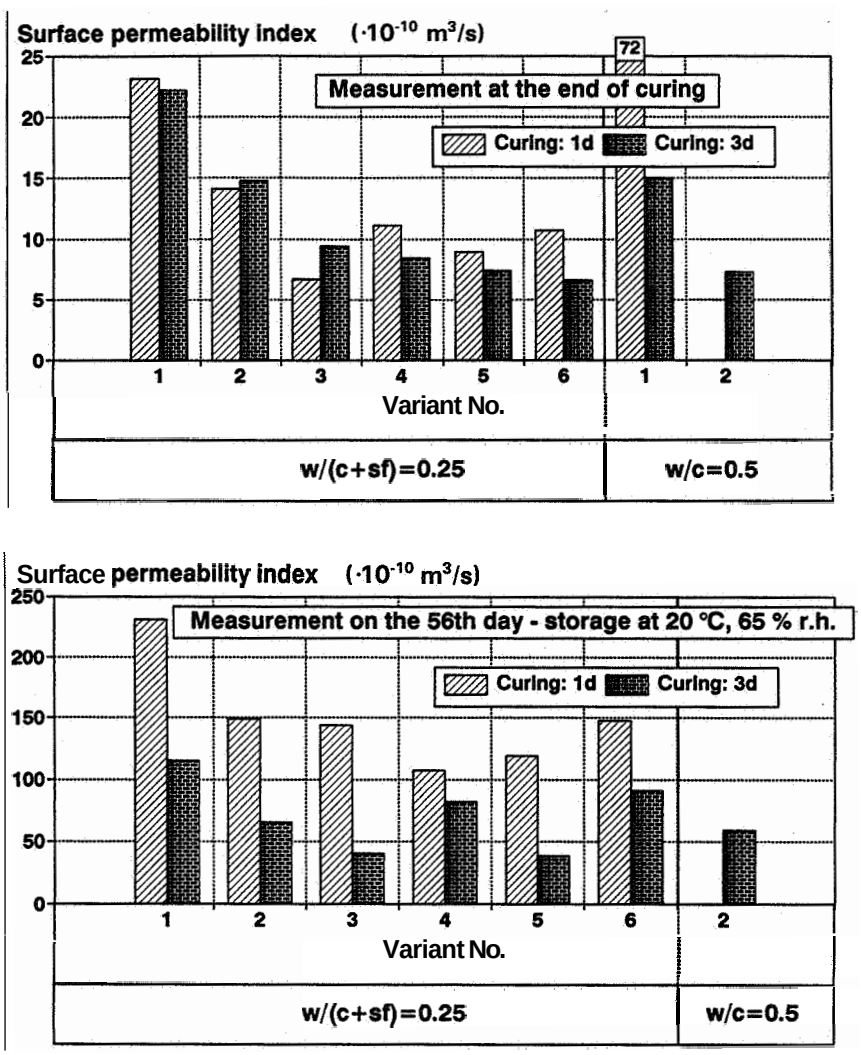

FIG.-3
Surface permeability of specimens cast in moulds lined with (No. 2 - 6) or without a fleece at the end of curing and after storage at 20 "C, 65 % r.h. up to the 56th day

Also at an age of 56 days the surface permeability of the specimens cast in moulds lined with a fleece was less than that of the reference specimens (No. 1). In all cases curing for 3 days led to a further reduction of the surface permeability. The lowest surface permeability was found in specimens which had been cured with the addition of water through the fleece in the mould for a period of **3** days (No. **3** and 5 acc. to TABLE-2).

FIG.-3 also gives the surface permeability of a conventional concrete with w/c = 0.5, kept in a steel mould with a fleece for **3** days, however, without the addition of water. The surface permeability of this concrete differs little from that of the HSC with w/(c+sf) = 0.25 and treated with the fleece. A microscopic examination showed, that the HSC cast in moulds with a fleece still showed surface cracks, however, the extent of cracking was significantly reduced compared to the surface cracks observed in the specimens manufactured without a fleece (TABLE-3). The values of the density of cracks in TABLE-3 are higher than the values given in FIG.-1. This effect may be traced back to the higher specific surface area of the silica fume which was employed in these experiments (24 m^2/g). The silica fume used in the earlier experiments (TABLE-1, FIG.-1) had a specific surface area of 14 m^2/g.

TABLE-3
Density of cracks in the surface of concretes with w/(c+sf) = 0.25 cast in moulds lined with (No. 2 -5) or without a fleece

Variant No. (acc. to TABLE-2)	Duration of curing (d)	Density of cracks (mm/cm^2)	Relative value
1	1 **3**	107.7 89.2	**1** 0.83
2	1 **3**	56.6 66.9	0.53 0.62
3	1 3	48.1 69.9	0.45 0.65
4	3	69.3	0.64
5	3	75.7	0.70

The pore size distribution of matrix samples taken from the surface near regions of HSC cast with and without fleece (No. 1, 3 and 6 acc. to TABLE-2, with 3 days of curing) has been determined by means of mercury intrusion porosimetry. The results are shown in FIG.-4. From this it follows, that the total pore volume intruded is higher in the case of applying a fleece with increased water storage capacity (No. 6) than that of the concrete treated with an ordinary fleece (No. **3)** and that of the concrete cast in steel moulds without a fleece. From this it may be concluded that the extra supply of water to the concrete surface immediately after casting with the help of a special composite led to an increase of the water/cement ratio of the surface near regions of the HSC which may have partially offset the positive effect of the supply of water at a later stage. Therefore, the optimum concrete age at which the supply of additional water should commence, has to be determined in more detailed studies.

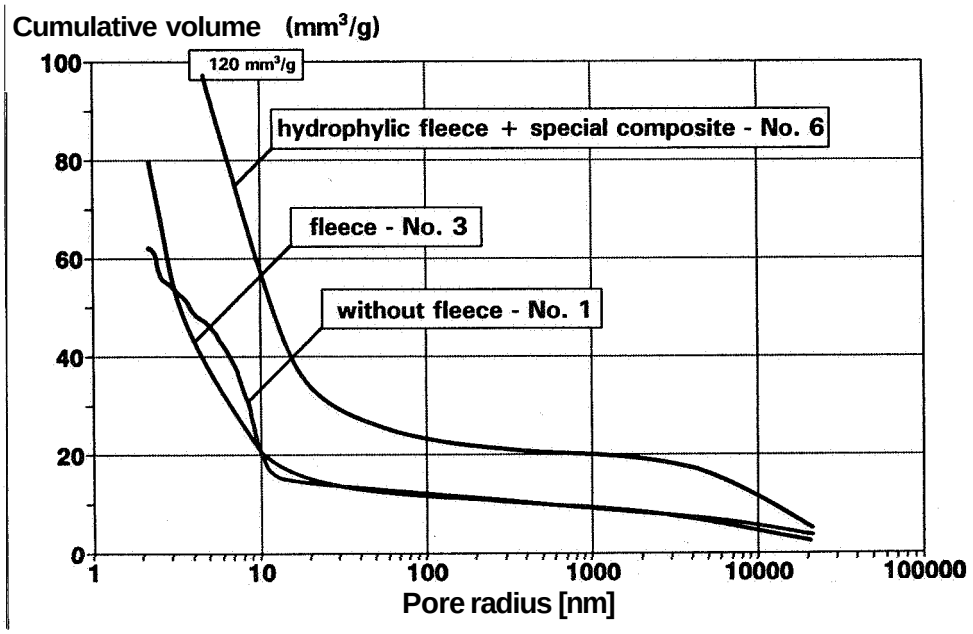

FIG.-4
Pore structure of the surface near regions

DISCUSSION

1. Effect of waterlcement ratio and autogeneous shrinkage on the extent of surface cracking

As pointed out in the problem statement of this paper, there is consensus among concrete researchers that early cracking in HSC is caused primarily by autogeneous shrinkage which in turn is due to self-desiccation of the concrete.

The effect of w/c on the process of self-desiccation and the corresponding volume changes can be demonstrated at least as a general trend on the basis of relations between capillary porosity, content of empty capillary pores due to self-desiccation and wlc as well as degree of hydration as given e.g. in [11] and [12]. These relations are based on the findings of Powers and Brownyard [13]. In FIG.-5 the decrease of capillary porosity with increasing degree of hydration $V_{cp} / V_{cp,m=0}$ as well as the fraction of capillary pores which became empty due to self-desiccation $V_{cp,empty} / V_{cp}$ are given as a function of the degree of hydration, m, for cement pastes with a waterlcement ratio of 0.25 and of 0.50, respectively. From this it follows, that the self-desiccation of pastes with w/c = 0.25 develops much more rapidly than that of pastes with w/c = 0.50. It should be kept in mind, however, that complete self-desiccation is not possible, because internal drying is accompanied by a reduction of the internal rel. humidity. As soon as the internal rel. humidity falls below approx. 80 %, hydration stops thus preventing further self-desiccation.

For the purpose of comparison let us consider the intersect of the relations for self-desiccation and for the reduction of capillary pore volume given in FIG.-5.

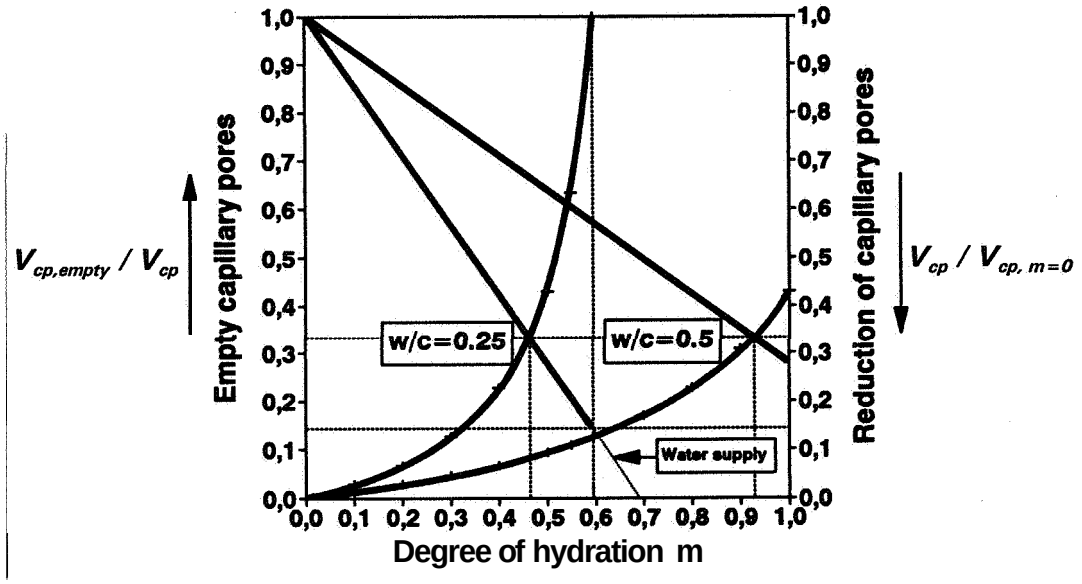

FIG.-5
Self-desiccation of capillary pores and reduction of capillary pore volume with increasing degree of hydration in cement pastes, w/c = 0.25 and 0.50, stored under sealed conditions

At this point the capillary porosity decreased to one third of its initial value, and one third of the capillary pores became empty due to self-desiccation. For a paste with w/c = 0.25 this intersect occurs for m = 0.46. For a paste made of a regular portland cement (CEM I) such a degree of hydration is likely to be reached already 24 hours after casting [14] and [15]. In contrast, in a paste with w/c = 0.50 the relations intersect at m = 0.93. For such a paste at least 28 days of storage under sealed conditions are necessary to reach such a degree of hydration [16]. This comparison underlines the significance of self-desiccation on the shrinkage behavior of low waterlcement ratio concretes and serves as a possible explanation for the effect of the waterlcement ratio on the cracking behavior of HSC.

In capillary pores which are not completely filled with water, capillary stresses develop acc. to well known relations given e. g. in [7] between capillary stresses and pore diameter. Based on these relations it may be shown that as w/c-ratio decreases the capillary pore radius decreases and the capillary stresses increase resulting in an increasing volume change of concrete [6]. Therefore the largest stresses should develop at our investigations in the concrete with silica fume and w/(c+sf) = 0.25 (TABLE-1). Acc. to FIG.-1 this concrete indeed showed the largest density of cracks both in the concrete surfaces and in the peripheral zone.

2. Discussion of experimental results

From the analysis of the crack patterns it follows that the extent of microcracking prior to the application of external stresses in HSC is 2 to 3 times larger than that in conventional concrete. Map cracking at the concrete surfaces which becomes visible under the microscope and which increases with decreasing waterlcement ratio is typical for this phenomenon. Such cracks

are initiated already at an early stage of hydration by self-desiccation and corresponding capillary stresses as has been discussed in the preceding section. Subsequent drying and the resulting drying shrinkage leads to a substantial growth of the cracks which had been initiated by self-desiccation in the surface near regions of the concrete. This follows from FIG.-1 which shows that the density of cracks in the concrete surfaces is 3 to 5 times the density of cracks in the peripheral zone of a section perpendicular to the concrete surface.

The use of a water absorbing fleece on the surface of the form work as a mean to add water to the concrete already during the early stages of hydration appears to be an effective method to improve the properties of the surface near regions of HSC if surface permeability and the density of cracks are taken as criteria. Continuous addition of water up to a concrete age of 3 days was particularly effective. However, the optimum concrete age at which the addition of water to the fleece should commence, still has to be investigated. From FIG.-4 it follows that too early addition of water may increase the water/cement ratio of the concrete whereas some self-desiccation may have occured already if the addition of water is initiated too late. An increase of the water storage capacity of the fleece did not result in a further improvement of the surface properties of the HSC. However, from FIG.-3 it follows that even without the addition of water the use of a fleece led to a reduction of the surface permeability of the HSC.

Furthermore, the fleece left a particular texture in the concrete surface which is free of larger pores. This texture of the fleece may have contributed to the increased resistance of the concrete surface to cracking.

CONCLUSIONS

In HSC self-dessication and subsequent drying shrinkage leads to the development of microcracks particularly in the surface near regions. As long as only the mechanical properties are of significance for a particular application of HSC, such microcracks are only of minor importance though they may lead to some reduction of the tensile strength of HSC.

However, the cracks have to be considered harmful, if the concrete has to satisfy certain durability requirements such as a high resistance to the penetration of liquids or gases, since the cracks will significantly increase the permeability of HSC particularly of the surface near regions.

Under such conditions the extent of cracking can be reduced and the permeability properties of the HSC may be improved by providing early water curing of the still immature concrete by means of a water absorbing fleece attached to the surface of the formwork facing the concrete. The sequence of an optimum curing regime should be investigated further.

REFERENCES

[1] Justness, H.; Reyniers, B.; Van Loo, D.; Sellevold, E.J.: An Evaluation of Methods for Measuring Chemical Shrinkage of Cementitious Pastes. Nordic Concrete Research, No. 1, 1994, pp. 45-61

[2] Paillere, A.M.; Buil, M.; Serrano, J.J.: Effect of Fiber Addition on Autogenous Shrinkage of Silica Fume Concrete. ACI Materials Journal, No. 2, 1989, pp. 139-144

[3] Bloom, R.; Bentur, A.: Restrained Shrinkage of High Strength Concrete. Proceedings International Conference High Strength Concrete 1993, Lillehammer 1993, pp. 139-144

[4] Summer, Th.; Schrage, I.: Hochfester Beton - Schwinden Kriechen und Reißneigung. DAfStb-Forschungskolloquium, TU Miinchen, 1993, pp. 147-150

[5] Dilger W.H.; Wang C.: Shrinkage and creep of high performance concrete (HPC). Adam Neville Symposium on Concrete Technology (eds. V.M.Malhotra), Las Vegas 1995, pp. 59-84

[6] Guse, U.; Hilsdorf, H.K.: Surface Cracking of High Strength Concrete. 4. Weimar Workshop on High Performance Concrete: Material Properties and Design (eds. F.H.Wittmann, P.Schwesinger), AEDIFICATIO, Freiburg 1995, pp. 69-89

[7] Grimsehl: Lehrbuch der Physik, Bd. 1., BSB B.G. Teubner, 1989

[8] Beddoe, R.E.; Springenschmid, R.: Einfluß von Schalungseinlagen auf die Dauerhaftigkeit von Beton. Concrete Precasting Plant and Technology, No. 2, 1995, pp. 80-88

[9] Marosszeky, M.; Chew, M.; Arioka, M.; Peck, Ph.: Textile Form Method to Improve Concrete Durability. Concrete International, No. 11, 1993, pp. 37-42

[10] Schonlin, K.: Permeabilitat als Kennwert der Dauerhaftigkeit von Beton. Heft Nr. 8 der Schriftenreihe des Instituts für Massivbau und Baustofftechnologie der Universitat Karlsruhe, 1989

[11] Hilsdorf H.K.: The Water Content of Hardened Concrete. Nuclear Radiation Shielding Studies, Report No. 4. University of Illinois, Urbana Ill., 1967

[12] Hansen T.C.: Physical structure of hardened cement paste. A classical approach. Matériaux et Constructions, N° 114, 1986, pp. 423-436

[13] Powers, T.C.,Brownyard, T.L.: Studies of the Physical Properties of Hardened Portland Cement Paste. Research and Development Laboratories of the Portland Cement Association, Research Department Bulletin, No. 22, Skokie Ill., 1947

[14] Yogendran, V.; Langan, B.W.; Ward, M.A.: Hydration of Cement and Silica Fume Paste. CCR, No. 5, 1991, pp. 691-707

[15] Zhang, M.H.; Gjorv, O.E.: Effect of Silica Fume on Cement Hydration in Low Porosity Cement Pastes. CCR, No. 5, 19 91, pp. 800-808

[16] Hilsdorf H.K.: Skriptum zur Vorlesung Baustofftechnologie. Sommersemester. Universität Karlsruhe, Institut für Massivbau und Baustofftechnologie, 1995

SHRINKAGE OF HOLLOW CORE SLAB CONCRETE

KLAUS JUVAS, ERIK NORDENSWAN
Partek Concrete Development Ltd.
FIN-21600 Pargas, Finland

ABSTRACT

The shrinkage of no-slump hollow-core slab concrete was studied at early age in a period of six to twelve months. It was noticed that increased water/cement ratio and dry curing conditions have a clear increasing effect on the shrinkage. The use of silica fume and wet curing have a decreasing effect on the shrinkage. The thermal expansion and the effect of the prestressing forces can also be noticed in the results. The general level of the shrinkage of no-slump concrete was rather low, 0,3 to 0,5 $^{o}/_{oo}$ in six months.

INTRODUCTION

The target of this investigation was to study the amount and effecting factors of shrinkage of no-slump concrete used in hollow-core slabs. A hollow-core slab is a prestressed concrete element, mostly used as a flooring structure. The main purpose of the hollows is to reduce the own weight of the element.
The extrusion technic is a normal production method of hollow-core slabs. In this method the water content of the concrete is very low and is often called no-slump concrete. The advantages of no-slump concrete are:

- good cohesion immediately after casting
- high early and ultimate strength
- good durability

TEST METHODS

The shrinkage was measured both at fresh stage and during the hardening time. The shrinkage of fresh concrete and the shrinkage during the first two days was measured by using an extensometer device combined to a computer data logger. The specimens were cylinders (o100*100 mm) made with the Intensive Compaction Tester (IC-tester). The IC-tester is a special device developed for testing no-slump concrete.

As the cylinders have a high fi-esh strength, it was possible to start the measurement immediately after casting. The cylinders were placed in plastic bags and two extensometer bridges (50 mm) were attached on the cylinders axially on both sides and pressed against the concrete with slack steel springs. The extensometer had a knife-type edge which guaranteed accurate positioning on the concrete surface. The pressure was adjusted so that the plastic bag was not perforated with the knife.
The water cured sample was prepared in the same way but the plastic bag was filled with a suitable amount of water. One sample was tested without cover in 40% relative humidity.

The shrinkage of hardened concrete was measured directly from a hollow-core slab with a mechanical measuring device. The slabs were cast at the Partek Precast Hyrylä factory in Finland.

The basic mix design of the concrete was:

- 300 kg/m^3 rapid hardening Portland cement
- 1980 kg/m^3 granite type sand and gravel
- waterlcernent ratio of 0,38

The variables in tests were:

- waterlcement ratio: 0.30 ...0.40
- different sections in hollow core slab: top and bottom surfaces
- use of silica fume: 0...8%
- use of superplasticizer: 0...1,5 %
- curing conditions: relative humidity40...100% and temperature 20...50°C

RESULTS AND CONCLUSIONS

The results are presented in the following Appendixes:

1. Effect of w/c-ratio, superplasticizer and silica. Curing of specimen in 20° C and 40% RH.
2. Effect of measured section and curing conditions of the hollow-core slab using the basic mix design.
3. Effect of curing conditions on early shrinkage using the basic mix design.

FIG.-1 in **App. 1** shows that the chance of waterlcement ratio has a clear effect but by adding a plasticizer the effect is weaker.
FIG.-2 shows that the use of silica fume has a clear reducing and retarding effect. The general shrinkage level after six months is between 0,3 to 0,5 $^{o}/_{oo}$ that is rather small compared to many other more flowable concretes used at the precast industry or ready mixed and cast-in-situ and presented in the literature (1), (2).

FIG.-3 in **App. 2.** The result presented shows that there is a clear difference if the shrinkage has been measured in the bottom or upper surface of the hollow-core slab. There is also a difference if the shrinkage has been measured lengthwise or crosswise. The shrinkage in the bottom is bigger than at the top. The reason is the prestressing force causing additional creep. Also the higher waterlcernent ratio at the lower section of the hollow-core slab has some effect. The prestressing force is probably also the reason why the lengthwise shrinkage in the top surface is smaller than the crosswise shrinkage.
FIG.-4 shows that both the temperature and humidity have a clear effect. In low temperatures the evaporation is slower which can be noticed in smaller shrinkage. In outdoor curing in wet conditions the slab swells and the shrinkage starts only after the slab is moved to dry indoor conditions.

Figures 5 and **6** in **App. 3** show the early shrinkage, the temperature rise and the effects of different curing conditions. It can clearly be seen that the part of the shrinkage occuring during the first **3** hours is very remarkable. After that period the shrinkage is retarding.

The thermal expansion due to the release of the heat of reaction and the heating from room temperature to 50°C is also effecting the results. The shrinkage without cover is three to four times larger than with cover during the observed period. The influence of an elevated temperature was smaller than expected, but this measurement had more disturbances than the others.

REFERENCES

A.M. Neville, Properties of Concrete, Longman Group Limited, 1995
Swedish Building Service Ltd. and Cements Ltd., Concrete Manual, Materials, Stockholm, 1994
K. Juvas, Very Dry Precasting Concretes, Proceedings of the International RILEM Conference "Production Methods and Workability of Concrete", Paisley, Scotland, 1996

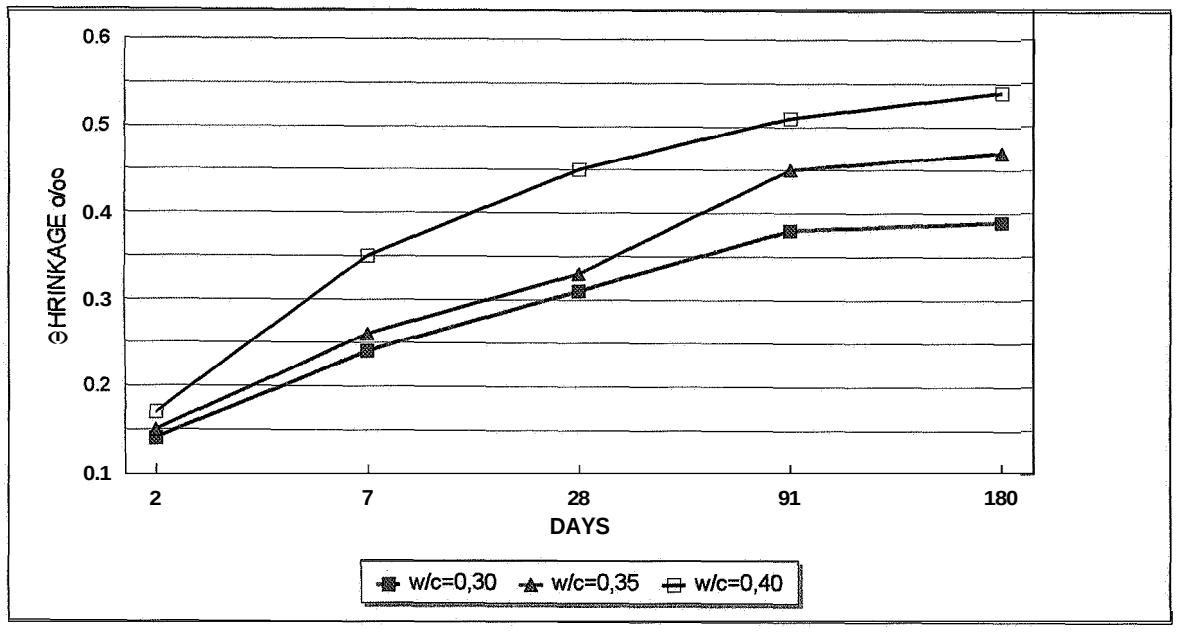

FIG.-1 The *effect* of different *w/c* ratios on the shrinkage of no-slump concrete

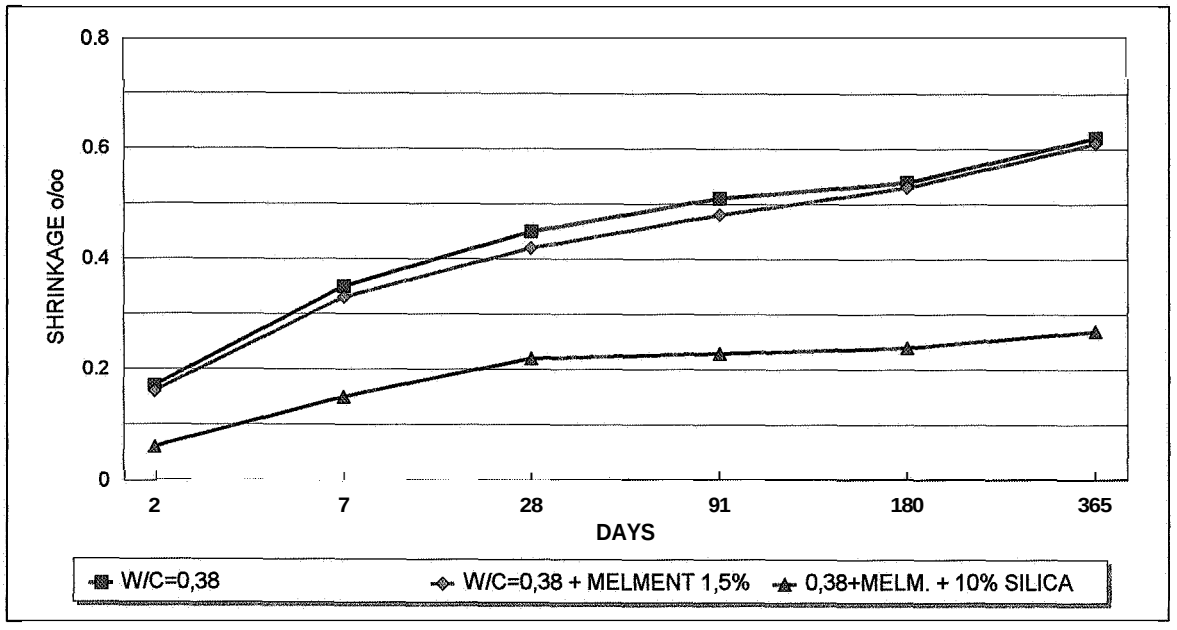

FIG.-2 The effect of superplasticizer and silica fume on the shrinkage of no-slump concrete

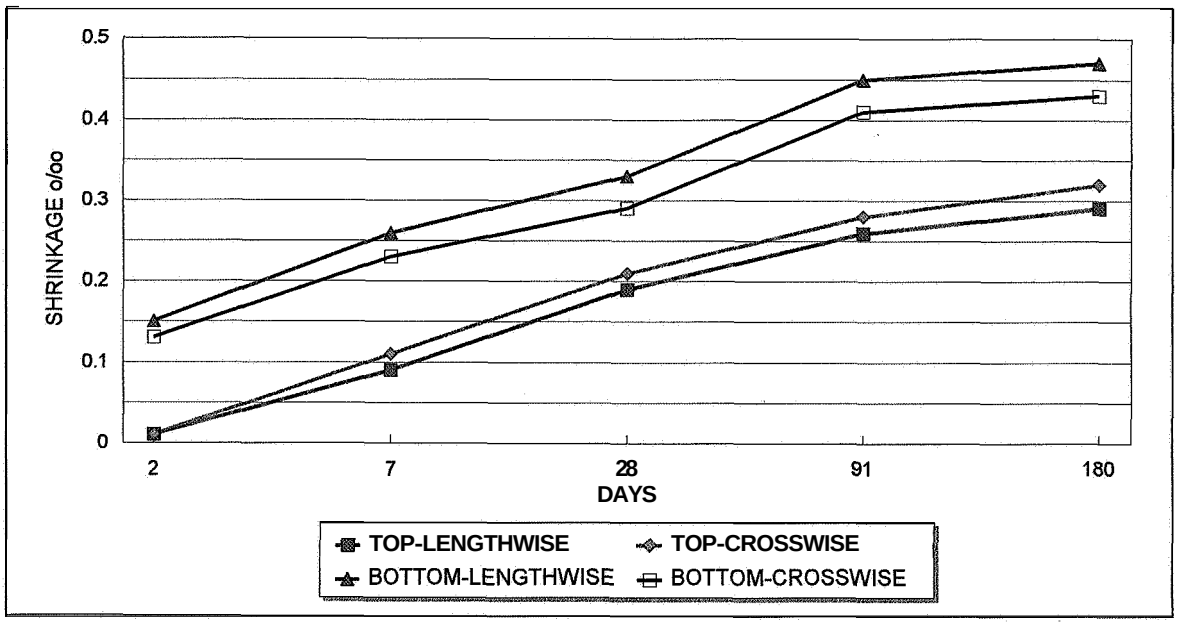

FIG.-3 The effect of measured section in hollow-core slab on shrinkage

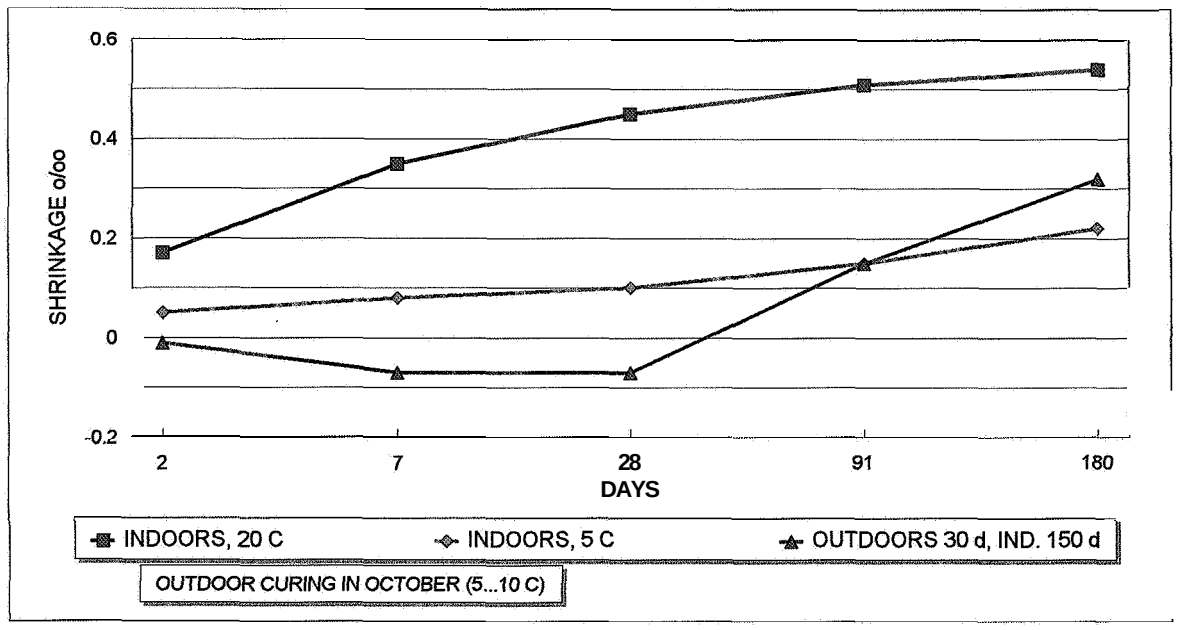

FIG.-4 The effect of curing conditions on shrinkage

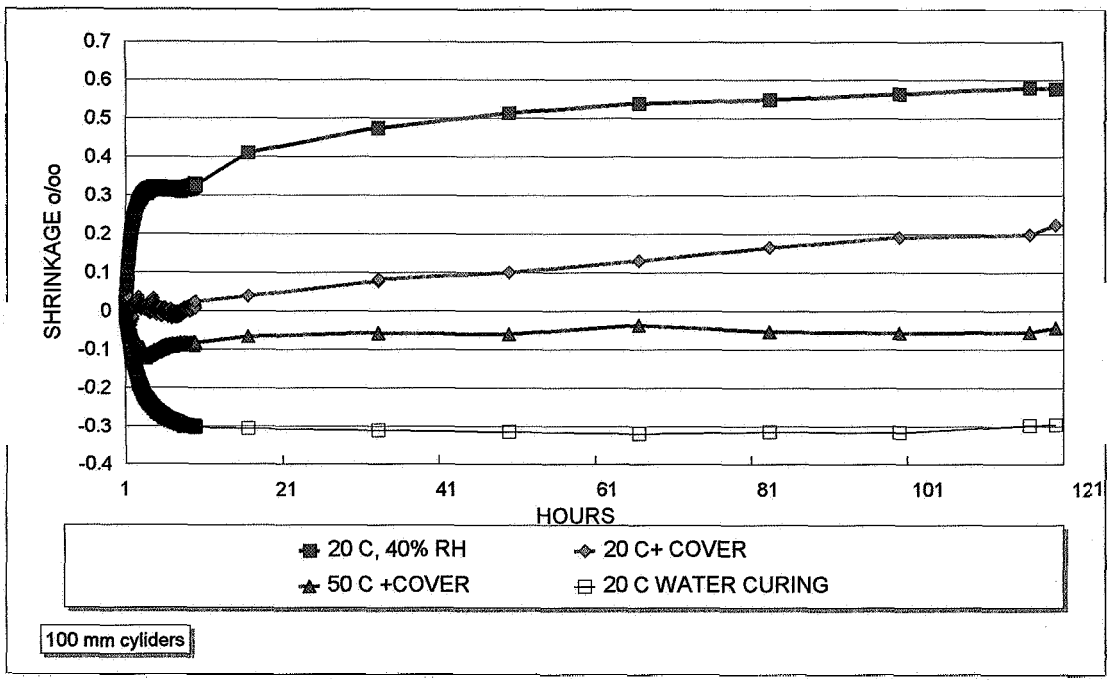

FIG.-5 **The effect of curing on early shrinkage**

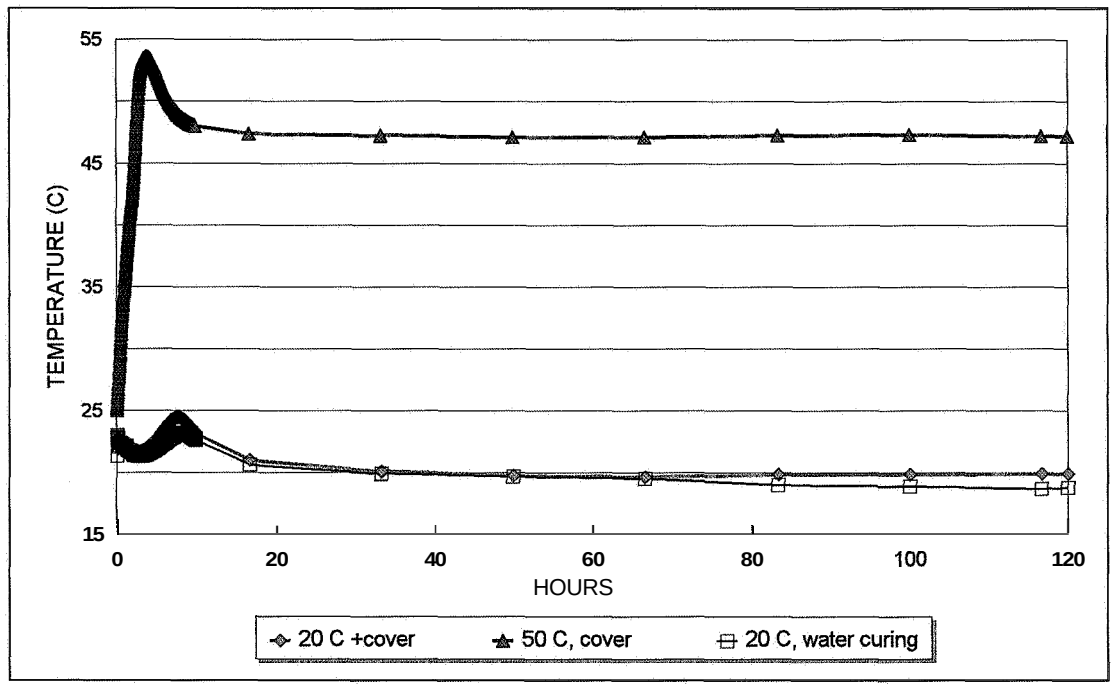

FIG.-6 Temperatures at early age tests